



UNIVERSITAT ROVIRA I VIRGILI

DEVELOPMENT AND CHARACTERIZATION OF BIOARTIFICIAL POLYSULFONE MEMBRANES FOR PROTON TRANSPORT APPLICATIONS

Kamila Szałata

ADVERTIMENT. L'accés als continguts d'aquesta tesi doctoral i la seva utilització ha de respectar els drets de la persona autora. Pot ser utilitzada per a consulta o estudi personal, així com en activitats o materials d'investigació i docència en els termes establerts a l'art. 32 del Text Refós de la Llei de Propietat Intel·lectual (RDL 1/1996). Per altres utilitzacions es requereix l'autorització prèvia i expressa de la persona autora. En qualsevol cas, en la utilització dels seus continguts caldrà indicar de forma clara el nom i cognoms de la persona autora i el títol de la tesi doctoral. No s'autoritza la seva reproducció o altres formes d'explotació efectuades amb finalitats de lucre ni la seva comunicació pública des d'un lloc aliè al servei TDX. Tampoc s'autoritza la presentació del seu contingut en una finestra o marc aliè a TDX (framing). Aquesta reserva de drets afecta tant als continguts de la tesi com als seus resums i índexs.

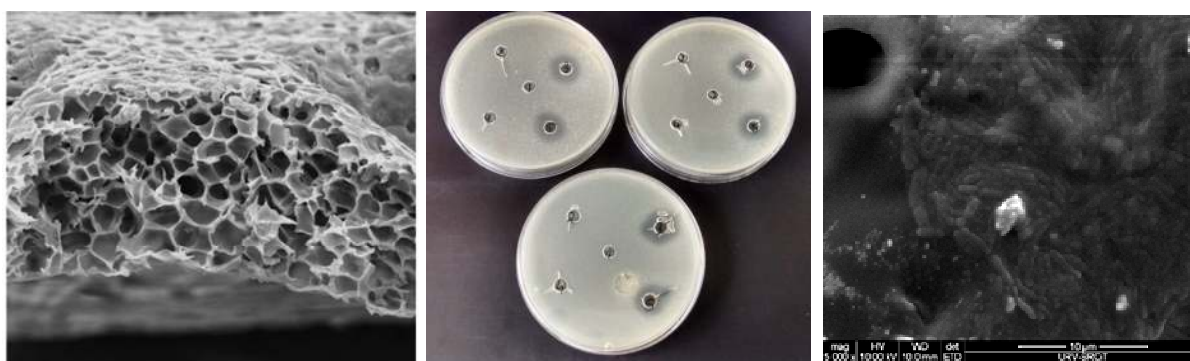
ADVERTENCIA. El acceso a los contenidos de esta tesis doctoral y su utilización debe respetar los derechos de la persona autora. Puede ser utilizada para consulta o estudio personal, así como en actividades o materiales de investigación y docencia en los términos establecidos en el art. 32 del Texto Refundido de la Ley de Propiedad Intelectual (RDL 1/1996). Para otros usos se requiere la autorización previa y expresa de la persona autora. En cualquier caso, en la utilización de sus contenidos se deberá indicar de forma clara el nombre y apellidos de la persona autora y el título de la tesis doctoral. No se autoriza su reproducción u otras formas de explotación efectuadas con fines lucrativos ni su comunicación pública desde un sitio ajeno al servicio TDR. Tampoco se autoriza la presentación de su contenido en una ventana o marco ajeno a TDR (framing). Esta reserva de derechos afecta tanto al contenido de la tesis como a sus resúmenes e índices.

WARNING. Access to the contents of this doctoral thesis and its use must respect the rights of the author. It can be used for reference or private study, as well as research and learning activities or materials in the terms established by the 32nd article of the Spanish Consolidated Copyright Act (RDL 1/1996). Express and previous authorization of the author is required for any other uses. In any case, when using its content, full name of the author and title of the thesis must be clearly indicated. Reproduction or other forms of for profit use or public communication from outside TDX service is not allowed. Presentation of its content in a window or frame external to TDX (framing) is not authorized either. These rights affect both the content of the thesis and its abstracts and indexes.

Doctoral Thesis

Development and Characterization of Bioartificial Polysulfone Membranes for Proton Transport Application

Kamila Maria Szałata



UNIVERSITAT ROVIRA I VIRGILI

2018



UNIVERSITAT ROVIRA I VIRGILI

DEPARTAMENT D'ENGINYERIA QUÍMICA

Escola Tècnica Superior d'Enginyeria Química (ETSEQ)

Av. Països Catalans 26, 43007 Tarragona (Spain)

I state that the present study entitled "DEVELOPMENT AND CHARACTERIZATION OF BIOARTIFICIAL POLYSULFONE MEMBRANES FOR PROTON TRANSPORT APPLICATION" presented by Ms. Kamila Szalata for the award of the Degree of Doctor has been carried out under my supervision at the Chemical Engineering Department of the Rovira i Virgili University and it fulfills all the requirements to be eligible for the International Doctorate Award.

Tarragona, March 20, 2018.

Doctoral Thesis Supervisor

Dra. Tània Gumí Caballero

Acknowledgments

I would like to express my gratitude to Dr. Tània Gumí for giving me the opportunity to develop my PhD thesis under her supervision. I am very thankful for her guidance, patience and unconditional comprehensiveness, which during those years induced both, my scientific and personal development.

Also I would like to acknowledge Dr. Krzysztof Bogdanowicz, my advisor and friend, for his advices and counsel, brain-storming discussions, and for his constant readiness to help.

My sincere gratitude to Dr. Sébastien Balme and all members of the Interfaces, Physical Chemistry and Polymers research group at the European Membrane Institute in Montpellier, for all their help and hospitality during my stay in Montpellier. Thank you Zaineb Bouaziz for your support and friendship.

The members of Servei de Recursos Científics i Tècnics (Universitat Rovira i Virgili) are acknowledged for their kindly guidance and advices through my samples analysis and characterization.

I would like to thank to Dr. Magdalena Constantí for successful collaboration, which has resulted in an article.

Dr. Bartosz Tylkowski is acknowledged for collaboration which resulted in a jointly published book chapter and article.

I acknowledge my friends and members of research group METEOR. Thank you for your help: Dr. Ricard García Valls, Dr. Marta Giamberinni, Dr. José Antonio Reina, Pepa, Xavi, Ruben, Mario, Mimmo, Rita, Gianmarco. I would like to thank to Jie for her help and participation in the work presented in the conference. Especially, I would like to thank to Ada, for her contribution and assistance to finish my work. Thanks to the rest of my Polish friends, Ania, Monika and Kasia for being by my side and to Martin for a nice company during mate-breaks. I could not forget to mention Hany, with which I was taking my first steps in science. Also, I would like to thank to Dr. Gaurav Pande for his collaboration and all good time full of interesting conversations and funny moments.

I am grateful to my parents and my brother, which were with me always when it was needed, for their help and love. Last but not least, I would like to thank to Andry. This work and all what I achieved would not have been possible without your support.

To my family, for their unconditional support

Table of contents

Chapter I: General introduction	1
1.1. Renewable energy and fuel cells concept	2
1.2. Bioartificial materials	5
1.2.1. Fabrication strategies	5
1.2.2. Biomolecules immobilization techniques	6
1.2.2.1. Adsorption	7
1.2.2.2. Covalent immobilization	7
1.2.2.3. Encapsulation	8
1.2.2.4. Entrapment of biomolecule	9
1.2.3. Bioartificial conjugates in membrane technology	10
1.2.3.1. Polysaccharydes	11
1.2.3.2. Enzymes	12
1.2.3.3. Ion channels	15
1.3. Design of bioartificial proton exchange membrane	17
1.4. References	21
Chapter II: Theoretical background	30
2.1. Introduction	31
2.2. Transport in proton exchange membrane	31
2.3. Proton exchange membranes characterization methods	32
2.4. References	36
Chapter III: Methodology and objectives	42
3.1. Introduction	43
3.2. Polysulfone membrane fabrication	43
3.2.1. Physical immobilization methods	44
3.2.1.1. Physical entrapment in polymeric matrix	44
3.2.1.2. Immobilization of gA on MNP	45
3.2.1.2.1. Role of MNP	45
3.2.1.2.2. Role of micelles	46
3.2.1.2.3. Strategy	46
3.2.2. Chemical immobilization method	47
3.2.2.1. Glutaraldehyde coupling	47
3.3. Polyethylene terephthalate (PET) membranes fabrication method	48
3.3.1. Track etching	48
3.3.2. Atomic Layer Deposition (ALD)	49
3.3.3. PET film surface modification and Gramicidin immobilization	50

3.3.4. Polysulfone membrane surface modification	51
3.4. Characterization methods	52
3.4.1. Membranes characterization methods	52
3.4.1.1. Hydrophobic/hydrophilic properties	52
3.4.1.1.1. Contact angle (CA)	52
3.4.1.1.2. Water uptake (WU)	53
3.4.1.2. Surface chemistry	53
3.4.1.2.1. Fourier Transform Infrared (FTIR)	53
3.4.1.3. Morphology analysis	54
3.4.1.3.1. Scanning Electron Microscopy (SEM) and Environmental Scanning Electron Microscopy (ESEM)	54
3.4.1.3.2. Porosity	54
3.4.1.4. Transport properties	55
3.4.1.4.1. Permeability calculation	55
3.4.1.4.2. Atomic Absorption Spectrometry (AAS)	57
3.4.1.4.3. Polarized Optical Microscope (POM)	58
3.4.1.4.4. Current-Voltage measurement (CV)	58
3.4.1.4.5. Self-diffusion coefficient calculation	59
3.4.2. Micelles characterization	61
3.4.2.1. Micelle solutions biological activity study	61
3.4.2.1.1. Activity study in solid media	61
3.4.2.2. Immobilized micelles biological activity study	62
3.4.2.2.1. Activity study in solid media	62
3.4.2.2.2. Activity study in liquid media	62
3.4.2.3. Interfacial tension measurement (IFT)	63
3.4.2.4. Viscosity	64
3.4.2.5. Electrical conductivity	66
3.4.2.6. Dynamic Light Scattering analysis (DLS)	66
3.5. Objectives	67
3.6. Acknowledgments	68
3.7. References	69
Chapter IV : Physical immobilization by entrapment	74
4.1. Introduction	75
4.2. Materials	75
4.3. Methods	76

4.3.1. Entrapment method process optimization	76
4.3.1.1. Phase inversion/precipitation in water-coagulation bath	76
4.3.1.2. Phase inversion/precipitation by solvent evaporation	76
4.4. Results	77
4.4.1. Morphology analysis (SEM and ESEM)	77
4.4.2. Contact angle (CA) and Water uptake (WU)	82
4.4.3. Permeability test	84
4.4.4. Current-Voltage measurement (CV)	84
4.5. Conclusions	84
4.6. References	86
Chapter V: Physical immobilization with the use of magnetic nanoparticles (MNP)	90
5.1. Introduction	91
5.2. Materials	91
5.3. Methods	92
5.3.1. Immobilization on a magnetic nanoparticles (MNP)	92
5.3.1.1. MNP preparation	92
5.3.1.2. MNP membranes preparation	93
5.3.1.3. TRX treatment	94
5.3.1.4. TRX/gA micelles immobilization	94
5.3.2. Plain Psf membrane modification	95
5.3.3. Characterization methods	97
5.3.3.1. Morphology analysis (ESEM)	97
5.3.3.2. Contact angle (CA)	97
5.3.3.3. Water uptake (WU)	97
5.3.3.4. Permeability test	98
5.3.3.5. Atomic Absorption Spectrometry (AAS)	98
5.3.3.6. Polarized Optical Microscope (POM)	98
5.3.3.7. Current-Voltage measurement (CV)	99
5.3.3.8. Self-diffusion coefficient calculation	99
5.4. Results	99
5.4.1. Morphology analysis (ESEM)	99
5.4.2. Contact angle (CA) and Water uptake (WU)	102
5.4.3. Permeability test	106
5.4.4. Atomic Absorption Spectrometry (AAS) and Polarized Optical Microscope (POM)	113
5.4.5. Current-Voltage measurement (CV)	113
5.4.6. Self-diffusion coefficient calculation	120
5.5. Conclusions	123
5.6. References	124

Chapter VI: Chemical immobilization by glutaraldehyde coupling	130
6.1. Introduction	131
6.2. Materials	131
6.3. Methods	132
6.3.1. Immobilization via glutaraldehyde coupling	132
6.3.2. Characterization methods	132
6.3.2.1. Morphology analysis (ESEM)	132
6.3.2.2. Contact angle (CA)	133
6.3.2.3. Water uptake (WU)	133
6.3.2.4. Permeability test	133
6.3.2.5. Current-Voltage measurement (CV)	134
6.3.2.6. Self-diffusion coefficient calculation	134
6.4. Results	134
6.4.1. Morphology analysis (ESEM)	134
6.4.2. Contact angle (CA) and Water uptake (WU)	135
6.4.3. Permeability test	138
6.4.4. Current-Voltage measurement (CV)	139
6.4.5. Self-diffusion coefficient calculation	143
6.5. Conclusions	145
6.6. References	146
Chapter VII : Preparation and characterization of track-etched polymeric membranes containing Gramicidin	148
7.1. Introduction	149
7.2. Materials and methods	149
7.2.1. PET film preparation	149
7.2.2. PET film surface modification and Gramicidin immobilization	150
7.2.3. Polysulfone membranes surface modification	151
7.2.4. Permeability test	152
7.3. Results	152
7.3.1. Selectivity to cations of PET membranes	152
7.3.2. Selectivity to anions of PET membranes	156
7.3.3. Selectivity of polysulfone membranes	158
7.3.4. Surface chemistry (FTIR)	159
7.4. Conclusions	160
7.5. Acknowledgments	161
7.6. References	162
Chapter VIII Surfactant/Gramicidin micelles bioactivity study	164
8.1. Introduction	165
8.2. Materials	167
8.3. Methods	167

8.3.1. Micelle solutions preparation	167
8.3.2. Inhibitory activity study of TRX/gA micelle solutions against <i>Listeria innocua</i> and <i>Bacillus subtilis</i>	168
8.3.3. Inhibitory activity study of polysulfone membranes with immobilized TRX/gA micelles against <i>Bacillus subtilis</i>	169
8.3.3.1. Experiment in solid medium	169
8.3.4. Membrane biofouling determination	170
8.4. Results	170
8.4.1. <i>Listeria innocua</i>	170
8.4.2. <i>Bacillus subtilis</i>	172
8.4.2.1. Gramicidin activity in micelles without presence of methanol	172
8.4.2.2. Gramicidin activity in micelles without presence of methanol at different concentration of bacteria	173
8.4.2.3. Gramicidin activity in micelles with presence of methanol	174
8.4.2.4. Gramicidin activity in micelles with presence of methanol and at different concentration of protein	175
8.4.2.5. Gramicidin activity in micelles and in the solution with presence of methanol	177
8.4.3. Inhibitory activity of polysulfone membranes containing immobilized TRX/gA micelles	180
8.4.3.1. Experiment in solid medium	180
8.4.3.2. Experiment in liquid medium	181
8.4.4. Membrane biofouling determination	183
8.4.5. Characterization of membrane with micelles containing methanol	184
8.4.5.1. Permeability test	184
8.4.5.2. Current-Voltage measurement (CV)	186
8.5. Conclusions	189
8.6. Acknowledgments	190
8.7. References	191
Chapter IX: Characterization of the surfactant/biomolecule micelles thermophysical properties	194
9.1. Introduction	195
9.2. Materials	196
9.3. Methods	197
9.3.1. Micelles solution preparation	197
9.3.2. Interfacial tension measurements	197
9.3.3. Dynamic Light Scattering analysis (DLS)	198
9.3.4. Viscosity measurement	198
9.3.5. Conductivity measurement	198
9.4. Results	199

9.4.1. Interfacial tension measurement (IFT)	199
9.4.2. Dynamic Light Scattering analysis (DLS)	202
9.4.3. Viscosity and conductivity measurement	205
9.5. Conclusions	206
9.6. Acknowledgments	207
9.7. References	208
Chapter X Conclusions	212
Appendices	218
Appendix A. List of Figures	219
Appendix B. List of Tables	223
Appendix C. Publications	224
Appendix D. Contribution to congresses	225
Appendix E. Other contributions	225
Appendix F. Curriculum Vitae	226

Abstract

Proton-exchange membrane fuel cells (PEMFCs) are promising technology as clean and efficient power source in the twenty-first century. Essential characteristics of those materials are high ion conductivity and selectivity, very good chemical and thermal stability, good mechanical properties and low production cost. One of the strategies for development of such membranes is design of bioinspired materials. Those materials are composed of biological and non-biological component, what connects the advantages of artificial polymeric films with biofunctionality of proteins. Nevertheless biomolecule immobilization is a challenging task, due to incompatibilities with polymer or lose of protein's biological activity.

The aim of this work was to develop a material combining robustness of polymer and bioactivity of protein. Polysulfone is known from its outstanding chemical, thermal and mechanical stability, and moreover, it was proved to be compatible with many biological components. Those characteristics, together with possibility of functionalization and facility in films preparation, make it to be a good base material for creation of bioartificial membrane. Gramicidin is a biological membrane ion channel, known from fast and selective transport of monopositively charged ions. Its transport properties studied also at elevated temperatures suggests its applicability in fuel cells applications.

Two different strategies for protein attachment: physical and chemical immobilization. Physical immobilization is considered to be a good strategy of protein immobilization, without affecting of their biofunctionality. Nevertheless, chemical attachment is stronger and prevent protein detachment. In this dissertation, two physical immobilization methods and one chemical immobilization method were evaluated. First, physical method was immobilization via entrapment, which consist of direct protein insertion into the polymeric matrix. The second method, was physical immobilization with use of magnetite nanoparticles, which consist of Surfactant/Gramicidin micelles formation and their immobilization on nanoparticles immersed in a membrane film. The chemical immobilization method was performed via glutaraldehyde coupling, which is known as a good method for covalent attachment of biomolecules to the artificial materials.

Accurate characterization of membrane is important to describe and understand occurring transport phenomena and is essential for further process optimization and

material improvement. In this thesis, obtained membranes were characterized in terms of morphology, interaction with water and transport properties. Moreover, Surfactant/Gramicidin micelles were examined in terms of their biological activity and thermophysical properties. Experimental results were analysed by means of statistical analysis. Additionally, ion permeability results were evaluated in terms of agreement with the Nernst-Einstein model.

The membrane system proposed herein have a potential to be used as ion exchange membranes, because its design combines the good mechanical properties of polysulfone and the selective ionic transport properties of Gramicidin. Moreover, the presented method intend to deliver a quick and easy way of membranes production, possibly easy to scale up. In this dissertation we present design and characterization of polysulfone membrane containing Gramicidin, immobilized via three strategies: two physical and one chemical method. Results show that influence of protein immobilization on membrane morphology was minimized. Immobilized protein changes hydrophobic and water swelling properties of the membrane (decrease of CA up to 25.2° and increase of water uptake up to 1.28 mg of water per mg of membrane). Physical protein immobilization by entrapment method does not improve membrane transport properties. Physical immobilization with use of magnetite nanoparticles and chemical immobilization via glutaraldehyde coupling improves ion transport properties (decrease of Ohmic resistance from 1366 $\Omega \cdot \text{cm}^2$ to 373 after physical immobilization, and to 455 $\Omega \cdot \text{cm}^2$ after chemical immobilization in the case of H^+ transport, and increase of H^+ diffusion rate from 7.02E-04 to 7.89E-03 $\text{cm}^2 \cdot \text{s}^{-1}$ in the case of physical immobilization and from 2.23E-03 to 7.53E-03 $\text{cm}^2 \cdot \text{s}^{-1}$ in the case of chemical immobilization). The use of magnetite nanoparticles in the membrane resulted in remarkable proton conductivity, in the range of 10^{-2} to 10^{-3} S/cm. Also, the influence of preparation solution was evaluated. For membranes containing $-\text{OH}$ and $-\text{NH}_2$ functionalized nanoparticles protein immobilization performed is more effective when performed in water and PBS respectively. Chemical immobilization is more effective when prepared in PBS buffer solution. The best performance in terms of ion transport selectivity was presented by the MNP-OH membranes with Gramicidin immobilized physically, which exhibit also the highest conductivity (0.71 S/cm for H^+). The highest diffusion permeability values was obtained for the membrane with chemically immobilized Gramicidin, prepared in PBS buffer solution (0.009 cm^2/s for Na^+) which has also relatively high conductivity (0.45 S/m for H^+) and good

selectivity values. Biological activity trial shows that Gramicidin maintains its antibacterial properties when the methanol is present in preparation solution. Micelles composed of surfactant Triton X100 and Gramicidin are biologically active in both, solution and immobilized on a membrane surface. Membranes with immobilized micelles have higher resistance to bacteria growth.

Resumen

Las celdas de combustible que utilizan membrana de intercambio de protones (PEMFC) son una tecnología prometedora como fuente de energía limpia y eficiente en el siglo XXI. Las características esenciales de esos materiales son su alta conductividad eléctrica, selectividad iónica, estabilidad química y térmica. Además, deben tener excelentes propiedades mecánicas y un bajo coste de producción. Una de las estrategias para incrementar el uso de estas membranas es su diseño empleando materiales bioinspirados, los cuales están compuestos de componentes biológicos y no biológicos. Esta estrategia permite combinar las ventajas de los polímeros artificiales con la biofuncionalidad de las proteínas. Sin embargo, la inmovilización de biomoléculas es una tarea desafiante, debido a incompatibilidades con el polímero o a la pérdida de la actividad biológica de la proteína. En esta tesis se han seleccionado la polisulfona y la Gramicidina como componentes para la fabricación de membranas de intercambio de protones. El objetivo de este trabajo ha sido desarrollar un material que combine la robustez de la polisulfona y la bioactividad de la Gramicidina.

La polisulfona es un polímero conocido por su excelente estabilidad química, térmica y mecánica, y además, se demostró que es compatible con muchos componentes biológicos. Esas características, junto con la posibilidad de funcionalización y facilidad en la preparación de películas poliméricas, hacen que sea un excelente material para la fabricación de una membrana bioartificial. La Gramicidina es una proteína de membrana biológica que actúa como canal, y es conocida por el transporte rápido y selectivo de iones con carga monopositiva. Dichas características de transporte que se mantienen también a temperaturas elevadas sugieren su aplicabilidad en celdas de combustible.

Existen dos maneras de inmovilizar proteínas: la inmovilización física se considera una buena estrategia de inmovilización de proteínas, sin afectar su biofuncionalidad. Sin embargo, la unión química es más fuerte y evita el desprendimiento de proteínas. En este trabajo, se han evaluado dos métodos de inmovilización física y un método de inmovilización química. El primer método físico fue la inmovilización por atrapamiento, que consiste en la inserción directa de proteínas en la matriz polimérica. El segundo método fue la inmovilización física con el uso de nanopartículas de magnetita, que consisten en la formación de micelas de Surfactante/Gramicidina y su posterior inmovilización en nanopartículas distribuidas en la película de membrana.

El método de inmovilización química se realizó mediante entrecruzamiento con glutaraldehído, el cual es comúnmente utilizado para el enlace covalente de biomoléculas con materiales artificiales.

La adecuada caracterización de la membrana es importante para describir y comprender los fenómenos de transporte que se producen y es esencial para una mayor optimización del proceso y mejora del material. En esta tesis, las membranas obtenidas se caracterizaron en términos de morfología, interacción con el agua y propiedades de transporte. Además, las micelas de Surfactante/Gramicidina se examinaron en términos de su actividad biológica y propiedades termofísicas. Los resultados experimentales se analizaron mediante análisis estadístico. Además, los resultados de la permeabilidad iónica se evaluaron en términos de acuerdo con el modelo de Nernst-Einstein.

El sistema de membrana propuesto en la presente tesis tiene el potencial de ser utilizado como membranas de intercambio iónico, debido a que su diseño combina las buenas propiedades mecánicas de la polisulfona y las propiedades de transporte iónico selectivo de la Gramicidina. Además, la estrategia utilizada permitió establecer que dos métodos presentados (inmovilización física con el uso de nanopartículas y inmovilización química) pretenden ofrecer una forma eficiente, rápida y fácil de producción de membranas, posiblemente fácil de escalar. La proteína inmovilizada modifica dos propiedades de la membrana como son su hidrofobicidad (disminuye el ángulo de contacto hasta 25.2°) y su capacidad para absorber agua (incrementa la capacidad de la membrana para absorber agua hasta 1.28 mg de agua por mg de membrana).

La inmovilización física con el uso de nanopartículas de magnetita y la inmovilización química a través del entrecruzamiento con glutaraldehído mejora las propiedades de transporte de iones. La resistencia óhmica disminuye desde $1366 \Omega \cdot \text{cm}^2$ a $373 \Omega \cdot \text{cm}^2$ después de la inmovilización física, y de $1366 \Omega \cdot \text{cm}^2$ a $455 \Omega \cdot \text{cm}^2$ después de la inmovilización química. También incrementa la velocidad de la difusión de H^+ desde $7.02\text{E-}04$ a $7.89\text{E-}03 \text{ cm}^2\text{s}^{-1}$ después de inmovilización física y desde $2.23\text{E-}03$ a $7.53\text{E-}03 \text{ cm}^2\text{s}^{-1}$ después de inmovilización química.

El uso de las nanopartículas de magnetita en la membrana dio como resultado una mejora/incremento conductividad de protones notable, en el rango de 10^{-2} a 10^{-3} S/

cm. La evaluación de la influencia de la solución inicial del proceso de inmovilización de la proteína en membranas con nanopartículas funcionalizadas con el grupo $-NH_2$ y $-OH$ mostro que el proceso es más efectivo cuando se utiliza PBS y agua como solvente respectivamente.

La inmovilización química es más efectiva cuando se prepara en solución tampón PBS. El mejor rendimiento en términos de selectividad del transporte iónico fue presentado por las membranas MNP-OH con Gramicidina inmovilizada físicamente, que exhiben también la conductividad eléctrica más alta (0.71 S/cm para H^+).

Los valores más altos de permeabilidad de difusión se obtuvieron para la membrana con Gramicidina químicamente inmovilizada, la cual fue preparada en solución tampón PBS (0.009 cm^2/s para Na^+) Esta membrana también tiene una conductividad relativamente alta (0.45 S/cm para H^+) y buena selectividad. La prueba de actividad biológica muestra que la Gramicidina mantiene sus propiedades antibacterianas cuando el metanol está presente en la solución de preparación. Las micelas compuestas de surfactante Triton X100 y Gramicidina son biológicamente activas tanto en solución como inmovilizadas en una superficie de membrana. Las membranas con micelas inmovilizadas tienen mayor resistencia al crecimiento de bacterias.

Chapter I

General introduction

1.1. Renewable energy and fuel cells concept

The continued exploitation of fossil fuels, followed by population growth and high energy demand, significantly influences environment causing irreversible changes in the climate. Emission of atmospheric CO₂ increases alarmingly and climatologists predict that by 2100 the global temperature will increase above dangerous level. Thus, mitigating the negative effects of global warming is extremely urgent. That implies a large amount of investments in renewable energy technologies sectors. The report of Bloomberg New Energy Finance says that by 2040 a total amount of 10.2 trillion dollars will be invested in alternative energy sources. European investments in this field grows 2,6% per year and in 2040 half of the produced electricity in the continent will come from various renewable energy sources, including solar, wind, geothermal and other types of energy obtained from sources that are endless and can be continuously refilled [1].

Electricity produced during renewable electrolysis of water into hydrogen and oxygen takes place in a device called fuel cell [2]. Fuel cells work continuously as long as an oxidant and a fuel is being supplied, converting the energy of a chemical reaction into electricity. Among many advantages of fuel cells, the following ones must be highlighted:

- Water is the main by-product, what is the most desirable characteristic of fuel cells, since it implies reduction of greenhouse emission.
- Possibility of continuous operation: they can be quickly refueled there is no need to change them after discharge, like in the case of batteries.
- Easy scale up: the fuel cell modules can be fabricated in both modular and industrial scale.
- High efficiency: fuel cells can produce large amount of energy, up to megawatt range.

Despite the recent advances in this novel technology, there are still some drawbacks which disable mass-market applications of fuel cells. High production and packaging costs and short lifetime in comparison to conventional energy sources are still a major

barrier for their full commercialization [3, 4]. For this reason, continuous research for new materials is necessary to overcome disadvantages presented by currently available fuel cells.

Until now several types of novel developed fuel cells have been introduced to the market, and the main ones can be classified as follows: direct methanol fuel cells (DMFC) used as a portable power source, alkaline fuel cells (AFC) for aeronautics energy sources applications, phosphoric acid fuel cells (PAFC), molten carbonate fuel cells (MCFC) and solid oxide fuel cells (SOFC) for stationary energy generation application, and proton exchange membrane fuel cells (PEMFC) used for transport applications [2, 3, 5]. During fuel cells operation process, heat, water and sometimes carbon dioxide are produced. The reactions taking place in different devices are collected in Table 1.1.

Table 1.1. Reactions on the electrodes in different fuel cells.

Fuel Cell	Anode reaction	Cathode reaction
DMFC	$\text{CH}_3\text{OH} + \text{H}_2\text{O} \rightarrow 6\text{H}^+ + 6\text{e}^- + \text{CO}_2$	$\frac{3}{2}\text{O}_2 + 6\text{H}^+ + 6\text{e}^- \rightarrow 3\text{H}_2\text{O}$
AFC	$2\text{H}_2 + 4\text{OH}^- \rightarrow 4\text{H}_2\text{O} + 4\text{e}^-$	$\text{O}_2 + 2\text{H}_2\text{O} + 4\text{e}^- \rightarrow 4\text{OH}^-$
PAFC	$\text{H}_2 \rightarrow 2\text{H}^+ + 2\text{e}^-$	$\text{O}_2 + 4\text{H}^+ + 4\text{e}^- \rightarrow 2\text{H}_2\text{O}$
MCFC	$\text{H}_2\text{O} + \text{CO}_3^{2-} \rightarrow \text{H}_2\text{O} + \text{CO}_2 + 2\text{e}^-$	$\frac{1}{2}\text{O}_2 + \text{CO}_2 + 2\text{e}^- \rightarrow \text{CO}_3^{2-}$
SOFC	$\text{H}_2 + \text{O}^{2-} \rightarrow \text{H}_2\text{O} + 2\text{e}^-$	$\frac{1}{2}\text{O}_2 + 2\text{e}^- \rightarrow \text{O}^{2-}$
PEMFC	$\text{H}_2 \rightarrow 2\text{H}^+ + 2\text{e}^-$	$\text{O}_2 + 4\text{H}^+ + 4\text{e}^- \rightarrow 2\text{H}_2\text{O}$

In general, fuel cells consist of an anode, an anodic catalyst layer, an electrolyte, a cathodic catalyst layer and a cathode. In order to obtain the desired voltage and current efficiency, fuel cells stacks are connected in parallel. The anode and cathode are usually fabricated from the highly conductive material, e.g. porous graphite. One of the most common catalysts used in low temperature fuel cell production is platinum. The electrolyte is produced from material with high proton conductivity and ideally no electron conductivity. The PEMFC is a fuel cell which specificity lies in a type of electrolyte employed in the operation. In a single cell, the main components are: an electron conducting anode, a proton conducting electrolyte which is solid polymeric

membrane, and an electron conducting cathode. The fuel used in an operation is air and hydrogen (Table 1.1.), which is processed at the anode, where protons separation occurs on the surface of a catalyst (platinum-based). While protons are crossing the solid electrolyte membrane to the cathode, the electrons migrate into an external circuit, generating the electrical power. Then, on the cathode side of the cell, metal-based electrode joins the protons, electrons and oxygen from air producing clean water [5, 6].

The proton exchange membrane (PEM) is a crucial PEMFC element, and its transport properties regulates the power production efficiency. PEMs ability to transport protons determines the chemical reactions speed and as a result- energy production. Nowadays, the most commonly PEM used in industry are sulfonated polymers, with Nafion from Dupont on the first place [5]. This membrane shows excellent ionic properties and good proton conductivity in hydrated state; and moreover it exhibits good mechanical stability. Despite multiple advantages presented by Nafion and other sulfonated polymers, their complicated synthesis and safety concerns related to the fabrication resulted in development of non-fluorinated hydrocarbons for PEMFC application (eg Victrex) [5]. Nevertheless, besides their availability, relatively good stability and easy processing and functionalization, their performance in a fuel cell is not very effective. Also, alternative styrene containing membranes (Ballard and Dais Analytics), found to be very unstable chemically and mechanically and thus their applications are very limited [5].

Based on the performed survey it can be concluded that an ideal PEM should poses the following characteristics: low fuel permeability, high proton transport speed, selectivity, good mechanical and chemical stability and low cost [7-9]. Up to now multiple strategies have been applied in order to develop a membrane with the desired properties. Many of the studies consist on the synthesis of new polymers, including polyimides [10, 11] or polyphosphazene based polymers [12, 13]. Synthesis of liquid crystalline polymers by Bogdanowicz [14-17] and Montané [18] lead to provide assembled polymeric wires, which in hybrid membrane system exhibits certain selectivity to proton. Also, formation of composite membranes [19-21] and mixed matrix membranes have been employed, joining functionality of inorganic component and polymer [22]. In order to enhance conductivity and water retention properties, some researchers used nanoparticles [23-25] or surface modification [26]. Another approach consist in connecting bioactivity of ion transporting molecules with robustness and

stability of polymer. This bioinspired concept lead to create bioartificial polymeric materials which combine the benefits coming from both sources- biological and synthetic ones. They can have advantages over the natural version, like improved mechanical robustness and reproducible chemistry but at the same time they may operate according to biological mechanism, with the same or even higher efficiency. In this work, bioartificial approach is employed with the purpose to develop proton transporting membrane with high ion speed and selectivity, which could serve as an alternative material for PEM fabrication.

1.2. Bioartificial materials

1.2.1. Fabrication strategies

One of the strategies to fabricate bioartificial materials is synthesis of new chemical compounds, able to adopt the same structure and functionality as pattern biomolecule. They are called biomimetic materials. Within this approach many stimuli-responsive polymers have been synthesized. An example of this kind of materials is a novel gel system was developed by Yoshida [27]. Over years of investigations, those polymeric gels have been improved, and are able to mimic autonomous oscillation movements, such as heart beat or brain waves. The working principle of this biomimetic actuators is based on converting a chemical oscillation process into a mechanical alteration in gels, which can be also controlled by changing temperature or substrates concentration. The work of Yoshida provides a smart material which can generate self-propelled motions, pendulum motions or directional motions and have found variety of applications in biomedicine. Another example of the same concept is the imitation of enzymes for sensing applications and biocatalysts [28, 29]. Recent improvements in this discipline allowed to overcome the challenges regarding poor selectivity of synthesized sensors by applying molecular imprinted polymers [30]. It is reported that MIP-based nitroreductase has been successfully used for effective determination of a metronidazole or hexazinone herbicide, which are pervasive ground water contaminants [31]. A known example of replacing a natural polymer by artificial one is synthetic rubber, which is

much easier to handle and thanks to that it is used e.g. for production of car wheels or artificial hair fabrication, as a synthetic substitute of keratin [32-35].

Another approach to create polymeric biomaterials is based on the concept of its biocompatibility with living cells. This is a great challenge in terms of application of many synthetic compounds- to be safely used *in vivo*, they need to be biodegradable and its decomposition products cannot exhibit any toxicity. Several synthetic polymers have been found to fulfill those characteristics and nowadays are commonly used in biomedical applications, for instance polymeric breast implants, polyurethane in artificial heart or poly(glycolic acid) as absorbable sutures [36-38].

Besides, great part of the investigations concerning the design of biological-like artificial systems, is dedicate to development of hybrid protein-synthetic polymer materials. The first trial performed to obtain synthetic polymers containing biomolecule was reported already in the 60's of XX century [39]. From that moment the knowledge in this discipline evolved significantly. The combination of synthetic parts with biological components is a step forward to the fabrication of hybrid bioinspired structures with unprecedented properties and plenty of new applications.

1.2.2. Biomolecules immobilization techniques

The crucial step in successful biomolecule immobilization is the preparation of material, which may possess the advantages of synthetic polymer, which includes good mechanical properties; reproducible chemistry which allows large scale production; and also, biocompatibility and functionality of biomolecule of natural systems. This establishment is related with many challenges which depend on the type of protein incorporated into artificial medium and on desired application of the material. However, the main defiance, present in all kind of used proteins is preserving their biological activity, which often is lost due to incompatibility with the polymer or change in a conformation during immobilization process [40-42]. Thus, within this particular concept different strategies of protein immobilization can be applied and are usually classified as follows.

1.2.2.1. Adsorption

Adsorption is the simplest and most commonly used method and consist in physical adsorption of the biomolecule on a support (Figure 1.1.). If performed in adequate conditions, this method can efficiently connect biomolecules to a artificial material via hydrophobic or van der Waals interactions. This method has found application in enzymes immobilization for drugs purification purposes [43-47]. Nevertheless, the interaction between support and protein, is usually too weak to cope high pressure or temperature conditions, thus in industrial applications is preferable to employ other techniques.

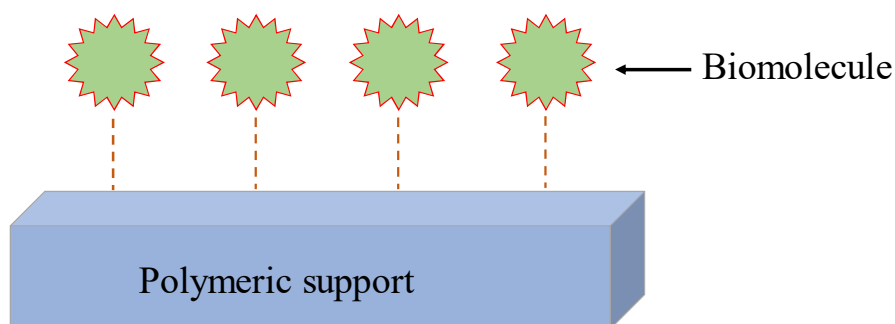


Figure 1.1. Scheme of physical adsorption of biomolecules on a polymeric support.

Adsorption is relatively easy to perform and since it is free from chemical modification is a very effective method which allows to maintain biological activity of proteins. Also, thanks to the fact that is reversible, purification of used biomolecules and supports is facilitated. Nevertheless, the main handicap of this method is requirement of mild working conditions and very careful selection of both, molecules and artificial carriers.

1.2.2.2. Covalent immobilization

This method results in obtaining much stronger linkages between polymers and biomolecules. Chemical reaction normally occurs between functional groups present in the support surface and the functional groups of protein. Common reactions used to create new bonds are 1,3-dipolar cycloadditions of terminal alkynes and azides, peptide

bonds formation, isourea linkage, alkylation reaction [48], coupling via tresyl chloride, coupling via cyanogen bromide, coupling via cyanuric chloride or glutaraldehyde coupling [49].

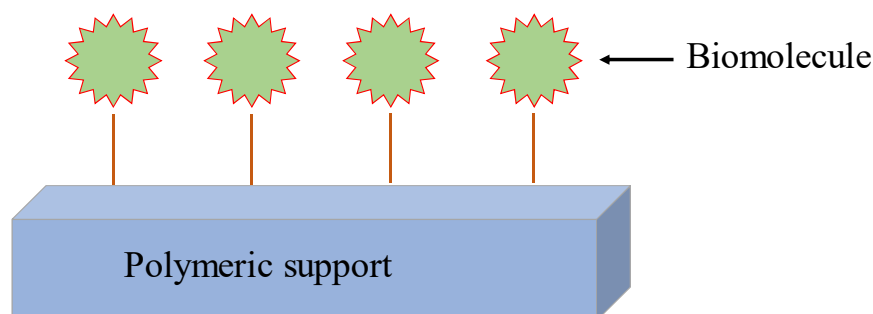


Figure 1.2. Schematic representation of a covalent biomolecule attachment to the polymeric support.

In the case of this immobilization strategy, leakage of biomolecule is minimized. However, due to the necessity of using chemicals, this is a much more expensive method in comparison to physical adsorption. Moreover, it is also often connected with use of organic solvents which may cause loss of protein biological activity.

1.2.2.3. Encapsulation

Encapsulation is commonly used in drug delivery systems as well as in biocatalysis. Biomolecule immobilized in a polymeric semi-permeable shell has enough free space to freely move and adapt various conformations, and it is isolated from environment (Figure 1.3.). Possibility to fabricate pH or light-sensitive microcapsules allows to release the entrapped protein from its core under desirable conditions [50, 51]. Thanks to the capability to produce capsules of different sizes it is possible to encapsulate even big biomolecules. The limitations related to this method consist in diffusion problems through the capsule. Also, an important factor is the sensitivity of polymer to external factors such as pH or temperature. Depending on the function of encapsulated protein, the properties of polymeric capsules need to be adjusted, to assure a release of biomolecule under the desired conditions.

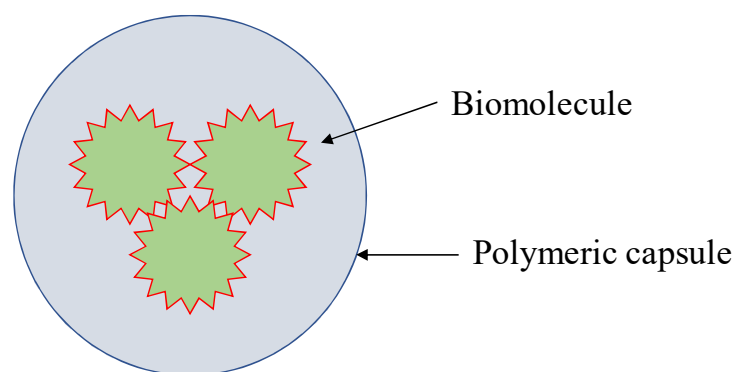


Figure 1.3. Schematic representation of biomolecule immobilization by encapsulation method.

1.2.2.4. Entrapment of biomolecule

Entrapment of biomolecules consists in dispersing them in a polymeric gel, which dense and viscous consistence delimits the movements and thus, stabilize protein/polymer structure (Figure 1.4.). In this system, the polymer acts also as a biomolecule protector, which separates it from harmful environmental conditions. Also, as the polymer porosity can be controlled, it is possible to design a gel-net adjusted to the protein size what can prevent leakage but also permits free moieties and adaptation of active form.

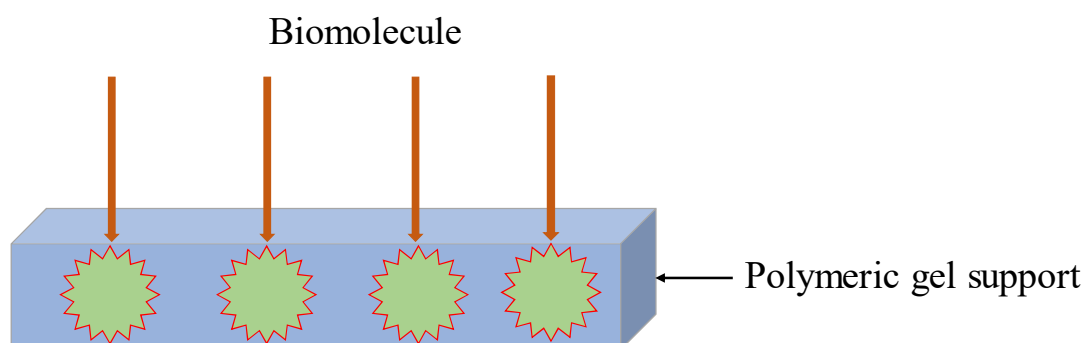


Figure 1.4. Scheme of biomolecule immobilization via entrapment.

Although protein loading achieved within this method can be very high there is a big disadvantage of this technique, related to diffusion limitation through the gel, similar like in the case of encapsulation.

All abovementioned immobilization techniques present certain disadvantages and the specific design of the optimum system needs to consider all type of limitations. However, development of new strategies and continuous improvements in terms of conditions optimization, allow to immobilize various biological elements in the polymers and has induced many remarkable discoveries in the area of bioconjugates. Election of the appropriate method depends on the type of immobilized biocompound and application of the final product.

Researchers from all over the world are facing challenges connected with specificity of particular biomolecules and polymers, struggling to overcome limitations to obtain desirable, perfect, defect free biomaterials with multiple functionalities. Bioartificial conjugates have found application in industry, technology, biosensing, tissue engineering and pharmacology [52, 53]. Our interest focus on application of those materials in membrane technology.

1.2.3. Bioartificial conjugates in membrane technology

Membranes are semipermeable barriers separating an initial mixture from a final solution, allowing the selective transport of certain species while prevent the passage of others, like in the case of biological membranes, that they maintain ionic balance in the cells. They gained tremendous importance in industrial applications due to their great advantages as low energy consumption, usually mild working conditions, easy to scale up and possibility to combine with other processes, and working in continuous mode. Many membrane separation techniques have been developed and among them; microfiltration, ultrafiltration, nanofiltration, reverse osmosis, membrane distillation, electrodialysis, membrane electrolysis, membrane gas separation, pervaporation or membrane contactors can be found. Different biomolecules, enzymes, ion channels or even cells, have been immobilized on membranes, whether ceramic or polymeric.

1.2.3.1. Polysaccharides

Polysaccharides are complex carbohydrates which are formed from at least two monosaccharides linked by a glycosidic bond. In living organisms they serve as energy storage and apart of that they possess building functions. They are widespread and easy to obtain from natural sources. They can be long-chain or short chain, soluble or insoluble in water and exhibit different functionalities. The most important in terms of their use for the synthesis of bioconjugates is their non-toxicity, and additionally they are completely environmentally safe.

Polysaccharides have found application in affinity membranes fabrication [54, 55]. The filtration mechanism through those membranes consist in capturing adsorbates (depending on the case it might be, for example, viruses, endotoxins, bacterias or heavy metals) onto functionalized membrane surface, allowing the feed to freely pass through it. Even if rejected substance is smaller than the pores present in a membrane, due to big affinity to the “capturing” area, it will get adsorbed. For example, the surface of the pores might be functionalized with positively charged active groups and through electrostatic interaction negatively charged species from the feed will get absorbed [56] (Figure 1.5).

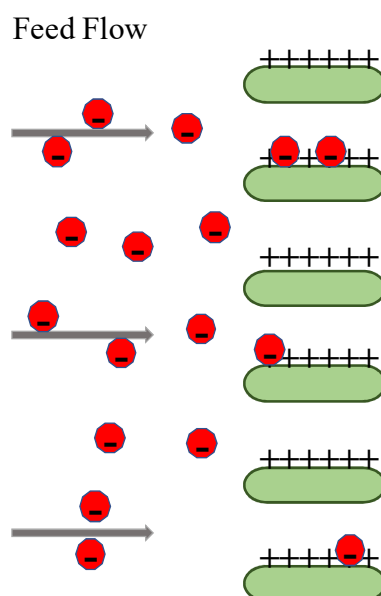


Figure 1.5. Scheme of affinity membrane separation mechanism.

This kind of membranes are characterized by low pressure drop resulting in low energy consumption, high efficiency, high fluxes with possibility to be easily regenerated. Various examples of the use of polysaccharide/polymer composites concern chitosan, which is a natural amino polymer extracted from chitin. Using its characteristic positive charge at low pH, it has found application in development of materials with big affinity to removal of species such as heavy metals which are negatively charged, such as nanofibers or membrane contactors (chitosan/carbon nanofibers/polyvinyl alcohol) reported by Prateek Khare et al.[57] or membranes (PET/chitosan membrane) described by Li [58]. One of the most interesting approaches of implementing this polysaccharide into artificial polymer is development of artificial liver studied among others by Teotia [59]. Authors have designed a system composed of polysulfone/tocopheryl polyethylene glycol succinate (Psf/TPGS) composite hollow fiber membrane, coated with chitosan. The coating procedure involved introducing negatively charged groups into the polymer composite (sulfonation) what afterwards facilitated electrostatic interaction with amine groups of chitosan. The surface after coating with polysaccharide exhibited good biocompatibility and supported growth of cells (HepG2 cell line) thus, it was able to mimic specific functions of liver. This particular achievement perfectly shows advantages of mechanical and chemical stability of synthetic Psf/TPGS membrane and biofunctionality of natural chitosan, what makes this polymer/polysaccharide conjugate a good material for artificial liver application.

1.2.3.2. Enzymes

Enzymes are proteins which function is assistance in catalytic reactions of biochemical processes. Their existence is crucial for all living organisms due to the fact, that most of the reactions do not occur spontaneously at normal temperature of the human body. The functionality of enzymes is related to their extremely high specificity, resulting from their particular geometric configuration, which allows to bind only those molecules which possess proper shape (key and lock mechanism). The catalytic activity of enzymes can be affected by different factors such as temperature, pH or concentration of the mixture (enzyme or substrate). They are also very sensitive to chemicals, which inhibits catalytic reactions in a reversible or irreversible way [60].

Thus, all those characteristics need to be taken into account during design of immobilization conditions and appropriate method selection.

High efficiency and selectivity of reactions performed with assistance of enzymes has always been an inspiration for the discoveries of novel bioreactors and biosensors. Recently the industrial competence in biocatalysis is achieved thanks to common use of lipases, esterase or peptidases [44, 47, 61-63]. Polymer/enzyme conjugates are reaching significance also in the field of water and soil decontamination. As a trend in green chemistry achievements, organophosphorus hydrolase was used [51, 52, 64]. This enzyme hydrolyzes organophosphorus (OP) compounds, which are present in soil as a result of being pesticides components. OP's are very toxic and can cause damage in central nervous system. An interesting approach, published by Xiao-Yu Yan and coworkers [65], implied the development of nanofibrous membrane containing OP hydrolase which fulfills both- filtration and degradation functions for biochemical protective applications. In this approach, hydrolase enzyme is immobilized covalently via glutaraldehyde coupling on polyamide nanofibers. This novel design of the material makes it potentially applicable in civilian and military protection equipment and clothier fabrication. Those clothes would be able to protect human body using double mechanisms: filtration of toxic products and as well converting it to nontoxic derivatives. This approach is schematically demonstrated in Figure 1.6.

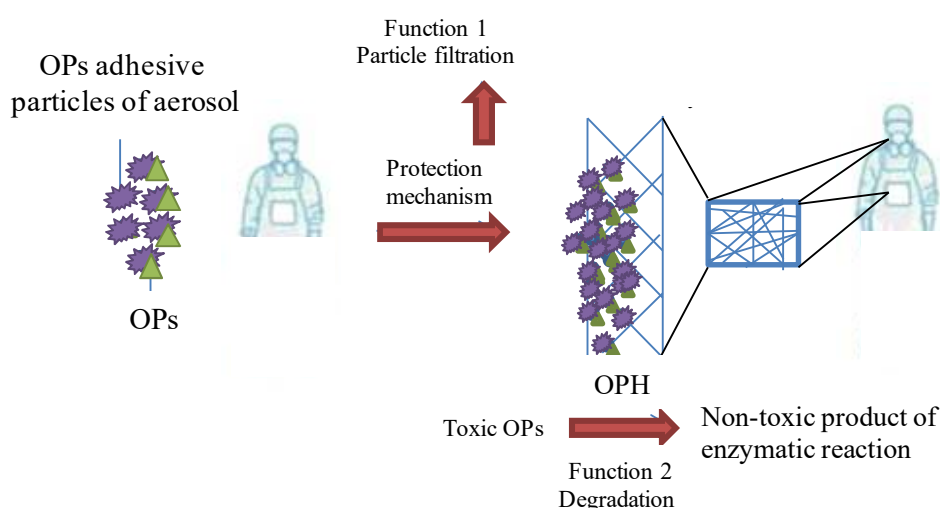


Figure 1.6. Schematic presentation of double mechanism of OP hydrolase-immobilized nanofibrous polymeric clothing.

Physical immobilization strategy was used to design a membrane which was able to immobilize up to three enzymes at the same time [66], which is presented schematically in Figure 1.7. This goal was reached by development of flat sheet polypropylene membrane coated with cellulose sublayer, and application of simple pressure driven filtration. Controlling of biofouling formation and driving it to form an enzyme cake layers, lead to obtain sheets which maintain activity of all three enzymes (formate dehydrogenase, formaldehyde dehydrogenase and alcohol dehydrogenase). This strategy provides a membrane which has excellent potential application in multienzymatic cascade reactions, in this particular case bioconversion of carbon dioxide into methanol. Among benefits coming from the strategy selected in this study it is necessary to highlight, that there is no need to use toxic and difficult to handle organic solvents which may influence enzyme bioactivity. Another interesting point found by authors of abovementioned work is simultaneous consideration of two immobilization mechanisms: physical immobilization on a surface by adsorption and physical entrapment of the biomolecule. Nevertheless, experimental results of CO_2 conversion proved that presented method still requires additional modifications and optimization.

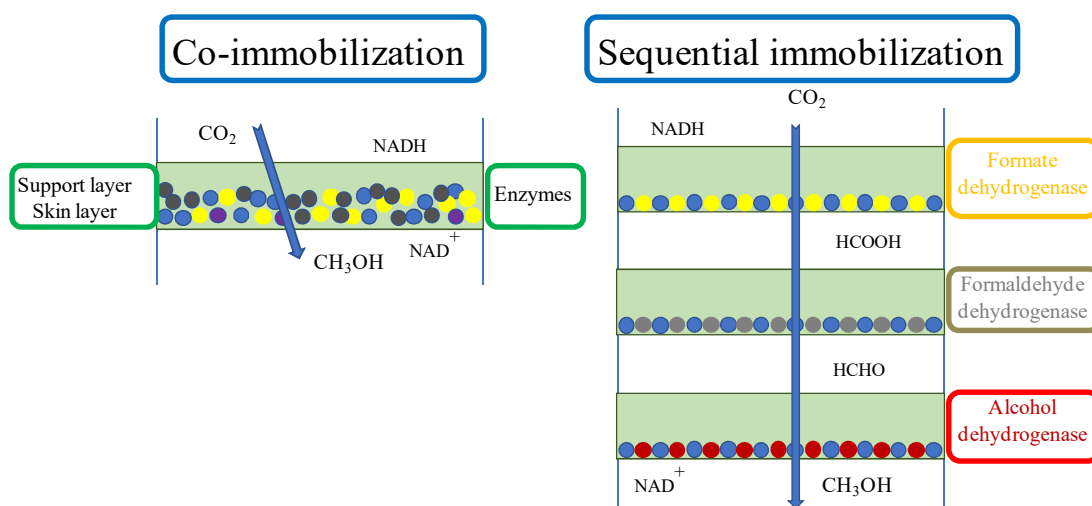


Figure 1.7. Scheme of the sequential enzyme immobilization and co-immobilization.

1.2.3.3. Ion channels

Another biocompounds widely used in development of bioartificial composites are ionic channels. Ion channels regulate the diffusion of ions across the biological membranes and thus, they are the proteins responsible for maintaining electrochemical balance between cell and its surrounding. Since cell membranes are electrical insulators, ionic channels work as a selective gate which opens allowing to pass some of the molecules into the cell and due to conformation change- closes preventing the passage of others [67]. Dependently of the type of factor which influences its “gating” motions, ion channels are classified into different groups.

One of the mechanisms allows the transport when ligand attached to the channel binds the ion what results in a conformational change, which allows it to pass through that formed door, in accordance to the concentration gradient. That type of receptor is called extracellular ligand gated ion channel and can be found in brain and muscles. Voltage-gated ion channels are activated by the change in membrane electrical potential. Those proteins are well known potassium and sodium pumps and also calcium and proton channels. When the signal influencing conformational change in the protein conformation comes from the interior of the cell, the protein is called intracellular ligand gated ion channel, which is e.g. cystic fibrosis transmembrane conductance regulator which is ATP-gating anionic channel. Complete understanding of all of this mechanisms leads to proper design of bioartificial conjugates with very specific functions and destiny. Ion channels have incredible importance in many biological processes that causes fast changes in cells, such as muscles contraction, selective transport of nutrients and ions or release of hormones. They work very specifically and its high selectivity is the result of responsive conformational changes which regulate the ionic transport [67]. Because of their extraordinary properties they have found a huge interest in development of new polymeric hybrid materials, mainly for biomedical and biosensing applications. Because functionality of ionic channels is related to the transportation, their properties are commonly applied in **biomimetic membrane technology**. To incorporate this biocompound into artificial polymeric matrix while maintaining its correct functionality and not affect the conformation it is necessary to imitate its natural environment, as much similar to the cell membrane as possible. To

achieve this, scientists tended to synthesize materials able to mimic conditions which are present in lipid bilayer. The most important criterion was obtaining materials with high thermal and chemical long-term stability, mechanical robustness but simultaneously exhibiting specific flexibility which would assure a proper free space necessary to enable ionic channels conformational changes.

Biological channel based biomimetic filters have good potential in recently developing application in novel concept of membrane crystallization technique [68]. Crystallization is a separation technique commonly used in the chemical industry and its crucial parameter is the ability to obtain crystals with desired, strict characteristics. However, conventional methods assimilate many handicaps which hamper reaching this goal. Incorrect agitation and non-homogenous solvent-non solvent distribution in traditional evaporators result in poor crystals reproducibility and thus, low efficiency of the process. Besides, high energy consumption related to this technology drives for looking for alternative solutions. Membrane crystallization technology is definitely more economic approach. It applies membrane technology to control grow of the crystals gradually from unsaturated solution. Aquaporin biomimetic membrane found an application in this technology [69]. Significantly enhanced water passage through the protein channels incorporated in the commercial polymeric membrane (AIM60 FO membrane from Aquaporin InsideTM) constitute an interesting alternative for use in sodium carbonate crystallization systems in carbon dioxide capturing purpose.

Apart of that, ion channels are perfect candidates to be used in applications related to ion exchange membranes and technologies such as fuel cells or energy conversion systems. In the literature, various examples of new polymers and copolymers with incorporated biological channels can be found [70]. Again, aquaporins attract the interest of researchers due to its improving water flux properties [71]. This membrane water channel is bidirectional, what means that it regulates flow of water which enters and goes out of the cell. Aquaporin structure consist in four monomers assembled in a way that the channel is narrow in the middle and wider at the ends, what allows passage of water molecule chain, but causes rejection of bigger solutes. Moreover, an internal local electrostatic field acts in a way that push the passing water molecules to rotate, what enhances transport. These extraordinary properties depict aquaporin channels as an excellent candidate to be used for increasing water passage in water treatment membranes. Since aquaporin works in two directions, its orientation in a membrane film

is not crucial for the membrane performance. This convenience allows applying various techniques for its immobilization such as: layer-by-layer immobilization [72], active layer formation [73, 74] or covalent bonding to lipid bilayer [75]. Improvement in gradient driven diffusion of water through the membrane containing ion channel have been discussed wider in recent reviews, considering various designs [76, 77]. Since incorporation of aquaporin aims mainly to increase water flow, random organization of channels does not affect reaching the goal.

However, to achieve selective ion transport, immobilization of channels requires the highest possible organization of biomolecule. But still, it is difficult to maintain high specificity of confined ionic gates, due to often difficulties in controlling immobilization process, which may affect conformation of the proteins. This challenge is continuously a main problem present in current investigations, in which researchers face difficulties in assembling ion channels in a desired orientation along the membrane. A study of well controlled immobilization of biological channels and their confinement in a precisely shaped and sized nanopores of polymers like polycarbonate (PC) and polyethylene terephthalate (PET) were performed by Balme et al [78-80]. The authors studied controlled incorporation of avidin, streptavidin, amphotericin B in a track etched membranes and also have successfully incorporated Gramicidin ion channel into nanopore, improving both flux and selectivity of membranes. Gramicidin was also reported as biomolecule used for enhancement of reverse osmosis desalination [81].

1.3. Design of bioartificial proton exchange membrane

Based on a literature review and state of the art in bioartificial membrane technology, a novel system based on its future applicability as a proton exchange membrane, has been designed. The goal was to obtain a membrane with connect the robustness and stability of a synthetic polymer with high ion transport speed and selectivity of a biomolecule. This strategy could deliver a membrane material, with desirable outstanding stability in both dry and hydrated state and very high ion conductivity and selectivity. Moreover, used components are available and membranes are easy to prepare, no dangerous procedures are employed and process is easy to scale up. Since

the protein immobilization is a challenging task, a polymer which has proven compatibility with biological materials has been chosen. Polysulfone, which is a thermoplastic polymer is widely used for the production of membranes for ultrafiltration or gas separation. The presence of diphenylene sulfone group in the subunit of this polymer, ensures its high mechanical stability and applicability in a broad range of pH conditions. It is also resistant to many oxidating agents, acids and alkali, what made it an extensively used material in the field of membrane technology [82, 83]. Ether linkage is responsible for the flexibility in the chain (Figure 1.8.). Thanks to its thermoplasticity it is easy formed in various shapes, thus, it is used for production of both, flat sheet and tubular membranes.

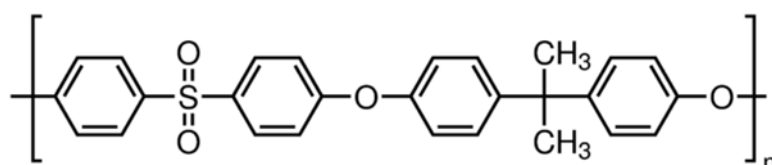


Figure 1.8. Polysulfone structure.

Hydrophobicity of polysulfone is often considered to be a disadvantage in terms of its application in water treatment industry, and many treatment methods aiming to increase its wetting properties have been developed [82, 84, 85]. However, designing a bioartificial hybrid membrane with polysulfone as a base material with hydrophobic nature is advantageous since it may benefit the resulting interactions between the polymer and immobilized biomolecule. Gramicidin, a pentadecapeptide produced by soil bacteria *Bacillus brevis* has been selected as the biomolecule. It is a natural cell membrane ion channel which is characterized by selective transport of monopositively charged cations over divalent ones. In solution, Gramicidin can adopt whether active channel form (the single stranded helical dimer [86]), or non-channel structure (the double stranded intertwined helix [87]). When properly conformed, Gramicidin in biological membranes can reach the proton transport velocity of 2×10^9 (H^+) s^{-1} [88], which is the fastest transport occurring in the ion channels. Moreover, Gramicidin is an antibiotic, active against gram-positive bacteria. It is composed exclusively from hydrophobic aminoacids, and can contain in its structure up to 4 tryptophan residues (Figure 1.9.), what suggests good affinity to polysulfone.

Mechanical stability and chemical resistance are key factors for the materials used as an ion-exchangers. Those properties allow non-disturbed, continuous process and long life-time of membranes. Together with high ion speed and selectivity of exchanger, those materials can provide highly efficient energy production process, desirable in fuel cells industry. This goal can be achieved by combination of outstanding resistance of polysulfone and excellent selectivity of Gramicidin.

Chapter I | **General introduction**

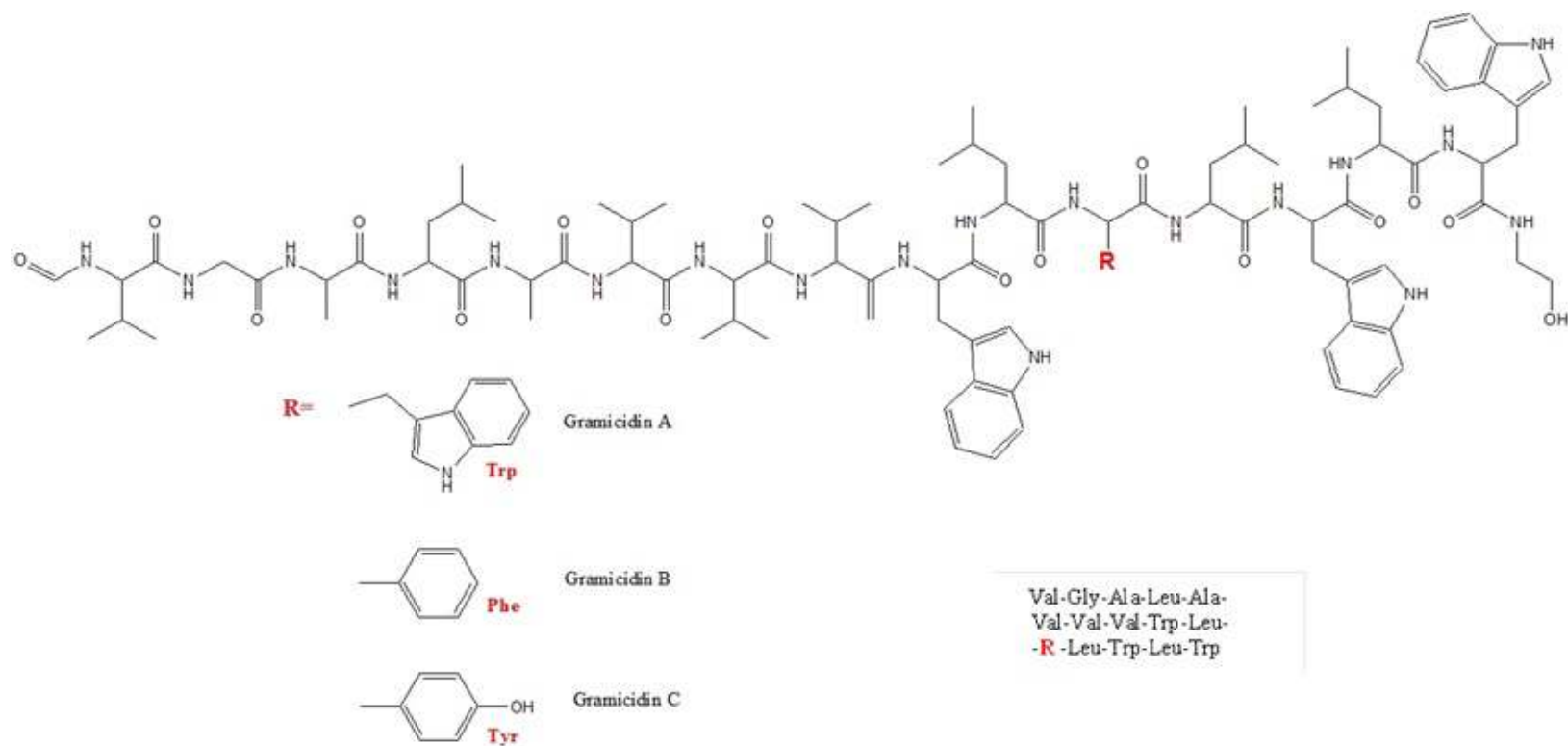


Figure 1.9. Structure of Gramicidin.

1.4. References

- [1] New Energy Outlook 2017, in, Bloomberg New Energy Finance, 2017.
- [2] O.Z. Sharaf, M.F. Orhan, An overview of fuel cell technology: Fundamentals and applications, *Renewable and Sustainable Energy Reviews*, 32 (2014) 810-853.
- [3] U. Lucia, Overview on fuel cells, *Renewable and Sustainable Energy Reviews*, 30 (2014) 164-169.
- [4] T. Sutharssan, D. Montalvao, Y.K. Chen, W.-C. Wang, C. Pisac, H. Elemara, A review on prognostics and health monitoring of proton exchange membrane fuel cell, *Renewable and Sustainable Energy Reviews*, 75 (2017) 440-450.
- [5] S.J. Peighambardoust, S. Rowshanzamir, M. Amjadi, Review of the proton exchange membranes for fuel cell applications, *International Journal of Hydrogen Energy*, 35 (2010) 9349-9384.
- [6] B. Paul, J. Andrews, PEM unitised reversible/regenerative hydrogen fuel cell systems: State of the art and technical challenges, *Renewable and Sustainable Energy Reviews*, 79 (2017) 585-599.
- [7] A. Jacques Roziere, J.J. Deborah, Non-Fluorinated Polymer Materials for Proton Exchange Membrane Fuel Cells, *Annual Review of Materials Research*, 33 (2003) 503-555.
- [8] S.J. Peighambardoust, S. Rowshanzamir, M. Amjadi, Review of the proton exchange membranes for fuel cell applications, *International Journal of Hydrogen Energy*, 35 (2010) 9349-9384.
- [9] L. Luis C. Pérez, José M.Sousa, Adélio Mendes, Segmented polymer electrolyte membrane fuel cells-A review, *Renewable and Sustainable Energy Reviews*, 15 (2011) 169-185.
- [10] H. Pu, D. Wang, Studies on proton conductivity of polyimide/H₃PO₄/imidazole blends, *Electrochimica acta*, 51 (2006) 5612-5617.
- [11] L.C. Jang Wonbong, Sundar Saimani, Shul Yong Gun, Han Haksoo, Thermal and hydrolytic stability of sulfonated polyimide membranes with varying chemical structure, *Polymer degradation and stability*, 90 (2005) 431-440.

- [12] P. Guo Qunhui, Tang Hao, O'Connor Sally, Sulfonated and crosslinked polyphosphazene-based proton-exchange membranes, *Journal of membrane science*, 154 (1999) 175-181.
- [13] H.R. Allcock, R.M. Wood, Design and synthesis of ion-conductive polyphosphazenes for fuel cell applications, *Journal of Polymer Science Part B: Polymer Physics*, 44 (2006) 2358-2368.
- [14] K.A. Bogdanowicz, *Liquid Crystalline Polymers for Smart Applications*, in: *Chemical Engineering, Universitat Rovira i Virgili, Doctoral Thesis*, Tarragona, 2015.
- [15] K.A. Bogdanowicz, Y. Li, I.F.J. Vankelecom, R. Garcia-Valls, J.A. Reina, M. Giamberini, Mimicking nature: Biomimetic ionic channels, *Journal of membrane science*, 509 (2016) 10-18.
- [16] K.A. Bogdanowicz, G.A. Rapsilber, A.J. Reina, M. Giamberini, Liquid crystalline polymeric wires for selective proton transport, part 1: Wires preparation, *Polymer*, 92 (2016) 50-57.
- [17] K.A. Bogdanowicz, P. Sistat, J.A. Reina, M. Giamberini, Liquid crystalline polymeric wires for selective proton transport, part 2: Ion transport in solid-state, *Polymer*, 92 (2016) 58-65.
- [18] X. Montané, A.J. Reina, M. Giamberini, Columnar liquid crystalline polyglycidol derivatives: A novel alternative for proton-conducting membranes, *Polymer*, 66 (2015) 100-109.
- [19] G. Alberti, M. Casciola, Composite membranes for medium-temperature PEM fuel cells, *Annual Review of Materials Research*, 33 (2003) 129-154.
- [20] W. Jia, B. Tang, P. Wu, Novel Composite PEM with Long-Range Ionic Nanochannels Induced by Carbon Nanotube/Graphene Oxide Nanoribbon Composites, *ACS Applied Materials & Interfaces*, 8 (2017) 28955-28963.
- [21] S.M.J. Zaidi, S.D. Mikhailenko, G.P. Robertson, M.D. Guiver, S. Kaliaguine, Proton conducting composite membranes from polyether ether ketone and heteropolyacids for fuel cell applications, *Journal of membrane science*, 173 (2000) 17-34.
- [22] E. Bakangura, L. Wu, L. Ge, Z. Yang, T. Xu, Mixed matrix proton exchange membranes for fuel cells: State of the art and perspectives, *Progress in Polymer Science*, 57 (2016) 103-152.

- [23] Y.-H. Su, Y.-L. Liu, Y.-M. Sun, J.-Y. Lai, D.-M. Wang, Y. Gao, B. Liu, M.D. Guiver, Proton exchange membranes modified with sulfonated silica nanoparticles for direct methanol fuel cells, *Journal of membrane science*, 296 (2007) 21-28.
- [24] S. Elakkiya, G. Arthanareeswaran, A.F. Ismail, D.B. Das, Functionalization and surface modification of TiO₂ nanoparticles for proton exchange membrane fuel cell, *International Journal of Hydrogen Energy* (2017).
- [25] K. Li, G. Ye, J. Pan, H. Zhang, M. Pan, Self-assembled Nafion/metal oxide nanoparticles hybrid proton exchange membranes, *Journal of membrane science*, 347 26-31.
- [26] J. Won, S.W. Choi, Y.S. Kang, H.Y. Ha, I.-H. Oh, H.S. Kim, K.T. Kim, W.H. Jo, Structural characterization and surface modification of sulfonated polystyrene-(ethylene-butylene)-styrene triblock proton exchange membranes, *Journal of membrane science*, 214 (2003) 245-257.
- [27] R. Yoshida, Self-oscillating polymer gels as novel biomimetic materials, in: T.D. Ngo (Ed.) *Biomimetic Technologies: Principles and Applications*, Woodhead Publishing, 2015, pp. 181-198.
- [28] R. Breslow, *Artificial Enzymes*, in, Wiley-VCH Verlag, 2005.
- [29] Z.Y. Qigang Wang, Xieqiu Zhang, Xudong Xiao, Chi K. Chang, Bing Xu, A Supramolecular-Hydrogel-Encapsulated Hemin as an Artificial Enzyme to Mimic Peroxidase, *Angewandte Chemie International Edition*, 46 (2007) 4285-4289.
- [30] W. Hu, S. Chen, Z. Yang, L. Liu, H. Wang, Flexible Electrically Conductive Nanocomposite Membrane Based on Bacterial Cellulose and Polyaniline, *The Journal of Physical Chemistry B*, 115 (2011) 8453-8457.
- [31] Y. Gu, X. Yan, C. Li, B. Zheng, Y. Li, W. Liu, Z. Zhang, M. Yang, Biomimetic sensor based on molecularly imprinted polymer with nitroreductase-like activity for metronidazole detection, *Biosensors and Bioelectronics*, 77 (2016) 393-399.
- [32] M.F. Dudley, Process for the preparation of synthetic rubber latex, in, *Google Patents*, 1966.
- [33] C.F. Fryling, Production of adhesives and adhesive bases from synthetic rubber latex by causing phase inversion with a protective colloid and adding organic solvent, in, *Google Patents*, 1956.
- [34] M.F. C, T. Zbikowski, Hair darts for implanting in live or artificial media, in, *Google Patents*, 1961.

- [35] M. Okazaki, M. Sone, Y. Ueyama, Synthetic fibers for artificial hair and production thereof, in, Google Patents, 1974.
- [36] G.T. Rodeheaver, J.G. Thacker, R.F. Edlich, Mechanical performance of polyglycolic acid and polyglactin 910 synthetic absorbable sutures, *Surg Gynecol Obstet*, 153 (1981) 835-841.
- [37] F. Mohammad, Specialty Polymers Materials and Applications, in, I. K. International Publishing House Pvt. Ltd., New Delhi, 2007.
- [38] L.S. Yu, B. Yuan, D. Bishop, S. Topaz, J. van Griensven, S. Hofma, P. Swier, J. Klinkmann, J. Kolff, W.J. Kolff, New polyurethane valves in new soft artificial hearts, *ASAIO Trans*, 35 (1989) 301-304.
- [39] A.D.V. K. P. Khomyakov, Z. Z. Rogovin, The prolongation of the action of pharmaceutical preparations by mixing or combining them with polymers, *Russ Chem Rev*, 33 (1964) 462-647.
- [40] J.J. Brady Dean, Advances in enzyme immobilization, *Biotechnol Lett* (2009) 1639–1650.
- [41] J.U. Bowie, Solving the membrane protein folding problem, *Nature*, 438 (2005) 581-589.
- [42] A. Jungbauer, W. Kaar, Current status of technical protein refolding, *Journal of Biotechnology*, 128 (2007) 587-596.
- [43] F.W. Ying LU, Method for preparing S-ibuprofen and S-ibuprofen ester by biological catalysis, in, Google Patents, 2008.
- [44] V.C. Gekas, Artificial membranes as carriers for the immobilization of biocatalysts *Enzyme Microb. Teehnol.* , 8 (1986) 450-460.
- [45] P.G. Wagh Priyesh, Viola Ronald E., Escobar Isabel C., A new technique to fabricate high-performance biologically inspired membranes for water treatment, *Separation and Purification Technology*, 156 (2015) 754-765.
- [46] T. Hideo Hirohara Shigeyasu Nabeshima; Masanori Fujimoto; Tsuneyuki Nagase, Enzyme immobilization with pullan gel, in, Sumitomo Chemical Company, Limited, Osaka, Japan, 1981.
- [47] S.S. Sekhon, J.-M. Park, J.-Y. Ahn, T.S. Park, S.-D. Kwon, Y.-C. Kim, J. Min, Y.-H. Kim, Immobilization of para-nitrobenzyl esterase-CLEA on electrospun polymer nanofibers for potential use in the synthesis of cephalosporin-derived antibiotics, *Molecular & Cellular Toxicology*, 10 (2014) 215-221.

- [48] M.M.M. Elnashar, The Art of Immobilization Using Biopolymers, Biomaterials and Nanobiotechnology, in: P.M. Elnashar (Ed.) Biotechnology of Biopolymers, InTech Europe, 2011.
- [49] M.D. Trevan, Enzyme Immobilization by Covalent Bonding, in: J.M. Walker (Ed.) New Protein Techniques, Humana Press, Totowa, NJ, 1988, pp. 495-510.
- [50] A.B. Okhamafe A., Chu W, Goosen M., Modulation of protein release from chitosan-alginate microcapsules using the pH-sensitive polymer hydroxypropyl methylcellulose acetate succinate, *J Microencapsul.*, 13 (1996) 497-508.
- [51] I. Gill, A. Ballesteros, Bioencapsulation within synthetic polymers (Part 2): non-sol-gel protein-polymer biocomposites, *Trends in Biotechnology*, 18 (2000) 469-479.
- [52] P.-S.B. Sassolas A., Marty J., Biosensors for pesticide detection: New Trends, *American Journal of Analytical Chemistry*, 3 (2012) 210-232.
- [53] K. Min, Y.J. Yoo, Recent progress in nanobiocatalysis for enzyme immobilization and its application, *Biotechnology and Bioprocess Engineering*, 19 (2014) 553-567.
- [54] M. Webster, J. Miao, B. Lynch, D.S. Green, R. Jones-Sawyer, R.J. Linhardt, J. Mendenhall, Tunable Thermo-Responsive Poly(N-vinylcaprolactam) Cellulose Nanofibers: Synthesis, Characterization, and Fabrication, *Macromolecular Materials and Engineering*, 298 (2013) 447-453.
- [55] T. Barroso, M. Temtem, A. Hussain, A. Aguiar-Ricardo, A.C.A. Roque, Preparation and characterization of a cellulose affinity membrane for human immunoglobulin G (IgG) purification, *Journal of Membrane Science*, 348 (2010) 224-230.
- [56] C.C. Angelo Basile, *Integrated Membrane Systems and Processes*, in: Wiley, 2016.
- [57] P. Khare, A. Yadav, J. Ramkumar, N. Verma, Microchannel-embedded metal-carbon-polymer nanocomposite as a novel support for chitosan for efficient removal of hexavalent chromium from water under dynamic conditions, *Chemical Engineering Journal*, 293 (2016) 44-54.
- [58] L. Li, Y. Li, C. Yang, Chemical filtration of Cr (VI) with electrospun chitosan nanofiber membranes, *Carbohydrate Polymers*, 140 (2016) 299-307.
- [59] R.S. Teotia, D. Kalita, A.K. Singh, S.K. Verma, S.S. Kadam, J.R. Bellare, Bifunctional Polysulfone-Chitosan Composite Hollow Fiber Membrane for Bioartificial Liver, *ACS Biomaterials Science & Engineering*, 1 (2015) 372-381.

- [60] T.K. Harris, M.M. Keshwani, Chapter 7 Measurement of Enzyme Activity, in: R.B. Richard, P.D. Murray (Eds.) *Methods in Enzymology*, Academic Press, 2009, pp. 57-71.
- [61] T. Gitlesen, M. Bauer, P. Adlercreutz, Adsorption of lipase on polypropylene powder, *Biochimica et Biophysica Acta (BBA) - Lipids and Lipid Metabolism*, 1345 (1997) 188-196.
- [62] R. Singh, M. Tiwari, R. Singh, J.-K. Lee, From Protein Engineering to Immobilization: Promising Strategies for the Upgrade of Industrial Enzymes, *International Journal of Molecular Sciences*, 14 (2013) 1232.
- [63] S.-F. Li, Y.-H. Fan, J.-F. Hu, Y.-S. Huang, W.-T. Wu, Immobilization of *Pseudomonas cepacia* lipase onto the electrospun PAN nanofibrous membranes for transesterification reaction, *Journal of Molecular Catalysis B: Enzymatic*, 73 (2011) 98-103.
- [64] M. Kim, M. Gkikas, A. Huang, J.W. Kang, N. Suthiwangcharoen, R. Nagarajan, B.D. Olsen, Enhanced activity and stability of organophosphorus hydrolase via interaction with an amphiphilic polymer, *Chemical Communications*, 50 (2014) 5345-5348.
- [65] X.-Y. Yan, Y.-J. Jiang, S.-P. Zhang, J. Gao, Y.-F. Zhang, Dual-functional OPH-immobilized polyamide nanofibrous membrane for effective organophosphorus toxic agents protection, *Biochemical Engineering Journal*, 98 (2015) 47-55.
- [66] J. Luo, A.S. Meyer, R.V. Mateiu, M. Pinelo, Cascade catalysis in membranes with enzyme immobilization for multi-enzymatic conversion of CO₂ to methanol, *New Biotechnology*, 32 (2015) 319-327.
- [67] D. J. Aidley, *Ion channels: molecules in action*, in, Cambridge University Press, Cambridge, 1996.
- [68] E. Drioli, G. Di Profio, E. Curcio, Progress in membrane crystallization, *Current Opinion in Chemical Engineering*, 1 (2012) 178-182.
- [69] W. Ye, J. Lin, H. Tækker Madsen, E. Gydesen Søgaard, C. Hélix-Nielsen, P. Luis, B. Van der Bruggen, Enhanced performance of a biomimetic membrane for Na₂CO₃ crystallization in the scenario of CO₂ capture, *Journal of Membrane Science*, 498 (2016) 75-85.
- [70] Z. Zhang, X.Y. Kong, K. Xiao, G. Xie, Q. Liu, Y. Tian, H. Zhang, J. Ma, L. Wen, L. Jiang, A Bioinspired Multifunctional Heterogeneous Membrane with Ultrahigh Ionic

Rectification and Highly Efficient Selective Ionic Gating, *Advanced materials*, 28 (2016) 144-150.

[71] P. Agre, D. Kozono, Aquaporin water channels: molecular mechanisms for human diseases, *FEBS Lett*, 555 (2003) 72-78.

[72] M. Wang, Z. Wang, X. Wang, S. Wang, W. Ding, C. Gao, Layer-by-Layer Assembly of Aquaporin Z-Incorporated Biomimetic Membranes for Water Purification, *Environmental Science & Technology*, 49 (2015) 3761-3768.

[73] P. Wagh, G. Parungao, R.E. Viola, I.C. Escobar, A new technique to fabricate high-performance biologically inspired membranes for water treatment, *Separation and Purification Technology*, 156 (2015) 754-765.

[74] W. Xie, F. He, B. Wang, T.-S. Chung, K. Jeyaseelan, A. Armugam, Y.W. Tong, An aquaporin-based vesicle-embedded polymeric membrane for low energy water filtration, *Journal of Materials Chemistry A*, 1 (2013) 7592-7600.

[75] W. Ding, J. Cai, Z. Yu, Q. Wang, Z. Xu, Z. Wang, C. Gao, Fabrication of an aquaporin-based forward osmosis membrane through covalent bonding of a lipid bilayer to a microporous support, *Journal of Materials Chemistry A*, 3 (2015) 20118-20126.

[76] C.Y. Tang, Y. Zhao, R. Wang, C. Hélix-Nielsen, A.G. Fane, Desalination by biomimetic aquaporin membranes: Review of status and prospects, *Desalination*, 308 (2013) 34-40.

[77] J. Habel, M. Hansen, S. Kynde, N. Larsen, S. Midtgaard, G. Jensen, J. Bomholt, A. Ogbonna, K. Almdal, A. Schulz, C. Hélix-Nielsen, Aquaporin-Based Biomimetic Polymeric Membranes: Approaches and Challenges, *Membranes*, 5 (2015) 307.

[78] S. Balme, F. Picaud, S. Kraszewski, P. Dejardin, J.M. Janot, M. Lepoitevin, J. Capomanes, C. Ramseyer, F. Henn, Controlling potassium selectivity and proton blocking in a hybrid biological/solid-state polymer nanoporous membrane, *Nanoscale*, 5 (2013) 3961-3968.

[79] S. Balme, J.-M. Janot, L. Berardo, F. Henn, D. Bonhenry, S. Kraszewski, F. Picaud, C. Ramseyer, New Bioinspired Membrane Made of a Biological Ion Channel Confined into the Cylindrical Nanopore of a Solid-State Polymer, *Nano letters*, 11 (2011) 712-716.

[80] D. Bonhenry, S. Kraszewski, F. Picaud, C. Ramseyer, S. Balme, J.M. Janot, F. Henn, Stability of the gramicidin-A channel structure in view of nanofiltration: a computational and experimental study, *Soft Matter*, 7 (2011) 10651-10659.

- [81] D. Saeki, T. Yamashita, A. Fujii, H. Matsuyama, Reverse osmosis membranes based on a supported lipid bilayer with gramicidin A water channels, *Desalination*, 375 (2015) 48-53.
- [82] Z. Zhang, Q. An, T. Liu, Y. Zhou, J. Qian, C. Gao, Fabrication of polysulfone ultrafiltration membranes of a density gradient cross section with good anti-pressure stability and relatively high water flux, *Desalination*, 269 239-248.
- [83] J.J. Min-suk, J. Parrondo, C.G. Arges, V. Ramani, Polysulfone-based anion exchange membranes demonstrate excellent chemical stability and performance for the all-vanadium redox flow battery, *Journal of Materials Chemistry A*, 1 (2013) 10458-10464.
- [84] M.L. Steen, L. Hymas, E.D. Havey, N.E. Capps, D.G. Castner, E.R. Fisher, Low temperature plasma treatment of asymmetric polysulfone membranes for permanent hydrophilic surface modification, *Journal of membrane science*, 188 (2001) 97-114.
- [85] A. Nabe, E. Staude, G. Belfort, Surface modification of polysulfone ultrafiltration membranes and fouling by BSA solutions, *Journal of membrane science*, 133 (1997) 57-72.
- [86] D.W. Urry, The Gramicidin A Transmembrane Channel: A Proposed $\pi(L,D)$ Helix, *Proceedings of the National Academy of Sciences*, 68 (1971) 672-676.
- [87] W.R. Veatch, E.T. Fossel, E.R. Blout, Conformation of gramicidin A, *Biochemistry*, 13 (1974) 5249-5256.
- [88] S. Cukierman, E.P. Quigley, D.S. Crumrine, Proton conduction in gramicidin A and in its dioxolane-linked dimer in different lipid bilayers, *Biophysical Journal*, 73 (1997) 2489-2502.

Chapter II

Theoretical background

2.1. Introduction

In this chapter, the fundamentals of transport occurring in Proton Exchange Membranes and possible proton transport mechanisms will be described. Also, the methods used for general characterization of ion transporting membranes, the information that they deliver and their importance for the application is summarized.

2.2. Transport in Proton Exchange Membrane

When considering proton exchange membrane evaluation, the first characteristic to take into account is its transport properties. In general, in proton exchange membranes, transport consists of proton and water passage [1, 2]. Proton transport is usually related to two different mechanisms: hopping or diffusion mechanism. Usually a combination of both of them is encountered. Hopping mechanism (or structural diffusion mechanism) consists of proton “jumps” from one hydrolysed ionic site to another within the polymer. Afterwards, produced proton is associated to form a water molecule. A schematic visualization of hopping mechanism occurring in sulfonated polymers (Nafion) is presented in Figure 2.1.

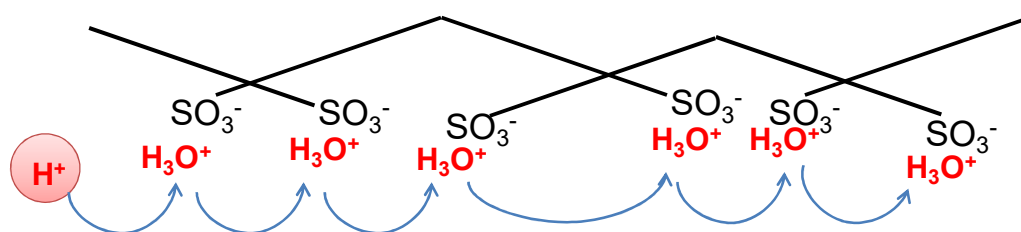


Figure 2.1. Schematic representation of hopping mechanism through the sulfonic groups of sulfonated polymer.

Another mechanism consist of diffusion of hydrated proton (H_3O^+) across the membrane as an effect of electrochemical gradient difference. This type of mechanism is possible only if membrane forming polymer chain has enough of free volume for

allowing to carry one or more water molecule together with the proton. A visualization of diffusion mechanism is represented on Figure 2.2.

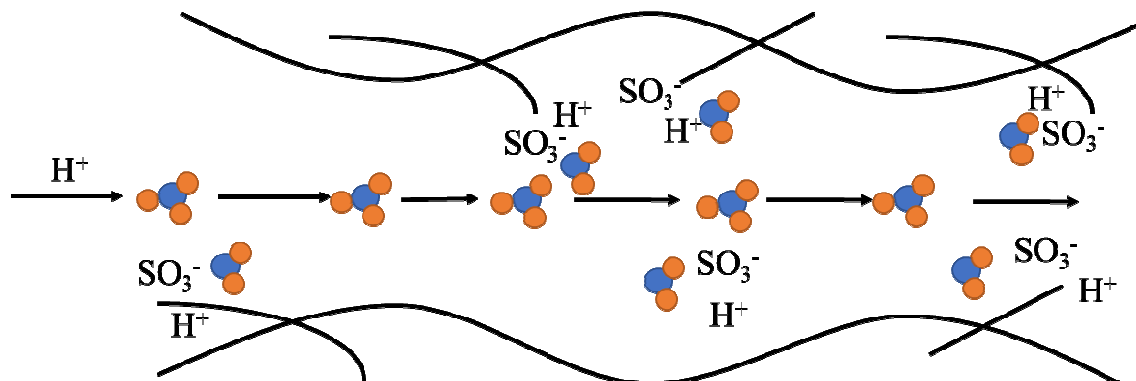


Figure 2.2. Schematic design of diffusion mechanism as proton conduction.

Regarding water, several mass transport phenomena occurs: electro-osmotic drag refers to the amount of water molecules which are transported together with proton to the cathode during electrochemical reaction; back diffusion (is the same phenomena taking place in opposite direction); less significant, although still present are pressure driven hydraulic water permeation and thermal-osmotic drag, an effect of the water movement as consequence of temperature increase [3].

2.3. Proton Exchange Membranes characterization methods

Characterization of membranes in order to understand both types of migration have been extensively discussed in the literature. However, it is considered that in order to deliver complete information about transport characteristics of the electrolyte it is necessary to determine its diffusion properties, electrical conductivity and transference number [4]. Diffusion transport refers to free movement of species across the membrane in the direction from high to low concentration. It is related to the hydration grade of the membrane and it is important in the evaluation of membrane applicability in a real system, since it is the measure of the efficiency of one of the general transport mechanisms (vehicular mechanism) [2]. To numerically express the diffusion transport

through the membrane, we can use permeability, which is correlated with diffusion coefficient according to the Fick's law, what will be further discussed in Chapter III, section 3.4.1.4.1 [5, 6].

Some researchers studied also the self-diffusion transport phenomena inside the membrane films, using Pulsed field gradient spin-echo ^1H NMR [7, 8]. This method not only delivers useful information about the solution interaction within the solid electrolyte but also, when applying Nernst-Planck or Nernst-Einstein relation [9], can be used to estimate electrical conductivity, what is less time consuming and still can deliver reliable data.

Conductivity refers to the membrane ability to transport ions when a potential is applied and is an actual ion transport value and a quantitative description of membrane performance [9, 10]. This is the most important characteristics of the PEM and it is evaluated for the membranes as well as for the stack of membrane assemblies (MEAs) [4, 11, 12]. In the case of proton exchange membranes, the most commonly used techniques for experimental characterization of conductivity are AC impedance spectroscopy [13, 14] and Current-Voltage measurements [15]. Electrochemical impedance spectroscopy (EIS) is a technique used also in modelling fuel cells with electrical circuits and can detect malfunctions and low membrane performance. Nevertheless, it requires selection of appropriate electrochemical model for correct data interpretation, what often causes difficulties in results analysis. Current-Voltage measurements also deliver information about ion transport through the membrane and conductivity can be calculated from the obtained membrane resistivity value.

In the absence of concentration gradient, the transference number is the fraction of the total electrical current present in the electrolyte solution which is carried by a particular ion [4]. This property is used to obtain information about the current density that can be produced by a fuel cell. Ideally, for good membrane performance the transference number of unity is desired [16]. Since direct determination of transport number is very delicate procedure, recently many models for transport number estimation have been developed [17]. Experimental determination consist of using potentiostatic methods such as cyclic voltammetry, applying different electrolyte

concentrations or; with the use of electrophoretic nuclear magnetic resonance [10, 18, 19].

Nevertheless, in order to have a complete data set of transport properties additional characterization of the membranes needs to be performed. Since in low temperature proton exchange membrane, water plays a key role in ions movement, material interaction with water is a crucial parameter [3]. In general, membrane conductivity increases with the increasing water content. Thus, in order to evaluate swelling properties of material, water uptake measurements are commonly conducted [20, 21] and, together with contact angle measurements, complete information about membrane film wetting characteristics may be reached [22, 23]. Hydration level of polymer chain is determined using NMR techniques and it is important from the point of view of material design in order to ensure the highest water and ion diffusion [2]. Also, direct water flow through the membrane and PEMFC flow channels is measured in order to understand general water passage abilities through the membrane [24].

Another very important source of information needed to characterize any membrane material is the complete morphological analysis. Various methods are known for the determination of membrane porosity like capillary flow porosimetry or pore volume determination [25, 26]. Porosity can be directly related with water absorption capability. The higher porosity, the higher absorption is expected. For determination of pores structure and shape, commonly used techniques include microscopic analysis (SEM or ESEM). Besides, surface topography is investigated by Atomic Force Microscopy (AFM) and usually delivers valuable information about the membrane roughness before and after operation, determining its degradation level [27-29].

In term of applicability, long lifetime of the electrolyte membrane is a very important factor for high efficiency and good performance of PEMFC. Thus, stability of membrane is an internal component in development of PEMFC. Concerning thermal stability, analysis such as TGA or DSC are performed, in order to evaluate the maximum possible operation temperature of the membrane [30, 31]. Chemical stability can be investigated via various soaking experiments, whether in alkaline or acidic solution and at various temperatures [2, 32-34]. Such treated membranes are then evaluated in terms of morphology changes (AFM, CA), chemical structure (FTIR or

elemental analysis) or performance (Ion Exchange Capacity). Detailed mechanical characterization should include measurements of thickness and dimensional stability in water or fuel, tensile strength and observation of all dimensional changes after any of experiments or treatments [35]. Those data can provide information about possible membrane performance during long term operation and give an idea about the membrane lifetime.

Although there are more characterization methods which can be employed for PEM description, determination of membrane Ion Exchange Capacity (IEC) is the most relevant [36, 37]. This parameter has influence on almost all other properties, especially if we consider new synthesized polymer. IEC is defined as the number of fixed charges per unit weight of the polymer from which a membrane is made. The higher IEC value, the better the membrane is expected to conduct protons. Usually, it is determined by titration method. Nevertheless to obtain reliable data it is necessary that charges are homogeneously distributed within membrane polymer matrix.

The abovementioned methods serve to obtain valuable information about proton exchange performance in fuel cell applications. Developing novel material which can fulfil all the requirements is a hard task. The focus of this Ph.D. thesis has been to achieve most of the desired characteristics by applying the concept of bioartificial membrane fabrication.

2.4. References

- [1] S.J. Peighambardoust, S. Rowshanzamir, M. Amjadi, Review of the proton exchange membranes for fuel cell applications, *International Journal of Hydrogen Energy*, 35 (2010) 9349-9384.
- [2] Jacques Rozière, J.J. Deborah, Non-Fluorinated Polymer Materials for Proton Exchange Membrane Fuel Cells, *Annual Review of Materials Research*, 33 (2003) 503-555.
- [3] W. Dai, H. Wang, X.-Z. Yuan, J.J. Martin, D. Yang, J. Qiao, J. Ma, A review on water balance in the membrane electrode assembly of proton exchange membrane fuel cells, *International Journal of Hydrogen Energy*, 34 (2009) 9461-9478.
- [4] M. Chintapalli, K. Timachova, K.R. Olson, S.J. Mecham, D. Devaux, J.M. DeSimone, N.P. Balsara, Relationship between conductivity, ion diffusion, and transference number in perfluoropolyether electrolytes, *Macromolecules*, 49 (2016) 3508-3515.
- [5] A.C. West, T.F. Fuller, Influence of rib spacing in proton-exchange membrane electrode assemblies, *Journal of applied electrochemistry*, 26 (1996) 557-565.
- [6] K.A. Bogdanowicz, S.V. Bhosale, Y. Li, I.F.J. Vankelecom, R. Garcia-Valls, J.A. Reina, M. Giamberini, Mimicking nature: Biomimetic ionic channels, *Journal of membrane science*, 509 (2016) 10-18.
- [7] G. Suresh, Y.M. Scindia, A.K. Pandey, A. Goswami, Self-diffusion coefficient of water in Nafion-117 membrane with different monovalent counterions: a radiotracer study, *Journal of membrane science*, 250 (2005) 39-45.
- [8] A. Goswami, A. Acharya, A.K. Pandey, Study of self-diffusion of monovalent and divalent cations in Nafion-117 ion-exchange membrane, *The Journal of Physical Chemistry B*, 105 (2001) 9196-9201.
- [9] A. Shirdast, A. Sharif, M. Abdollahi, Prediction of proton conductivity of graphene oxide-containing polymeric membranes, *International Journal of Hydrogen Energy*, 39 (2014) 1760-1768.
- [10] P.G. Bruce, J. Evans, C.A. Vincent, Conductivity and transference number measurements on polymer electrolytes, *Solid State Ionics*, 28 (1988) 918-922.
- [11] Y.-H. Su, Y.-L. Liu, D.-M. Wang, J.-Y. Lai, M.D. Guiver, B. Liu, Increases in the proton conductivity and selectivity of proton exchange membranes for direct methanol

fuel cells by formation of nanocomposites having proton conducting channels, *Journal of Power Sources*, 194 (2009) 206-213.

[12] X. Ye, H. Bai, W.S.W. Ho, Synthesis and characterization of new sulfonated polyimides as proton-exchange membranes for fuel cells, *Journal of membrane science*, 279 (2006) 570-577.

[13] M.E. Orazem, Application of impedance spectroscopy to characterize polymer-electrolyte-membrane (PEM) fuel cells, *ECS Transactions*, 50 (2013) 247-260.

[14] C. Brunetto, A. Moschetto, G. Tina, PEM fuel cell testing by electrochemical impedance spectroscopy, *Electric Power Systems Research*, 79 (2009) 17-26.

[15] S. Gouws, Electrolysis, in: J.K. Vladimir Linkow (Ed.) *Voltammetric Characterization Methods for the PEM Evaluation of Catalysts*, InTech, 2012.

[16] M. Gasik, *Materials for Fuel Cells*, in, Woodhead Publishing Limited and CRC Press LLC, Boca Raton, Boston, New York, Washington, 2008.

[17] M. Watanabe, S. Nagano, K. Sanui, N. Ogata, Estimation of Li⁺ transport number in polymer electrolytes by the combination of complex impedance and potentiostatic polarization measurements, *Solid State Ionics*, 28 (1988) 911-917.

[18] J. Evans, C.A. Vincent, P.G. Bruce, Electrochemical measurement of transference numbers in polymer electrolytes, *Polymer*, 28 (1987) 2324-2328.

[19] H. Dai, T.A. Zawodzinski, Determination of lithium ion transference numbers by electrophoretic nuclear magnetic resonance, *Journal of The Electrochemical Society*, 143 (1996) L107-L109.

[20] V. Sproll, T.J. Schmidt, L. Gubler, Effect of glycidyl methacrylate (GMA) incorporation on water uptake and conductivity of proton exchange membranes, *Radiation Physics and Chemistry* (2018).

[21] J.-P. Melchior, G.n. Majer, K.-D. Kreuer, Why do proton conducting polybenzimidazole phosphoric acid membranes perform well in high-temperature PEM fuel cells?, *Physical Chemistry Chemical Physics*, 19 (2017) 601-612.

[22] R.P. Dowd, C.S. Day, T. Van Nguyen, Engineering the Ionic Polymer Phase Surface Properties of a PEM Fuel Cell Catalyst Layer, *Journal of The Electrochemical Society*, 164 (2017) F138-F146.

- [23] S. Rajendran, M.R. Prabhu, A Study of influence on sulfonated TiO₂-Poly (Vinylidene fluoride-co-hexafluoropropylene) nano composite membranes for PEM Fuel cell application, *Applied Surface Science*, 418 (2017) 64-71.
- [24] J.M. Sergi, Z. Lu, S.G. Kandlikar, In Situ Characterization of Two-Phase Flow in Cathode Channels of an Operating PEM Fuel Cell With Visual Access, (2009) 303-311 C301 - ASME 2009 2007th International Conference on Nanochannels, Microchannels and Minichannels.
- [25] M. Halisch, E. Vogt, C. Müller, D. Pattyn, P. Hellebaut, K. Van Der Kamp, Capillary Flow Porometry-Assessment Of An Alternative Method For The Determination Of Flow Relevant Parameters Of Porous Rocks (2013).
- [26] L.-Y. Yu, Z.-L. Xu, H.-M. Shen, H. Yang, Preparation and characterization of PVDF-SiO₂ composite hollow fiber UF membrane by sol-gel method, *Journal of membrane science*, 337 (2009) 257-265.
- [27] A. Lehmani, S. Durand-Vidal, P. Turq, Surface morphology of Nafion 117 membrane by tapping mode atomic force microscope, *Journal of applied polymer science*, 68 (1998) 503-508.
- [28] Z.Y. Zhai, Y.G. Shen, B. Jia, Y. Yin, Surface morphology studies on PBI membrane materials of high temperature for proton exchange membrane fuel cells, in: *Advanced Materials Research*, Trans Tech Publ, (2013) pp. 239-242.
- [29] M.A. Smit, A.L. Ocampo, M.A. Espinosa-Medina, P.J. Sebastian, A modified Nafion membrane with in situ polymerized polypyrrole for the direct methanol fuel cell, *Journal of Power Sources*, 124 (2003) 59-64.
- [30] D.H. Jung, S.Y. Cho, D.H. Peck, D.R. Shin, J.S. Kim, Performance evaluation of a Nafion/silicon oxide hybrid membrane for direct methanol fuel cell, *Journal of Power Sources*, 106 (2002) 173-177.
- [31] H. Tang, S. Peikang, S.P. Jiang, F. Wang, M. Pan, A degradation study of Nafion proton exchange membrane of PEM fuel cells, *Journal of Power Sources*, 170 (2007) 85-92.
- [32] A. Amel, S.B. Smedley, D.R. Dekel, M.A. Hickner, Y. Ein-Eli, Characterization and Chemical Stability of Anion Exchange Membranes Cross-Linked with Polar Electron-Donating Linkers, *Journal of The Electrochemical Society*, 162 (2015) F1047-F1055.

- [33] J.J. Min-suk, J. Parrondo, C.G. Arges, V. Ramani, Polysulfone-based anion exchange membranes demonstrate excellent chemical stability and performance for the all-vanadium redox flow battery, *Journal of Materials Chemistry A*, 1 (2013) 10458-10464.
- [34] D. Banham, S. Ye, S. Knights, S.M. Stewart, M. Wilson, F. Garzon, UV-visible spectroscopy method for screening the chemical stability of potential antioxidants for proton exchange membrane fuel cells, *Journal of Power Sources*, 281 (2015) 238-242.
- [35] J. Tan, Y.J. Chao, H. Wang, J. Gong, J.W. Van Zee, Chemical and mechanical stability of EPDM in a PEM fuel cell environment, *Polymer Degradation and Stability*, 94 (2009) 2072-2078.
- [36] L. Jones, P.N. Pintauro, H. Tang, Ion exclusion properties of polyphosphazene ion-exchange membranes, *Journal of membrane science*, 162 (1999) 135-143.
- [37] X. Tongwen, Y. Weihua, Fundamental studies of a new series of anion exchange membranes: membrane preparation and characterization, *Journal of membrane science*, 190 (2001) 159-166.

Chapter III

Methodology and objectives

3.1. Introduction

Proton exchange membranes need to show high proton conductivity, low permeability to fuel, very good chemical and thermal stability, good mechanical properties and low cost [1, 2]. In order to design a membrane which could fulfil all these requirements, the mechanical and chemical properties of polysulfone with high ion transport velocity provided by biological ion channel Gramicidin (gA) have been combined. In the present work both physical and chemical immobilization of gA on polysulfone (Psf) membrane have been studied. Besides, Poly(Ethylene Terephthalate) polymeric membranes containing gA have been also investigated.

3.2. Polysulfone membranes fabrication

Ion exchange membranes are available in flat sheet, hollow fiber and tubular configurations. In this work flat sheet membranes configuration has been selected, since this is the configuration used in fuel cell system. Moreover, sheets are easy to fabricate and a notable variety of available films characterization methods are known.

The principal method for preparing flat sheet polymeric membranes is phase inversion/precipitation [3-5]. The principle of this method is the presence of two solutions: a phase high-concentrated in polymer (solvent), and another phase low-concentrated in polymer (non-solvent). High-concentrated phase, consists in a polymer completely and homogeneously dissolved. Low-concentrated phase, consist in a component which is miscible with the polymer solvent, but does not dissolve the polymer. Thus, in the moment of contact, when the two phases start to mix, the non-solvent molecules exchange the solvent molecules in a mixture, resulting in polymer precipitation. Schematic diagram of phase inversion/precipitation process for flat sheet membrane fabrication is presented below (Figure 3.1.).

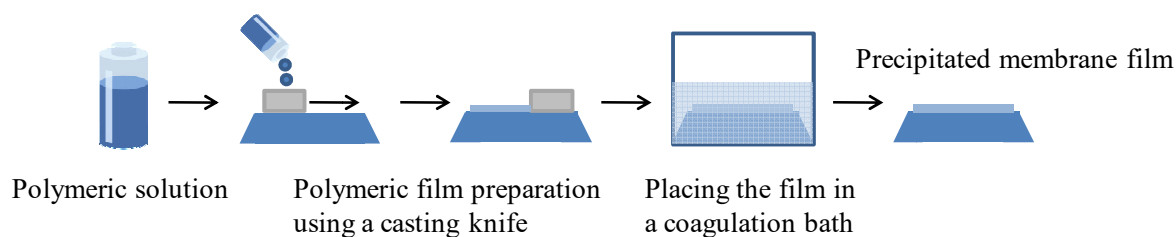


Figure 3.1. Scheme of phase inversion/precipitation process for membrane fabrication.

All membranes studied in this work were prepared via phase inversion/precipitation method, either in water coagulation bath or by solvent evaporation. Detailed description of fabrication method, dependently of immobilization strategy is further described in this Chapter.

3.2.1. Physical immobilization methods

3.2.1.1. Physical entrapment in a polymeric matrix

The first approach consists in biomolecule entrapment within polysulfone matrix. As it is shown in the Figure 3.2., hydrophobic subunits of gA have a high affinity to the fatty acid chains of lipid bilayer. Interior of the folded dimer of gA is filled with water molecules, what allows the ion transport through the channel [6, 7]. Since Psf is a very hydrophobic material, it is a good environment for hydrophobic ion channel immobilization, providing numerous hydrophobic and aromatic interactions.

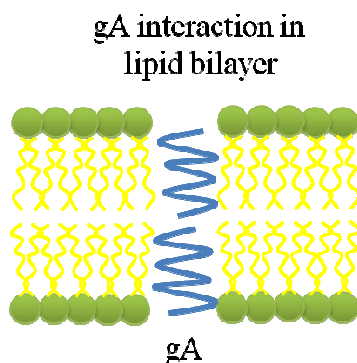


Figure 3.2. Scheme of the gA interaction in lipid bilayer. The hydrophobic exterior of the channel is attracted to the hydrophobic chains of lipid bilayer, while hydrophilic interior of gA filled with water molecules, allows the ions transport.

For membrane preparation, different gA concentrations were used. Nevertheless, at high protein concentration the components were immiscible, thus in order to achieve the highest possible protein loading without phase separation, process optimization needed to be performed. Subsequent steps as well as detailed description of experimental conditions will be described in Chapter IV, section 4.3.1.

3.2.1.2. Immobilization of gA on MNP

3.2.1.2.1. Role of MNP

The second approach, implies immobilization of gA on magnetic nanoparticles (MNP) surface. MNP are one of the nanomaterials most commonly used within the last years in applications like biotechnology, sensors and biomedical devices [8-10]. They are characterized by good thermal and chemical stability, mechanical hardness and low electrical losses [11]. Apart of that, iron oxide is widespread in nature and easy to obtain. Magnetite nanoparticles are facile to prepare, comparing to polymeric nanoparticles, and exhibit good dispersion capability, which is essential, taking into account that the preparation method investigated, includes dispersion of them in the polymeric solution. Moreover, they are reusable and easy to separate [12-14], what makes them much more ecofriendly than e.g. conductive silver nanoparticles, which apart of its potential toxicity are much more expensive [15]. Besides, the possibility of their functionalization, made them good material to be used to improve characteristics of Psf membrane and enhance the efficiency of gA immobilization. The first step of this strategy consists of MNP's functionalization with hydrophilic –OH or -NH₂ groups, and then introducing them to the Psf membrane. This step is essential in order to obtain a material with hydrophilic groups on the surface, which will increase the surface affinity to the micelles.

3.2.1.2.2. Role of micelles

Micelles are spherical structures composed of amphiphilic molecules (e.g. surfactants), which spontaneously self assemble at concentrations equal or above critical micelle concentration (CMC), which is characteristic for each compound [16]. Dependently on the environment and the character of the surrounding solvent, amphiphiles self-aggregate into micelles with hydrophobic core and hydrophilic shell in the case of water, or the other way around in non-polar solvents. The double nature of these components gives them plenty of possibilities for application. Thanks to that they can be used as emulsifiers, detergents or vesicles for drug delivery purposes. Their size, shape and CMC depend on the temperature, solvent or ionic strength. This last effect is the less significant in the case of non-ionic surfactants, which does not have any charge, as the interactions with electrolyte ions are low. To minimize the possibility of undesirable effects, in this study, a non-ionic surfactant Triton X-100, which have relatively low CMC and its micelles are well known and characterized has been employed. It is also widely used for biological membranes permeabilization, as it solubilise hydrophobic membrane proteins with good efficiency.

3.2.1.2.3. Strategy

The schematic presentation of the process is enclosed in Figure 3.3. Each preparation step is described further in Chapter V.

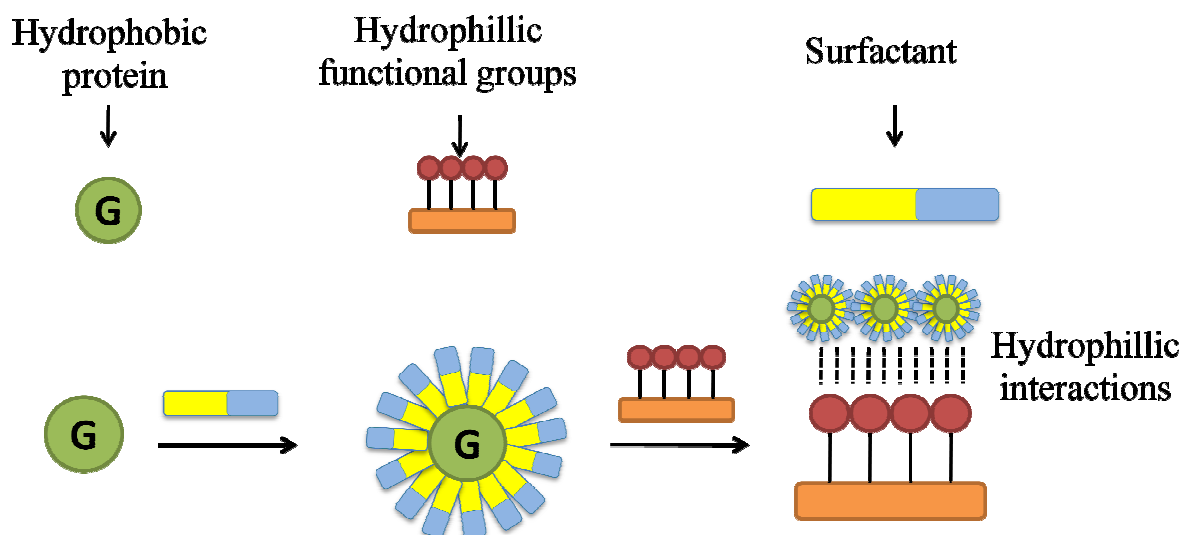


Figure 3.3. Scheme of the surfactant (Triton X100)/protein (gA) micelles immobilization on Psf membrane containing MNP's. On the top the components which are used to the membrane preparation are shown: hydrophobic protein, gA; Psf membrane containing magnetic nanoparticles functionalized with hydrophilic groups; surfactant (Triton X100). On the bottom, the schematic representation of the micelle formed in the aqueous solution containing gA and Triton X100, and the theoretical mechanism of the micelles attachment to the MNP membrane is presented.

3.2.2. Chemical immobilization method

3.2.2.1. Glutaraldehyde coupling

Covalent attachment of biomolecule to artificial components is often related to conformational changes that disable protein functions. Nevertheless, crosslinking with use of glutaraldehyde is known as an effective method to produce protein-synthetic component conjugates, with good maintenance of bioactivity [17, 18]. Thus, covalent gA immobilization on the Psf membrane with glutaraldehyde has been selected. In the first step, glutaraldehyde reacts with the amino group from artificial component (in the case of this work, amine group of MNP immersed in Psf membrane) and forms imine bonds, while its terminal aldehyde group is left without modification. During the second step of crosslinking, terminal aldehyde group reacts with the amino residues of the biomolecule. The schematic representation of this reaction is presented in the Figure below (Figure 3.4). In this case, functional groups of MNP

immersed in the polymer membrane matrix are involved in the first step. Then, the coupling reaction was performed directly on the membrane surface, containing $-NH_2$ functionalized nanoparticles.

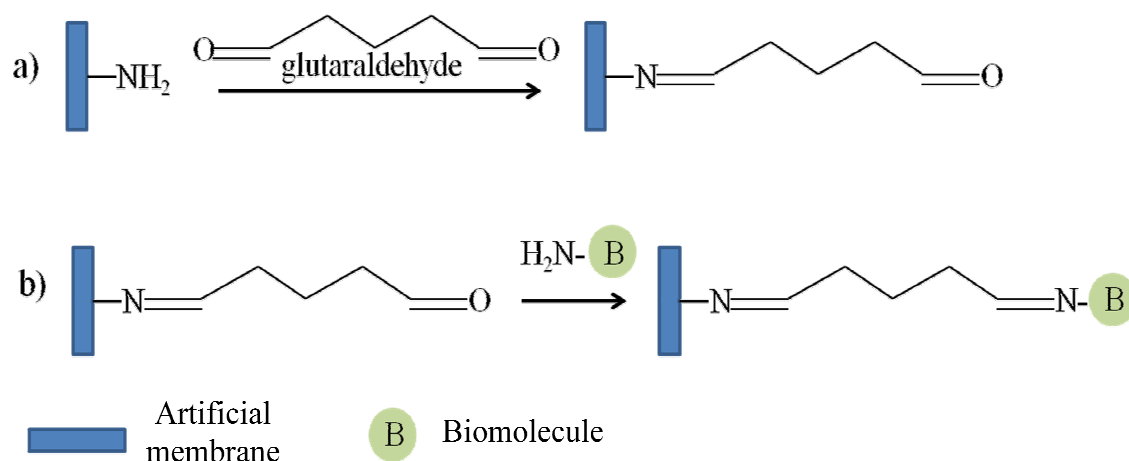


Figure 3.4. Schematic representation of glutaraldehyde coupling with biomolecule: a) the first step of the reaction with $-NH_2$ group from the membrane, and b) coupling with $-NH_2$ terminal group from biomolecule.

3.3. Polyethylene terephthalate (PET) membranes fabrication methods

3.3.1. Track etching

Track etching is another very useful technique applied in membrane technology. Production of membranes using this methodology allows to obtain materials with precisely determined pore size, shape and density, which can be controlled and thus, is an attractive tool to obtain membranes with the desired characteristics. The most commonly used materials which found commercial application for the production of track etched membranes are polyethylene terephthalate (PET), polypropylene (PP) and polycarbonate (PC) [19-21]. Possibility of producing membranes with cylindrical, conical, funnel-like, or cigar-like pores, gave to track etched membranes application in many filtration processes.

Track etching membranes fabrication contains several steps. The first one aims to produce the latent tracks in a smooth polymeric film, which will be converted to pores afterwards. This micro-damages can be induced by irradiation by fragments of heavy nuclei, or irradiation by ion beam. The latter is considered to be a better method because produced films are not contaminated with radioactive components. Once the breakages are performed, the next step consist in chemical etching, which is the actual pore formation process. Exposure to the chemical agent, which usually is an aqueous alkali solution, removes the latent tracks. At this stage, by choosing appropriate conditions, it is possible to determine pores size and shape. In order to achieve reproducible results, parameters such as temperature and etching agent composition and concentration and also the duration of exposure must be determined. Therefore, fabricated membranes have already fixed porosity and pore shape. However, many film modifications can be performed afterwards in order to obtain desired surface properties. Within common modification procedures, hydrophillization or hydrophobization, graft polymerization or introduction of new functional groups to the membrane surface, can be found [19]. Possible structure modification after etching include also pore size reduction, which is the case of the present work.

3.3.2. Atomic Layer Deposition (ALD)

ALD technique allows to cover surfaces with a layer of various substances introduced previously to a vapour phase [22, 23]. It is considered to be a variant of chemical vapour deposition (CVD), because it consists in chemical reaction between the surface and precursor gases in a reactor filled with an inert gas. The chemical nature of the precursor is important for the process. Above all, the precursor must be volatile and thermally stable and can be either a gas, a liquid or even a solid. The key property of the precursor is its ability to chemisorb on the modified material surface. It can also react with the functional groups on the film and with another precursor. It is crucial to achieve the required saturation stage in a short time and ensure a fast rate of deposition. There are non-metallic and metallic precursors [23]. For deposition of non-metallic hydrides, the presence of hydroxylic groups on the film surface is necessary. Those precursors have found to be volatile and thermally stable. Among the most common metal precursors, halides, alkyls and alkoxides are found. The mechanism of

deposition consist in reaction of the surface with two precursors (reactants), but not at the same time (Figure 3.5.). When the surface is properly pretreated or functionalized, the precursor A, which reacts with a limited number of reactive sites on the surface, is introduced in the reaction chamber . Then, when this process is finished, the excess of the precursor A and the byproducts of the reaction are flushed away by an inert gas, and precursor B is introduced to react with the surface afterwards. The excess of precursor B and byproducts is flushed away with an inert gas. This process is repeated in cycles in order to obtain a desired and fully controlled layer thickness. Since vapour easily penetrate the surface and is not sensitive to the inequalities and roughness, it gets deposited also in the pores, what reduces its size.

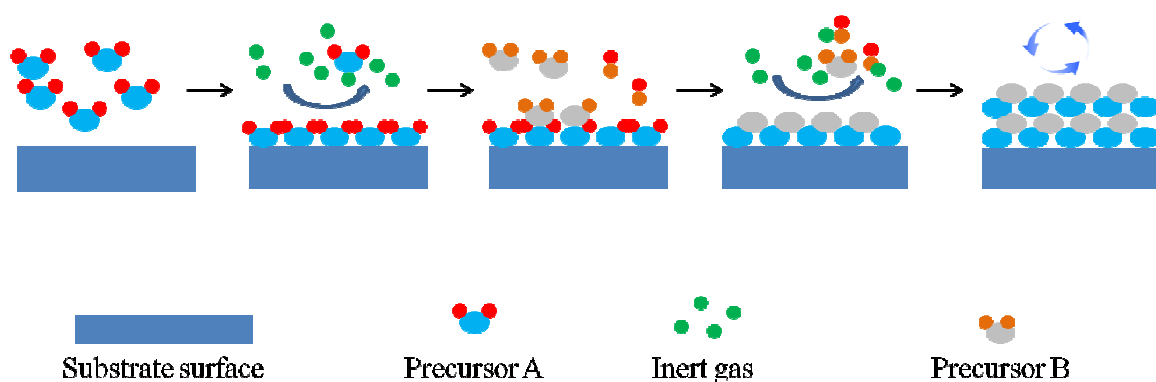


Figure 3.5. Scheme of Atomic Layer Deposition process.

3.3.3. PET film surface modification and Gramicidin immobilization

Track etched PET membranes were functionalized and various gA immobilization methods were applied.

- Triton X100/Gramicidin micelles immobilization (the same procedure as described above in the case of polysulfone membranes)
- Isopropylamine modification: this method aims to perform aminolysis of PET film in order to introduce to the surface alkyl functional groups. This process is a well-known method to modify PET polymer structure to convert it to less thermally stable derivative, for recycling purposes [24, 25]. Introduction of hydrophobic alkyl groups

aims to imitate the interaction of Gramicidin with the lipid bilayer in biological membrane.

- c) Hexamethyldisilazane modification: this method, like the previously described one, tends to introduce the $-CH_3$ methyl hydrophobic groups and mimic the interaction between protein and biological membrane.

3.3.4. Polysulfone membrane surface modification

An additional modification of Polysulfone membrane has been performed, in order to evaluate another method for increasing water passage through the membrane with the use of biological channel and compare the results with the data obtained for PET modified membranes.

Nystatin is antifungal medicament which is also a membrane active polyene with amphiphilic structure (Figure 3.6.). This properties allows it to self-assemble into channels and increase ion passage through the membrane [26]. We expect that Nystatin can interact with polysulfone film within the same mechanism as Triton X100 does, when immobilizing micelles. Thus, Nystatin treatment was performed in order to check the influence of another channel-forming molecule immobilization on ion permeability across polysulfone membrane.

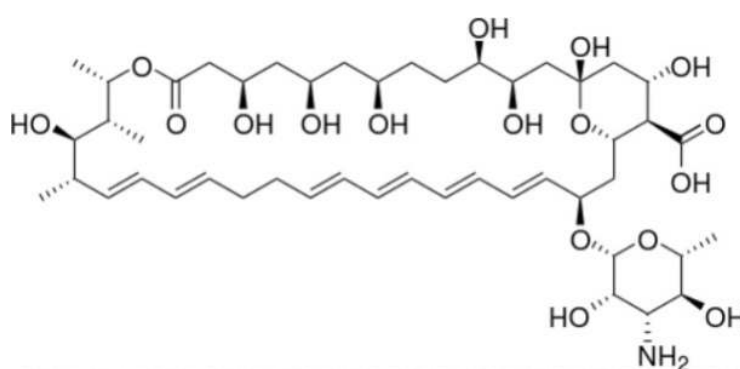


Figure 3.6. Nystatin structure.

3.4. Characterization methods

Characterization includes both, new membrane materials as well as micelles used for physical immobilization method. All the membranes were characterized to determine their hydrophobic/hydrophilic properties, morphology, surface chemistry and transport properties. Thermophysical properties of micelles such as surface tension, viscosity, conductivity as well as their size were studied, and biological activity of the entrapped Gramicidin has been investigated.

3.4.1. Membranes characterization methods

3.4.1.1. Hydrophobic/hydrophilic properties

3.4.1.1.1. Contact angle (CA)

Hydrophobic/hydrophilic properties of materials plays an important role in terms of application. Those characteristics influence cleaning properties, wetting, and floating properties, among others. Hydrophobicity and hydrophilicity are terms introduced in order to describe affinity of solids to water, when spread on their surface. A contact angle is a value related to the surface energies of two surfaces: solid material and water drop. Water drop is spreaded on the surface of the membrane and the contact angle is measured (Figure 3.7.). Surfaces characterized by a contact angle smaller than 90 are considered to be hydrophilic and those above 90 as hydrophobic [27].

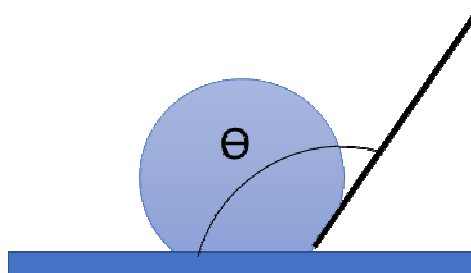


Figure 3.7. Water drop behaviour and contact angle on hydrophobic surface.

Contact angle is also related to the roughness parameter of the outer membrane surfaces. In the present work, contact angle measurement deliver an important information, because it is expected that surface hydrophilicity will change after immobilizing the hydrophobic protein.

3.4.1.1.2. Water uptake (WU)

Ability of membrane to swell water is an important parameter which often has impact on membrane transport properties. It is the complementary characterization method, often used together with the contact angle measurement [27, 28]. Weighted dry membranes were immersed in deionized water and weighted after 4, 6, 8 and 24 hours and after drying process. The water uptake can be calculated from the Equation 3.1.:

$$\text{Water uptake (\%)} = \frac{(W_{wet} - W_{dry})}{W_{dry}} \cdot 100\% \quad \text{Eq. 3.1.}$$

This method provides information about protein immobilization influence on hydrophobic properties of polysulfone. Moreover, is a source of data necessary for the correct interpretation of transport properties results.

3.4.1.2. Surface chemistry

3.4.1.2.1. Fourier Transform Infrared (FTIR)

FTIR (Fourier Transform Infrared) spectroscopy is based on radiation which passes through a sample. Compounds with covalent bonds are not rigid and can be stretched or bent and in addition, the groups around the single bonds rotate easily. Those properties result in a variety of rotational/vibrational movements within the molecules, characteristic of the atoms present in their structure. In a consequence, all the compounds may absorb the infrared radiation corresponding to the energy of their vibrations. The resulting spectrum is a representation of the molecular absorption or transmission, characteristic for each compound,

which create so called molecular fingerprint of the sample. This makes infrared spectroscopy useful tool for organic analysis for specific determination and monitoring of chemistry changes in a sample [29]. Possibility of registration new appearing amine bonds in a membrane can be a proof of successful protein immobilization. In order to evaluate changes in surface chemistry of membranes, FTIR spectra before and after gA immobilization were performed. This method can offer information about efficiency of protein immobilization by registration of new appeared amide bonds from protein.

3.4.1.3. Morphology

3.4.1.3.1. Scanning Electron Microscopy (SEM) and Environmental Scanning Electron Microscopy (ESEM)

Electron microscope allows imaging a sample by means of a focused beam of electrons which interact with atoms present in a material. Interactions of material atoms emit secondary electrons, which deliver information about the sample's surface [30]. Therefore, sample topography may be obtained, and its composition may be determined, if using elementary analysis module. SEM can reproduce the sample image with relatively high resolution. Samples can be analyzed in high vacuum, in low vacuum and at different temperatures. In the case of Environmental Scanning Electron Microscope (ESEM), samples can be observed in wet conditions, what is extremely useful for biological samples analysis.

3.4.1.3.2. Porosity

Porosity is a parameter which influence all the membrane properties, thus, it is fundamental for optimization of their performance [31]. Porosity is calculated as a fraction of pores volume over a total volume of membrane and can be calculated as follows:

$$\phi = \frac{V_p}{V_m} \cdot 100\% \quad \text{Eq. 3.2.}$$

where V_p is a volume of pores and V_m is a total volume of the membrane. In order to obtain all the necessary information for the calculation, exact membrane area and thickness must be measured. The pore volume is measured gravimetrically, by measuring the membrane mass in dry state and after its saturation with water. The mass of water in the pores is obtained:

$$M_w = M_{sm} - M_{dm} \quad \text{Eq. 3.3.}$$

Where M_{sm} refers to the mass of swelled membrane and M_{dm} is the mass of dried membrane.

The last step is calculation of water entrapped within membrane pores, which is equal to the pores volume.

$$V_w = V_p = \frac{M_w}{d_w} \quad \text{Eq. 3.4.}$$

Where M_w is the mass of water calculated from the Equation 3.2. and d_w is water density.

3.4.1.4. Transport properties

3.4.1.4.1. Permeability calculation

Diffusivity is defined as the rate at which particles or heat can spread. The method of its determination is based on the occurrence of heat transfer related to the macroscopic movement of the molecules within fluids, called convection. It is an effect of a concentration gradient and is described by Fick's laws. When two solutions are contacted through a membrane, the solutes pass from the more concentrated solution to the less concentrated one. The registered ion concentration change is linear. From the slope value of the graphical data representation diffusion coefficient can be obtained. Diffusion coefficient is a factor by which the mass of a solute diffusing in time t across the surface, is proportional to the concentration

gradient of this substance. It depends on the molecule size, temperature and pressure. From the pH change slope, ion diffusion coefficient and permeability were calculated according to the Fick's First law [32, 33] :

$$J = \frac{P \cdot \Delta C}{l} \cdot 10^{-3} \quad \text{Eq. 3.5.}$$

where l (cm) is the membrane thickness and ΔC is the difference in concentration (mol/l) between the initial feed solution (C_0) and the final stripping solution. At used experimental conditions, C_0 was much greater than the final concentration, so we considered $\Delta C \sim C_0$. P is the ion permeability (cm^2/s), defined as:

$$P = D \cdot S \quad \text{Eq. 3.6.}$$

where D is the diffusion coefficient and S is the sorption equilibrium parameter. The flux is related to the permeability coefficient p (cm/s), as:

$$J = P \cdot C_0 \quad \text{Eq. 3.7.}$$

$$P = p \cdot l \quad \text{Eq. 3.8.}$$

The permeability coefficient can be described by the following Equation:

$$-\ln \frac{C_f}{C_0} = \frac{A \cdot P}{V_f} \cdot t \quad \text{Eq. 3.9.}$$

where C_0 (mol/l) is the initial concentration of the feed solution and C_f (mol/l) is the feed concentration calculated from the stripping solution at time t (s):

$$C_f = C_0 - C_s \quad \text{Eq. 3.10.}$$

V_f is the feed volume (ml) and A is the actual membrane area (cm^2). The ion permeability is calculated according to the above Equations. Concerning the cation antiport mechanism, in order to maintain the electrochemical balance, the cation diffusion through the membrane, forces a passage of the ion with the same electrochemical charge from the other side. Under this hypothesis, proton transport in these experiments should be limited by the bigger cation permeability, since the size of H^+ is smaller in comparison to the rest of ions in stripping

solutions. In this work, the permeability value for Na^+ , K^+ , Ca^{2+} and Mg^{2+} have been determined using a subsequent chloride salts as stripping solutions and hydrochloric acid as a feed. Experimental setup for those measurements is presented in Figure 3.8.

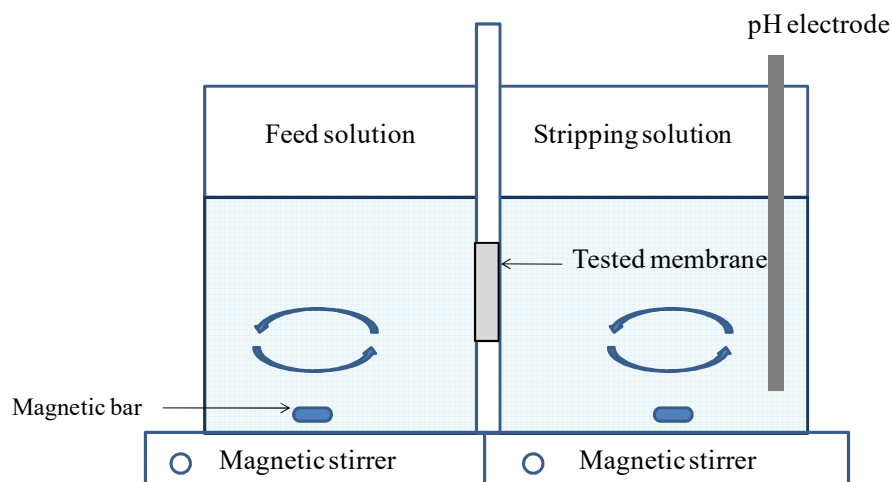


Figure 3.8. Scheme of the permeability experiments test cell consisting in Teflon cell with two compartments of 200 ml volume, separated by tested membrane placed between two rubber o-rings.

3.4.1.4.2. Atomic Absorption Spectrometry (AAS)

AAS is a characterization method which allows, with relatively high sensitivity, to determine quantitatively chemical elements. This technique is based on the absorption of the light emitted by free atoms, in gaseous state released by a combustion reaction. When the sample is introduced to the spectroscopic atomizer, the electrons of the atoms present in the sample are excited by absorption of a characteristic wavelength, which is specific for each element. This absorbance value is conveniently detected and then converted to the concentration value according to the Beer-Lambert Law [34]. In the case of this work, in order to ensure the reliability of diffusion measurements, randomly collected samples from permeability experiments were collected and correspondence of Mg^{2+} ion concentration change between a feed and a stripping solution was evaluated.

3.4.1.4.3. Polarized Optical Microscope (POM)

Polarized Optical Microscopy (POM) is a simple characterization technique that consist in illuminating a sample with polarized light, that enhances the contrast of the image providing a good quality view of the sample surface [35]. During permeability experiment, membranes are exposed to the effect of osmotic pressure. Therefore, after experiments samples may be used to verify if micro-damages have appeared.

3.4.1.4.4. Current-Voltage measurement (CV)

Concentration polarisation is a phenomena which occurs in cation exchange membrane systems and it is a direct consequence of membrane selectivity. It refers to the presence of concentration gradients at a membrane/solution interface which occurs because of the transfer of one kind of species through the membrane (as an effect of driving forces) while the other species are not transported, or transported slower. Concentration of transported ions decreases while the retained species have higher concentration at the membrane surface. Studying this phenomena for membrane systems leads to consideration of so called limiting current value and conditions under which ionic transport occurs in the range below and above this value. According to the Nernst classical model, the shape of Current-Voltage curve for ion exchange membrane should be composed of three regions, as shown on the Figure below (Figure 3.9.) [36].

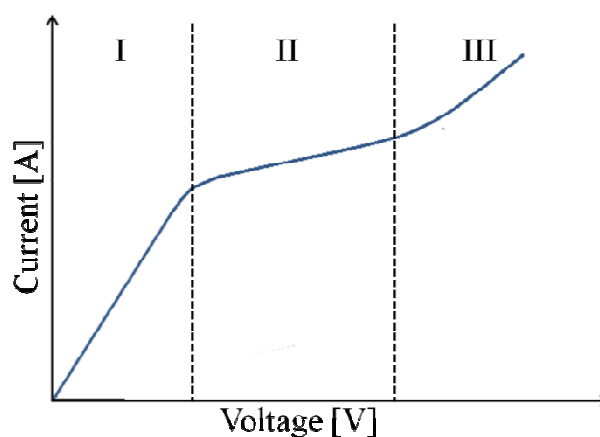


Figure 3.9. Typical Current-Voltage curve for proton exchange membranes, containing three characteristic regions: Ohmic (I), limiting current (II) and convective region (III).

Linear Ohmic region (I) , a flat or almost flat limiting current region- in which the ion transport occurs (II), and third region, where usually current flow increases, that is known as convective region (III). Performing C-V measurements with the membranes under study provides useful information about the optimal transport conditions, such as: membrane resistance, capacity and ion conductivity capability. The experimental set-up is presented in Figure 3.10.

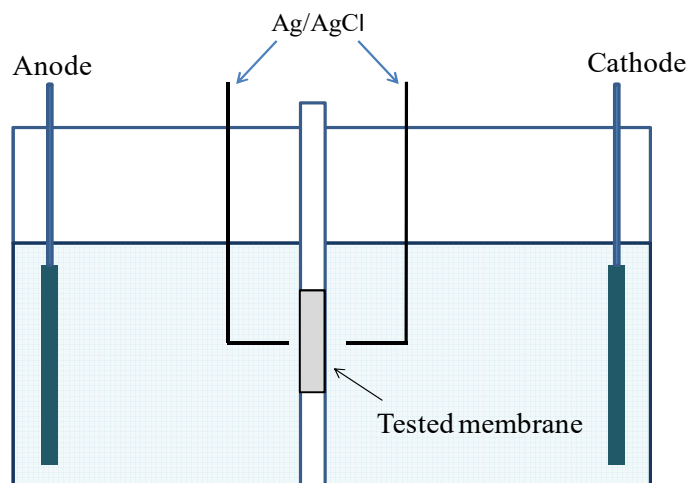


Figure 3.10. Experimental set-up for Current-Voltage measurements. It contains a cell with two compartment of equal volume of 200 ml separated by the membrane, and two working and two reference electrodes.

The value of samples voltage may be calculated according to Equation 3.11.:

$$U_{comp} = U_m - R_{sol} \cdot I_m \quad \text{Eq. 3.11.}$$

where U_{comp} is the compensated voltage value, U_m is measured voltage value, R_{sol} is the solution resistance, and I_m is the measured current value.

3.4.1.4.5. Self-diffusion coefficient calculation

In many studies devoted to model and predict ion transport through polymeric composite membranes it is highlighted the importance of determination of self-diffusion coefficient in the membrane. Experimental data of permeabilities are often difficult to interpret, because apart of the electrolyte ions fluxes another impact on the average diffusion coefficient has an

unknown gradient of electrolyte and water concentration which exists inside the porous membrane phase. In fact it is considered that the liquid in the pores is the medium in which diffusion transport occurs and thus, the movement of ions through the liquid in the pore is the diffusion rate determining step.

There are known several methods to determine self-diffusion coefficient: non-equilibrium thermodynamics phenomenological model, radiotracer technique, models based on Stefan-Maxwell Equation and the one based on the Nernst-Einstein Equation. In the present work the results of calculations of self-diffusion coefficient of ions with use of Nernst-Einstein generalized model, which can be expressed by the Equation 3.12. [37-39] are reported.

$$\sigma = \frac{F^2 z^2 D_\sigma}{RT} \quad \text{Eq. 3.12.}$$

Where σ is conductivity, F is Faraday constant, z is a charge number of ion, R is gas constant, T is temperature in Kelvin, D_σ is diffusion coefficient and C is the concentration of the ion in a membrane film. Diffusion coefficient D_σ can be expressed by:

$$D_\sigma = \frac{\Lambda RT}{F^2 z^2} \quad \text{Eq. 3.13.}$$

Where Λ is molar conductivity and f is a correction factor applied for the porous media, calculated from the Equation 3.14. [40]:

$$f = \frac{\varepsilon}{\tau} \quad \text{Eq. 3.14.}$$

Where ε refers to the membrane porosity and τ is the tortuosity factor, calculated from the Bruggeman relation, which has been proven to be good approximation for the porous materials and is expressed as follow [41, 42]:

$$\tau = \varepsilon^{-0.5} \quad \text{Eq. 3.15.}$$

Conductivity data for calculations were obtained from Current-Voltage measurements and calculated from the relations [43]:

$$R = \rho \frac{l}{A} \quad \text{Eq. 3.16.}$$

$$\sigma = \frac{1}{\rho} \quad \text{Eq. 3.17.}$$

Where R is resistance, ρ is resistivity, l is a membrane thickness and A is a membrane area.

3.4.2. Micelles characterization

3.4.2.1. *Micelle solutions biological activity study*

3.4.2.1.1. *Activity study in solid media*

One of the method to evaluate biofunctionality of a solution containing protein is the study of its activity against bacteria [44]. One of the method to realize antimicrobial activity experiment is agar diffusion technique. The principle of this technique is based on growing bacteria against which the test will be performed, on Petri dishes filled with nutrient agar. Once the medium is solidified, small holes are made using a sterile Pasteur pipet. After that, tested solutions are placed in the holes and let to diffuse into the agar gel. Then, the plates need to be incubated in the adequate temperature for bacteria incubation, for optimal period of time. The inhibitory activity of solution against bacteria can be detected as clear zones around the holes, visible after incubation. The inhibition growth diameter is determinant of antimicrobial activity. Schematic representation of the experimental procedure is shown in Figure 3.11.

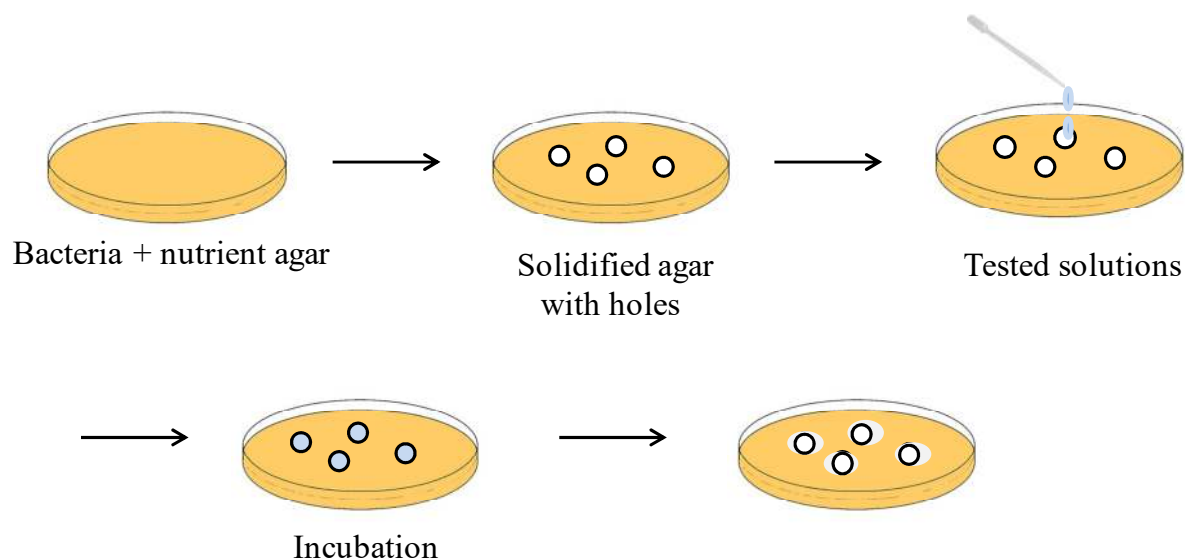


Figure 3.11. Experimental procedure of antibacterial activity assay with use of solid media.

3.4.2.2. Immobilized micelles biological activity study

3.4.2.2.1. Activity study in solid media

Antibacterial properties of membranes can be studied using the same agar assay mentioned above. The difference consists in placing pieces of membranes on the agar surface, instead of the holes drilling.

3.4.2.2.2. Activity study in liquid media

Activity against bacteria can be observed also in liquid medium. For this purpose, bacteria cell concentration is indirectly determined by optical density, measured with the use of a spectrophotometer. Within this procedure, light is emitted through the suspension of bacteria in liquid medium and is scattered. The amount of registered scatter is an indication of the bacteria present in the solution [45]. Absorption spectra is registered at 600 nm. By comparing the optical density (OD) at the same wavelength of the suspensions with immersed

membrane without micelles and with micelles, we can monitor the inhibition growth effect, which will be reflected as a lower OD value.

3.4.2.3. Interfacial tension measurement (IFT)

This key thermodynamic property refers to elastic capacity of fluids and it is often used to characterize micelle solutions [46]. Interfacial tension (IFT) refers to the surface tension occurring on a interface of two non-miscible phases (in the case of the system used in this work, liquid and air). This value informs about surfactant efficiency, and the lowest it is, the better functions fulfils in many practical applications. In oil recovery, lowering interfacial tension by surfactants increase oil mobility and allows easier extraction of the oil. In domestic applications, surfactants' amphiphilic nature permits the grease removal through the micelle formation and dispersion of oily stains in water. In this work, measurement of IFT could provide valuable information about ability of micelle solutions to penetrate and permeabilize the cell membrane and thus, deliver micellized gA to the bacteria. Measurement of interfacial tension is carried out by the pendant drop method.

The pendant drop technique is used to determine the interfacial tension between two immiscible phases, where the gravity, hydrostatic pressure, and surface tension effects, influence the shape of the solution drop, which is suspended on a syringe tip. Because of the tension present between inner and outer phase of the drop, the pressure inside it increases. The Young-Laplace Equation describes correlation between the pressure difference Δp , the radii of surfaces curvature r_1 and r_2 and the interfacial tension σ (Equation 3.18.) [47]:

$$\Delta p = \sigma \cdot \left(\frac{1}{r_1} + \frac{1}{r_2} \right) \quad \text{Eq. 3.18.}$$

Under the gravity, shape of the drop changes in vertical direction (see Figure 3.12.), and has a characteristic “pear” form. The deviation range from the spherical shape is expressed by the ratio between the drop weight and its surface or interfacial tension. It is necessary to know the difference in density between the two phases and then, the surface or interfacial tension is calculated from the shape of the drop. An schematic setup for pendant drop method is shown in Figure 3.12.

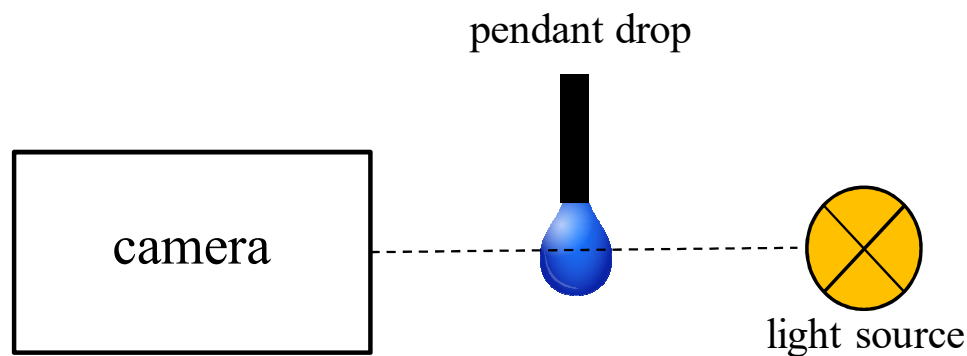


Figure 3.12. Schematic setup for pendant drop technique.

3.4.2.4. Viscosity

Viscosity is defined as the liquid resistance to deformation caused by tensile stress or in other words, its ability to flow. Knowing this value it is possible to model or to predict the liquid system behaviour and understand its properties [48]. In order to measure viscosity, Ostwald viscometer may be used. This viscometer works on the basis of the Hagen-Poiseuille law which can be expressed as follows:

$$V = \frac{Pr^4\pi}{8l\eta} t \quad \text{Eq. 3.19.}$$

Where η is viscosity of homogenous fluid passing through a capillary tube of length l and radius r at pressure P per time t . The Ostwald viscometer is a U-tube with a capillary which separates two bulb reservoirs (see Figure 3.13.).

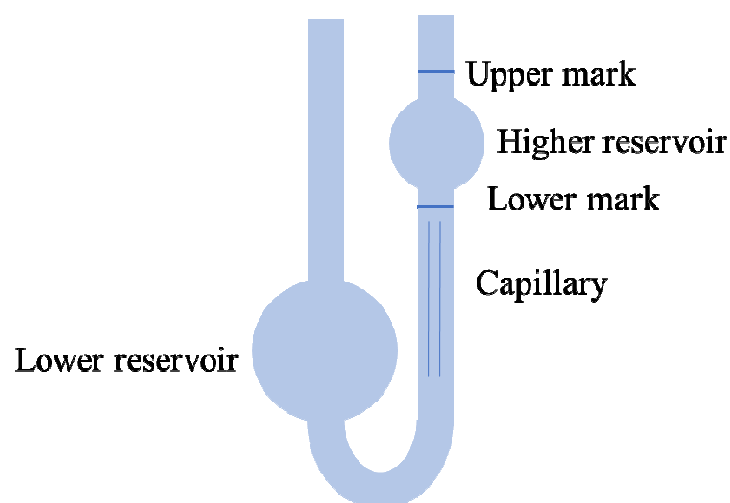


Figure 3.13. Ostwald viscometer scheme.

The procedure consists of liquid addition to the viscometer and pump it to the upper reservoir, and then allowed to fall by gravity back into the lower reservoir. The measured time that it takes for the liquid to pass between two etched marks, is used for viscosity calculations. The kinematic viscosity is:

$$\eta = K \cdot t \quad \text{Eq. 3.20.}$$

Where t is the flow time in seconds and the K is the instrument constant determined with use comparative measurements with reference viscometers. Dynamic viscosity was calculated by dividing the obtained value of kinematic viscosity over the density of each sample. Density was measured with the use of vibrating-tube densitometer. This simple vibrating system contains a spring and a mass, which when displaced, causes vibrations at known frequency. The frequency of vibration of the tubing is related to the fluid density in the tube.

3.4.2.5. Electrical conductivity

Conductivity is the ability of materials to conduct electric current. It is an essential property to understand the structure of ionic systems and the interaction occurring in it. In the case of electrical conductivity of micelle solutions, information about micelles structure may be provided. If with increasing surfactant concentration, decrease of conductivity is observed, it suggests micelles association, what is related to lower amount of moving charged species. Contrary, an increase of conductivity suggests that micelles do not form aggregates [49]. This is especially useful for investigation if micelles formed by ionic surfactants. Nevertheless, influence on this property can be also investigated in the case of non-ionic detergents. The measuring equipment is built of a probe with two electrodes, between which a voltage is applied when the probe is immersed in a solution. The drop in voltage caused by electrical resistance from the solution is then read by the detector and converted to conductivity units.

3.4.2.6. Dynamic Light Scattering analysis (DLS)

Dynamic light scattering (DLS) is a technique widely utilized to determine the particle size and distribution. The analysis is performed in terms of temporal fluctuations, usually expressed as intensity. Since it is possible to perform analysis at different temperature, it can be also used to predict and monitor the stability of colloidal formulations. The particle motions in the solutions are called Brownian motions and are the result of the collisions occurring between the solvent molecules and the particles. When a laser beam crosses a particle solution, light will be scattered due to the abovementioned motions [50]. Particles with different size will scatter light in different times (Figure 3.14.).

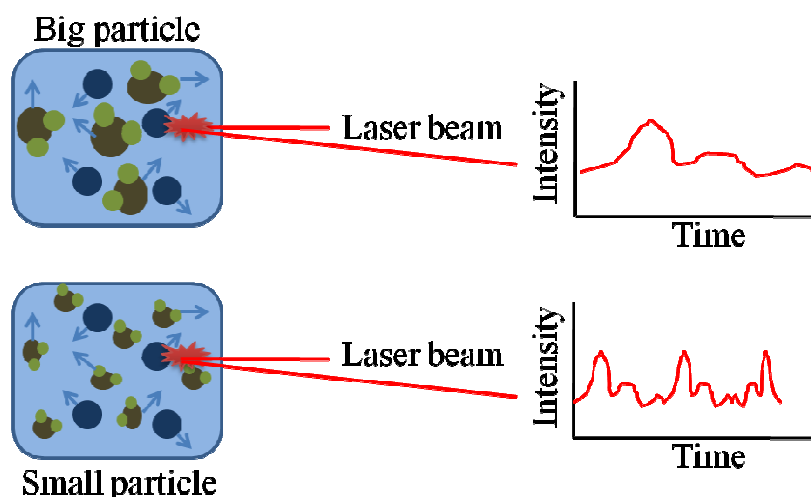


Figure 3.14. Theoretical dynamic light scattering of two samples: containing big particles on the top, and small particles on the bottom.

Afterwards, collected data is analyzed and correlated according to an adequate model. Information which could be extracted from this analysis is average particle size and distribution, diffusion coefficient, hydrodynamic radius and polydispersity index.

3.5. Objectives

The main objective of the present thesis is the design and the preparation of a novel bioartificial membrane, composed of polysulfone and Gramicidin, joining robustness and durability of polymer with ion selectivity of protein, resulting in enhanced ion transport properties in regards to Plain polysulfone membrane. The detailed objectives of this work are as follows:

- Preparation of a functional bioartificial membrane by physical entrapment of biomolecule within polymer matrix.
- Preparation of a functional bioartificial membrane by physical immobilization of Surfactant/Protein micelles on a membrane using magnetic nanoparticles.
- Preparation of a functional bioartificial membrane by chemical immobilization method employing glutaraldehyde coupling.

- To study the effect of nanoparticles functional group on protein immobilization efficiency.
- To characterize the membranes obtained in terms of morphology using SEM, surface using FTIR, CA, WU and transport properties measuring diffusion transport and ion conductivity and basing on obtained characteristics evaluate their potential applicability as proton exchange membrane in fuel cells.
- To characterize the thermophysical properties of surfactant/protein micelles and evaluate biological activity of immobilized Gramicidin against gram positive bacteria.
- To evaluate the bioactivity and antibacterial activity against gram positive bacteria of Gramicidin immobilized on membrane.

3.6. Acknowledgments

Analysis of FTIR and ESEM/SEM was performed thanks to resources and technical support from Servei Recursos Científic del Universidad Rovira i Virgili. Track etched membranes were fabricated and characterized in Interfaces, Physical Chemistry and Polymers research group at the European Membrane Institute in Montpellier thanks to Dr. Sébastien Balme. Dynamic Light Scattering measurements were performed thanks to Dr. Pierfrancesco Cerruti from the Institute of Polymers, Composites and Biomaterials – CNR, Via Campi Flegrei, 3480128 Pozzuoli (Naples), Italy. Biological activity assay was performed in the microbiological laboratory of Interfibio research group at the Chemical Engineering Department of Universitat Rovira i Virgili. The rest of analysis were performed in the laboratory of METEOR research group of the Chemical Engineering Department at Universitat Rovira i Virgili.

3.7. References

- [1] S.J. Peighambardoust, S. Rowshanzamir, M. Amjadi, Review of the proton exchange membranes for fuel cell applications, *International Journal of Hydrogen Energy*, 35 (2010) 9349-9384.
- [2] A. Kraytsberg, Y. Ein-Eli, Review of Advanced Materials for Proton Exchange Membrane Fuel Cells, *Energy & Fuels*, 28 (2014) 7303-7330.
- [3] C.A. Smolders, A.J. Reuvers, R.M. Boom, I.M. Wienk, Microstructures in phase-inversion membranes. Part 1. Formation of macrovoids, *Journal of membrane science*, 73 (1992) 259-275.
- [4] C.F. Fryling, Production of adhesives and adhesive bases from synthetic rubber latex by causing phase inversion with a protective colloid and adding organic solvent, in, *Google Patents*, 1956.
- [5] M.-J. Han, S.-T. Nam, Thermodynamic and rheological variation in polysulfone solution by PVP and its effect in the preparation of phase inversion membrane, *Journal of membrane science*, 202 (2002) 55-61.
- [6] J.A. Lundbæk, S.A. Collingwood, H.I. Ingólfsson, R. Kapoor, O.S. Andersen, Lipid bilayer regulation of membrane protein function: Gramicidin channels as molecular force probes, *Journal of The Royal Society Interface*, 7 (2010) 373-395.
- [7] R. Ketchum, W. Hu, T. Cross, High-resolution conformation of Gramicidin A in a lipid bilayer by solid-state NMR, *Science-New York Then Washington-*, 261 (1993) 1457-1457.
- [8] Y.F. Shen, J. Tang, Z.H. Nie, Y.D. Wang, Y. Ren, L. Zuo, Preparation and application of magnetic Fe₃O₄ nanoparticles for wastewater purification, *Separation and Purification Technology*, 68 (2009) 312-319.
- [9] K. Abdollahi, F. Yazdani, R. Panahi, Covalent immobilization of tyrosinase onto cyanuric chloride crosslinked amine-functionalized superparamagnetic nanoparticles: Synthesis and characterization of the recyclable nanobiocatalyst, *International Journal of Biological Macromolecules*, 94, Part A (2017) 396-405.
- [10] L. Cabrera, S. Gutierrez, N. Menendez, M.P. Morales, P. Herrasti, Magnetite nanoparticles: Electrochemical synthesis and characterization, *Electrochimica Acta*, 53 (2008) 3436-3441.

- [11] H. Yun, J. Chen, V. Doan-Nguyen, J. Kikkawa, C. Murray, Synthesis, characterization, and fabrication of magnetic nanoparticles for low energy loss applications, in: APS Meeting Abstracts, 2013, pp. 14003.
- [12] X. Jin, K. Zhang, J. Sun, J. Wang, Z. Dong, R. Li, Magnetite nanoparticles immobilized Salen Pd (II) as a green catalyst for Suzuki reaction, *Catalysis Communications*, 26 (2012) 199-203.
- [13] P. Yuan, M. Fan, D. Yang, H. He, D. Liu, A. Yuan, J. Zhu, T. Chen, Montmorillonite-supported magnetite nanoparticles for the removal of hexavalent chromium [Cr (VI)] from aqueous solutions, *Journal of Hazardous materials*, 166 (2009) 821-829.
- [14] B. Movassagh, A. Yousefi, Magnetite (Fe₃O₄) nanoparticles: an efficient and reusable catalyst for the synthesis of thioethers, vinyl thioethers, thiol esters, and thia-Michael adducts under solvent-free condition.
- [15] Q.H. Tran, A.-T. Le, Silver nanoparticles: synthesis, properties, toxicology, applications and perspectives, *Advances in Natural Sciences: Nanoscience and Nanotechnology*, 4 (2013) 033001.
- [16] P. Mukerjee, K.J. Mysels, Critical micelle concentrations of aqueous surfactant systems, in, National Standard reference data system, 1971.
- [17] G.I. Bayramoglu, B. Hazer, B. Atlintaş, M.Y. Arica, Covalent immobilization of lipase onto amine functionalized polypropylene membrane and its application in green apple flavor (ethyl valerate) synthesis, *Process biochemistry*, 46 (2002) 372-378.
- [18] P. Ye, Z.-K. Xu, J. Wu, C. Innocent, P. Seta, Nanofibrous poly (acrylonitrile-co-maleic acid) membranes functionalized with gelatin and chitosan for lipase immobilization, *Biomaterials*, 27 (2006) 4169-4176.
- [19] P. Apel, Track etching technique in membrane technology, *Radiation Measurements*, 34 (2001) 559-566.
- [20] F. Tasselli, Membrane Preparation Techniques, in: E. Drioli, L. Giorno (Eds.) *Encyclopedia of Membranes*, Springer Berlin Heidelberg, Berlin, Heidelberg, 2015, pp. 1-3.
- [21] R.W. Baker, *Membrane technology*, Wiley Online Library, 2000.
- [22] R.W. Johnson, A. Hultqvist, S.F. Bent, A brief review of atomic layer deposition: from fundamentals to applications, *Materials today*, 17 (2014) 236-246.
- [23] M. Leskelä, M. Ritala, Atomic layer deposition (ALD): from precursors to thin film structures, *Thin solid films*, 409 (2002) 138-146.
- [24] W.H. Cook, Process for modifying linear polymer resins, in, Google Patents, 1980.

- [25] M. Drobota, M. Aflori, I. Stoica, F. Doroftei, Surface characterization of amine functionalized pet films after collagen immobilization, *Rev Roum Chim*, 58 (2013) 203-207.
- [26] K. Boukari, G. Paris, T. Gharbi, S. Balme, J.-M. Janot, F. Picaud, Confined Nystatin Polyenes in Nanopore Induce Biologic Ionic Selectivity, *Journal of Nanomaterials* (2016).
- [27] B. Tylkowski, I. Tsibranska, Overview of main techniques used for membrane characterization, *Journal of Chemical Technology & Metallurgy*, 50 (2015).
- [28] V. Sproll, T.J. Schmidt, L. Gubler, Effect of glycidyl methacrylate (GMA) incorporation on water uptake and conductivity of proton exchange membranes, *Radiation Physics and Chemistry* (2018).
- [29] J. Schmitt, H.-C. Flemming, FTIR-spectroscopy in microbial and material analysis, *International Biodeterioration & Biodegradation*, 41 (1998) 1-11.
- [30] W. Zhou, R. Apkarian, Z.L. Wang, D. Joy, Fundamentals of scanning electron microscopy (SEM), in: *Scanning microscopy for nanotechnology*, Springer (2006) pp. 1-40.
- [31] M.B. Berger, The importance and testing of density/porosity/permeability/pore size for refractories, in: *Proceeding of the Southern African Institute of Mining and Metallurgy Refractories Conference*, (2010) pp. 101e116.
- [32] K.A. Bogdanowicz, S.V. Bhosale, Y. Li, I.F.J. Vankelecom, R. Garcia-Valls, J.A. Reina, M. Giamberini, Mimicking nature: Biomimetic ionic channels, *Journal of membrane science*, 509 (2016) 10-18.
- [33] K.A. Bogdanowicz, P. Sistas, J.A. Reina, M. Giamberini, Liquid crystalline polymeric wires for selective proton transport, part 2: Ion transport in solid-state, *Polymer*, 92 (2016) 58-65.
- [34] R. García, A.P. Báez, Atomic absorption spectrometry (AAS), in: *Atomic Absorption Spectroscopy*, InTech (2012).
- [35] R. Oldenbourg, *Polarized light microscopy: principles and practice*, Cold Spring Harbor Protocols, 2013 pdb. top078600.
- [36] S. Gouws, Electrolysis, in: J.K. Vladimir Linkow (Ed.) *Voltammetric Characterization Methods for the PEM Evaluation of Catalysts*, InTech, 2012.
- [37] I. Ressay, M. Lahcini, A. Belen Jorge, H. Perrot, O. Sel, Correlation between the proton conductivity and diffusion coefficient of sulfonic acid functionalized chitosan and Nafion composites via impedance spectroscopy measurements, *Ionics*, 23 (2017) 2221-2227.
- [38] L. Pasquini, F. Ziarelli, S.p. Viel, M.L. Di Vona, P. Knauth, Fluoride-ionic-conducting Polymers: Ionic Conductivity and Fluoride Ion Diffusion Coefficient in Quaternized Polysulfones, *ChemPhysChem*, 16 (2015) 3631-3636.

- [39] A. Shirdast, A. Sharif, M. Abdollahi, Effect of the incorporation of sulfonated chitosan/sulfonated graphene oxide on the proton conductivity of chitosan membranes, *Journal of Power Sources*, 306 (2016) 541-551.
- [40] M.G. Marino, J.P. Melchior, A. Wohlfarth, K.D. Kreuer, Hydroxide, halide and water transport in a model anion exchange membrane, *Journal of membrane science*, 464 (2014) 61-71.
- [41] L. Pisani, Simple expression for the tortuosity of porous media, *Transport in Porous Media*, 88 (2011) 193-203.
- [42] R.E. Meredith, Tobias, C.W., Conduction in heterogenous systems., in: C.W. Tobias (Ed.) *Advances in Electrochemistry and Electrochemical Engineering 2.*, Interscience Publshers, New York, 1962.
- [43] J.R. Luch, T. Higuchi, L.A. Sternson, Electrical charge conduction mechanism of a polymer membrane electrode selective for hydrophobic cations, *Analytical Chemistry*, 54 (1982) 1583-1588.
- [44] C. Panisello, B. Peña, G. Gilabert Oriol, M. Constantí, T. Gumí, R. Garcia-Valls, Polysulfone/vanillin microcapsules for antibacterial and aromatic finishing of fabrics, *Industrial & Engineering Chemistry Research*, 52 (2013) 9995-10003.
- [45] C.L. Lewis, C.C. Craig, A.G. Senecal, Mass and density measurements of live and dead gram-negative and gram-positive bacterial populations, *Applied and environmental microbiology*, 80 (2014) 3622-3631.
- [46] B. Binks, D. Furlong, *Modern characterization methods of surfactant systems*, CRC Press, 1999.
- [47] G.M. Kontogeorgis, S. Kiil, Surface and Interfacial Tensions-Principles and Estimation Methods, in: *Introduction to Applied Colloid and Surface Chemistry*, John Wiley & Sons, Ltd, (2016) pp. 34-73.
- [48] D.S. Viswanath, T.K. Ghosh, D.H.L. Prasad, N.V.K. Dutt, K.Y. Rani, Theories of viscosity, *Viscosity of Liquids: Theory, Estimation, Experiment, and Data*, Springer Netherlands, Dordrecht, 2007, pp. 109-133.
- [49] G.D. Parfitt, A.L. Smith, Conductivity of sodium dodecyl sulfate solutions below the critical micelle concentration, *The Journal of Physical Chemistry*, 66 (1962) 942-943.
- [50] B.J. Berne, R. Pecora, *Dynamic light scattering: with applications to chemistry, biology, and physics*, Courier Corporation, 2000.

Chapter IV

Physical immobilization by entrapment

4.1. Introduction

Through this thesis work, two types of physical immobilizations of Gramicidin (gA) have been studied. The first approach is discussed in this chapter and consists in direct biomolecule entrapment within the polysulfone matrix. Hydrophobic subunits of gA have high affinity to the fatty acid chains of lipid bilayer. Interior of the folded dimer is filled with water molecules, what allows the ion transport through the channel [1, 2]. Since Psf is a very hydrophobic material, it is a good environment for hydrophobic ion channel immobilization, providing numerous hydrophobic and aromatic interactions. In this Chapter the effect of protein immobilization on membrane morphology using Environmental Scanning Electron Microscope (ESEM) is discussed. Contact angle measurements (CA) and water uptake experiments (WU) were used to assess the influence of gA on the material hydrophobicity and on the wetting properties. Ion transport characterization was evaluated during ion permeability experiments, checking diffusion properties and Current-Voltage measurement, giving information about actual ion transport across the membrane. All the experimental results were additionally examined by means of statistical analysis using Student's t hypothesis test.

4.2. Materials

Polysulfone (Mw 35,000) in transparent pellet form, N,N-Dimethylformamide (DMF, 99 %) used for flat sheet membrane fabrication were purchased from Sigma Aldrich. Gramicidin from *bacillus aneurinolyticus* (*Bacillus brevis*) was purchased from Sigma Aldrich.

4.3. Methods

4.3.1. Entrapment method process optimization

In order to optimize the procedure to immobilize gA, two membrane preparation methods were evaluated: phase inversion/precipitation in water-coagulation bath and phase inversion/precipitation by solvent evaporation.

4.3.1.1. Phase inversion/precipitation in water-coagulation bath

In the first case, polymeric solutions were prepared by dissolving 10^{-7} M; 0.25, 0.5 and 5 wt% of gA in DMF (providing subsequently 10×10^{-7} M, 6×10^{-3} M and 12×10^{-3} M, and 12×10^{-2} M solutions) and afterwards, Psf pellets up to 15 wt% were added. The total amount of gA used was selected according to both being able to observe the effect of protein incorporation into membrane and to avoid eventual aggregates formation. Mixtures were stirred at 300 rpm during at least 12 h at room temperature using a magnetic stirrer. Then, the polymeric solutions were allowed to stabilize for 24 h, without stirring, to remove air bubbles formed. Membranes were obtained by phase inversion precipitation method [3-5] using a casting knife of 200 μm thickness in water as a non-solvent phase.

4.3.1.2. Phase inversion/precipitation by solvent evaporation

In order to ensure that the protein was not flushed out of the membrane, during precipitation in a coagulation bath, solvent evaporation method was also considered. For this purpose, different concentration of gA in Psf solution were prepared and left for observation during 72 hours. The highest concentration at which the phase separation after this time did not occur was selected. In that way, it was pretended to obtain the highest possible concentration immobilized. Polymeric solutions were prepared by dissolving 0.75; 1 or 1.5 wt% of gA in DMF (providing subsequently 4.5×10^{-3} M, 6×10^{-3} M and 9×10^{-3} M solutions)

and afterwards, Psf pellets up to 15 wt% were added. The mixtures were stirred at 300 rpm during at least 12 h at room temperature using magnetic stirrer. Then, the polymeric solutions were allowed to stabilize for 24 h, without stirring, to remove air bubbles formed. Membranes were formed using a casting knife of 200 μm thickness. Polymeric films were left overnight, at room temperature, to allow solvent evaporation.

4.4. Results

After preparation, membranes were characterized in detail, in terms of protein detection and analysis its influence on membrane morphology and hydrophobicity. Probably due to very low content of incorporated Gramicidin, despite the use of variety of different techniques, including FTIR, Raman spectroscopy and X Ray diffraction, the presence of protein have not been detected.

4.4.1. Morphology analysis (SEM and ESEM)

On the pictures below (Figure 4.1.) cross sectional views of the membranes prepared by phase inversion precipitation method in a coagulation bath are presented.

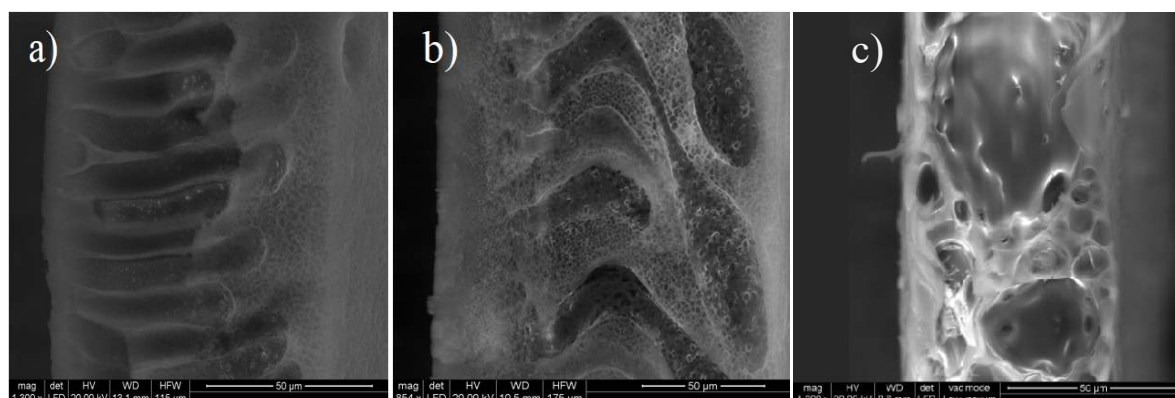


Figure 4.1. Cross-section micrographs of the membranes prepared by phase inversion/precipitation method in a water-coagulation bath, Plain Psf (left), 0.5 wt% of gA (middle) and 5 wt% of gA (right).

As can be observed, in Plain Psf membrane, finger-like pores are clearly formed. After addition of 0.5 wt% of protein, pores deformation is observed. Also, the internal morphology

seems to adjust the sponge-like form. When the Gramicidin content is as high as 5 wt%, the pore structure is permanently lost. This is an effect of phase separation, which appears as microvoids formation. Influence of additives on internal morphology of polysulfone have been reported previously by Conesa et al [6]. As far as phase separation in the 5 wt% membrane is clearly visible, the cause of pore deformation in the case of membrane 0.5 wt% is not unequivocal. In contrast, when in membranes the concentration of protein is very low, finger like pores are not observed at all, and membrane interior has a sponge-like structure, as presented in Figure 4.2.

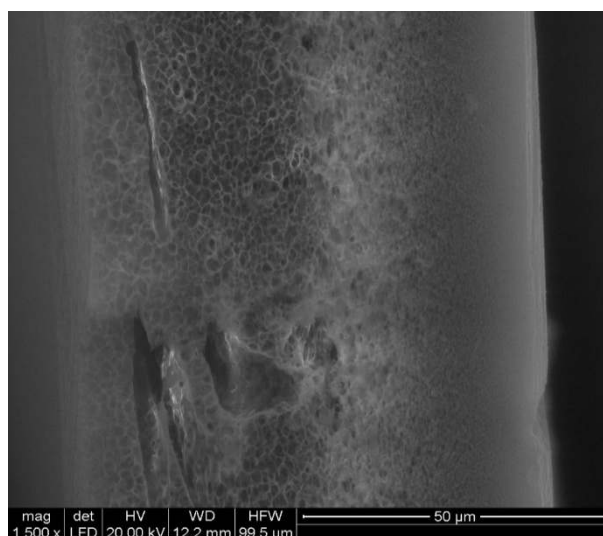


Figure 4.2. Cross-sectional view of the membrane containing 10^{-7} M of gA.

Moreover, as the protein is added, the surface become denser and pores are smaller and rare. In Figure 4.3. top surfaces of the plain Psf membrane and the membrane with the smallest gA content (10^{-7} M) are presented. As it can be concluded from the Table 4.1., the pore size change in the case of these two membranes is not significant, since statistically the pore size change was not demonstrated (p-value 0.55). Nevertheless, membranes containing 0.25 wt% and 0.5 wt% of gA (Figure 4.4.) have significantly bigger pores than Plain Psf membrane (p-values <0.0001).

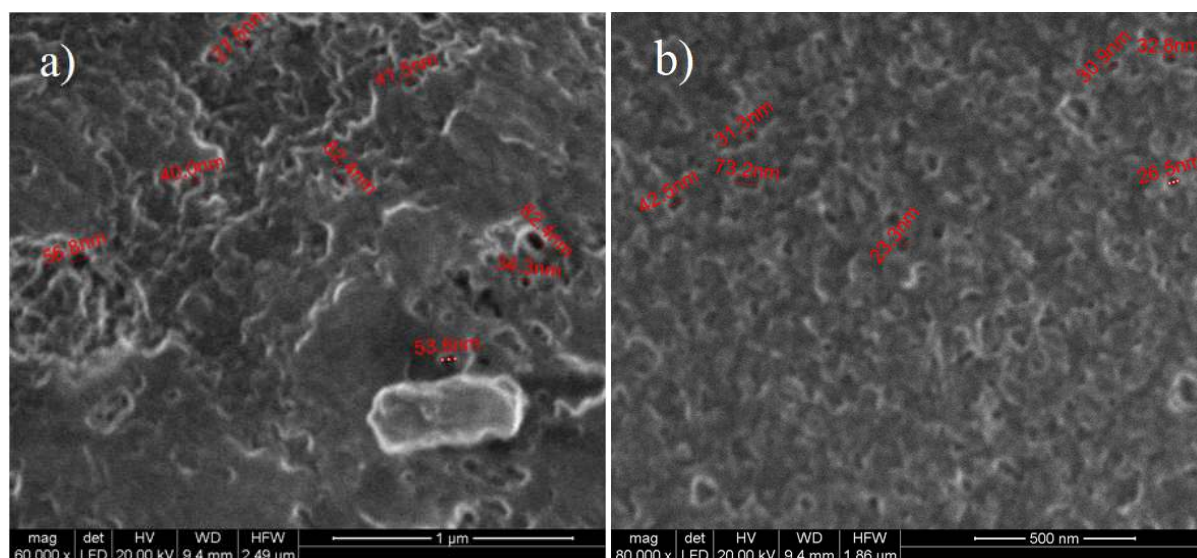


Figure 4.3. Plain polysulfone membrane (a) and Psf/10⁻⁷ M of gA membrane (b) prepared by phase inversion/precipitation method in water-coagulation bath (top surface).

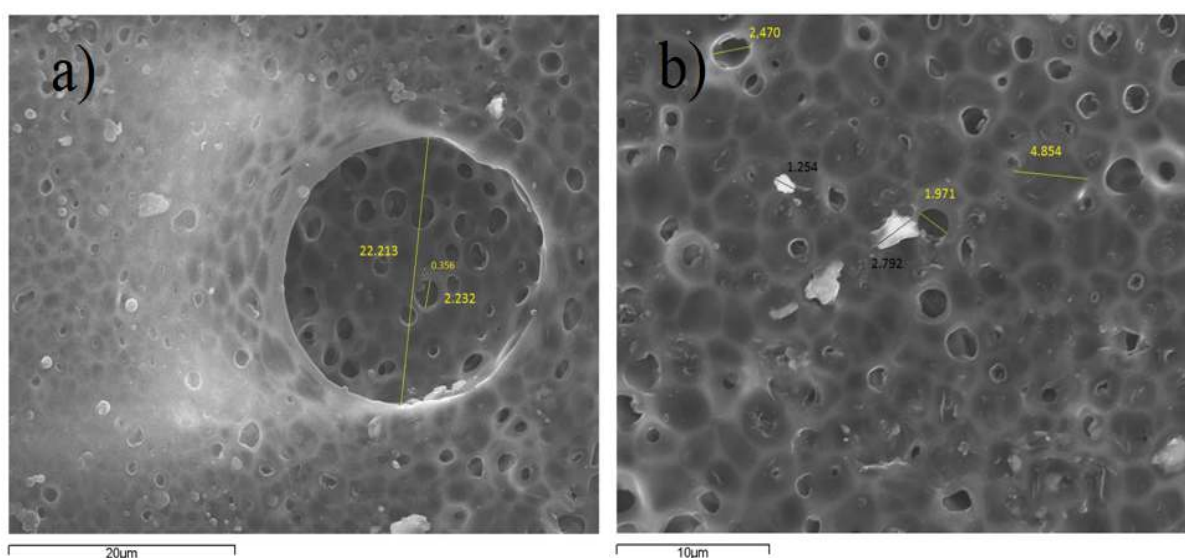


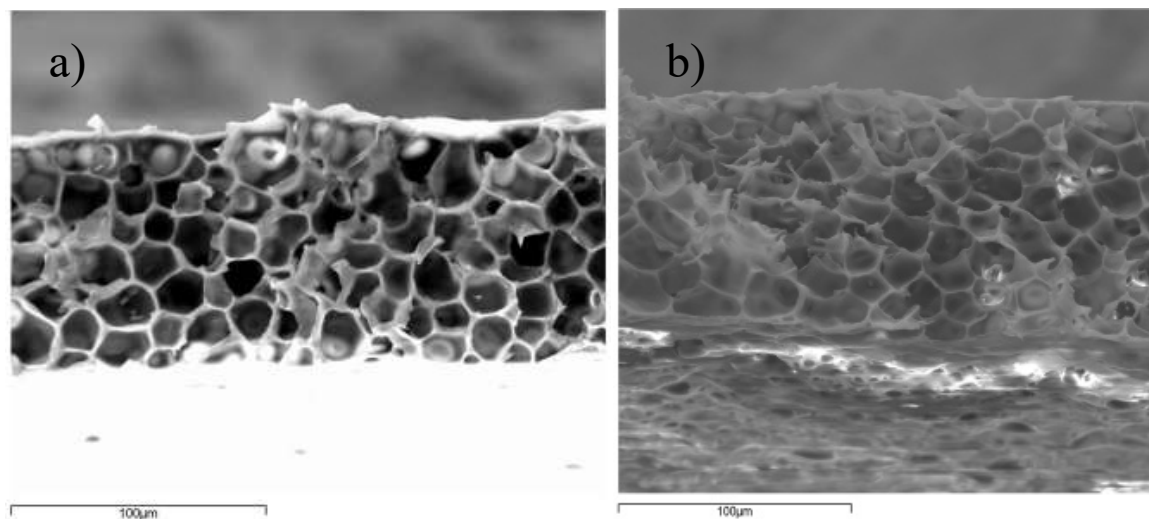
Figure 4.4. SEM micrograph of the top surface of the membrane prepared by phase inversion/precipitation method in water-coagulation bath, with 0.25 wt% (a) and 0.5 wt% of gA content (b).

Table 4.1. Pore sizes of the membranes prepared by phase inversion/precipitation method in water-coagulation bath.

Membrane	Plain Psf	10 ⁻⁷ M gA	Membrane	0.25 wt% gA	0.5 wt% gA
Pore size [nm]	45.14 ± 21.54	37.04 ± 20.48	Pore size [μm]	5.16 ± 3.07	3.12 ± 1.12

Previous studies also show, that addition of additives affect the pores formation in polysulfone membranes [6, 7]. From this result it can be concluded that even a small amount of protein as 0.25 wt% added to the polysulfone polymeric solution influences the membrane morphology by changing pores shape and increasing their size.

SEM micrographs of the membranes prepared by solvent evaporation are presented in Figure 4.5. The pictures of membranes with entrapped gA were compared with the ones of plain Psf membrane. All the membranes present a sponge-like morphology. Collected morphology analysis data of average pore sizes and membranes thickness, performed by ImageJ software, are shown in Table 4.2. It can be noticed, that the final thickness of the films is smaller than 200 μm , as expected. This is a consequence of preparation procedure, in which the casting solution after being distributed on the support, it is not introduced into the coagulation bath immediately, and the solution is let to dry on the air. Thus, the solution is still spilling a little bit, making the final membrane thinner. Very low p-values indicate, that gA immobilization has a significant influence on the membrane pore size. Regarding the membrane thickness, very large p-values state that the protein immobilization does not affect thickness of the membrane.



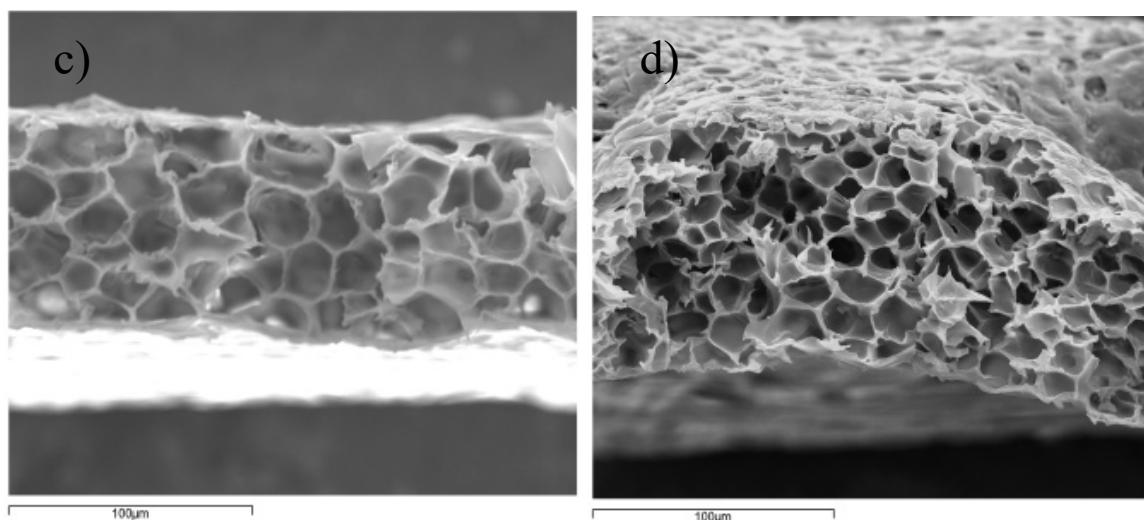


Figure 4.5. SEM cross section micrographs of membranes: a) Plain Psf, b) 0,75 wt% of gA, c) 1 wt% of gA, d) 1,5 wt% of gA in magnification 500x times.

Although a relatively uniform appearance of the film, protein agglomerates were observed on the membrane surface and within the pores (Figure 4.6.). It has been previously reported that gA tends to form aggregates [8, 9] as it is also seen in the present case.

This suggests the occurrence of two phenomena: entrapment within the polymeric matrix and immobilization on the surface (since some of the aggregates are visible on the membrane film). Relatively high protein concentration and probably too fast solvent evaporation result in macromolecular crowding effect, which can cause proteins aggregation [10]. Therefore, instead of obtaining a desired ion channel structure within the polymeric matrix, the gA precipitated on the membrane surface and inside the film.

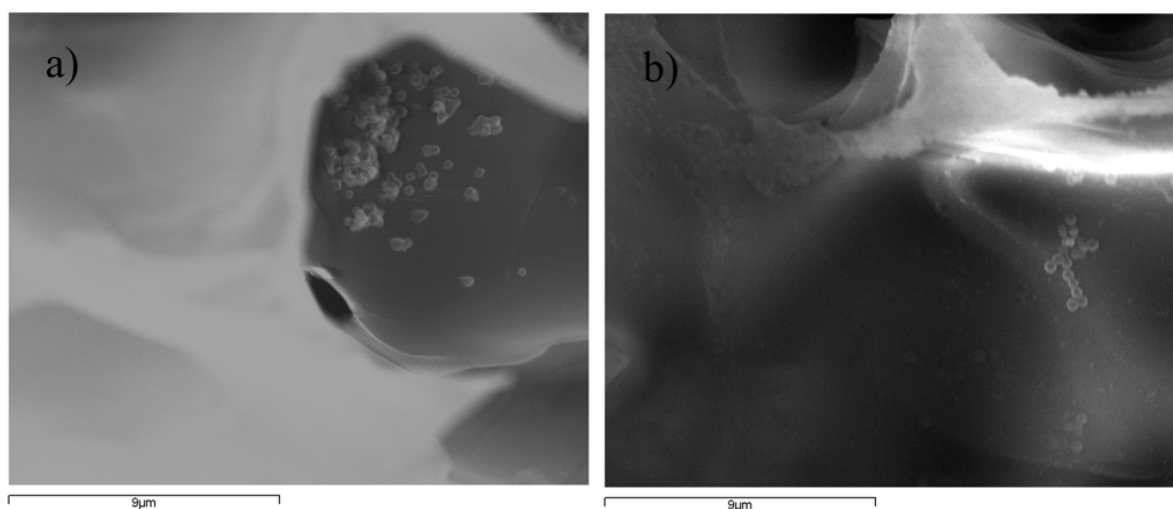


Figure 4.6. SEM micrographs of cross section of membranes: a) Psf/1wt% of gA and b) Psf/0.75 wt% of gA, with visible protein aggregates.

Table 4.2. Pore sizes and thicknesses of the membranes prepared by gA entrapment.

Parameter	Plain Psf	0.75 wt% of gA	1 wt% of gA	1.5 wt% of gA
Average pore size [μm]	22.2 ± 2.2	2.7 ± 2.4	9.0 ± 6.8	11.8 ± 5.4
Membrane thickness [μm]	97.2 ± 6.7	$98.2 \pm 6,9$	95.8 ± 7.1	96.7 ± 9.5

Values of pore sizes and membrane thicknesses are the average of 3 measurements taken from 3 parts of the 3 different membranes.

4.4.2. Contact angle (CA) and Water uptake (WU)

Because of the observed phase separation in the case of membranes prepared in a coagulation bath, only the membranes prepared by solvent evaporation method were further analyzed. Due to the limited sensitivity of the contact angle technique, for the statistical analysis we presumed a difference in CA of at least 5 degrees to be meaningful.

In the case of membranes prepared by solvent evaporation method, addition of gA slightly influence the hydrophobic character of the surface (Table 4.3.). The p-values demonstrate that especially the bottom of the surface was affected by immobilization of gA, and the decrease of CA was at least of 5 degrees. It is probably due to the sedimentation of gA at the bottom of the film, that increases of the concentration in this part of the membrane, which favors protein aggregation. Thus, precipitated gA settled on the bottom surface, what was also visible on the SEM analysis discussed above.

Table 4.3. Contact angle (CA) measurement for membranes prepared by gA entrapment.

Membrane	CA on the top surface	St. dev	p- value	CA on the bottom surface	St. dev.	p- value
Plain Psf	96.1	0.4		96.4	0.6	
Psf/0.75 wt% of gA	91.0	0.9	0.458	87.3	0.7	< 0.0001
Psf/1 wt% of gA	91.1	0.4	0.576	86.0	1.1	< 0.0001
Psf/1.5 wt% of gA	89.5	0.15	< 0.0001	89.0	1.1	0.002

The p-values **below** 0.05 correspond to the samples in which the hydrophilicity change is significant (bolded).

Analyzing the data of the WU experiments (Figure 4.7.), it may be seen that membranes containing protein swells water much slower than pure Psf material. This can be explained by the observed before change in the membrane surface and smaller pore size, which decreases water access. The p-values obtained for membranes 0.75 wt%, 1 wt% and 1.5 wt% of gA were respectively: 0.029; 0.391 and 0.206, what indicates, that only the membrane containing 0.75 wt% of gA has significantly lower water uptake properties, comparing to Plain Psf. However after 24 h, when the membranes are fully saturated with water, among the membranes containing gA it may be we observed that as the content of protein increases, the total amount of absorbed water increases as well (the membrane with 1,5 wt% of gA seems to absorb even more than Plain Psf membrane).

It has been previously reported, that although Gramicidin structure is determined mainly by hydrophobic interactions, water also plays an important role in the protein assembling [11-13]. It confirms that the more gA is entrapped in the membrane, the more water is swelled to form a hydration coat. This result means that the hydrophobic properties of Psf were affected mainly on the surface, but it seems that swelling properties were not affected significantly, when the protein concentration was 1 wt% or 1.5 wt%. The effect of gA on water uptake seems to be present at the lowest protein concentration, what implies, that at higher concentrations, gA is not homogenously distributed in the film and agglomerates, which results in its precipitation, confirmed in SEM analysis. The same weight of dry membranes after experiment suggests that there was no effect of flushing out or protein dissolving.

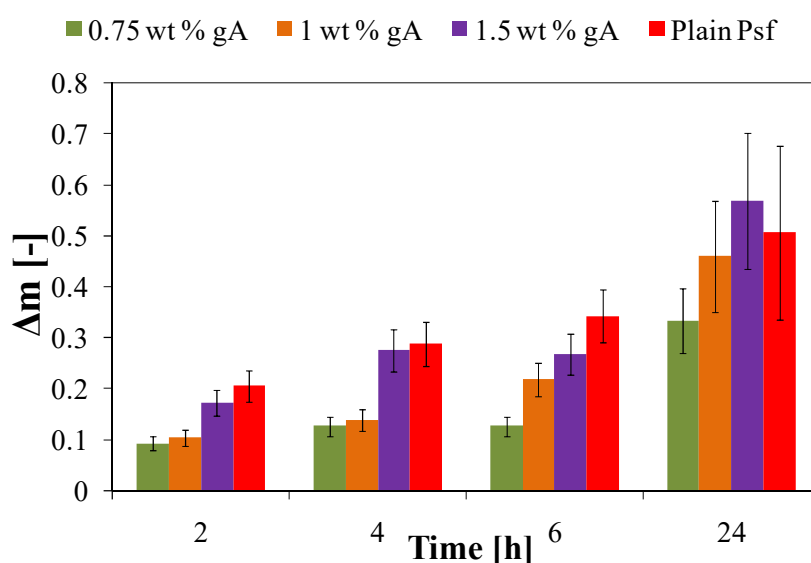


Figure 4.7. Water uptake results for membranes prepared by entrapment. The error bars refers to the standard deviation of the measurements. Values of mg of water absorbed per mg of membrane (Δm) are average of 3 measurements taken from 3 different membranes.

4.4.3. Permeability test

Ionic diffusion was not observed by any membranes. It may be due to the protein influence on internal porosity, since a plain polysulfone membrane prepared within solvent evaporation method presents also sponge-like morphology and does not transport ions. Besides, it could be also caused by very low protein content employed or to the procedure used, not being an appropriate method for gA immobilization.

4.4.4. Current-Voltage measurement (CV)

In order to ensure system stabilization, the membranes were soaked during 5 hours before each analysis. Any significant impact of the distance between the electrodes on the results have not been observed, thus the measurements have been carried out maintaining 1 cm of space between reference electrodes (see Chapter III, section 3.4.1.4.4.). No improvement of ion transport properties in comparison to Plain polysulfone membrane have been registered. Experimental results have shown that resistance does not decrease after Gramicidin immobilization, and its value reach $16,666 \text{ Ohm}\cdot\text{cm}^2$. Besides, in any of the examined cases presence of pseudo- plateau region, characteristic for ion transporting materials have not been observed.

4.5. Conclusions

Membranes prepared by entrapment method were characterized in terms of hydrophobic properties, morphology and ion transport properties. Two methods were evaluated- phase inversion/precipitation in coagulation bath and solvent evaporation. After previous optimization, a proper protein concentration was used and in the case of solvent evaporation, influence on membrane morphology was minimized. Membranes containing Gramicidin are more hydrophobic, and swell more water in comparison to the blank polysulfone, what confirms presence of entrapped protein- what could not be determined by FTIR, Raman or

XRD, probably due to a very low protein content. Nevertheless, in terms of ionic transport, improvement in ion diffusion transport, nor in electrically driven passage through the membrane was neither observed. This can be probably a result of low protein content or bioactivity loss, due to protein aggregation and precipitation, as observed on SEM micrographs.

4.6. References

- [1] J.A. Lundbæk, S.A. Collingwood, H.I. Ingólfsson, R. Kapoor, O.S. Andersen, Lipid bilayer regulation of membrane protein function: Gramicidin channels as molecular force probes, *Journal of The Royal Society Interface*, 7 (2010) 373-395.
- [2] R. Ketchum, W. Hu, T. Cross, High-resolution conformation of Gramicidin A in a lipid bilayer by solid-state NMR, *Science-New York Then Washington-*, 261 (1993) 1457-1457.
- [3] C.F. Fryling, Production of adhesives and adhesive bases from synthetic rubber latex by causing phase inversion with a protective colloid and adding organic solvent, in, *Google Patents*, 1956.
- [4] J.-H. Kim, K.-H. Lee, Effect of PEG additive on membrane formation by phase inversion, *Journal of Membrane Science*, 138 (1998) 153-163.
- [5] M. Mulder, Membrane preparation | Phase Inversion Membranes A2 - Wilson, Ian D, in: *Encyclopedia of Separation Science*, Academic Press, Oxford, 2000, pp. 3331-3346.
- [6] A. Conesa, T. Gumi, C. Palet, Membrane thickness and preparation temperature as key parameters for controlling the macrovoid structure of chiral activated membranes (CAM), *Journal of Membrane Science*, 287 (2007) 29-40.
- [7] C. Mbareck, Q.T. Nguyen, Study of Polysulfone and Polyacrylic Acid (PSF/PAA) Membranes Morphology by Kinetic Method and Scanning Electronic Microscopy, *Journal of Membrane Science & Technology*, 5 (2013) 1.
- [8] T.R. Besanger, J.D. Brennan, Ion Sensing and Inhibition Studies Using the Transmembrane Ion Channel Peptide Gramicidin A Entrapped in Sol-Gel-Derived Silica, *Analytical Chemistry*, 75 (2003) 1094-1101.
- [9] M.R. Hicks, A. Damianoglou, A. Rodger, T.R. Dafforn, Folding and Membrane Insertion of the Pore-Forming Peptide Gramicidin Occur as a Concerted Process, *Journal of Molecular Biology*, 383 (2008) 358-366.
- [10] D. Homouz, L. Stagg, P. Wittung-Stafshede, M.S. Cheung, Macromolecular Crowding Modulates Folding Mechanism of α/β Protein Apoflavodoxin, *Biophysical Journal*, 96 (2009) 671-680.
- [11] T.W. Allen, O.S. Andersen, B. Roux, Energetics of ion conduction through the Gramicidin channel, *Proceedings of the National Academy of Sciences*, 101 (2004) 117-122.

[12] J.A. Killian, B. De Kruijff, Importance of hydration for Gramicidin-induced hexagonal HII phase formation in dioleoylphosphatidylcholine model membranes, *Biochemistry*, 24 (1985) 7890-7898.

[13] M. Poxleitner, J. Seitz-Beywl, K. Heinzinger, Ion Transport through Gramicidin A. Water Structure and Functionality, *Zeitschrift für Naturforschung C*, 48 (1993) 654-665.

Chapter V

Physical immobilization with the use of magnetic nanoparticles (MNP)

5.1. Introduction

MNP are one of the nanomaterials commonly used during recent years in applications like biotechnology, sensors and biomedical devices [1-3]. They are characterized by good thermal and chemical stability, mechanical hardness and low electrical losses [4]. Iron oxide is widespread in nature and easy to obtain. Magnetite nanoparticles are facile to prepare, compare to polymeric nanoparticles, and exhibit good dispersion capability. Moreover, they are reusable and easy to separate [5-7], what makes them much more ecofriendly than e.g. conductive silver nanoparticles, which apart of its potential toxicity are much more expensive [8]. Besides, it is also possible to functionalize them, what provide a variety of immobilization possibilities. In this chapter the effect of protein immobilization (by means of MNP) on the membrane morphology is being analyzed using Environmental Scanning Electron Microscope (ESEM). Contact angle measurements (CA) and water uptake experiments (WU) were used to assess the influence of gA on the material hydrophobicity and on the wetting properties. Ion transport characterization was evaluated by ion permeability experiments, checking concentration driven diffusion properties and by Current-Voltage measurement, what leads information about actual ion transport across the membrane. All the experimental results were additionally examined by means of statistical analysis using Student's t hypothesis test.

5.2. Materials

Polysulfone (Mw 35,000) in transparent pellet form, N,N-Dimethylformamide (DMF, 99 %) used for flat sheet membrane fabrication were purchased from Sigma Aldrich. Gramicidin from *bacillus aneurinolyticus* (*Bacillus brevis*) was purchased from Sigma Aldrich. Salts used for PBS (phosphate buffer saline) preparation and for permeability experiments: sodium chloride, magnesium chloride hexahydrate and potassium chloride were purchased from Sigma Aldrich,

potassium phosphate dibasic trihydrate, disodium hydrogen phosphate dihydrate and calcium chloride dihydrate were purchased from Panreac. Hydrochloric acid $\geq 37\%$ was purchased from Sigma Aldrich. Iron (II) chloride tetrahydrate, Iron (III) chloride hexahydrate, Ammonium hydroxide 25%, Aminopropyltriethoxysilane (APTS) for magnetic nanoparticles (MNP) fabrication were purchased from Sigma Aldrich. Surfactant Triton X-100 (TRX) was purchased from Sigma Aldrich. All solutions were prepared in MiliQ water from Millipore.

5.3. Methods

5.3.1. Immobilization on a magnetic nanoparticles (MNP)

5.3.1.1. MNP preparation

MNP were prepared by iron (II) and iron (III) salts co-precipitation in alkaline solution according to the protocol described by Cruz-Izquierdo et al [9]. A volume of 450 ml of 1M ammonia hydroxide solution was added dropwise to the solution containing 0.72 M FeCl_3 and 0.36 M FeCl_2 salts, at room temperature. The solution was continuously stirred and nitrogen was continuously bubbled during addition of ammonia hydroxide. The obtained black precipitate was separated by centrifugation. The precipitate was washed three times with MilliQ water and twice with Phosphate buffer saline (PBS). The pellets after centrifugation were left to dry in an oven at 60 °C overnight. It was reported that obtained Fe_3O_4 nanoparticles, are covered with hydroxyl groups (-OH) groups, when prepared in the aqueous phase [10-12]. A scheme of the reaction is presented in Figure 5.1.

The next step was the conversion of -OH functionalized nanoparticles, to - NH_2 functionalized ones. With this purpose, 1 ml (per 10 mg of MNP-OH) of 2% Aminopropyltriethoxysilane (APTS) solution in dry acetone was used. As reported, APTS immobilizes directly on the MNP-OH surface through silanization reaction, introducing - NH_2 functional groups (Figure 5.2.). The

APTS solution with MNP-OH was stirred with orbital shaker for 24 h at the temperature of 70° C. After stirring, the resultant brown coloured precipitate was washed again as in the case of MNP-OH, three times with MilliQ water and twice with PBS solution, and left to dry overnight in an oven at 60 °C. The dried precipitate was powdered using an agate mortar and pestle.

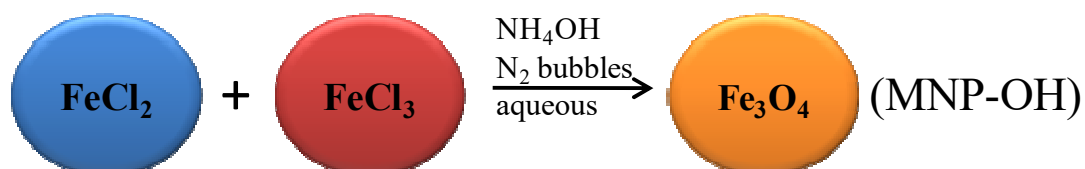


Figure 5.1. Scheme of the reaction of the synthesis of magnetite nanoparticles (Fe_3O_4) from iron salts FeCl_2 and FeCl_3 .

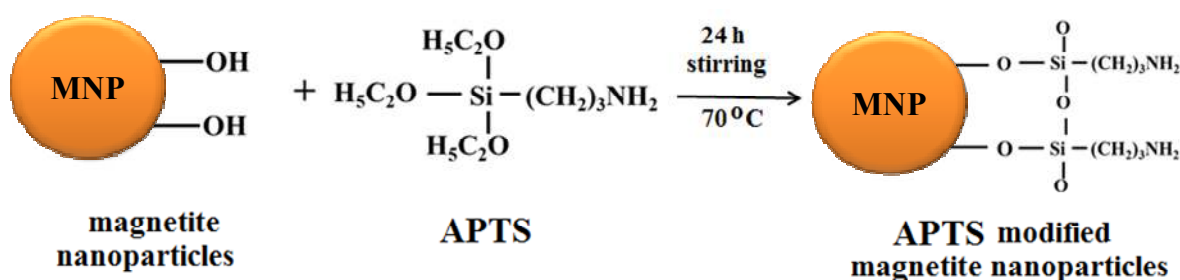


Figure 5.2. Scheme of the MNP-OH functionalization through the silanization reaction with APTS. The products of the reaction are MNPs functionalized with $-\text{NH}_2$ groups.

5.3.1.2. MNP membranes preparation

The first step of this strategy consists of MNP's functionalization with hydrophilic $-\text{OH}$ or $-\text{NH}_2$ groups, and then introducing them to the Psf membrane. This process increases the membrane surface affinity to the surfactant/protein micelles, which are spontaneously forming in the aqueous solutions over the critical micelle concentration (CMC) of the surfactant [13, 14]. It is noteworthy, that gA have been already successfully introduced to the micellar systems [13, 15].

Polymeric solutions were prepared by dissolving 15 wt% of Psf pellets in DMF. The mixtures were stirred at 300 rpm using magnetic stirrer during at least 12 h at room temperature. Afterwards, the polymeric solutions were allowed to stabilize for 24 h, without stirring, to avoid air bubbles formation. After that, 25 wt% of MNP was added to the solution (final weight ratio 1:3 MNP:Psf) and the mixture was sonicated for 10 minutes. Membrane films were prepared using a casting knife with thickness of 200 μm and films were left overnight to evaporate the solvent.

5.3.1.3. TRX treatment

The membranes were immersed in 210 ml of aqueous or phosphate buffer saline (PBS) solution. Both stock solutions (water and PBS) were used in order to check the salts effect on immobilization efficiency. Next, surfactant Triton X100 (TRX) was added. Surfactant concentration was 0.29 mM, which is the range of critical micelle concentration (CMC) [16]. Surfactants, as they reach their CMC, start to spontaneously self-associate into micelles, what is expected also in this case. Samples were stirred during 72 h at 300 rpm using magnetic stirrer, at room temperature. This treatment was performed in order to study the effect of surfactant micelles immobilization, without gA entrapped inside, on membrane performance. To avoid confusion, from now on, the term “TRX treatment” will be used to refer to this modification.

5.3.1.4. TRX/gA micelles immobilization

Protein was immobilized by immersing the membranes in an aqueous or phosphate buffer saline (PBS) solution, similarly as in the case of TRX treatment. Next, TRX and gA were added. Surfactant concentration was 0.29 mM. Izquierdo et. al have reported that activity of enzyme immobilized on MNP is maintained, when the concentration does not exceed 0.4 mg protein/mg of MNP. When the concentration is higher, protein forms aggregates and precipitates, loosing activity [9]. Thus, added gA quantity was calculated according to the amount of MNP in the membrane, and it was always 0.4 mg protein to 1 mg of MNP. That means that to prepare a

membrane with a weight of 200 mg that contains 50 mg of MNP, 20 mg of gA was used. Samples were stirred during 72 h at room temperature. This treatment aimed to immobilize TRX/gA micelles on the membrane surface and from now on will be referred as TRX/gA micelles immobilization.

5.3.2. Plain Psf membrane modification

Permeability tests, were designed in order to check if the MNP's improves the TRX treatment and TRX/gA micelles immobilization efficiency, as well as transport properties. Also, one set of Plain Psf membranes (without MNP) was modified using TRX treatment and TRX/gA micelles immobilization for comparison. A Table with all the membranes prepared and tested in this investigation is shown below (Table 5.1.).

Table 5.1. List of all the membranes used in this investigation and characterization performed.

Membranes prepared by TRX treatment and TRX/gA micelles immobilization method				
Stock solution	Base material	No.	Membrane	Performed tests
H ₂ O	Psf membranes:	1	Plain Psf	permeability test
		2	Psf/TRX	permeability test
		3	Psf/TRX/gA	permeability test
	MNP-NH ₂ membranes:	4	MNP-NH ₂	SEM, CA, WU, permeability test, CV
		5	MNP-NH ₂ /TRX	SEM, CA, WU, permeability test, CV
		6	MNP-NH ₂ /TRX/gA	SEM, CA, WU, permeability test, CV
	MNP-OH membranes:	7	MNP-OH	SEM, CA, WU, permeability test CV
		8	MNP-OH/TRX	SEM, CA, WU, permeability test, CV
		9	MNP-OH/TRX/gA	SEM, CA, WU, permeability test, CV
PBS	Psf membranes:	10	Plain Psf	permeability test
		11	Psf/TRX	permeability test
		12	Psf/TRX/gA	permeability test
	MNP-NH ₂ membranes:	13	MNP-NH ₂	SEM, CA, WU, permeability test, CV
		14	MNP-NH ₂ /TRX	SEM, CA, WU, permeability test, CV
		15	MNP-NH ₂ /TRX/gA	SEM, CA, WU, permeability test, CV
	MNP-OH membranes:	16	MNP-OH	SEM, CA, WU, permeability test, CV
		17	MNP-OH/TRX	SEM, CA, WU, permeability test, CV
		18	MNP-OH/TRX/gA	SEM, CA, WU, permeability test, CV

5.3.3. Characterization methods

5.3.3.1. Morphology analysis (ESEM)

Surface and cross-sectional morphologies of membranes with MNP before and after TRX/gA micelles immobilization were observed at 20 kV with high-vacuum ESEM FEI Quanta 600 apparatus, without sputter coating. Membrane cross-sections were prepared by fracturing in liquid nitrogen. The images were analysed with ImageJ software to observe the effect of protein immobilization on pore size and membrane thickness. Values of pore sizes and membrane thicknesses are the average of 3 measurements taken from 3 membranes prepared with the same experimental conditions.

5.3.3.2. Contact angle (CA)

Static Contact Angle analysis was performed on a Dataphysics OCA15EC contact angle analyzer with MiliQ water as testing liquid. The angle was measured immediately after the drop (3 μm) was released on membrane's surface. Measurements were repeated 5 times on different areas of 3 different membranes prepared under the same experimental conditions.

5.3.3.3. Water uptake (WU)

Membranes were weighted before and after 2, 4, 6 and 24 h of water immersion, in order to ensure complete saturation with the solvent. The surface water drops were removed from wet membranes with the use of filter paper and the mass was measured immediately. Then the membranes were dried in the oven (Nabertherm L9/12/P330) at the temperature of 100° C for 24 h, and weighted. The water uptake was calculated as a difference between the wet membrane mass and dry membrane mass and expressed as mg of water gain per mg of the membrane.

Experiments were repeated 3 times for each membrane prepared under the same experimental conditions.

5.3.3.4. Permeability test

Ion diffusion experiments were performed in the system described in Chapter III, section 3.4.1.4.1. For all experiments performed, initial feed solution was 0.1 M HCl aqueous solution and stripping solutions tested were 0.1 M aqueous electrolyte solutions: NaCl, KCl, MgCl₂, CaCl₂ or pure MiliQ water. The ion transport was monitored by pH change of stripping solution. The pH of the stripping solution was measured every 10 s by an Orion Dual Star pH/ISE Multimeter. From the pH change slope, ion diffusion coefficient and permeability were calculated according to the procedure described in Chapter III, section 3.4.1.4.1.

5.3.3.5. Atomic Absorption Spectrometry (AAS)

Magnesium content in selected solutions before and after permeability test was determined by flame emission spectrometry (Perkin Elmer 3110 spectrometer). To accomplish this, standard solutions of MgCl₂ were prepared to establish the regression model between the emission intensity of the solutions and their metal content expressed in ppm (mg/L). Then, the magnesium concentration values expressed in mol/L were determined by AAS.

5.3.3.6. Polarized Optical Microscope (POM)

Surfaces of the samples after the permeability experiment were observed with an Axiolab Zeiss optical microscope.

5.3.3.7. Current-Voltage measurement (CV)

Current-voltage (CV) measurements were performed using Autolab PGstat100 in potentiostatic mode with current ranging (automatic) from 100 mA to 100 μ A, potential range from 0 V to 5 V, with the step of 0.01 V and scan rate 0.01 V/s. The distance between the reference electrodes (Ag/AgCl) and membrane was 1 cm. The solution volume in each compartment was 200 ml. Tested solutions were 0.1 M concentrated HCl, NaCl, KCl, MgCl₂ and CaCl₂. The measurements were performed at the ambient temperature (24 \pm 1°C).

5.3.3.8. Self-diffusion coefficient calculation

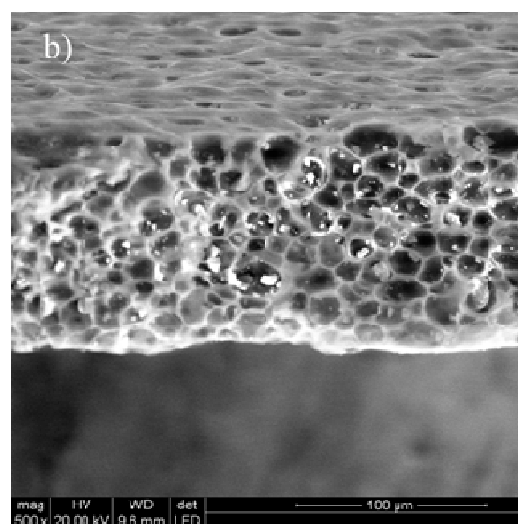
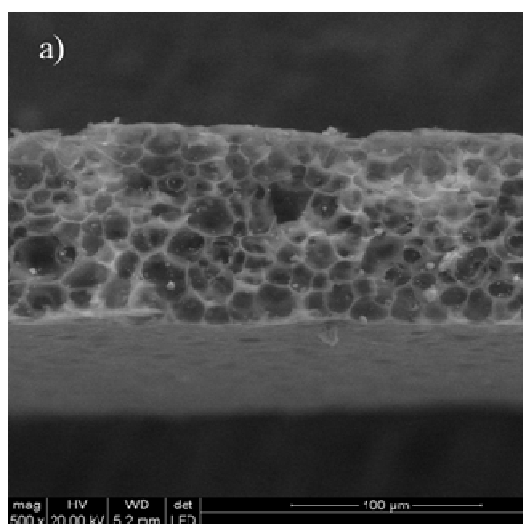
The self-diffusion coefficient of ions in the membranes was calculated from conductivity values obtained from CV measurements. Exact procedure is described in Chapter III, section 3.4.1.4.5.

5.4. Results

5.4.1. Morphology analysis (ESEM)

ESEM micrographs of the membranes are presented in Figure 5.3. As it can be seen in the Figure, all the membranes here investigated present a sponge-like morphology. Collected morphology analysis data of average pore sizes and membranes thickness, performed by ImageJ software, are shown in Table 2. It can be noticed, that the final thickness of the films is smaller than 200 μ m. This is a consequence of preparation procedure, in which the casting solution after being distributed on the support, it is not introduced to the coagulation bath but the solution is let to dry on air. Thus, the solution is still spilling a little bit, making the final membrane thinner. It has been previously reported that gA tends to form aggregates [17, 18]. However in this case, the

presence of protein agglomerates was not observed, what suggests that gA could be very well and homogeneously dispersed within the micelles. Pictures taken after TRX/gA micelles immobilization look similar to the ones taken before (Figure 5.3.). Although some particles can be seen in both MNP and MNP/TRX/gA membranes, their size is definitely too big to be protein precipitates. Thus, we suppose that it corresponds to MNP, which are not homogeneously distributed within membrane, and form big agglomerates of nanoparticles of micrometric size. Membranes with -OH functionalized MNP seems to have smaller pores than membranes with -NH₂ functionalized MNP. After TRX/gA immobilization, in both MNP membranes formulations, the pore size and the membrane thickness remain unaffected, what is indicated statistically (difference is not significant according to the p-value).



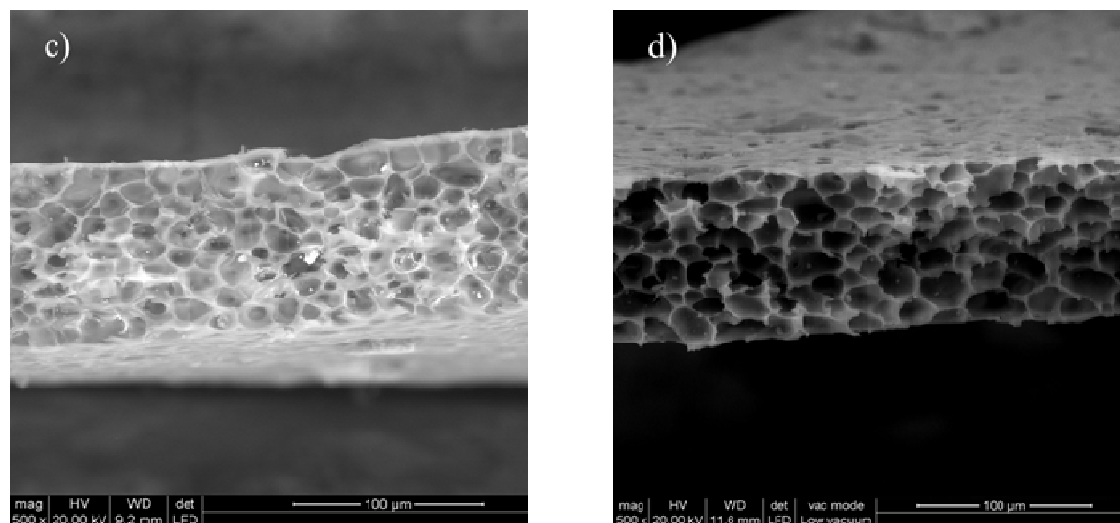


Figure 5.3. ESEM micrographs of cross sections in magnification x500: a) MNP-NH₂, b) MNP-NH₂/TRX/gA, c) MNP-OH, d) MNP-OH/TRX/gA membranes, with visible particles.

Table 5.2. Pore sizes and thicknesses of membranes prepared before and after TRX/gA immobilization.

Parameter	MNP-NH ₂	St.dev.	MNP-NH ₂ /gA	St.dev.	p-value	MNP-OH	St.dev.	MNP-OH/gA	St.dev.	p-value
Average pore size [µm]	30.9	11	23.5	8.9	0.416	20.2	6.1	15.6	7.3	0.639
Membrane thickness [µm]	104.7	16.9	110.9	20.7	0.708	99.5	10.2	94.7	12.6	0.635

Values of pore sizes and membrane thicknesses are the average of 3 measurements taken from 3 membranes prepared under the same experimental conditions. For the statistical evaluation, the following *null hypothesis* were made: (i) the pore size of the MNP membranes before TRX/gA immobilization is different than the pore size of the membranes after immobilization (ii) the thickness of MNP membranes before TRX/gA immobilization is different than the thickness of membranes with immobilized TRX/gA. The p-values **below** 0.05 are in agreement with those hypotheses (none of them).

5.4.2. Contact angle (CA) and Water uptake (WU)

It has been previously reported, that although Gramicidin structure is determined mainly by hydrophobic interactions, water also plays an important role in the protein assembling [19-21]. Thus, in order to extract more information about hydrophilic/hydrophobic properties of the membrane systems, the results of contact angle measurements and water uptake test will be discussed together. Due to the limited sensitivity of the method, for the statistical analysis we presumed a difference in CA of at least 5 degrees to be meaningful.

Results of contact angle are shown in Table 5.3. MNP-NH₂ membranes, after TRX treatment and after TRX/gA micelles immobilization, when prepared in water solution do not exhibit significant change of hydrophilicity (82.4, 81.1 and 86.9 subsequently for untreated, TRX treated and TRX/gA treated membrane). However, when the modification is performed in PBS buffer environment, MNP-NH₂ membrane became more hydrophilic (from 83.3 for untreated membrane, to 78.4 and 69.9 for TRX and TRX/gA treated, subsequently), what is supported also by low p-values. That could suggest that membranes stored in water have higher affinity to interact with non-micellized surfactant (very low increase in hydrophobicity, caused by attaching hydrophilic head of surfactant and leaving on the surface hydrophobic tie), while after storage in PBS, micelles are more attracted to the surface (hydrophilicity increase is caused by hydrophilic nature of the micelles, which have hydrophobic core and fully hydrophilic shell).

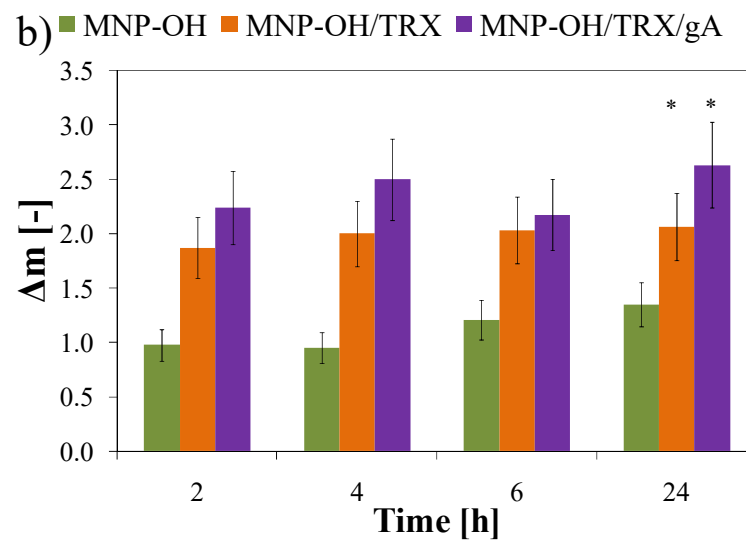
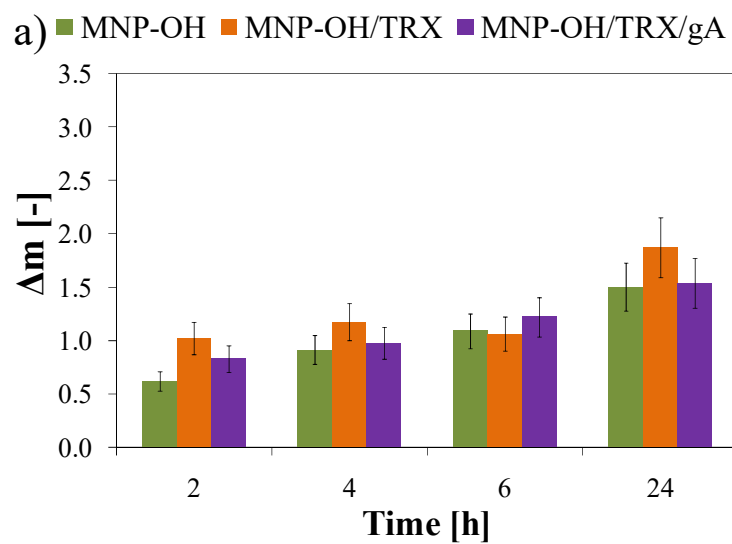
In the case of MNP-OH membranes, in both stock solutions, after TRX treatment, the membranes hydrophobicity increases from 73.3 to 80.7 (very low p-values). Nevertheless, after TRX/gA micelles immobilization, membranes recover their hydrophilicity (75.1). This can suggest that in aqueous environments, OH groups of MNP's interact stronger with the non-micellized surfactant, but when TRX/gA micelles are present, MNP-OH immobilize them on the surface. Those data are in complete agreement with the data of water uptake experiment, which present the general trend, that more hydrophilic membranes after TRX treatment or TRX/gA micelles immobilization swell water faster and more than hydrophobic ones (Figure 5.4.). Only for the MNP-OH membrane modified in water solution, this tendency was not statistically demonstrated, giving a p-value higher than 0.05 (0.051 and 0.071 after TRX treatment and after

TRX/gA micelles immobilization, respectively), as shown in Table 5.4. Much lower p-values of other membranes states that amount of water absorbed by membranes after TRX treatment or after TRX/gA micelles immobilization is significantly different than the amount of water absorbed by non-modified membranes.

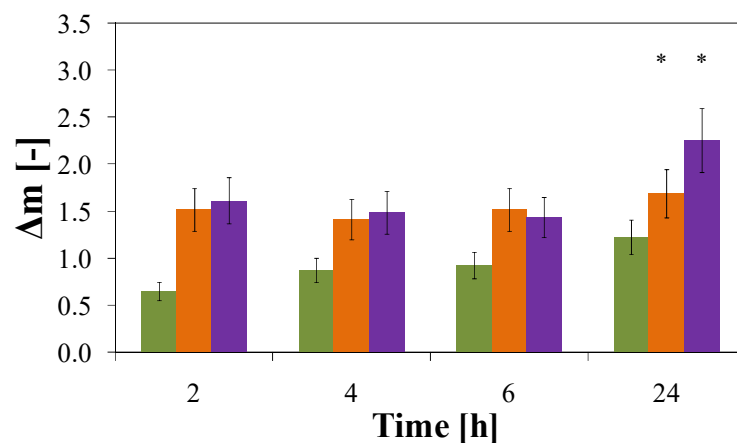
Table 5.3. Results of contact angle (CA) measurement for MNP membranes.

Membrane	Preparation solution	CA on the top surface	St. dev.	p-value	CA on the bottom surface	St. dev.	p-value
MNP-NH ₂	H ₂ O	82.4	1.1	0.997	78.3	0.3	0.997
MNP-NH ₂ /TRX		81.1	0.6		75.2	1.1	
MNP-NH ₂ /TRX/gA		86.9	1.4		82.1	0.4	
MNP-NH ₂	PBS	83.3	0.3	0.592	80.8	1.2	0.001
MNP-NH ₂ /TRX		78.4	0.7		69.1	0.9	
MNP-NH ₂ /TRX/gA		69.9	1.2		69.4	1.1	
MNP-OH	H ₂ O	73.3	0.7	0.003	73.1	0.6	0.006
MNP-OH/TRX		80.7	0.4		80.6	0.9	
MNP-OH/TRX/gA		75.1	0.9		73.1	0.6	
MNP-OH	PBS	61.9	0.4	0.0001	48.9	1.1	0.0001
MNP-OH/TRX		83.8	0.7		79.8	0.8	
MNP-OH/TRX/gA		68.4	0.8		65.8	1	

Values of contact angle are the average of 5 measurements taken from 3 parts of the 3 membranes prepared at the same experimental conditions. For the statistical evaluation, the following hypothesis was made: (i) the CA of the non-modified MNP membrane is more than 5 degrees different from the CA of modified membranes (whether MNP/TRX or MNP/TRX/gA). The p-values **below** 0.05 correspond to the samples which are in agreement with this assumption (the samples which does not exhibit a significant change in CA are bolded).



c) ■ MNP-NH₂ ■ MNP-NH₂/TRX ■ MNP-NH₂/TRX/gA



d) ■ MNP-NH₂ ■ MNP-NH₂/TRX ■ MNP-NH₂/TRX/gA

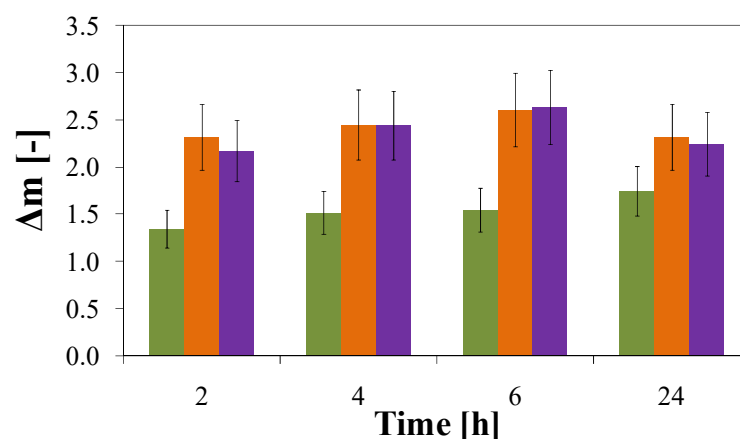


Figure 5.4. Water uptake experiment results for MNP membranes: MNP-OH membranes prepared in H₂O (a) and in PBS (b). MNP-NH₂ membranes prepared in H₂O (c) and in PBS (d). Values of mg of water absorbed per mg of membrane (Δm) are average of 3 measurements taken from 3 different membranes. The error bars refers to the standard deviation from the measurements. Columns highlighted with * refers to the samples for which obtained p-value was <0.05 . The hypothesis in this case was: the amount of water absorbed by membranes after TRX treatment or after TRX/gA micelles immobilization is different than amount of water absorbed by non-modified membrane. Values below 0.05 are in agreement with this hypothesis.

Table 5.4. Statistical analysis performed for WU experiments corresponding to MNP membranes.

Membrane	Preparation solution	After TRX treatment p-value	After TRX/gA immobilization p-value
MNP-NH ₂	H ₂ O	0.017	0.018
	PBS	0.018	0.018
MNP-OH	H ₂ O	0.051	0.073
	PBS	0.013	0.014

For the statistical evaluation, the following *null hypothesis* was made: (i) the amount of water absorbed by membranes after TRX treatment or after TRX/gA micelles immobilization is different than amount of water absorbed by non-modified membrane. The p-values **below** 0.05 correspond to the samples which are in agreement with this assumption (the values for which there is no significant difference are bolded).

5.4.3. Permeability tests

MNP membranes (after TRX treatment and after TRX/gA immobilization) were analyzed in order to study both the surfactant treatment and the protein immobilization effect on the membrane performance. Influence of bulk preparation solution (whether water or PBS) on treatment efficiency was also studied. Plain Psf membranes modified in the same way as MNP membranes, were tested in order to evaluate the treatment efficiency when the membrane does not contain hydrophilic MNP's.

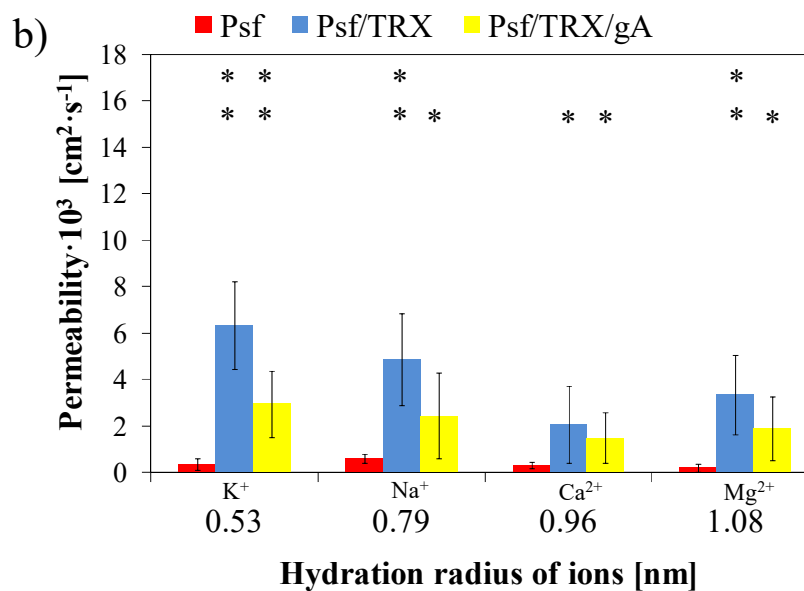
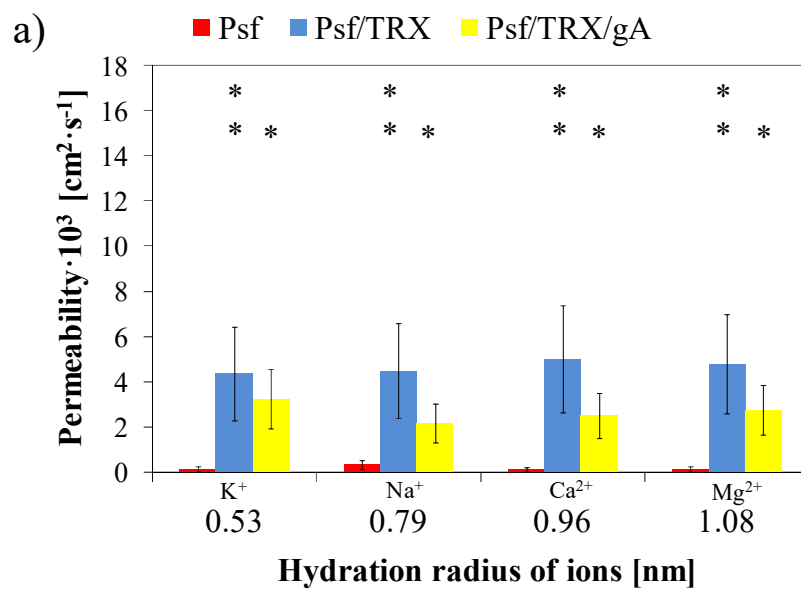
The influence of Triton X100 (TRX) on the water flux properties of the polymeric membranes, has been previously reported, and it was found, that treatment with surfactant significantly enhances water passage through the polymeric membranes [22-25]. Since the water flux is expected to increase after treatment with Triton solution, the overall ion passage is going to increase as well. Since TRX treatment, as well as TRX/gA micelles immobilization, imply interaction of membrane surface with surfactant, we expect both modifications to improve ion permeability. Figure 5.5. shows the values of ion permeability for Psf and MNP membranes, in

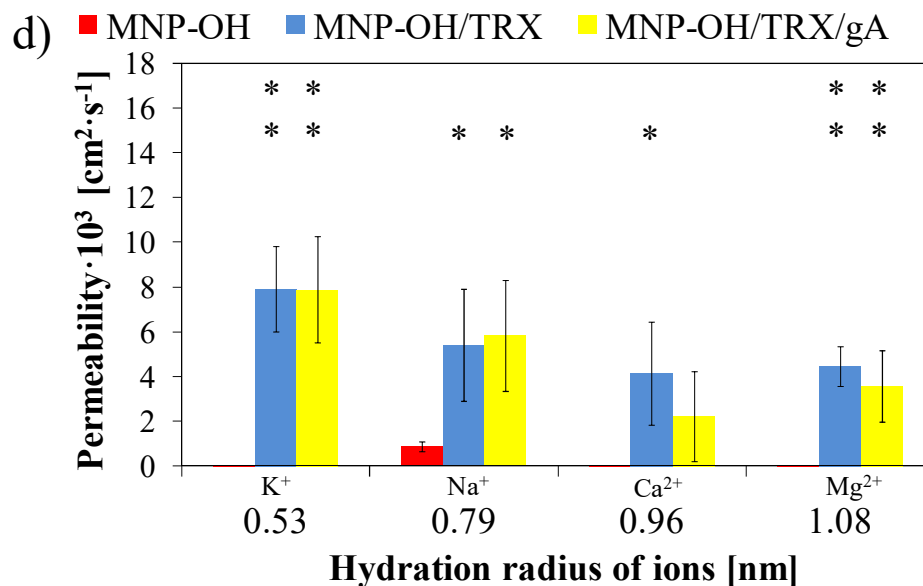
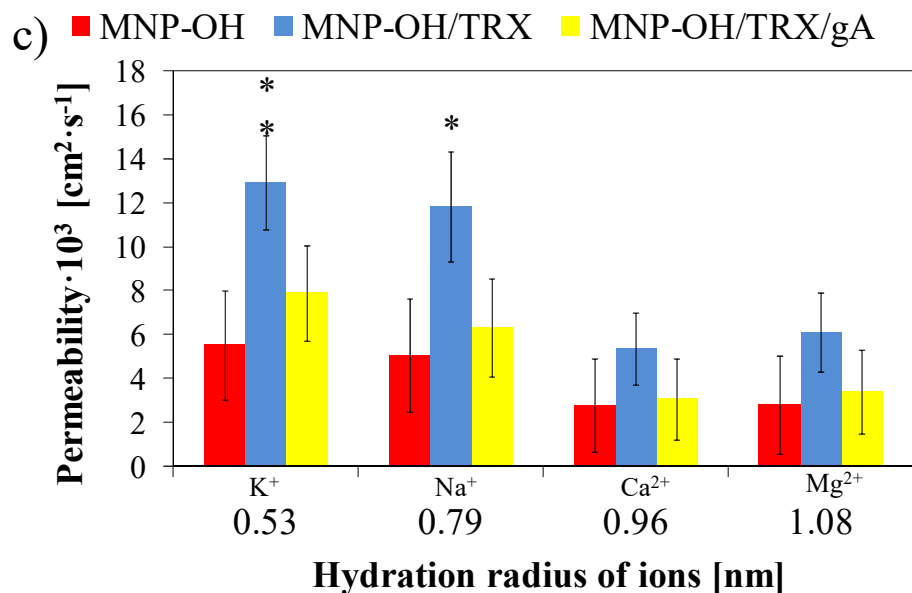
regards with the increment on the hydration radius. The statistical results enclosed in the Table 5.5. confirm that almost all the experiments are in agreement with above *hypothesis*, presenting very low p-values (below 0.05). This effect is more visible in the case of the treatment performed in PBS solution environment (very low p-values). A similar behaviour, related to increase of hydrophilicity, was also observed during CA measurements (Section 5.4.2). Because Triton X100 is a non-ionic surfactant, its interactions with salts are minimized. Thus, it is probably, that the ions of the PBS buffer are getting entrapped within the immobilized micelles, which causes stronger interactions with tested electrolytes. In consequence, for MNP-NH₂ membranes an increase of ion flux, when the stock preparation solution was PBS (e.g. from 3.55E-03 to 7.83E-03 cm²·s⁻¹ for Na⁺ and from 6.83E-03 to 1.42E-02 cm²·s⁻¹ for K⁺ after TRX treatment) has been observed.

The same tendency was registered after modification of Plain Psf membrane (an increase from 4.4E-03 to 4.9E-03 cm²·s⁻¹ for Na⁺ and 4.38E-03 to 6.33E-03 cm²·s⁻¹ for K⁺ after TRX treatment), but in the case of MNP-OH membrane this effect was not noticed and permeability values were higher when the membranes were prepared in water (1.82E-02 cm²·s⁻¹ in water and 5.4E-03 cm²·s⁻¹ in PBS in the case of Na⁺ and 1.29E-02 cm²·s⁻¹ in water and 7.91E-03 cm²·s⁻¹ in PBS in the case of K⁺ ion after TRX treatment). One of the explanation for this behaviour could be stronger hydrophilic nature of –OH group in comparison to –NH₂, what causes better transport performance in pure aqueous environment, without saline interferences. Ion diffusion, kinetics can be influenced by several factors, such as, temperature, ion mobility, ionic radius or hydration radius [26]. Generally, for MNP membranes, permeability decreases in the order K⁺>Na⁺>Ca²⁺; then, it slightly increases with the hydration ratio of Mg²⁺ ion. One of the explanations for this observation can be the very small size of non-hydrated Mg²⁺, which in this case, has visible impact on permeability. For Plain Psf membrane, although the ion flux significantly increases after TRX treatment and TRX/gA micelles immobilization, selective behaviour is not clearly highlighted. After TRX/gA micelles immobilization on Psf membrane, a decrease of permeability comparing to the membrane after TRX treatment (e.g. from 4.9E-03 to 2.43E-03 cm²·s⁻¹ for K⁺ in PBS and from 4.49E-03 to 2.17E-03 cm²·s⁻¹ in water for Na⁺) is detected. This could be a consequence of losing interactions between membrane and surfactant when the protein is present, due to the lack of hydrophilic groups in the Plain membrane.

For both types of MNP membranes (-OH and -NH₂ functionalized), ion permeability values are higher in comparison to the Plain Psf membranes. This may be the result of successful introduction of hydrophilic functional groups to the membrane surface, what enhances interaction with surfactant micelles. In the case of MNP-OH membrane, decrease of permeability after TRX/gA micelles immobilization, comparing to membrane after TRX treatment, is also observed (except for the 2 smallest ions, for the membrane prepared in PBS, where the permeability values are similar, Figure 5.5. d). It could be an effect of losing interactions with micelles, like in the case of Psf membrane. However, the selective behaviour to the smallest ions (monovalent K⁺ with hydration radius 0.53 nm and Na⁺ with hydration radius 0.79 nm) suggests, that interaction with entrapped gA occurs. The same tendency is visible for MNP-NH₂ membrane. When prepared in water solution, the transport of smaller ions seems to increase even more, comparing to membrane after TRX treatment. It is worth to mention, that also before the immobilization of TRX/gA micelles, MNP membranes seems to contribute to membrane selectivity, and thus, observed results probably combine this effect with influence of immobilized gA. The actual ion transport occurring within the modified membranes is probably a combination of a few mechanisms, like free diffusion through the water channels in the membrane pores, or through the central ion channel, which has been previously reported in other cases of immobilization [27, 28].

It can be stated that efficiency of membrane treatment depends also from the composition of the bulk solution used during preparation. Interactions between surfactant micelles are stronger when the membranes are prepared in PBS solution in the case of MNP-NH₂. On the other hand, in the case of MNP-OH membranes, the treatments are more efficient in water environment (probably due to the nature of -OH group, which has higher affinity to water comparing to -NH₂ group). Above all, it may be concluded, that both types of MNP membranes, enhance interaction with Triton, due to its hydrophilic functional groups, and also improve TRX/gA micelles immobilization efficiency. Observed ion diffusion velocity of TRX treated membranes is higher comparing with the membrane containing TRX/gA micelles. Nevertheless, it proves the presence of ionic interactions with immobilized protein. Decrease of membrane permeability after protein immobilization was also reported previously [29, 30].





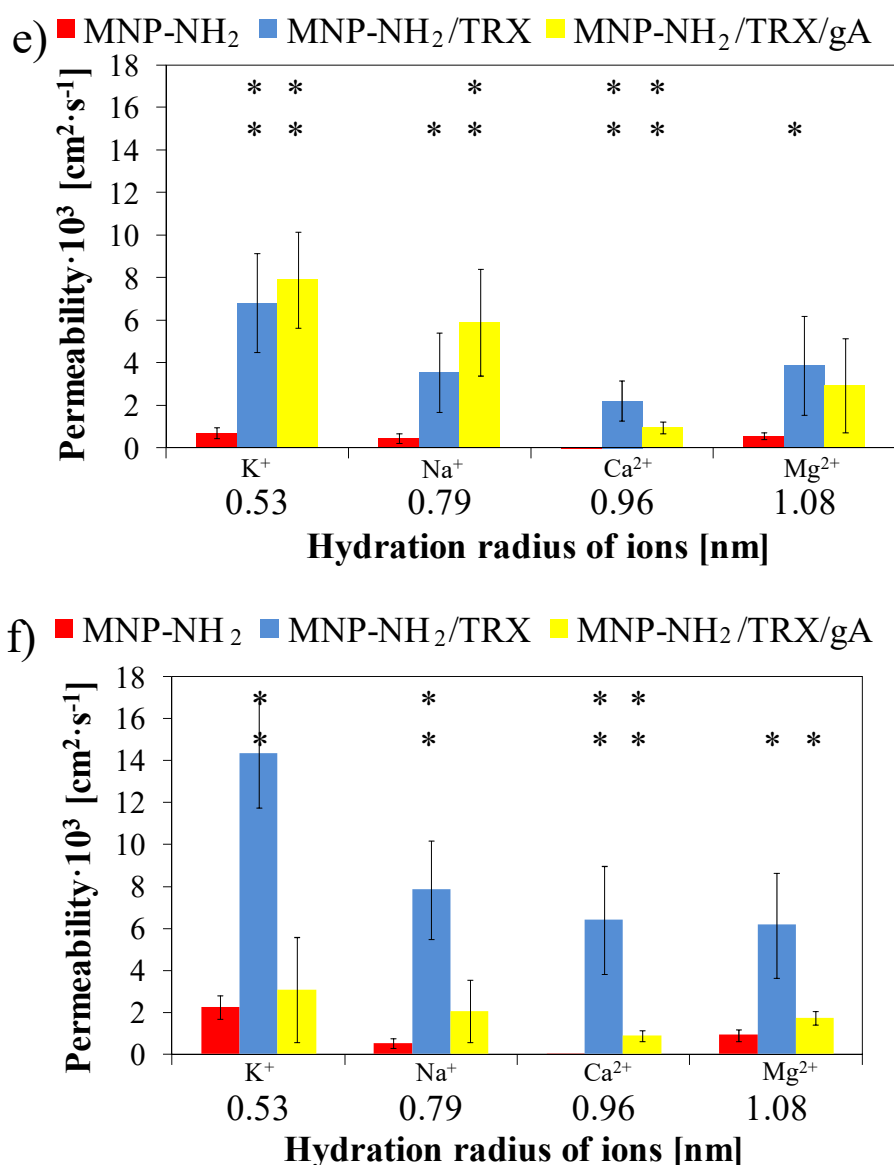


Figure 5.5. Permeability test results in respect to the hydration radius of ions K⁺, Na⁺, Ca²⁺ and Mg²⁺ respectively [31, 32] for Psf membranes: Plain Psf prepared in H₂O (a) and in PBS (b), MNP-OH prepared in H₂O (c) and in PBS (d), MNP-NH₂ prepared in H₂O (e) and in PBS (f). Values of permeability are average of 3 measurements taken from 3 different membranes prepared under the same experimental conditions. The error bars refers to the standard deviation from the measurements. Columns highlighted with * refers to the samples for which obtained p-value was <0.05, with ** refers to the samples for which p-value was <0.01. For the statistical evaluation, the following hypothesis was made: (i) the permeability value of membranes after TRX treatment or after TRX/gA micelles immobilization is different than permeability value of non-modified membrane. The p-values **below** 0.05 correspond to the samples which are in agreement with this assumption.

Table 5.5. Statistical analysis performed for permeability tests for Plain Psf and MNP membranes.

Membrane	Preparation solution	K ⁺	p-values		
			Na ⁺	Ca ²⁺	Mg ²⁺
Psf/TRX	H ₂ O	0.003	0.004	0.003	0.003
Psf/TRX/gA		0.012	0.033	0.016	0.028
Psf/TRX	PBS	< 0.001	0.003	0.039	0.006
Psf/TRX/gA		0.006	0.048	0.037	0.025
MNP-OH/TRX	H ₂ O	0.009	0.015	0.085	0.059
MNP-OH/TRX/gA		0.139	0.276	0.433	0.375
MNP-OH/TRX	PBS	0.001	0.017	0.018	0.001
MNP-OH/TRX/gA		0.002	0.013	0.063	0.009
MNP-NH ₂ /TRX	H ₂ O	0.005	0.022	0.007	0.035
MNP-NH ₂ /TRX/gA		0.003	0.010	0.002	0.069
MNP-NH ₂ /TRX	PBS	0.001	0.003	0.006	0.011
MNP-NH ₂ /TRX/gA		0.301	0.078	0.002	0.015

For the statistical evaluation, the following hypothesis was made: (i) the permeability value of membranes after TRX treatment or after TRX/gA micelles immobilization is different than permeability value of non-modified membrane. The p-values **below** 0.05 correspond to the samples which are in agreement with this assumption (the ones which are not significantly different, of value above 0.05 are bolded).

In conclusion, treatment with surfactant significantly enhances ion transport properties of all the membranes, especially those with nanoparticles. After this treatment, the best performance is exhibited by MNP-OH membrane prepared in water, with high permeability value for both monovalent ions (1.29E-02 cm²·s⁻¹ for K⁺ and 1.82E-02 cm²·s⁻¹ for Na⁺), and by membrane MNP-NH₂ prepared in PBS with the highest permeability for potassium (1.43E-02 cm²·s⁻¹). Both membranes exhibit certain selectivity to small, monovalent cations. Nevertheless, immobilization of TRX/gA micelles is more effective in MNP-OH membranes, which maintains relatively high ion passage velocity when prepared either in water (7.89E-03 cm²·s⁻¹ for K⁺ and 6.33E-03 cm²·s⁻¹ for Na⁺) or in PBS (7.88E-03 cm²·s⁻¹ for K⁺ and 5.83E-03 cm²·s⁻¹ for Na⁺).

5.4.4. Atomic Absorption Spectrometry (AAS) and Polarized Optical Microscope (POM)

Atomic Absorption Spectrometry analysis were performed for the samples collected in Table 5.6. together with the theoretical concentration change value calculated according to the registered pH values of Mg^{2+} concentration.

Table 5.6. Results of Mg^{2+} ion concentration in the stripping solution according to the pH meter measurements and Atomic Absorption Spectrometry.

Membrane	Concentration AAS [ppm]	Concentration pH meter [ppm]
Psf/TRX in PBS	6.88 ± 0.34	7.15 ± 1.07
MNP-OH/TRX in PBS	0.045 ± 0.01	0.046 ± 0.007

As can be seen from the results, the difference in registered magnesium concentration values (3.78% for Psf/TRX membrane and 1.76 % for MNP-OH/TRX membrane) is very small. It confirms that observed ion diffusion passage is related to the actual transport across the membrane and not the diffusion of ions entrapped in the membrane before (as a result of saturation with PBS solution in which was stored).

Moreover, pictures taken with POM did not show any mechanical damage of the membrane, what confirms that the results are free from the inconsistency resulted from the membrane leak. It also proves that after treatments membranes are still mechanically resistant.

5.4.5. Current-Voltage measurement (CV)

In order to characterise the ion transport, current-voltage measurements were performed using the set-up described in Chapter III, section 3.4.1.4.4. in Figure 3.9. The Current-Voltage (C-V) curves, obtained for some of the membranes show the characteristic regions: Ohmic and limiting current and for MNP-NH₂/TRX membrane also an electroconvective region was registered as presented in Figure 5.6. Ohmic resistance values are collected in Table 5.7. In the case of

membranes for which experiment does not present a typical C-V curve, although the limiting current region was not defined, in most of the measurements the differences between Ohmic and convectional regions were possible to be distinguished. The limiting current region was possible to be observed only during a few experiments and it is highlighted in Table 5.7. In the case of all the membranes, treatment with TRX or TRX/gA immobilization resulted in significant decrease of membrane's Ohmic resistance, what was also statistically proved by p-values calculation (Table 5.7).

Table 5.7. Ohmic resistance values for all the tested membranes.

Membrane	Preparation solution	Ohmic resistance · 10 ⁻¹ [$\Omega \cdot \text{cm}^2$]				
		H ⁺	Na ⁺	K ⁺	Mg ²⁺	Ca ²⁺
MNP-OH		83.3 ± 0.0*	227.8 ± 36.0*	172.2 ± 13.6	136.2 ± 7.6	111.1 ± 0.0
MNP-OH/TRX	H ₂ O	23.4 ± 0.6	43.5 ± 1.2	36.4 ± 3.5	32.1 ± 0.8	33.0 ± 1.5
MNP-OH/TRX/gA		11.2 ± 0.4	53.1 ± 1.2	38.8 ± 4.0*	32.8 ± 0.9	34.7 ± 1.4
MNP-OH		63.4 ± 11.8	200.0 ± 0.0	150.7 ± 12.3	111.1 ± 0.0	100.0 ± 0.0
MNP-OH/TRX	PBS	33.7 ± 0.9	93.9 ± 4.7	54.7 ± 11.4*	39.3 ± 1.3	38.9 ± 2.6
MNP-OH/TRX/gA		17.9 ± 1.0	60.0 ± 1.9	56.7 ± 9.2*	42.3 ± 0.9	41.4 ± 3.8
MNP-NH ₂		136.6 ± 23.9*	450.0 ± 122.5	333.3 ± 0.0	250.0 ± 0.0	208.3 ± 20.4
MNP-NH ₂ /TRX	H ₂ O	14.7 ± 0.6	54.6 ± 1.5	52.2 ± 9.6	41.1 ± 0.9	37.6 ± 1.7
MNP-NH ₂ /TRX/gA		37.8 ± 1.6	111.1 ± 0.0	83.3 ± 0.0	60.1 ± 3.2	51.4 ± 2.3
MNP-NH ₂		122.7 ± 5.7	319.4 ± 34.0*	250.0 ± 0.0	200.0 ± 0.0	194.4 ± 13.6
MNP-NH ₂ /TRX	PBS	37.3 ± 0.6**	88.4 ± 19.1**	78.8 ± 18.1**	72.6 ± 5.6	67.8 ± 5.6
MNP-NH ₂ /TRX/gA		28.5 ± 3.4	57.2 ± 1.8	59.7 ± 13.1	44.2 ± 1.7	52.1 ± 9.2

Measurements for which pseudo-plateau region was possible to be distinguished are marked with *, the membranes with visible 3 characteristic regions with pseudo plateau and convective region are marked with **.

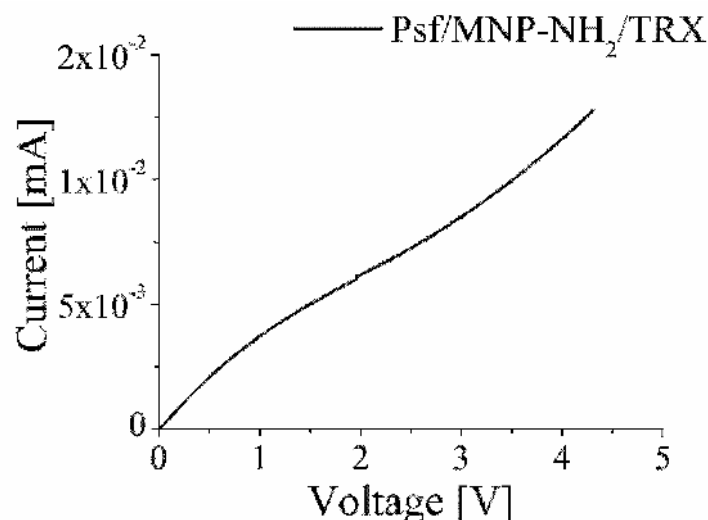


Figure 5.6. Current- Voltage curve of MNP-NH₂/TRX membrane prepared in PBS, with visible 3 characteristic regions: limiting current (0-1 V), pseudo-plateau (1-3 V) and convective region (3-5 V).

Table 5.8. Statistical analysis of the Ohmic resistance values.

Membrane	Preparation solution	p-values			
		K ⁺	Na ⁺	Ca ²⁺	Mg ²⁺
MNP-OH/TRX	H ₂ O	<0.0001	<0.0001	<0.0001	<0.0001
MNP-OH/TRX/gA		<0.0001	<0.0001	0.292	0.183
MNP-OH/TRX	PBS	<0.0001	<0.0001	<0.0001	<0.0001
MNP-OH/TRX/gA		<0.0001	<0.0001	0.737	0.001
MNP-NH ₂ /TRX	H ₂ O	<0.0001	<0.0001	<0.0001	<0.0001
MNP-NH ₂ /TRX/gA		<0.0001	<0.0001	<0.0001	<0.0001
MNP-NH ₂ /TRX	PBS	<0.0001	<0.0001	<0.0001	<0.0001
MNP-NH ₂ /TRX/gA		<0.0001	<0.0001	<0.0001	<0.0001

Hypothesis developed for statistical analysis: for the membranes after treatment with TRX: the resistance of membranes after TRX treatment is lower than the resistance of unmodified membrane; and for the membranes after TRX/gA immobilization: the resistance of membranes after TRX/gA immobilization is different than the resistance of membranes after TRX treatment. The p-values below 0.05 are in agreement with this hypotheses.

Graphical representation of the results is shown on the Figures 5.7.-5.10. To show the membranes selectivity in the Tables 5.9.-5.12. a ratio of admittance (reverse resistance, Y) values of tested ions over proton's ion ($Y_{\text{ion}}/Y_{\text{H}^+}$) are presented.

In the case of membranes MNP-OH prepared in water solution (Figure 5.7.) it can be seen that both modified materials show a significant decrease of the Ohmic resistance for all used alkaline ions. This increase of ion transport velocity is related- as in the case of diffusion transport- to better wetting of the material which facilitates ion passage. Considering simultaneously the selectivity calculation presented in Table 5.9. it may be observed that after treatment with TRX, membranes have high ion transport speed and loose selectivity. Nevertheless, when the membrane performance after TRX/gA micelles immobilization is analyzed, it can be observed that in comparison with untreated membrane, the MNP-OH/TRX/gA membrane has better selectivity to monovalent ions- the passage is reduced 51.56% for Mg^{2+} permeability and 56.93% for Ca^{2+} permeability, and moreover modified membrane exhibits much lower Ohmic resistance (decrease from $83.3 \Omega \cdot \text{cm}^2 \cdot 10^{-1}$ in unmodified membrane to $12.2 \Omega \cdot \text{cm}^2 \cdot 10^{-1}$ for membrane after TRX/gA micelles immobilization, in the case of transport of H^+ ion). This improvement of selectivity, visible for the exclusion of divalent ions over monovalent ones, especially for proton, suggests that a successful Gramicidin immobilization was accomplished and that it has a positive influence on membrane selectivity enhancement.

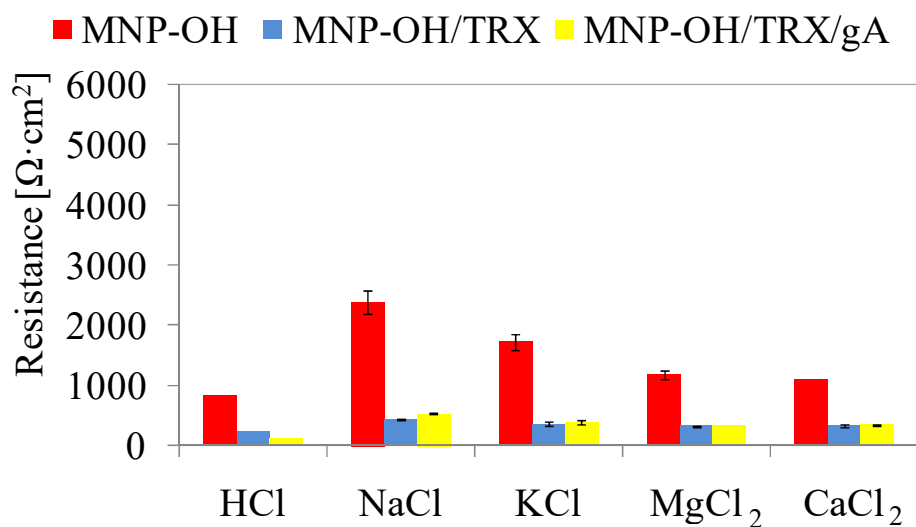


Figure 5.7. Ohmic resistance of MNP-OH membranes prepared in water.

Table 5.9. Selectivity values for MNP-OH membranes prepared in water.

Ion	Selectivity [$Y_{\text{ion}}/Y_{\text{H}^+}$]		
	MNP-OH	MNP-OH/TRX	MNP-OH/TRX/gA
H ⁺	1	1	1
Na ⁺	0.37 ± 0.06	0.54 ± 0.00	0.21 ± 0.00
K ⁺	0.49 ± 0.04	0.64 ± 0.04	0.29 ± 0.02
Mg ²⁺	0.71 ± 0.05	0.73 ± 0.00	0.34 ± 0.00
Ca ²⁺	0.75 ± 0.00	0.71 ± 0.02	0.32 ± 0.00

The results obtained for the membrane prepared in PBS are presented in Figure 5.8. A decrease in resistance after treatment with TRX or TRX/gA, as in the previous case was also detected. After treatment with TRX, MNP-OH membrane loses its selectivity, which is recovered when the TRX/gA micelles are immobilized. Selectivity in comparison to the unmodified membrane was also improved- permeability of divalent ions decreased from (57.15 ± 10.66 % to 42.35 ± 1.51%) for Mg²⁺ and from (63.5 ± 11.85% to 43.38 ± 1.5%) for Ca²⁺. Also, permeability to bigger monovalent ion (K⁺) was slightly reduced (from 41.87 ± 4.46% to 31.94 ± 3.43%) while increasing selectivity to proton (Table 5.10.).

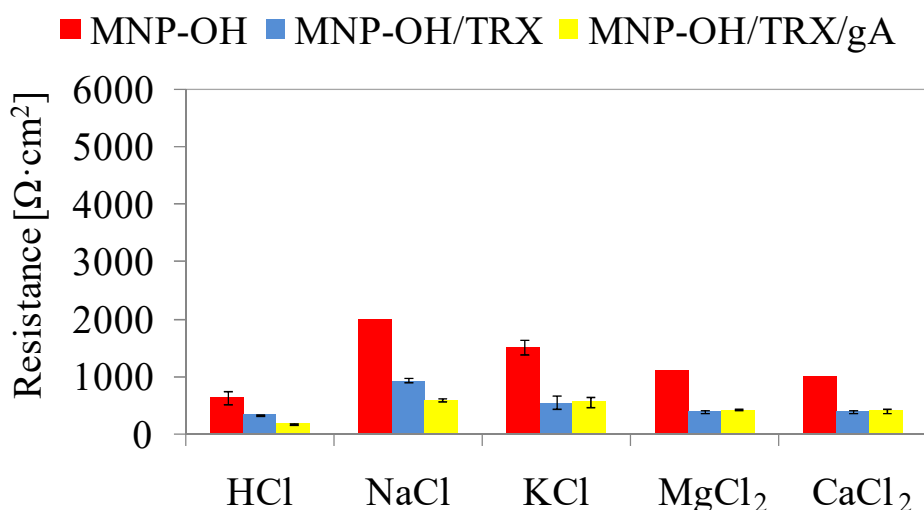


Figure 5.8. Ohmic resistance of the MNP-OH membranes prepared in PBS.

Table 5.10. Selectivity values for MNP-OH membranes prepared in PBS.

Ion	Selectivity [$Y_{\text{ion}}/Y_{\text{H}^+}$]		
	MNP-OH	MNP-OH/TRX	MNP-OH/TRX/gA
H ⁺	1	1	1
Na ⁺	0.32 ± 0.06	0.36 ± 0.0	0.30 ± 0.0
K ⁺	0.42 ± 0.04	0.63 ± 0.12	0.32 ± 0.03
Mg ²⁺	0.57 ± 0.11	0.86 ± 0.0	0.42 ± 0.02
Ca ²⁺	0.64 ± 0.12	0.87 ± 0.04	0.43 ± 0.02

In the case of membrane MNP-NH₂ prepared in water solution, a similar behaviour (as in the case of MNP-OH membrane) is observed: a decrease of resistance after treatments and loss of selectivity when TRX treatment was applied and selectivity enhancement after TRX/gA micelles immobilization (Figure 5.9). Reduction of permeability for divalent ions is 34.78% for Mg²⁺ and 40.19% for Ca²⁺. Also permeability to monovalent ions have been reduced 13.20% for Na⁺ and 30.29% for K⁺, increasing even more selectivity to proton, what is summarized in a Table 5.11.

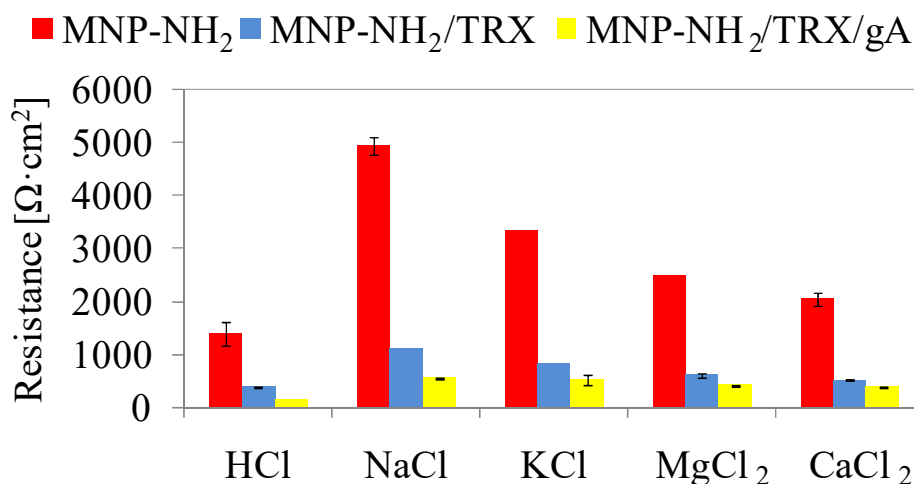


Figure 5.9. Ohmic resistance of the MNP-NH₂ membranes prepared in water.

Table 5.11. Selectivity values for the MNP-NH₂ membranes prepared in water.

Ion	Selectivity [$Y_{\text{ion}}/Y_{\text{H}^+}$]		
	MNP-NH ₂	MNP-NH ₂ /TRX	MNP-NH ₂ /TRX/gA
H ⁺	1	1	1
Na ⁺	0.31 ± 0.03	0.34 ± 0.01	0.27 ± 0.0
K ⁺	0.41 ± 0.07	0.45 ± 0.02	0.29 ± 0.04
Mg ²⁺	0.55 ± 0.10	0.63 ± 0.0	0.36 ± 0.0
Ca ²⁺	0.65 ± 0.05	0.74 ± 0.0	0.39 ± 0.0

As shown in Figure 5.10., MNP-NH₂ membrane preparation in PBS solution leads to obtain membrane which exhibit lower resistance values after treatment with TRX (decrease from 122.7 to 37.3 $\Omega \cdot \text{cm}^2 \cdot 10^{-1}$ in the case of H⁺) and TRX/gA micelles (decrease from 122.7 to 28.5 $\Omega \cdot \text{cm}^2 \cdot 10^{-1}$ in the case of H⁺). However, significant changes in terms of selectivity (Table 5.12.) were not detected, although in the resistance results it may be seen that micelles immobilization reduces Ohmic resistance even more than TRX treatment. The lack of selectivity improvement suggests that the effect of surfactant treatment is more visible than the protein immobilization. It may be caused by weaker interaction of micelles with the -NH₂ functional group in comparison to -OH group, since it is less hydrophilic and might have lower affinity for hydrophilic micelle shell.

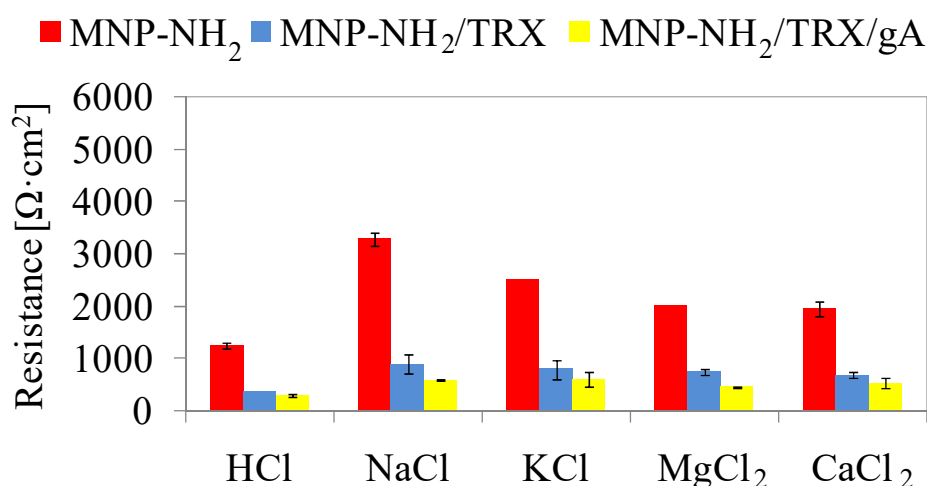


Figure 5.10. Ohmic resistance of the MNP-NH₂ membranes prepared in PBS.

Table 5.12. Selectivity values for the MNP-NH₂ membranes prepared in PBS.

Ion	Selectivity [$Y_{\text{ion}}/Y_{\text{H}^+}$]		
	MNP-NH ₂	MNP-NH ₂ /TRX	MNP-NH ₂ /TRX/gA
H ⁺	1	1	1
Na ⁺	0.38 ± 0.02	0.42 ± 0.09	0.50 ± 0.04
K ⁺	0.49 ± 0.02	0.47 ± 0.11	0.48 ± 0.05
Mg ²⁺	0.61 ± 0.03	0.51 ± 0.03	0.64 ± 0.05
Ca ²⁺	0.63 ± 0.02	0.55 ± 0.04	0.55 ± 0.03

Both treatments investigated, whether with a surfactant or with surfactant/protein micelles, drastically reduce Ohmic resistance of the membranes which is coming along with higher ions permeability. In three of the four cases, immobilization of TRX/gA micelles enhances membrane selectivity, what is a critical property for the membrane performance evaluation. The best results in terms of ion transport efficiency and selectivity is disclosed by the membrane MNP-OH prepared in water, which has both, the lowest resistance values after gA immobilization and the highest selectivity. For both types of membranes, MNP-OH and MNP-NH₂, immobilization in water seems to be more effective, probably due to the high interferences caused by ionic strength in PBS, which could cause interactions between charged micelles in a solution, while reducing reaction with a functional groups on the surface. Due to the unusual structure of these hybrid membranes, they cannot be directly compared with typical polymeric ion-exchange membranes.

5.4.6. Self-diffusion coefficient calculation

From the above Current-Voltage experiments, conductivity (molar) and self-diffusion coefficient values have been calculated. Obtained data together with diffusion coefficient values are collected in Table 5.13. Comparing those two coefficient's values can give an idea about the accuracy of the estimation and applicability of the Nernst-Einstein equation to MNP membranes system.

In the case of all the membranes, the calculated self-diffusion coefficient values are at least five orders of magnitude higher than the diffusion coefficient values obtained via permeability experiment. In fact, mobility of ion inside the membrane film should be a limiting factor determining diffusion speed, thus this big difference is not desirable if only diffusion transport is expected. It might be then an indication of the occurrence of viscous flow through the membrane, what have been reported previously [33, 34]. Also, considering the fact that other researchers [35] have obtained similar values of experimental and calculated self-diffusion coefficient values for Nafion 117 membrane, it is also possible that for such a complex and unusually structured novel system proposed in this work, this simple Nernst-Einstein equation based model is not applicable.

Chapter V | Physical immobilization with the use of magnetic nanoparticles (MNP)

Table 5.13. Results of conductivity and self-diffusion coefficient calculated from the resistance data, and the diffusion coefficient values calculated from permeability data, for the membranes prepared in water and in PBS.

Membrane	Prep. Sol.	H ⁺			Na ⁺			K ⁺			Mg ²⁺			Ca ²⁺		
		σ [S/m]	D σ [cm ² /s] ($\cdot 10^{-8}$)	D	σ [S/m]	D σ [cm ² /s] ($\cdot 10^{-8}$)	D [cm ² /s] ($\cdot 10^{-3}$)	σ [S/m]	D σ [cm ² /s] ($\cdot 10^{-8}$)	D [cm ² /s] ($\cdot 10^{-3}$)	σ [S/m]	D σ [cm ² /s] ($\cdot 10^{-8}$)	D [cm ² /s] ($\cdot 10^{-3}$)	σ [S/m]	D σ [cm ² /s] ($\cdot 10^{-8}$)	D [cm ² /s] ($\cdot 10^{-3}$)
MNP-OH		0.13	4.98		0.05	1.82	5.06	0.06	2.41	5.52	0.01	0.09	2.83	0.10	0.93	2.78
MNP-OH/TRX	H ₂ O	0.43	16.92		0.23	9.08	11.80	0.28	10.86	12.90	0.13	1.32	6.11	0.30	2.99	5.37
MNP-OH/TRX/gA		0.71	28.16		0.15	5.95	6.33	0.21	8.14	7.89	0.22	2.15	3.41	0.23	2.28	3.07
MNP-OH		0.17	6.53		0.05	2.08	0.86	0.07	2.75	<0.01	0.02	0.15	<0.01	0.11	1.04	<0.01
MNP-OH/TRX	PBS	0.24	9.37		0.09	3.37	5.40	0.15	5.78	7.92	0.06	0.60	4.46	0.21	2.03	4.14
MNP-OH/TRX/gA		0.45	17.65		0.13	5.27	5.83	0.14	5.57	7.88	0.11	1.04	3.57	0.19	1.91	2.23
MNP-NH ₂		0.10	3.01		0.03	0.91	0.44	0.04	1.23	0.70	0.01	0.03	0.56	0.06	0.49	<0.01
MNP-NH ₂ /TRX	H ₂ O	0.61	19.44		0.17	5.22	3.55	0.172	5.45	6.82	0.15	1.18	3.87	0.24	1.90	2.22
MNP-NH ₂ /TRX/gA		0.27	8.37		0.09	2.85	5.90	0.12	3.80	7.89	0.04	0.35	2.94	0.20	1.54	0.96
MNP-NH ₂		0.07	2.32		0.03	0.89	0.52	0.04	1.14	2.23	0.01	0.03	0.91	0.05	0.37	<0.01
MNP-NH ₂ /TRX	PBS	0.32	10.19		0.14	4.30	7.83	0.15	4.82	14.30	0.04	0.35	6.15	0.18	1.40	6.38
MNP-NH ₂ /TRX/gA		0.35	11.16		0.18	5.53	2.06	0.17	5.30	3.07	0.08	0.63	1.72	0.19	1.52	0.88

5.5. Conclusions

Physical method of biomolecule immobilization on a Psf membrane with the use of magnetic nanoparticles MNP has been studied in this work. Results show that immobilization of Gramicidin impacts hydrophilic/hydrophobic properties of Psf membrane and does not affect membrane morphology. Membrane functionalization with $-OH$ and $-NH_2$ groups of nanoparticles effectively increase hydrophilicity. However, performed treatment with surfactant or TRX/gA micelles immobilization present various effects on the surface character, making it whether more hydrophilic or more hydrophobic, dependently of the type of nanoparticles used. Immobilization on nanoparticles enhances ion diffusion speed by treatment with Triton: an increase of transport rate of at least 10 times is reached. In most of the cases, permeability of ions decrease after gA immobilization. This is related to the lower water passage confirmed by water uptake experiment. The results of permeability tests revealed that ion diffusion transport depends also on the composition of bulk solution used for preparation and seems to have higher efficiency when performed in water. ASA analysis confirmed that registered amount of ions which passed through the membrane comes from a feed solution and not from the preparation solution remaining on the surface. Membranes containing MNP have higher selectivity to monovalent ions comparing to Plain Psf membranes modified in the same way. Ion transport characterization with use of Current-Voltage measurements evidenced that all prepared membranes, with two different modification degrees (either treated with surfactant or with micelles) disclose higher ions conductivity and high proton selectivity compared to unmodified membrane (selectivity enhancement higher than 50%). Also, three of four prepared membrane exhibit improved ion selectivity after gA immobilization, comparing to the membranes after TRX treatment. This interesting findings could indicate that potential use in application requiring selective ion transport, such as artificial photosynthesis, nanofiltration or fuel cells and proves functionality of immobilized protein. The Nernst-Einstein equation based model for self-diffusion coefficient estimation seems to be not applicable for this kind of membranes.

5.6. References

- [1] Y.F. Shen, J. Tang, Z.H. Nie, Y.D. Wang, Y. Ren, L. Zuo, Preparation and application of magnetic Fe_3O_4 nanoparticles for wastewater purification, *Separation and Purification Technology*, 68 (2009) 312-319.
- [2] K. Abdollahi, F. Yazdani, R. Panahi, Covalent immobilization of tyrosinase onto cyanuric chloride crosslinked amine-functionalized superparamagnetic nanoparticles: Synthesis and characterization of the recyclable nanobiocatalyst, *International Journal of Biological Macromolecules*, 94, Part A (2017) 396-405.
- [3] L. Cabrera, S. Gutierrez, N. Menendez, M.P. Morales, P. Herrasti, Magnetite nanoparticles: Electrochemical synthesis and characterization, *Electrochimica Acta*, 53 (2008) 3436-3441.
- [4] H. Yun, J. Chen, V. Doan-Nguyen, J. Kikkawa, C. Murray, Synthesis, characterization, and fabrication of magnetic nanoparticles for low energy loss applications, in: *APS Meeting Abstracts*, 2013, pp. 14003.
- [5] X. Jin, K. Zhang, J. Sun, J. Wang, Z. Dong, R. Li, Magnetite nanoparticles immobilized Salen Pd (II) as a green catalyst for Suzuki reaction, *Catalysis Communications*, 26 (2012) 199-203.
- [6] P. Yuan, M. Fan, D. Yang, H. He, D. Liu, A. Yuan, J. Zhu, T. Chen, Montmorillonite-supported magnetite nanoparticles for the removal of hexavalent chromium [Cr (VI)] from aqueous solutions, *Journal of Hazardous materials*, 166 (2009) 821-829.
- [7] B. Movassagh, A. Yousefi, Magnetite (Fe_3O_4) nanoparticles: an efficient and reusable catalyst for the synthesis of thioethers, vinyl thioethers, thiol esters, and thia-Michael adducts under solvent-free condition (2013).
- [8] Q.H. Tran, A.-T. Le, Silver nanoparticles: synthesis, properties, toxicology, applications and perspectives, *Advances in Natural Sciences: Nanoscience and Nanotechnology*, 4 (2013) 033001.
- [9] A. Cruz-Izquierdo, E.A. Pico, C. Lopez, J.L. Serra, M.J. Llama, Magnetic Cross-Linked Enzyme Aggregates (mCLEAs) of *Candida antarctica* lipase: an efficient and stable biocatalyst for biodiesel synthesis, *PLoS One*, 9 (2014).
- [10] M.H.R. Farimani, N. Shahtahmasebi, M. Rezaee Roknabadi, N. Ghows, A. Kazemi, Study of structural and magnetic properties of superparamagnetic $\text{Fe}_3\text{O}_4/\text{SiO}_2$ core-shell nanocomposites

synthesized with hydrophilic citrate-modified Fe_3O_4 seeds via a sol-gel approach, *Physica E: Low-dimensional Systems and Nanostructures*, 53 (2013) 207-216.

[11] X.-C. Shen, X.-Z. Fang, Y.-H. Zhou, H. Liang, Synthesis and characterization of 3-aminopropyltriethoxysilane-modified superparamagnetic magnetite nanoparticles, *Chemistry Letters*, 33 (2004) 1468-1469.

[12] Z.L. Liu, Y.J. Liu, K.L. Yao, Z.H. Ding, J. Tao, X. Wang, Synthesis and Magnetic Properties of Fe_3O_4 Nanoparticles, *Journal of Materials Synthesis and Processing*, 10 (2002) 83-87.

[13] S.V. Sychev, L.I. Barsukov, V.T. Ivanov, Conformation of Gramicidin A in Triton X-100 micelles from CD and FTIR data: a clean example of antiparallel double β 5.6 helix formation, *Journal of Peptide Science*, 19 (2013) 452-458.

[14] K. Simons, A. Helenius, K. Leonard, M. Sarvas, M. Gething, Formation of protein micelles from amphiphilic membrane proteins, *Proceedings of the National Academy of Sciences*, 75 (1978) 5306-5310.

[15] S.S. Rawat, D.A. Kelkar, A. Chattopadhyay, Effect of Structural Transition of the Host Assembly on Dynamics of an Ion Channel Peptide: A Fluorescence Approach, *Biophysical Journal*, 89 (2005) 3049-3058.

[16] Z. Huang, T. Gu, Mixed adsorption of nonionic and cationic surfactants on silica gel and methylated silica gel, *Colloids and Surfaces*, 28 (1987) 159-168.

[17] T.R. Besanger, J.D. Brennan, Ion Sensing and Inhibition Studies Using the Transmembrane Ion Channel Peptide Gramicidin A Entrapped in Sol-Gel-Derived Silica, *Analytical Chemistry*, 75 (2003) 1094-1101.

[18] M.R. Hicks, A. Damianoglou, A. Rodger, T.R. Dafforn, Folding and Membrane Insertion of the Pore-Forming Peptide Gramicidin Occur as a Concerted Process, *Journal of Molecular Biology*, 383 (2008) 358-366.

[19] T.W. Allen, O.S. Andersen, B. Roux, Energetics of ion conduction through the Gramicidin channel, *Proceedings of the National Academy of Sciences*, 101 (2004) 117-122.

[20] J.A. Killian, B. De Kruijff, Importance of hydration for Gramicidin-induced hexagonal HII phase formation in dioleoylphosphatidylcholine model membranes, *Biochemistry*, 24 (1985) 7890-7898.

[21] M. Poxleitner, J. Seitz-Beywl, K. Heinzinger, Ion Transport through Gramicidin A. Water Structure and Functionality, *Zeitschrift für Naturforschung C*, 48 (1993) 654-665.

- [22] K. Yamagiwa, H. Kobayashi, M. Onodera, A. Ohkawa, Y. Kamiyama, K. Tasaka, Surfactant pretreatment of a polysulfone ultrafilter for reduction of antifoam fouling, *Biotechnology and bioengineering*, 43 (1994) 301-308.
- [23] H. Rabiee, S.M. Seyedi, H. Rabiei, N. Alvandifar, Improvement in permeation and fouling resistance of PVC ultrafiltration membranes via addition of Tetronic-1107 and Triton X-100 as two non-ionic and hydrophilic surfactant, *Water Science and Technology*, (2016).
- [24] A. Rahimpour, S.S. Madaeni, Y. Mansourpanah, The effect of anionic, non-ionic and cationic surfactants on morphology and performance of polyethersulfone ultrafiltration membranes for milk concentration, *Journal of Membrane Science*, 296 (2007) 110-121.
- [25] I. Roh, C. Bartels, Method for wetting hydrophobic porous polymeric membranes to improve water flux without alcohol treatment, in, *Google Patents*, 2005.
- [26] A. Ciferri, A. Perico, *Ionic interactions in natural and synthetic macromolecules*, Wiley Online Library, 2012.
- [27] F. Picaud, S. Kraszewski, C. Ramseyer, S. Balme, P. Déjardin, J.M. Janot, F. Henn, Enhanced potassium selectivity in a bioinspired solid nanopore, *Physical Chemistry Chemical Physics*, 15 (2013) 19601-19607.
- [28] S. Balme, J.-M. Janot, L. Berardo, F. Henn, D. Bonhenry, S. Kraszewski, F. Picaud, C. Ramseyer, New Bioinspired Membrane Made of a Biological Ion Channel Confined into the Cylindrical Nanopore of a Solid-State Polymer, *Nano Letters*, 11 (2011) 712-716.
- [29] S. Hernandez, C. Porter, X. Zhang, Y. Wei, D. Bhattacharyya, Layer-by-layer assembled membranes with immobilized porins, *RSC Advances*, 7 (2017) 56123-56136.
- [30] N. Anuraj, S. Bhattacharjee, J.H. Geiger, G.L. Baker, M.L. Bruening, An all-aqueous route to polymer brush-modified membranes with remarkable permeabilities and protein capture rates, *Journal of membrane science*, 389 (2012) 117-125.
- [31] F. Kara, G. Gurakan, F. Sanin, Monovalent cations and their influence on activated sludge floc chemistry, structure, and physical characteristics, *Biotechnology and bioengineering*, 100 (2008) 231-239.
- [32] R.P.a.S.M. E., *Processes Involved in Sodic Behaviour*, Oxford University Press, New York, 1998.
- [33] J.R. Abney, B.A. Scalettar, J.C. Owicki, Self diffusion of interacting membrane proteins, *Biophysical Journal*, 55 (1989) 817-833.

- [34] T. Uragami, S. Kido, M. Sugihara, Studies on syntheses and permeabilities of special polymer membranes. 37. Permeabilities of poly(\hat{I}^3 -methyl L-glutamate) membranes, *Polymer*, 23 (1982) 617-620.
- [35] I.A. Stenina, P. Sizat, A.I. Rebrov, G. Pourcelly, A.B. Yaroslavtsev, Ion mobility in Nafion-117 membranes, *Desalination*, 170 (2004) 49-57.

Chapter VI

Chemical immobilization by glutaraldehyde coupling

6.1. Introduction

Covalent immobilization methods have been also considered to link proteins to membrane supports. However, formation of chemical bonds between biomolecule and solid supports is connected very often with a change of protein structure, and thus, lose of bioactivity. Besides, it is often related with the use of organic solvents, which are known to denature proteins. Among most common immobilization strategies can be found click chemistry reaction, 1,3-dipolar cycloaddition of terminal alkynes and azides, isourea linkage, peptide bond formation and glutaraldehyde coupling [1, 2]. The criteria for the selection of appropriate method were the degree of polymer modification needed for the reaction, invasiveness in terms of use of harmful chemicals and the reaction complexity. In this work glutaraldehyde coupling method for covalent gA immobilization has been selected. Plenty of successful use of this technique [3-6] for immobilization of proteins have been previously reported. Moreover, it does not require any use of toxic chemicals, is quick and the procedure and conditions are very easy to reproduce.

6.2. Materials

Polysulfone (Mw 35,000) in transparent pellet form, N,N-Dimethylformamide (DMF, 99 %) used for flat sheet membrane fabrication were purchased from Sigma Aldrich. Gramicidin from *bacillus aneurinolyticus* (*Bacillus brevis*) was purchased from Sigma Aldrich. Salts used for PBS (phosphate buffer saline) preparation and for permeability experiments: sodium chloride, magnesium chloride hexahydrate and potassium chloride were purchased from Sigma Aldrich, potassium phosphate dibasic trihydrate, disodium hydrogen phosphate dihydrate and calcium chloride dihydrate were purchased from Panreac. Hydrochloric acid $\geq 37\%$ was purchased from Sigma Aldrich. Surfactant Triton X-100 (TRX) was purchased from Sigma Aldrich. Glutaraldehyde, Ammonium sulphate, sodium borohydrate were purchased from Sigma Aldrich. All solutions were prepared in MiliQ water from Millipore.

6.3. Methods

6.3.1. Immobilization via glutaraldehyde coupling

In order to immobilize gA on a MNP-NH₂ membrane, 4 cm x 4 cm pieces of membrane were immersed in 210 ml of aqueous or in a phosphate buffer saline (PBS) solution in the presence of ammonium sulphate (precipitation agent) in a concentration of 1.3 M. Both stock solutions (water and PBS) were used in order to check the salts effect on immobilization efficiency. Next, surfactant Triton X100 (TRX) was added. Surfactant concentration was 0.29 mM, like in the case of physical micelles immobilization. After 5 minutes of stirring at 300 rpm, a 50% glutaraldehyde solution was added (to achieve a final concentration of 500 mM). Samples were stirred during 24 h at 300 rpm at room temperature. After this time, membranes were washed three times with PBS. Next, the membranes were placed in 210 ml of carbonate/bicarbonate buffer (pH 10) and 0.02 g of NaBH₄ was added. Membranes were stirred in this solution for 2h at room temperature in order to reduce unreacted aldehyde groups. After this process, membranes were washed with 2 M NaCl in PBS and then with 1% (v/v) Triton X-100 in PBS.

6.3.2. Characterization methods

6.3.2.1. Morphology analysis (ESEM)

Surface and cross-sectional morphologies of membranes with MNP before and after TRX/gA micelles immobilization were observed at 20 kV with high-vacuum ESEM FEI Quanta 600 apparatus, without sputter coating. Membrane cross-sections were prepared by fracturing them in liquid nitrogen. The images were analysed with ImageJ software to observe the effect of protein immobilization on pore size and membrane thickness. Values of pore size and membrane thickness are the average of 3 measurements taken from 3 membranes prepared with the same experimental conditions.

6.3.2.2. Contact angle (CA)

Static Contact angle analysis was performed on a Dataphysics OCA15EC contact angle analyzer with MiliQ water as testing liquid. The angle was measured immediately after the drop (3 μm) was released on membrane's surface. Measurements were repeated 5 times on different areas of 3 different membranes prepared under the same experimental conditions.

6.3.2.3. Water uptake (WU)

Membranes were weighted before and after 2, 4, 6 and 24 h of water immersion, in order to ensure complete saturation with the solvent. The surface water drops were removed from wet membranes with the use of filter paper and the mass was measured. Then the membranes were dried in the oven (Nabertherm L9/12/P330) at the temperature of 100° C for 24 h, and weighted afterwards. The water uptake was calculated as the difference between the wet membrane mass and the dry membrane mass and expressed as mg of water gain per mg of membrane. Experiment was repeated 3 times for each membrane prepared under the same experimental conditions.

6.3.2.4. Permeability test

Ion diffusion experiments were performed in the system described in Chapter III, section 3.4.1.4.1. For all experiments performed, initial feed solution was 0.1 M HCl aqueous solution and stripping solutions tested were 0.1 M aqueous electrolyte solutions: NaCl, KCl, MgCl₂, CaCl₂ or pure MiliQ water. The ion transport was monitored by pH change of stripping solution. The pH of the stripping solution was measured every 10 s by an Orion Dual Star pH/ISE Multimeter. From the pH change slope, ion diffusion coefficient and permeability were calculated according to the procedure described in Chapter III, section 3.4.1.4.1.

6.3.2.5. Current-Voltage measurement (CV)

Current-Voltage (CV) measurements were performed using Autolab PGstat100 in potentiostatic mode with current ranging (automatic) from 100 mA to 100 μ A, potential range from 0 V to 5 V, with a step of 0.01 V and scan rate 0.01 V/s. The distance between the reference electrodes (Ag/AgCl) and membrane was 1 cm. The solution volume in each compartment was 200 mL. Tested solutions were 0.1 M concentrated HCl, NaCl, KCl, MgCl₂ and CaCl₂. The measurements were performed at the ambient temperature ($24 \pm 1^\circ\text{C}$).

6.3.2.6. Self-diffusion coefficient calculation

The self-diffusion coefficient of ions in the membranes was calculated from conductivity values obtained from CV measurements. Exact procedure is described in Chapter III, section 3.4.1.4.5.

6.4. Results

6.4.1. Morphology analysis (ESEM)

Regarding morphology analysis, influence on the pore size of the membranes was not observed. Also, the thickness is maintained unaffected (Table 6.1.). In conclusion, even though this immobilization method involves a chemical reaction with the membrane surface, the conditions are mild enough to not damage membrane structure. In the interior of the membrane small particles are found (Figure 6.1. a-b), which most probably are not well distributed nanoparticles, as it was also encountered in previously prepared membranes containing MNP (See Chapter V, Figure 5.4.).

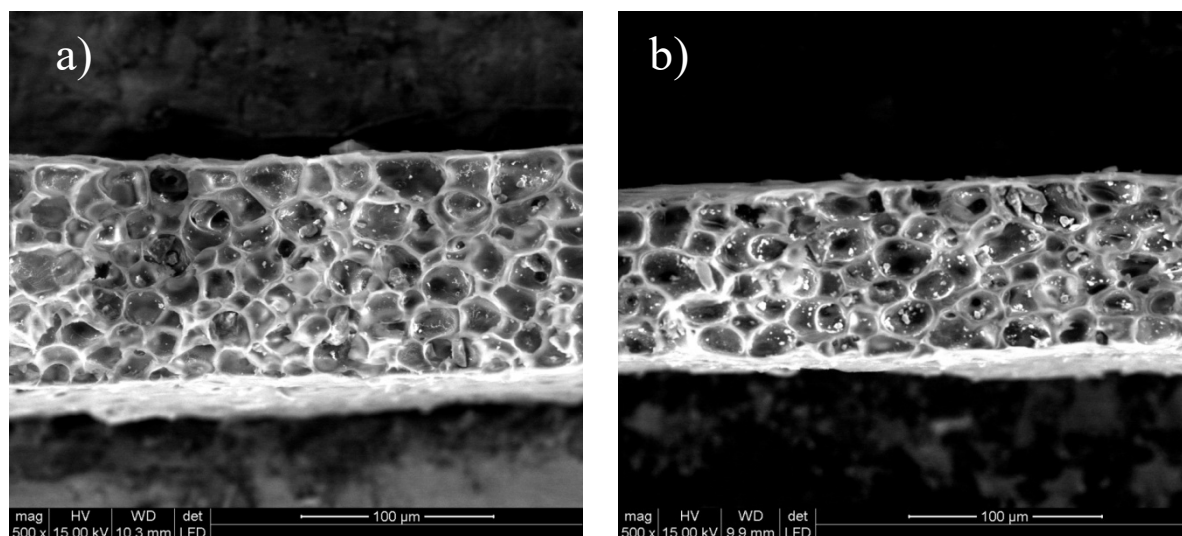


Figure 6.1. ESEM micrographs of membrane cross sections in magnification x500: a) MNP-NH₂/glutar/gA prepared in PBS, b) MNP-NH₂/glutar/gA prepared in water.

Table 6.1. Pore sizes and thicknesses of membranes prepared before and after glutaraldehyde coupling reaction, compared also with the values obtained previously for the MNP-NH₂ membrane with physically immobilized TRX/gA micelles and MNP-NH₂ membrane before modification (Chapter V, Table 5.2.).

Parameter	MNP-NH ₂	St.dev.	MNP-NH ₂ /TRX/gA	St.dev.	MNP-NH ₂ /glutar/gA	St.dev.	p-value
Average pore size [μm]	30.9	11	23.5	8.9	22.2	6.4	0.302
Membrane thickness [μm]	104.7	16.9	110.9	20.7	104.0	8.2	0.950

Values of pore sizes and membrane thicknesses are the average of 3 measurements taken from 3 membranes prepared under the same experimental conditions. For the statistical evaluation, the following *null hypothesis* were made: (i) the pore size of the MNP membranes before glutaraldehyde coupling reaction is different than the pore size of the membranes after the reaction (ii) the thickness of MNP membranes before glutaraldehyde coupling reaction is different than the thickness of membranes after the reaction. The p-values **below** 0.05 are in agreement with those hypotheses (none of them).

6.4.2. Contact angle (CA) and Water uptake (WU)

All the results of CA and WU measurements were compared with the MNP membranes without any modification and with the membranes with physically immobilized TRX/gA micelles. In the case of the membranes prepared in both stock solutions, large increase of

hydrophilicity may be observed, compare to MNP-NH₂ and MNP-NH₂/TRX/gA membranes (in both cases the p-value was <0.001, which means that hydrophilicity change is significant).

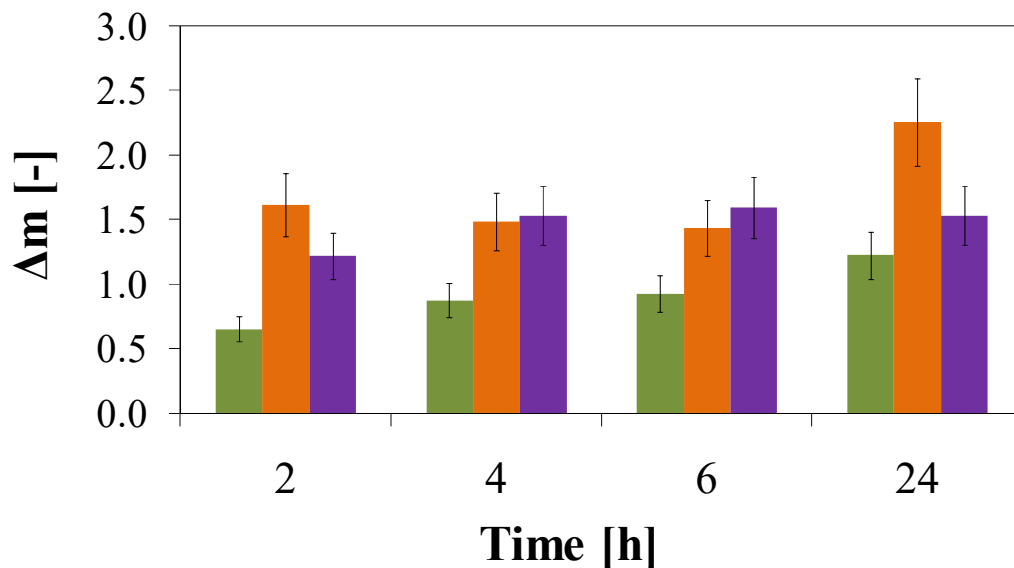
Table 6.2. Results of contact angle (CA) measurement for MNP membranes with gA immobilized via glutaraldehyde coupling (5-6) compared with the values obtained previously for the MNP-NH₂ membrane with physically immobilized TRX/gA micelles and MNP-NH₂ membrane before modification (1-4, see Chapter V, Table 5.3.).

Membrane	CA top	CA bottom	p-value
1. MNP-NH ₂ /H ₂ O	82.35 ± 3.05	72.05 ± 0.25	
2. MNP-NH ₂ /PBS	83.25 ± 3.25	80.85 ± 1.25	
3. MNP-NH ₂ /TRX/gA/H ₂ O	86.9 ± 1.4	82.1 ± 0.4	
4. MNP-NH ₂ /TRX/gA/PBS	69.9 ± 1.2	69.4 ± 1.1	
5. MNP-NH ₂ /glutar/gA/H ₂ O	55.7 ± 6.33	24.75 ± 5.04	<0.0001
6. MNP-NH ₂ /glutar/gA/PBS	57.09 ± 5.66	59.16 ± 5.46	<0.0001

Values of contact angle are the average of 5 measurements taken from 3 parts of the 3 membranes prepared at the same experimental conditions. For the statistical evaluation, the following hypothesis was made: (i) the CA of the non-modified MNP membrane is more than 5 degrees different from the CA of membranes prepared via glutaraldehyde coupling. The p-values **below** 0.05 correspond to the samples which are in agreement with this assumption (both).

According to water uptake assay it can be seen that although membranes with gA immobilized via glutaraldehyde coupling are more hydrophilic on the surface, compare to MNP-NH₂/TRX/gA membranes, they absorb less water (Figure 6.2). This suggests stronger surface modification after chemical reaction, but lower modification degree within the membrane matrix.

a) ■ MNP-NH₂ ■ MNP-NH₂/TRX/gA ■ MNP-NH₂/glutar/gA



b) ■ MNP-NH₂ ■ MNP-NH₂/TRX/gA ■ MNP-NH₂/glutar/gA

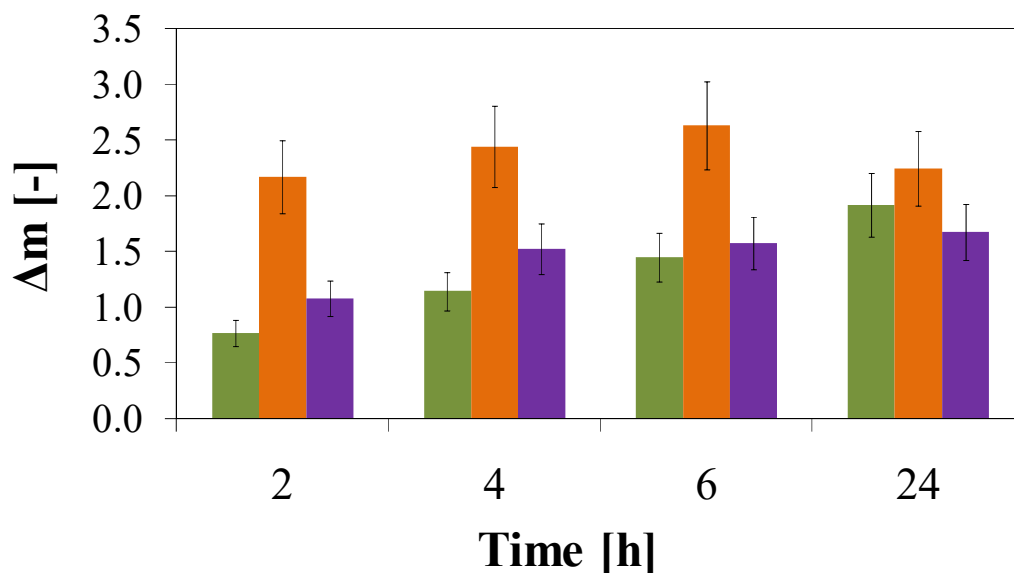


Figure 6.2. Water uptake experiment results for MNP-NH₂ membranes: described previously Plain MNP-NH₂ and MNP-NH₂/TRX/gA (see Chapter V, Figure 4 c-d) and MNP-NH₂/glutar/gA prepared in water (a) and PBS (b). Values of mg of water absorbed per mg of membrane (Δm) are average of 3 measurements taken from 3 different membranes. The error bars refers to the standard deviation from the measurements.

6.4.3. Permeability test

Permeability experiments were performed under the same conditions as for the membranes with physically immobilized gA. Results are presented in Figure 6.3. It may be seen that diffusive transport of membrane modified by glutaraldehyde coupling is lower than the membrane prepared with the use of TRX/gA micelles.

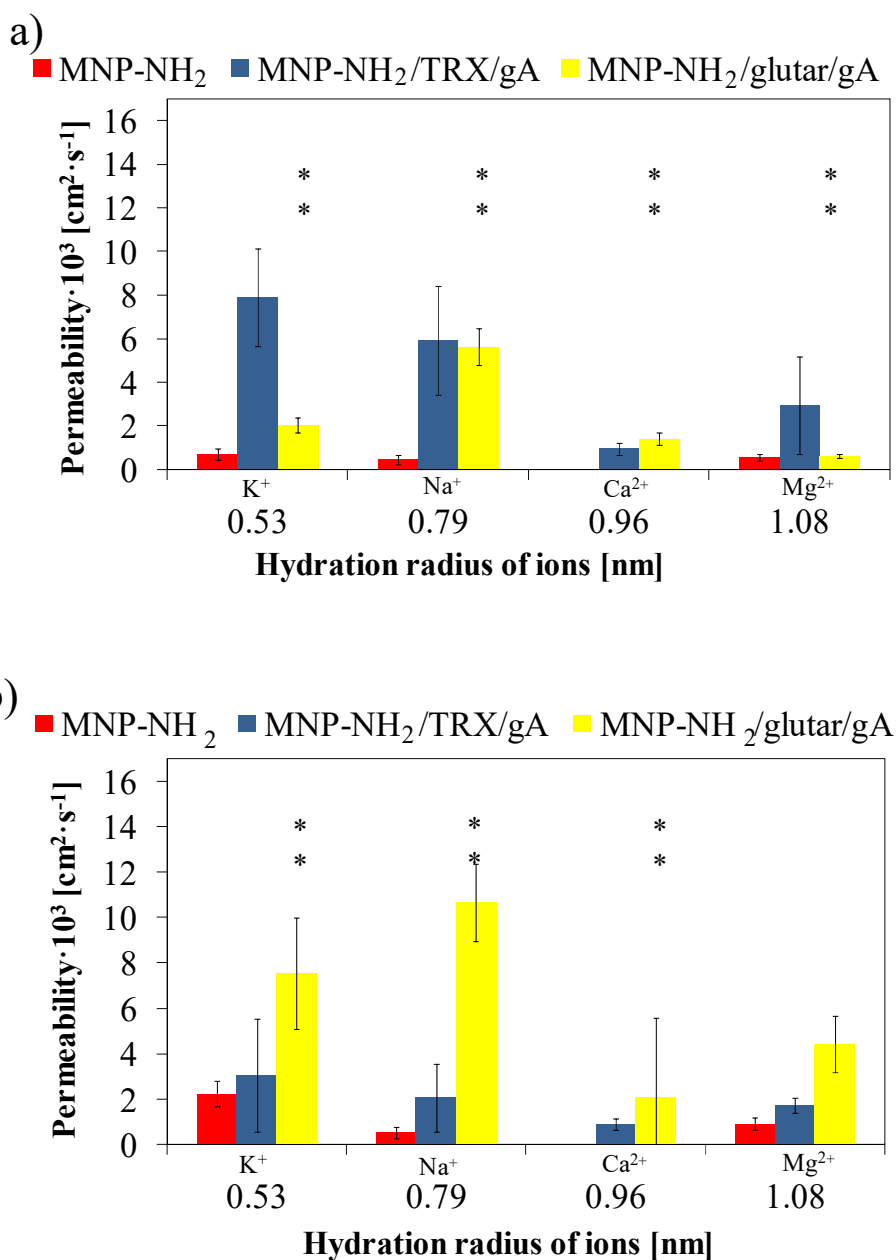


Figure 6.3. Permeability test results versus the hydration radius of ions K⁺, Na⁺, Ca²⁺ and Mg²⁺ respectively [7, 8] for membranes: MNP-NH₂, MNP-NH₂/TRX/gA presented previously (see

Chapter V, Figure 5.5. e-f) and MNP-NH₂/glutar/gA prepared in H₂O (a) and in PBS (b). Values of permeability are average of 3 measurements taken from 3 different membranes prepared under the same experimental conditions. The error bars refers to the standard deviation from the measurements. Columns highlighted with ** refer to samples for which p-value was <0.01. For the statistical evaluation, the following hypothesis was made: (i) the permeability value of membranes after glutaraldehyde coupling reaction is different than permeability value of non-modified membrane. The p-values **below** 0.05 correspond to the samples which are in agreement with this assumption.

Concerning the membranes prepared in PBS buffer solution (Figure 6.3 b), it can be seen that their performance enhances drastically in comparison to the membrane after physical gA immobilization. This difference is caused most probably by the use of the buffer, which maintains constant pH value, and favours the efficiency of the chemical reaction. Comparing these data with the results of water uptake experiment it can be concluded, that the fast ion diffusion speed is not related only to the highest water content in the membrane, since it was found that membranes after chemical gA immobilization swells less water. This result not only provide an encouraging message about membrane performance but is also a prove that chemical reaction that occurred in the membrane surface enhanced ion passage speed, most probably due to the protein attachment.

6.4.4. Current- Voltage measurement (CV)

The results of Current-Voltage measurements are shown in Figure 6.4. The three characteristic regions of the curves can be clearly observed. These curves are characteristic of ion exchange membranes [9]. Although convective region is not clearly highlighted in all the cases, it is possible to distinguish limiting current region. The resistance values for the membranes prepared via glutaraldehyde coupling are collected in Table 6.3.

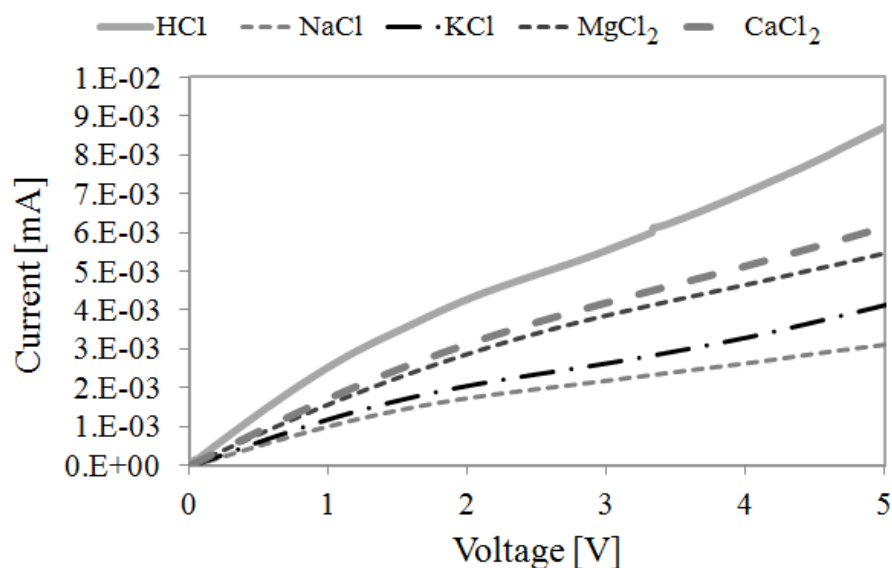


Figure 6.4. Current-Voltage curves obtained for all electrolyte solutions for the membrane MNP-NH₂/glutar prepared in PBS solution.

Table 6.3. Ohmic resistance values for the membranes: MNP-NH₂, MNP-NH₂/TRX/gA presented previously (see Chapter V, Table 6.7.) and MNP-NH₂/glutar/gA prepared in water and in PBS.

Membrane	Preparation solution	Ohmic resistance · 10 ⁻¹ [Ω·cm ²]				
		H ⁺	Na ⁺	K ⁺	Mg ²⁺	Ca ²⁺
MNP-NH ₂		136.6 ± 23.9*	450.0 ± 122.5	333.3 ± 0.0	250.0 ± 0.0	208.3 ± 20.4
MNP-NH ₂ /TRX/gA	H ₂ O	14.7 ± 0.6	54.6 ± 1.5	52.2 ± 9.6	41.1 ± 0.9	37.6 ± 1.7
MNP-NH ₂ /glutar/gA		83.6 ± 11.0	100.0 ± 0.0	92.6 ± 14.3	66.8 ± 2.8	66.4 ± 6.3
MNP-NH ₂		122.7 ± 5.7	319.4 ± 34.0*	250.0 ± 0.0	200.0 ± 0.0	194.4 ± 13.6
MNP-NH ₂ /TRX/gA	PBS	37.3 ± 0.6**	88.4 ± 19.1**	78.8 ± 18.1**	72.6 ± 5.6	67.8 ± 5.6
MNP-NH ₂ /glutar/gA		45.5 ± 0.0	111.1 ± 0.0	103.7 ± 5.7	88.1 ± 10.6	75.4 ± 6.1

It can be observed, that chemical reaction with glutaraldehyde causes decrease in membrane resistance, comparing to the untreated material. Nevertheless, in comparison to the membranes prepared by TRX/gA micelles immobilization in PBS solution, it is still significantly higher. It might be related to the higher water content in the membranes after physical protein immobilization, since membrane exposition to the surfactant treatment in this case was higher.

In Figure 6.5. the graphical representation of the resistance values for the membranes prepared in water can be seen. In the case of all the ions, chemical immobilization of gA decreases the membrane resistance. In comparison to the physical immobilization method, membranes exhibit resistance values of the same range, but for proton. Membranes after physical immobilization of gA present even lower resistance values than membranes with chemically immobilized protein. In Table 6.4., calculated values of selectivity are presented. As can be observed, no enhancement is encountered in selectivity, in any case.

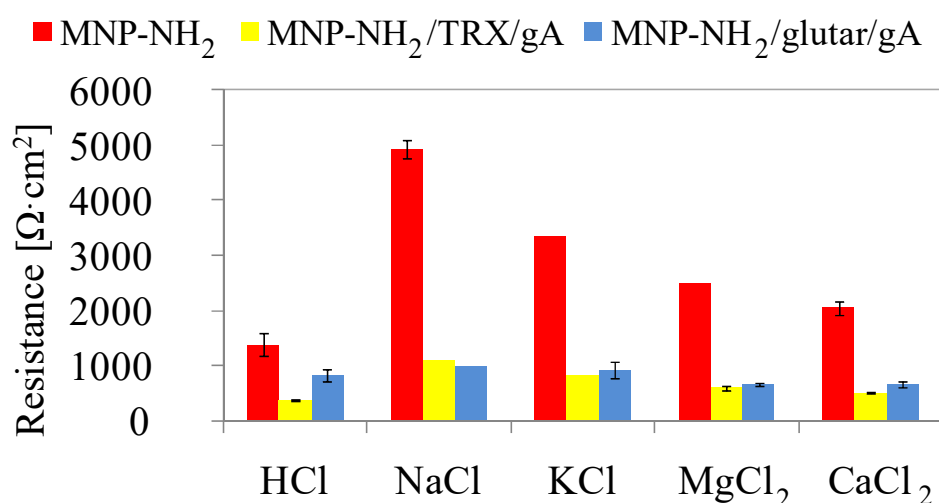


Figure 6.5. Ohmic resistance values the membranes: MNP-NH₂, MNP-NH₂/TRX/gA presented previously (see Chapter V, Figure 5.9.) and MNP-NH₂/glutar/gA prepared in water.

Table 6.4. Selectivity values the membranes: MNP-NH₂, MNP-NH₂/TRX/gA presented previously (see Chapter V, Table 5.11.) and MNP-NH₂/glutar/gA prepared in water.

Ion	Selectivity [Y_{ion}/Y_{H^+}]		
	MNP-NH ₂	MNP-NH ₂ /TRX/gA	MNP-NH ₂ /glutar/gA
H ⁺	1	1	1
Na ⁺	0.31 ± 0.0	0.27 ± 0.0	0.54 ± 0.0
K ⁺	0.41 ± 0.07	0.29 ± 0.04	0.45 ± 0.0
Mg ²⁺	0.55 ± 0.1	0.36 ± 0.0	0.49 ± 0.0
Ca ²⁺	0.65 ± 0.05	0.39 ± 0.0	0.68 ± 0.0

In Figure 6.6. the data collected for the membranes prepared in PBS solution is presented. It can be seen that the initial trend is similar as in the case of the membranes prepared in water, but resistance values obtained for the membrane prepared via chemical coupling are much lower than the ones of untreated membrane. Even though they are significantly higher

than the values obtained for the membranes after physical treatment. Higher water content in the membranes prepared by TRX/gA micelles immobilization (confirmed also in water uptake experiments) can result in higher ion passage. However, considering those results together with selectivity calculation (Table 6.5.) it can be seen, that although the resistance is higher, membrane exhibit better selectivity, slightly improved in regards to the initial, untreated membrane (about 6, 11, 16 and 4% better for sodium, potassium, magnesium and calcium, respectively) and notably enhanced in comparison to the membrane after physical immobilization (of 18, 8, 20 and 10% better for sodium, potassium, magnesium and calcium, respectively).

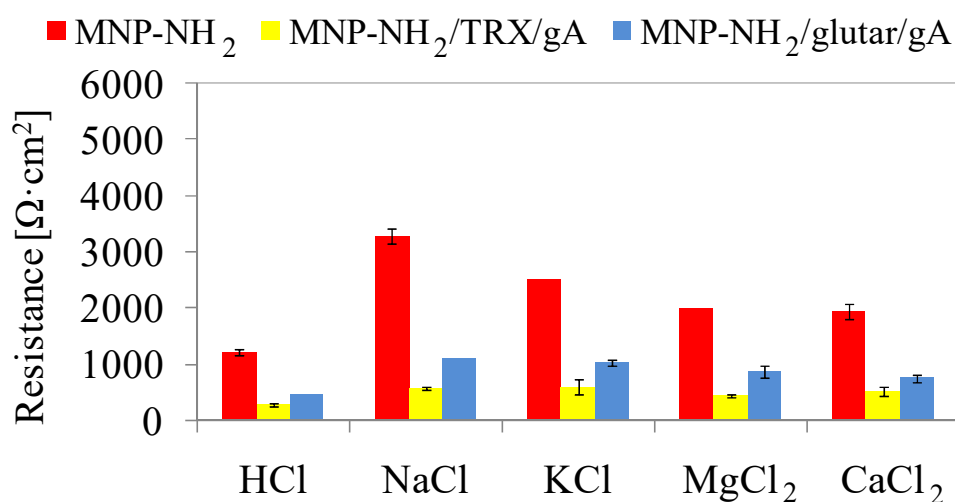


Figure 6.6. Ohmic resistance values for the membranes: MNP-NH₂, MNP-NH₂/TRX/gA presented previously (see Chapter V, Figure 5.10.) and MNP-NH₂/glutar/gA prepared in PBS.

Table 6.5. Selectivity values for the membranes: MNP-NH₂, MNP-NH₂/TRX/gA presented previously (see Chapter V, Table 5.12.) and MNP-NH₂/glutar/gA prepared in PBS.

Ion	Selectivity [Y_{ion}/Y_{H^+}]		
	MNP-NH ₂	MNP-NH ₂ /TRX/gA	MNP-NH ₂ /glutar/gA
H ⁺	1	1	1
Na ⁺	0.38 ± 0.02	0.50 ± 0.04	0.41 ± 0.0
K ⁺	0.49 ± 0.02	0.48 ± 0.05	0.44 ± 0.0
Mg ²⁺	0.61 ± 0.03	0.64 ± 0.05	0.52 ± 0.0
Ca ²⁺	0.63 ± 0.02	0.55 ± 0.03	0.60 ± 0.0

Nevertheless, it still maintains unexplained, why there is a contrast between results obtained by ion diffusion assay and ion conductivity experiments regarding the membranes

prepared in PBS. Permeability experiment suggested, that since the permeability values obtained for MNP-NH₂/glutar/gA membrane were the highest, the lowest ohmic resistance in Current-Voltage assay would be expected. To better understand this phenomena, transport mechanism study is essential. For better interpretation of obtained results, transport properties data analysis was performed, and will be discussed in the following section 6.4.4. Nevertheless, it can be stated that the observed increase in selectivity seems to be a consequence of successful protein immobilization. Even though the membrane prepared via glutaraldehyde coupling has higher resistance compare to the membrane with immobilized TRX/gA micelles, it is still significantly lower than the resistance of untreated MNP membrane. This property, together with high selectivity is an important advance in achieving the main goal of ion exchange membrane fabrication.

6.4.4. Self-diffusion coefficient calculation

From the above Current-Voltage experiments, conductivity (molar) and self-diffusion coefficient values have been calculated. Data obtained together with diffusion coefficient values are collected in Table 6.6. The data obtained for the membranes prepared via glutaraldehyde coupling were compared with the values obtained for the membranes with physically immobilized gA. Similar like in the case of all the previously studied membranes, the calculated self-diffusion coefficient values are at least five orders of magnitude higher than the diffusion coefficient values obtained from permeability experiment. It suggests that those hybrid membrane systems do not apply to the Nernst-Einstein equation based model.

Chapter VI | **Chemical immobilization by
glutaraldehyde coupling**

Table 6.6. Results of conductivity and self-diffusion coefficient calculated from the resistance data, and the diffusion coefficient values calculated from permeability data, for the membranes: MNP-NH₂, MNP-NH₂/TRX/gA presented previously (see Chapter V, Table 5.14.) and MNP-NH₂/glutar/gA.

Membrane	Prep. Sol.	H ⁺		Na ⁺		K ⁺		Mg ²⁺		Ca ²⁺					
		σ [S/m]	D σ [cm ² /s] ($\cdot 10^{-08}$)	σ [S/m]	D σ [cm ² /s] ($\cdot 10^{-8}$)	D [cm ² /s] ($\cdot 10^{-3}$)	σ [S/m]	D σ [cm ² /s] ($\cdot 10^{-8}$)	D [cm ² /s] ($\cdot 10^{-3}$)	σ [S/m]	D σ [cm ² /s] ($\cdot 10^{-8}$)	D [cm ² /s] ($\cdot 10^{-3}$)			
MNP-NH ₂		0.10	3.01	0.03	0.91	0.44	0.04	1.23	0.70	0.01	0.03	0.56	0.06	0.49	<0.01
MNP-NH ₂ /TRX/gA	H ₂ O	0.27	8.37	0.09	2.85	5.90	0.12	3.80	7.89	0.04	0.35	2.94	0.20	1.54	0.96
MNP-NH ₂ /glutar/gA		0.71	3.40	0.15	2.85	2.03	0.21	3.08	4.65	0.22	0.13	1.41	0.23	1.07	0.60
MNP-NH ₂		0.07	2.32	0.03	0.89	0.52	0.04	1.14	2.23	0.01	0.03	0.91	0.05	0.37	<0.01
MNP-NH ₂ /TRX/gA	PBS	0.35	11.16	0.18	5.53	2.06	0.17	5.30	3.07	0.08	0.63	1.72	0.19	1.52	0.88
MNP-NH ₂ /glutar/gA		0.45	8.35	0.13	3.42	7.54	0.14	3.66	10.7	0.11	0.24	2.06	0.19	1.26	4.43

6.5. Conclusions

A chemical method of biomolecule immobilization on a Psf membrane containing magnetic nanoparticles MNP, via glutaraldehyde coupling reaction have been investigated. It have been found that immobilization significantly increase surface hydrophilicity of MNP-NH₂ membrane and does not affect membrane morphology. Immobilization enhances also ion diffusion speed in comparison to untreated MNP-NH₂ membrane, and when the reaction is performed in PBS, the membrane performance is better than the membranes with physically immobilized gA. Ion transport characterization by Current-Voltage shows that membranes after gA immobilization exhibit lower resistance than unmodified membrane, but when prepared in PBS solution, resistance is slightly higher when compared to the membrane with physically immobilized protein. Nevertheless, with relatively low resistance value, membrane selectivity was significantly improved. This indicates the potential use of this material to be used in application requiring selective ion transport such as: artificial photosynthesis, nanofiltration or fuel cells. For this system, as in the case of membranes with physically immobilized gA, Nernst-Einstein model for self-diffusion coefficient estimation does not apply.

6.6. References

- [1] M.M.M. Elnashar, The Art of Immobilization Using Biopolymers, Biomaterials and Nanobiotechnology, in: P.M. Elnashar (Ed.) Biotechnology of Biopolymers, InTech Europe, 2011.
- [2] M.D. Trevan, Enzyme Immobilization by Covalent Bonding, in: J.M. Walker (Ed.) New Protein Techniques, Humana Press, Totowa, NJ, 1988, pp. 495-510.
- [3] D.R. Walt, V.I. Agayn, The chemistry of enzyme and protein immobilization with glutaraldehyde, TrAC Trends in Analytical Chemistry, 13 (1994) 425-430.
- [4] S. Avrameas, Coupling of enzymes to proteins with glutaraldehyde: use of the conjugates for the detection of antigens and antibodies, Immunochemistry, 6 (1969) 43IN949-948IN1152.
- [5] I. Migneault, C. Dartiguenave, M.J. Bertrand, K.C. Waldron, Glutaraldehyde: behavior in aqueous solution, reaction with proteins, and application to enzyme crosslinking, Biotechniques, 37 (2004) 790-806.
- [6] P.D. Weston, S. Avrameas, Proteins coupled to polyacrylamide beads using glutaraldehyde, Biochemical and biophysical research communications, 45 (1971) 1574-1580.
- [7] F. Kara, G. Gurakan, F. Sanin, Monovalent cations and their influence on activated sludge floc chemistry, structure, and physical characteristics, Biotechnology and bioengineering, 100 (2008) 231-239.
- [8] R.P.a.S.M. E., Processes Involved in Sodic Behaviour, Oxford University Press, New York, 1998.
- [9] G.I. Chamoulaud, D. Belanger, Modification of ion-exchange membrane used for separation of protons and metallic cations and characterization of the membrane by current-voltage curves, Journal of Colloid and Interface Science, 281 (2005) 179-187.

Chapter VII

Preparation and characterization of track-etched polymeric membranes containing Gramicidin

7.1. Introduction

In this chapter another membrane preparation method is introduced. The applicability of TRX/gA micelles immobilization technique in membranes different than polysulfone is checked. Polyethylene terephthalate (PET) membranes, fabricated by track etching technique have been used. Besides, different immobilization methods of Gramicidin have been performed on PET track etched films and tested, in order to compare the efficiency of the micelles between modification methods.

7.2. Materials and methods

In this section, the preparation of various polymeric membranes will be described.

7.2.1. PET film preparation

Poly(Ethylene Terephthalate) (PET) film (thickness 13 μm , biaxial orientation) was purchased from Goodfellow (ES301061). The tracks were done by Xe irradiation fluence (8,98 MeV u^{-1} , density $1.63 \times 10^8 \text{ cm}^{-2}$) at GANIL, SME line, Caen, France. Previous to the etching, track activation was performed by exposition to UV light (Fisher bioblock; VL215.MC) at 365 nm wave length. Next, films were etched with 3M NaOH solution. In order to study also the impact of pore shape on immobilization procedures efficiency, two types of membranes were prepared: membrane with conical pores and membrane with cylindrical pores. In both cases, irradiation and etching procedures were adjusted independently.

- a) Membranes with conical pores: 24 hours irradiation from one side, etching at the temperature of 40° C for 3 minutes in order to obtain membranes with a pore size of 20 nm (TR20C), and 4.5 minutes to obtain membranes with a pore size of 40 nm

(TR40C). TR40C membrane was further treated with Atomic Layer Deposition (ALD) to obtain the pore size of around 20 nm.

- b) Membranes with cylindrical pores: 8 hours irradiation from each side, etching at the temperature of 50° C for 5 minutes in order to obtain membranes with a pore size of 40 (TR40), and for 7 minutes to obtain membranes with a pore size of 80 nm (TR80). Both membranes were further treated with Atomic Layer Deposition (ALD) to obtain the pore size of around 20 nm.

Pore size after chemical etching was determined by SEM analysis.

7.2.2. PET film surface modification and Gramicidin immobilization

In order to immobilize gA on track etched membranes various methods were applied.

- a) Triton micelles immobilization: micelle immobilization was performed using the same procedure carried out for the functionalization of polysulfone membranes reported before (see Chapter V, section 5.3.1.4.), that implies immersing the membrane in the TRX and 10^{-7} M of gA solution and stirring during 72 h. Within this technique, TR20C membrane was obtained.
- b) Isopropylamine modification: this method aims to perform aminolysis of PET film in order to introduce alkyl functional groups to the surface. This process is a well-known method to modify PET polymer structure to convert it to less thermally stable derivative, for recycling purposes [1, 2]. Introduction of hydrophobic alkyl groups aims to imitate the interaction of Gramicidin with the lipid bilayer in biological membrane. Modification was performed by immersion of the membrane film in an isopropylamine solution for 24 hours. Next, impregnation with methanolic 10^{-6} M concentrated Gramicidin solution was performed by soaking the membrane for 72 hours. Within this technique, TR40C A membrane was obtained.
- c) Hexamethyldisilazane modification: this method, as the previously described one, tends to introduce $-CH_3$ methyl hydrophobic groups to the PET membrane and was performed by film exposition to HMDS vapors for 24 hours [3, 4]. Next, impregnation

with methanolic Gramicidin solution was carried out by soaking the membrane for 72 hours. Within this technique, were obtained membranes: TR40, TR40C B and TR80.

7.2.3. Polysulfone membranes surface modification

Polysulfone modification with Nystatin has been performed by immersing polysulfone membranes in an aqueous 0.58 mM concentrated solution of nystatine and stirred for 72 hours. Results of permeability test for this membrane were compared with the results obtained for the Plain polysulfone membranes modified by TRX/gA micelles immobilization (physical methods).

Nystatin is an antifungal drug which is also a membrane active polyene with amphiphilic structure (Figure 7.1.). This properties allows it to self-assemble into channels and increase ion passage through the membrane [5].

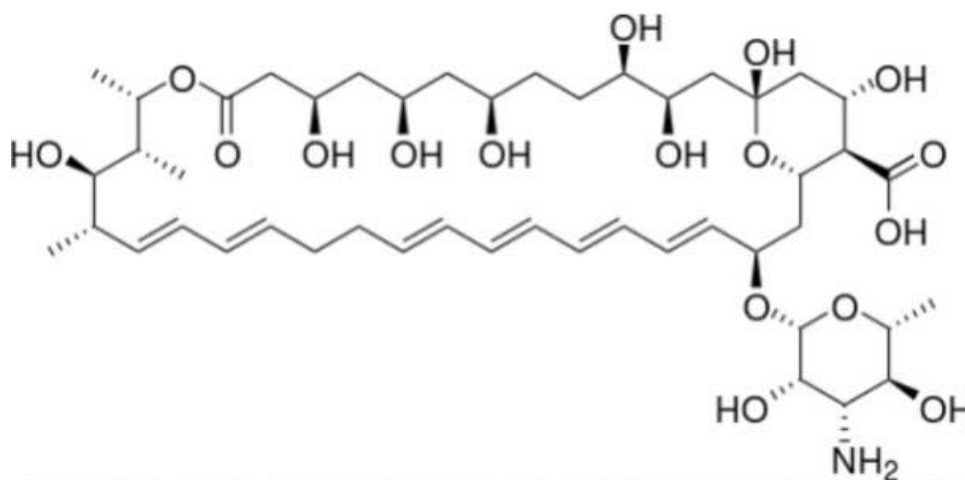


Figure 7.1. Nystatin structure.

The amphiphilic character of Nystatin could interact with polysulfone film within the same mechanism as Triton does, when immobilizing micelles. Thus, Nystatin treatment was performed in order to check the influence of another channel-forming molecule immobilization on ion permeability across polysulfone membrane.

7.2.4. Permeability test

Prepared membranes were tested in order to examine ion diffusion properties. This experiment type has been chosen as a representative characterization method for novel prepared membranes, due to its simplicity and possibility to extract the basic information about membrane ion transport properties. The electrolytes used were 0.1 M solutions of: NaCl, KCl, MgCl₂ and CaCl₂. Membranes with immobilized TRX/gA micelles were additionally tested in terms of selectivity to anions, with the 0.1 M solutions of NaNO₃, Na₂SO₄ and saturated solution of NaHCO₃. The rest of the membranes was tested also with 0.1 M Na₂SO₄ solution. The concentration change during time was measured with Hanna HI 255 combined meter with conductivity and electrode HI 76310. Experiments were carried out at least 2 times, using different piece of membrane.

7.3. Results

7.3.1. Selectivity to cations of PET membranes

Micelle immobilization effect was evaluated, studying the membrane permeability. As can be seen on the graphic below (Figure 7.2.), permeability of the membranes concerning to small monovalent cations (sodium and potassium, on the left side of the graphics) is only slightly lower in comparison to the non-modified track etched PET film. However, bigger divalent ions (magnesium and calcium, on the right side of the graphics) seem to pass much slower after TRX/gA micelles immobilization. It shows an improvement of selectivity in respect to smaller ions, but the velocity of transport did not change significantly. Since it is known, that Gramicidin in the biological membranes is characterized by the fastest ion transport, an increase in ion transport could indicate that not only free ion diffusion occurs. Thus, it cannot be ensured if selectivity is a result of gA role in transport mechanism or it is only due to the blocking of the small conical pore by micelle, that would obstruct the passage of bigger ions.

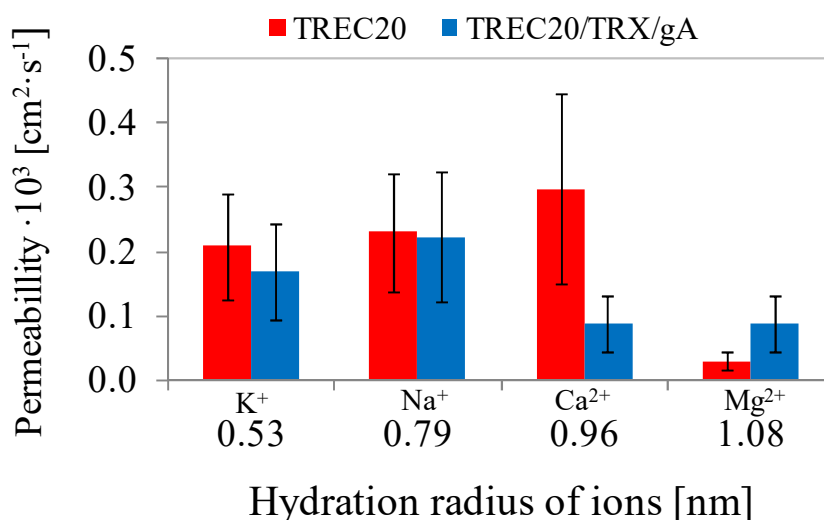


Figure 7.2. Permeability of track etched membranes with conical pores, before and after TRX/gA micelles immobilization versus the hydration radius of ions K⁺, Na⁺, Ca²⁺ and Mg²⁺ respectively [6, 7]. Values of permeability are average of 2 measurements taken from 2 different membranes prepared under the same experimental conditions. The error bars refers to the standard deviation from the measurements.

Results for the conical pore membrane, functionalized with HMDS and initial pore size of 40 nm are presented below (Figure 7.3.). In general, permeability values are lower in comparison to the results corresponding to membrane with immobilized TRX/gA micelles. This is due to the fact that membrane treatment with surfactant increase its wetting properties and higher ion passage is related to higher water flux. In contrast, treatment with HMDS increase hydrophobicity of the surface, thus the water access is impeded and so is the ion passage. Nevertheless, transporting tendency is not regular and neither improvement nor deterioration in modified membrane performance is observed with respect to the material before gA immobilization.

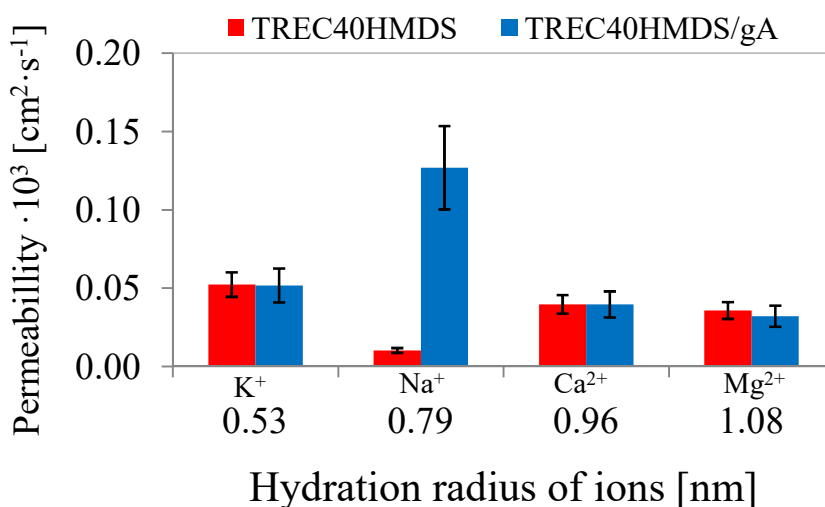


Figure 7.3. Permeability of HMDs functionalized track etched membranes with conical pores, before and after gA immobilization versus the hydration radius of ions K⁺, Na⁺, Ca²⁺ and Mg²⁺ respectively [6, 7]. Values of permeability are average of 2 measurements taken from 2 different membranes prepared under the same experimental conditions. The error bars refers to the standard deviation from the measurements.

Concerning membranes with cylindrical pores, after gA immobilization, permeability to monovalent ions has been reduced in both cases: from 1.21E-04 to 1.01E-04 cm²·s⁻¹ for Na⁺ and from 1.22E-04 to 9.77E-05 cm²·s⁻¹ for K⁺ in the case of TR40 membrane; and from 1.53E-04 to 7.75E-05 cm²·s⁻¹ for Na⁺ and from 7.53E-05 to 3.85E-05 cm²·s⁻¹ for K⁺ in the case of TR80 membrane (Figure 7.4.). In the case of divalent ions, for TR40 membrane only the value of permeability for Ca²⁺ has been obtained. Result shows, that permeability for this ion is smaller after modification (reduction from 8.39E-05 to 3.35E-05 cm²·s⁻¹), in contrast to the membrane TR80, which represents slightly higher values of permeability for divalent ions after immobilization (increase from 1.8E-05 to 2.83E-05 cm²·s⁻¹ for Ca²⁺ and from 1.34E-05 to 2.49E-05 cm²·s⁻¹ for Mg²⁺). Similarly as in the previous case, those velocities are smaller in comparison to the micelle immobilized membrane, as a result of more hydrophobic surface. The results shows undoubtedly, the dependence of ion transport efficiency on the ion size, which could be an effect of both, gA selective function or simply blocking of the pores.

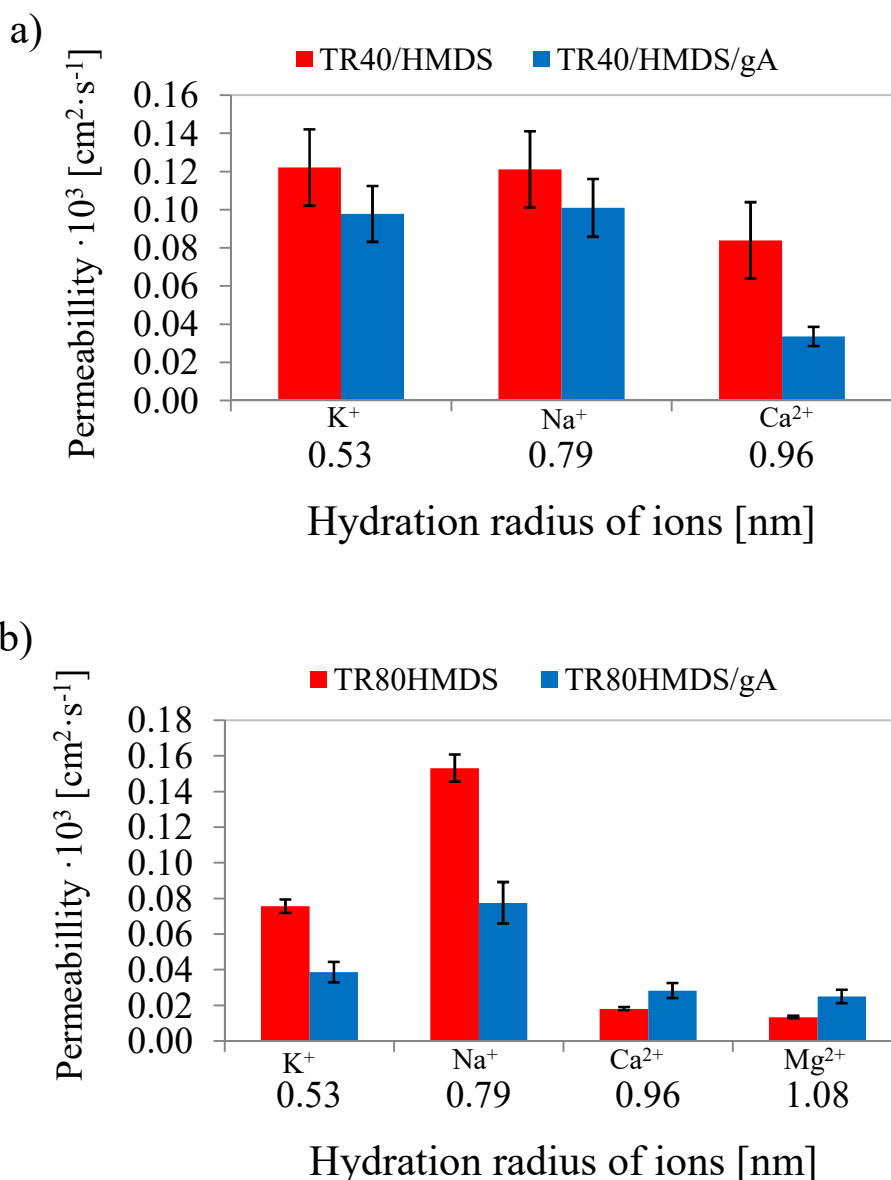


Figure 7.4. Permeability of HMDS functionalized track etched membranes with cylindrical pores of initial size of 40 (7.4.a) and 80 nm (7.4.b), before and after gA immobilization versus the hydration radius of ions K⁺, Na⁺, Ca²⁺ and Mg²⁺ respectively [6, 7]. Values of permeability are average of 2 measurements taken from 2 different membranes prepared under the same experimental conditions. The error bars refers to the standard deviation from the measurements.

Results obtained for membrane TRC40, corresponding to 40 nm pore diameter, having conical pore, functionalized with isopropylamine are collected in Figure 7.5., together with all experimental results of other membranes obtained. In the case of all the track etched membranes, dependence of the ion transport speed on the ionic size is clear. The highest

selectivity is visible for the membrane with immobilized TRX/gA micelles and TR40/HMDS modified membrane with cylindrical pore. The membrane modified with isopropylamine has lower permeability than the one modified with surfactant micelle, but higher permeability than the ones modified with HMDS. This is due to the intermediate hydrophilicity between both surface modifying agents. In the case of all the membranes with immobilized Gramicidin, an increase of Na⁺ permeability over other ions is visible. That might be an effect of the participation of gA in transport mechanism. Nevertheless, for any of the cases those tendencies were not proved statistically.

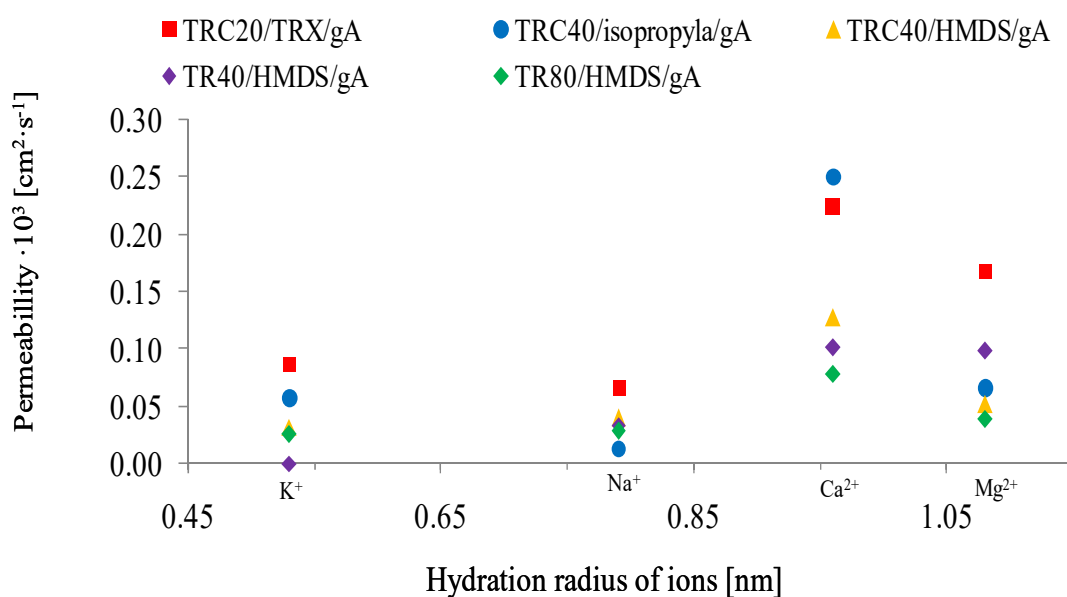


Figure 7.5. Permeability of all the track etched membranes modified with various techniques.

7.3.2. Selectivity to anions of PET membranes

Track etched membrane with conical pore with immobilized TRX/gA micelles were tested in terms of its selective behavior according to anions. The results are presented below (Figure 7.6.). Immobilization of micelles seems to have no drastic influence on anion permeability in case of small chloride ions (0.33 nm ionic diameter), but it is notable affected for bigger NO₃⁻ and SO₄²⁻. For bicarbonate ions (0.36 nm an improvement in permeability speed was observed (from 1.32E-04 to 2.13E-04 cm²s⁻¹).

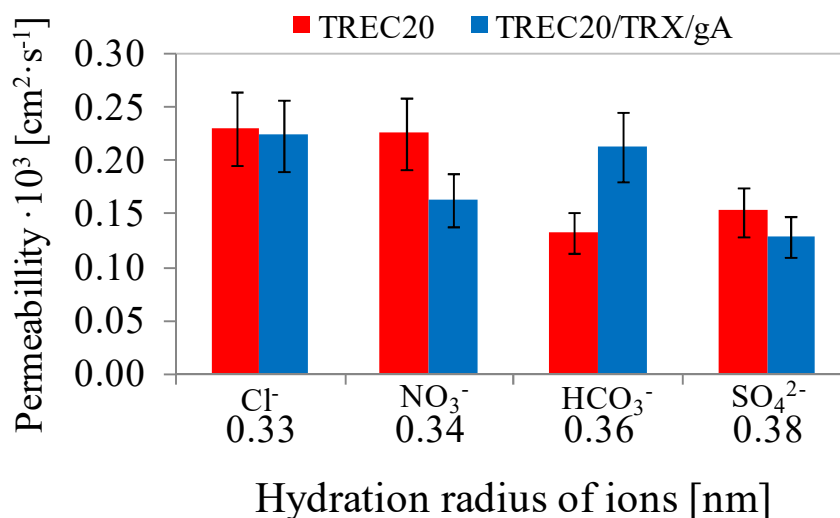


Figure 7.6. Permeability of track etched membranes with conical pores, before and after TRX/gA micelles immobilization versus the hydration radius of ions Cl^- , NO_3^- , CO_3^- and SO_4^{2-} respectively. Values of permeability are average of 2 measurements taken from 2 different membranes prepared under the same experimental conditions. The error bars refers to the standard deviation from the measurements.

All the membranes were tested with the solution of sodium chloride and sodium sulfate, in order to check the transport behavior of small and big anions. Except of TR40 membrane, functionalized with HMDS, all the membranes exhibit certain selectivity (Figure 7.7.). The most visible effect detected is in the case of membrane functionalized with isopropylamine. However those tendencies were not proved statistically.

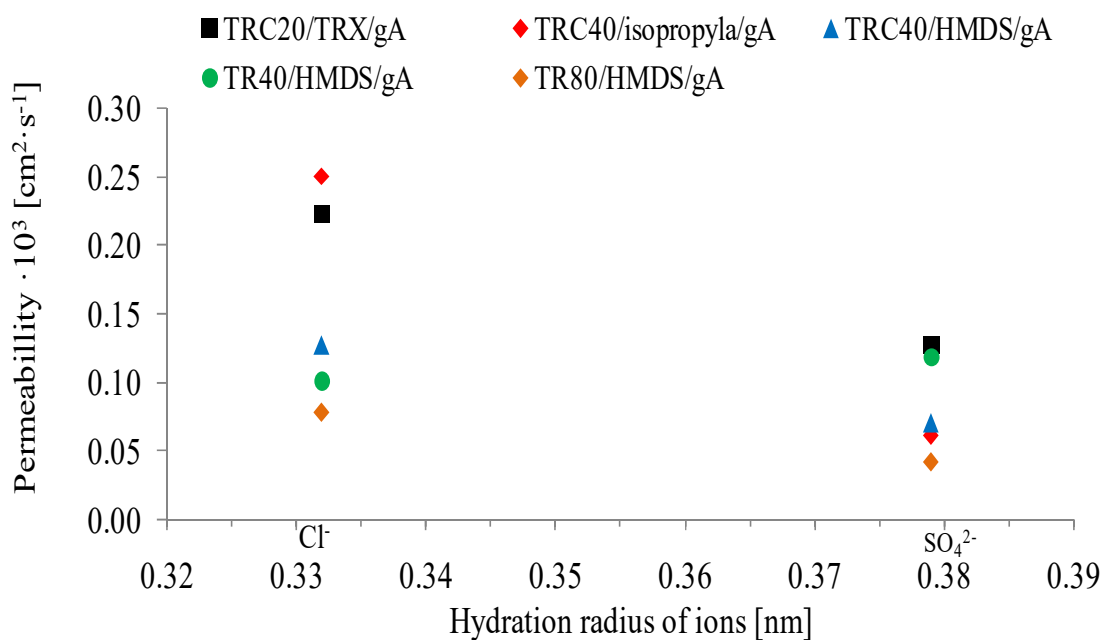


Figure 7.7. Permeability trends of all the track etched membranes modified with various techniques.

7.3.3. Selectivity of polysulfone membranes

Nystatine-treated polysulfone membrane with has been compared with Triton- and Triton/gA micelle-treated polysulfone. As reference, untreated polysulfone membrane was used. The results undoubtedly shows that treatment with use of surfactant leads to the best performance in terms of permeability (Figure 7.8.). As expected, also immobilization of Nystatin improved ion passage, nevertheless it is still much lower in comparison to the membranes treated with the use of surfactant or surfactant/gA micelles. It is also confirmed, as in the case of the same treatments performed on MNP membranes described before, that permeability decrease after gA incorporation within micelles. This influence of the protein immobilization could be a result of the interaction of ions with the protein, or only due to the blocking the pores by protein agglomerates. Regarding the selective behavior of the membranes, it is not clearly highlighted in the case of Nystatin functionalized polysulfone. The membrane containing TRX/gA micelles shows to be selective to the smallest ion.

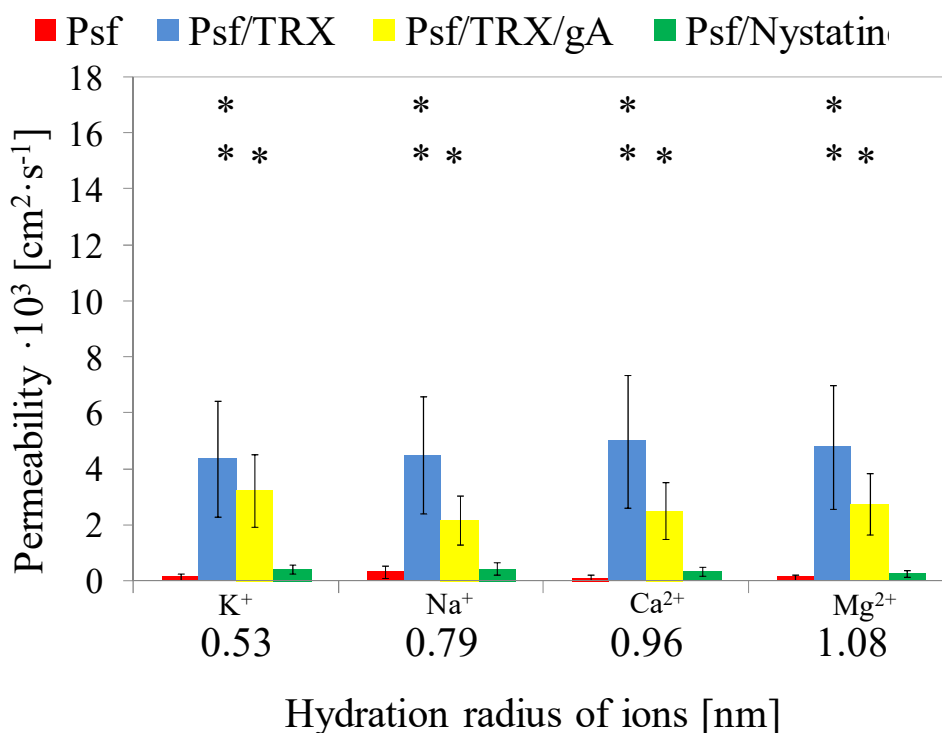


Figure 7.8. Permeability of polysulfone membranes modified with various techniques: previously presented Plain Psf, Psf/TRX and Psf/TRX/gA membrane (see Chapter V, Figure 5.6.b) and Psf/Nystatine membrane versus the hydration radius of ions K^+ , Na^+ , Ca^{2+} and Mg^{2+} respectively [6, 7]. Values of permeability are average of 2 measurements taken from 2 different membranes prepared under the same experimental conditions. The error bars refers to the standard deviation from the measurements. Columns highlighted with * refers to the samples for which obtained p-value was <0.05 , with ** refers to the samples for which p-value was <0.01 . For the statistical evaluation, the following hypothesis was made: (i) the permeability value of Psf membranes after TRX treatment, after TRX/gA micelles immobilization or after Nystatin immobilization is different than permeability value of non-modified membrane. The p-values **below** 0.05 correspond to the samples which are in agreement with this assumption.

7.3.4. Surface chemistry (FTIR)

FTIR spectra were performed for all the membranes, however only representative samples after immobilization are presented. In Figure 7.9. spectra of PET/isopropylamine/gA and PET/TRX/gA membranes, compared with non-modified PET film are shown. In all the spectra a peak around 2970 cm^{-1} , characteristic for PET coming from methyl group is visible. Besides, a strong and sharp carbonyl group signal was also detected [8, 9]. Only in the spectra

of isopropylamine functionalized membrane it can be seen additional sharp peaks between 3000-2850 cm^{-1} coming from alkane C-H stretching of new attached alkyl chain [10]. Treatment with TRX/gA micelles on the other hand does not show any changes in the surface chemistry, and non additional peaks are visible at all. Regarding the protein detection, no changes in a characteristic amide bond zone, which would be expected after gA immobilization were present [11]. That was not observed in any of the spectra, although the surface modifications through the applied treatments could be noticed. This is probably due to the fact the very low content of protein with respect to polymer.

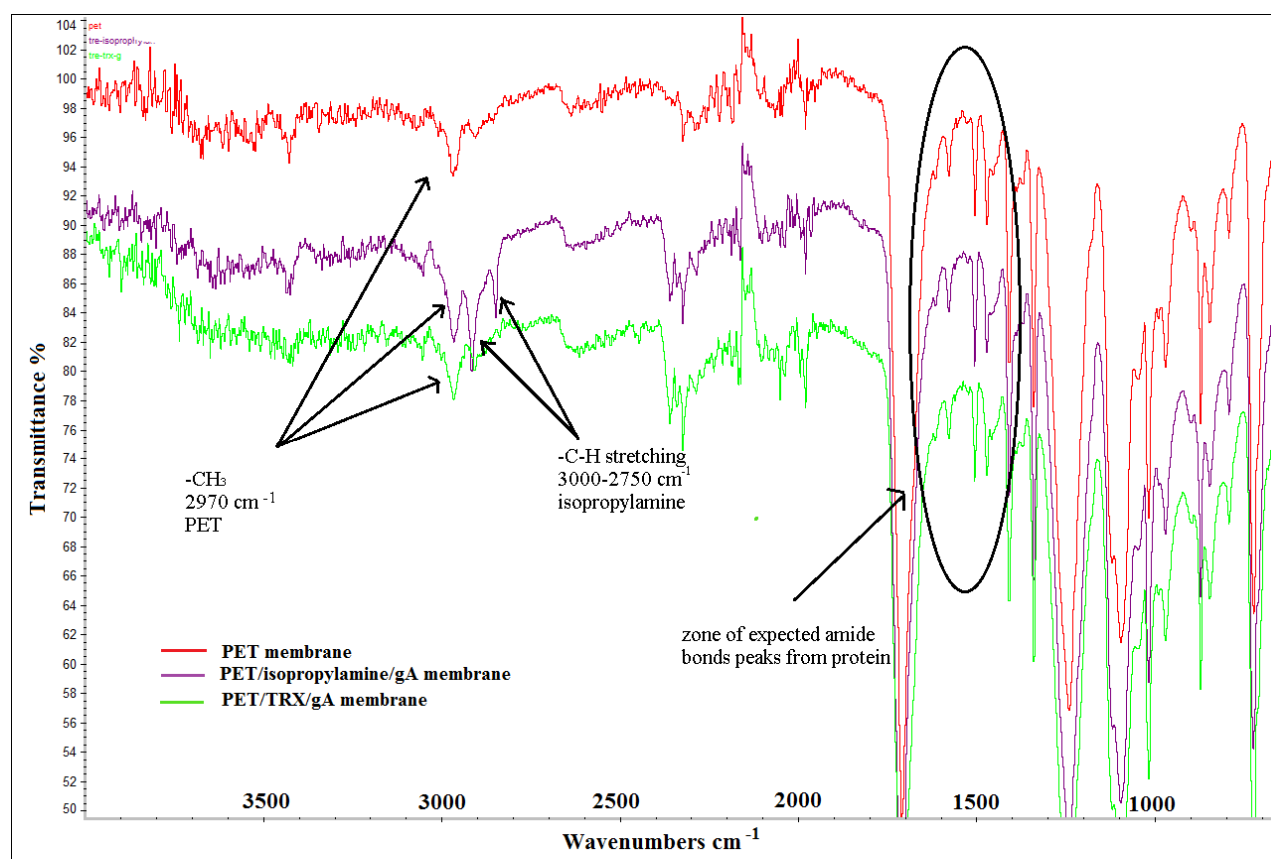


Figure 7.9. FTIR spectra of track etched membranes: plain PET film, functionalized with isopropylamine and gA, and with TRX/gA micelles.

7.4. Conclusions

Another method of porous polymeric membrane preparation was presented in this chapter. Applicability of TRX/gA micelles immobilization on material different than polysulfone was

evaluated. Also, various types of Gramicidin immobilization were tested: TRX/gA micelles immobilization, gA immobilization on isopropylamine or HMDS functionalized membrane, with different pore shapes. Permeability test results show, that among many techniques, the highest permeability values for both, cations and anions are obtained for membranes after TRX/gA micelles immobilization. This is due to surfactant treatment, which increases water passage and, also ion flux. In contrast, high increase of hydrophobicity caused by introduction of methyl groups by use of HMDS, provided the lowest membrane permeability values. In no cases, significant increase of selectivity after gA immobilization was observed, however the general trend is, that after protein confinement, permeability slightly decreases. This effect suggests occurrence of interaction between ion channel and electrolyte ions. This confirms the successful protein immobilization with all the used techniques. Nevertheless, the efficiency of protein exact loading amount on the membranes is difficult to determine. FTIR analysis did not provide information about protein presence in the film, probably due to a very low gA concentration. Additionally, another modification of polysulfone membrane was performed. Nystatin immobilization enhanced ion permeability, without impact on its selectivity. However, obtained values of permeability are still significantly lower in comparison to the polysulfone membranes after TRX/gA micelles immobilization.

7.5. Acknowledgments

Track-etched membranes and Polysulfone/Nystatin membrane were fabricated and characterized in Interfaces, Physical Chemistry and Polymers research group at the European Membrane Institute in Montpellier. Dr Sébastien Balme is kindly acknowledge for his assistance, collaboration and help.

7.6. References

- [1] W.H. Cook, Process for modifying linear polymer resins, in, Google Patents, 1980.
- [2] M. Drobot, M. Aflori, I. Stoica, F. Doroftei, Surface characterization of amine functionalized pet films after collagen immobilization, *Rev Roum Chim*, 58 (2013) 203-207.
- [3] Y. Mor, T. Chang, P. Liu, T. Tsai, C. Chen, S. Yan, C. Chu, W. Wu, F. Pan, W. Lur, Effective repair to ultra-low-k dielectric material ($k \sim 2.0$) by hexamethyldisilazane treatment, *Journal of Vacuum Science & Technology B: Microelectronics and Nanometer Structures Processing, Measurement, and Phenomena*, 20 (2002) 1334-1338.
- [4] S.C. Lim, S.H. Kim, J.H. Lee, M.K. Kim, T. Zyung, Surface-treatment effects on organic thin-film transistors, *Synthetic Metals*, 148 (2005) 75-79.
- [5] K. Boukari, G. Paris, T. Gharbi, S. Balme, J.-M. Janot, F. Picaud, Confined Nystatin Polyenes in Nanopore Induce Biologic Ionic Selectivity, *Journal of Nanomaterials*, 2016 (2016).
- [6] F. Kara, G. Gurakan, F. Sanin, Monovalent cations and their influence on activated sludge floc chemistry, structure, and physical characteristics, *Biotechnology and bioengineering*, 100 (2008) 231-239.
- [7] R.P.a.S.M. E., Processes Involved in Sodic Behaviour, Oxford University Press, New York, 1998.
- [8] Z. Huang, L. Bi, Z. Zhang, Y. Han, Effects of dimethylolpropionic acid modification on the characteristics of polyethylene terephthalate fibers, *Molecular medicine reports*, 6 (2012) 709-715.
- [9] Z. Chen, J.N. Hay, M.J. Jenkins, FTIR spectroscopic analysis of poly(ethylene terephthalate) on crystallization, *European Polymer Journal*, 48 (2012) 1586-1610.
- [10] W. Duncan, W.H. Soine, Identification of Amphetamine Isomers by GC/IR/MS, *Journal of Chromatographic Science*, 26 (1988) 521-526.
- [11] W.-P. Ulrich, H. Vogel, Polarization-Modulated FTIR Spectroscopy of Lipid/Gramicidin Monolayers at the Air/Water Interface, *Biophysical Journal*, 76 (1999) 1639-1647.

Chapter VIII

Surfactant/Gramicidin micelles bioactivity study

8.1. Introduction

Apart of its excellent transport properties, Gramicidin A is also an antibiotic that destroys gram-positive bacteria. This antimicrobial peptide (AMP) is characterized by very high bacteria killing rate (of 100% in comparison with other AMP [1]). The most common killing mechanism of that kind of peptides is based on pore formation followed by destroying pathogen cell membranes. Gramicidin instead of pore, forms single ion channel and apart of membrane permeabilization, uses also another mechanism, based on hydroxyl radical formation [1]. Antibacterial activity of gA against bacteria such as *Staphylococcus aureus* or *Streptococcus pneumoniae* has been proved [1, 2]. Thus, it has been evaluated whether Gramicidin immobilized in micelles exhibited the same characteristics.

Surfactants are characterized by amphiphilic structure, what means that contain both hydrophilic and hydrophobic groups. This unique property of having both water- and oil-soluble components, have made them useful as detergents, emulsifiers or dispersants. In a solution, surfactants above their particular concentration (called critical micelle concentration) self-organize into micelles and dependently of the character of the solvent, they create structures called micelles, with hydrophobic interior and hydrophilic exterior (in water) or contrary (in organic solvent). Those aggregates of surfactant molecules can adapt different shapes, from spheres, vesicles, wormlike micelles to reverse micelles [3]. They have found application in various fields, like enhanced oil recovery [4, 5], cosmetics [6, 7] or wastewater treatment [8]. Thanks to its affinity to lipids, they are also commonly used in biology for cell membranes permeabilization, which allows to create capsules dispersed in water, containing functional insoluble proteins. This approach enabled the possibility to create biologically functional microreactors and perform processes unavailable till now in aqueous environment [9-11]. Besides, possibility of micelles adsorption on solid supports has tremendous importance for enhancement of many technological processes, like pollution control, wetting and lubrication or heterogeneous catalysis [12-14].

Bacteria studied were selected based on possible future application and were *Listeria innocua* and *Bacillus subtilis*.

Listeria innocua is a Gram-positive bacteria of the *Listeria* genus. *Listeria*'s are commonly found in the soil. They are resistant to various pH range and salts. Their optimal development occurs in the range of 30-37° C. One of them, *Listeria monocytogenes*, is extremely harmful food-borne pathogen. It can survive food-processing conditions and refrigeration temperatures what makes it a serious danger to human health. Listeriosis, induced by intoxication with *monocytogenes* is caused by food poisoning and is a virulent and highly lethal disease which in United States, together with salmonella and toxoplasmosis is responsible for over 1500 deaths every year [15]. *Listeria innocua* was found to have a similar genom to this dangerous pathogen and thus, was chosen to be a great candidate to study the effect of TRX/gA micelles on those species. This investigation can bring information about potential use of membranes with immobilized micelles in food industry separation processes, helpful in solving the problem of high mortality of food poisonings caused by *Listeria monocytogenes*.

Bacillus subtilis is found in soil and vegetations. Is one of the most studied bacteria which serves as a model gram-positive species, corresponding to gram negative *Escherichia Coli*. As *Listeria innocua*, it is a facultative anaerobe. It is not pathogenic and moreover it found application as a fungicide because does not affect human health. Since this is a model gram-positive bacteria, *Bacillus subtilis* was chosen to study general antibacterial activity of Gramicidin immobilized in micelles. *Bacillus subtilis* was also found to be a component of ultra and nanofiltration membranes fouling. Thus, the study of activity against this bacteria could give potential antifouling properties of membranes with immobilized micelles. In this Chapter the antimicrobial properties of micelle solutions and of micelles immobilized on a membrane surface have been evaluated.

8.2. Materials

Gramicidin (gA) from *Bacillus aneurinolyticus* (*Bacillus brevis*) were purchased from Sigma Aldrich. Salts used for PBS (phosphate buffer saline) preparation: sodium chloride and potassium chloride were purchased from Sigma Aldrich, potassium phosphate dibasic trihydrate, disodium hydrogen phosphate dihydrate were purchased from Panreac. Surfactant Triton X-100 (TRX) was purchased from Sigma Aldrich. Methanol was purchased from Sigma Aldrich. All the solutions were prepared in MiliQ water from Millipore. Lyophilized cells of *Bacillus subtilis* (CECT 356) was used as bacteria strain for antimicrobial test. Tryptic soy agar and yeast extract were purchased from Scharlab. Natural seawater from Tarragona Mediterranean Sea was used as water for soaking test sample preparation. To accelerate biofilm formation on the membrane surface, glucose purchased from Sigma was added to water samples.

8.3. Methods

8.3.1. Micelle solutions preparation

PBS, used to obtain all the micelle solutions, was prepared by dissolving the salts at the following concentrations: 137 mM of NaCl, 2.7 mM of KCl, 10 mM of Na₂HPO₄ and 1.8 mM of K₂HPO₄. Final pH value was 7.4. For some of the samples preparation, 10wt% of CH₃OH was added. Next, the gA and TRX were added and the mixture was stirred overnight with use of magnetic stirrer.

The list of samples prepared, together with their contents of protein and surfactant is presented below (Table 8.1).

Table 8.1. List of the samples prepared for bioactivity assay.

Samples used for bioactivity assay
1. PBS
2. PBS+10% CH ₃ OH
3. PBS+ 320 µl/ml TRX+100µg/ml gA
4. PBS+ 320 µl/ml TRX+50µg/ml gA
5. PBS+ 10% CH ₃ OH+100µg/ml gA
6. PBS+ 10% CH ₃ OH+50µg/ml gA
7. PBS+10% CH ₃ OH+25µg/ml gA
8. PBS+10% CH ₃ OH+5µg/ml gA
9. PBS+10%CH ₃ OH+320 µl/ml TRX+100µg/ml gA
10. PBS+10%CH ₃ OH+320 µl/ml TRX+50µg/ml gA
11. PBS+ 10%CH ₃ OH+320 µl/ml TRX+5µg/ml gA
12. PBS+10%CH ₃ OH+320 µl/ml TRX
13. PBS+10%CH ₃ OH +480µg/ml TRX+ 50µg/ml gA

8.3.2. Inhibitory activity study of TRX/gA micelle solutions against *Listeria innocua* and *Bacillus subtilis*

Petri dishes were filled with a mixture of 200µL of standard 10⁸ Colony Forming Unit (CFU)/ml (grown in liquid media: tryptic soy broth 30g/L + yeast extract 6g/L) of *Bacillus subtilis* and 100µL of standard 10⁸ Colony Forming Unit (CFU)/ml of *Listeria innocua* and 15 mL of nutrient agar. Once the medium was solidified (after 4-5 hours), holes with diameters of 7 mm were made using a sterile Pasteur pipet. After that, they were filled either with 25µL of micelle or control solutions. Plates were left for 2 hours at room temperature to allow diffusion of the samples into agar. Then, the plates were incubated at 30°C for 24 h in the case of *Bacillus* and for 48 h at 37°C in the case of *Listeria*. The inhibitory activity of TRX/gA micelles against bacteria was detected as clear zones around the holes, which were measured after incubation. All the experiments were done per triplicate. Statistical analysis using student-T test was performed using XLStat software, using means comparison method with a significance level of 0.05.

8.3.3. Inhibitory activity study of polysulfone membranes with immobilized TRX/gA micelles against *Bacillus subtilis*

8.3.3.1. Experiment in solid medium

Petri dishes were filled with a mixture of 200 μ l of standard 10^8 Colony Forming Unit (CFU)/ml (grown in liquid media: tryptic soy broth 30g/L + yeast extract 6g/L) of *Bacillus subtilis* and 15 ml of nutrient agar. Once the medium was solidified (after 4-5 hours), pieces of 1 cm x 1 cm of polysulfone membrane containing MNPs and the same membrane with immobilized TRX/gA micelles were placed on the agar surface and the plates were incubated at 30°C for 24 h. The inhibitory activity of immobilized TRX/gA micelles against bacteria was detected as clear zones around the membranes, which were measured after incubation. All the experiments were done per triplicate. Statistical analysis using student-T test was performed using XLStat software, using means comparison method with a significance level of 0.05.

8.3.3.2. Experiment in liquid medium

Glass tubes, filled with 5 ml of 5% tryptic soy broth and 1 cm x 1 cm pieces of membranes (containing TRX/gA micelles and without them), were placed into the glassware. Then 100 μ l of standard 10^8 Colony Forming Unit (CFU)/ml of *Bacillus subtilis* were added, and optical density at wavelength of 600 nm of samples were measured immediately. Next, the tubes were incubated at 30°C and the OD were measured again after 24 and 48 h. The inhibitory activity of immobilized TRX/gA micelles against bacteria was evaluated comparing the difference between the values of bacteria density in the samples with the membrane without micelles and the membrane with immobilized TRX/gA micelles. All the experiments were done per triplicate. Statistical analysis using student-T

test was performed using XLStat software, using mean comparison method with a significance level of 0.05. After the experiment, membranes were observed under ESEM in order to check the presence of bacteria growth on the membrane surface.

8.3.4. Membrane biofouling determination

Bacterial stock were prepared by growing overnight cultures in 3% tryptic soy broth at 30°C for 24 hours. Next, 500 µl of *Bacillus subtilis* solution was added to seawater, in order to obtain bacteria concentration around 1×10^7 cfu/ml. Next, 1 mM of glucose was added. The membranes MNP and MNP-OH/TRX/gA were cut using sterile scissors into 3 cm × 3 cm pieces. Three of each membranes were placed in separate 100 ml volume beakers with 50 ml of testing water, seawater without bacteria and glucose or MiliQ water (control). The beakers were wrapped in aluminum foil and shaken at 100 rpm, at 30 °C, to allow biofilm formation, for 24 hours. After that, membranes were analyzed by ESEM to evaluate biofilm growth on surfaces.

8.4. Results

8.4.1. *Listeria innocua*

Although in liquid media the culture growth was easily observed even after 24 hours of incubation, no bacteria growth in solid medium was detected (Figure 8.1.).



Figure 8.1. Petri dishes with *Listeria innocua*, without visible growth of bacteria culture.

In order to check if chosen bacteria concentration was not too low, the same experiment was performed adding to nutrient agar: 100, 200 and 300 µl of liquid media. Plates were incubated for 48 hours at 37°C. However, any of adjusted concentrations did not bring expected effect of bacteria growth as can be seen in the pictures (Figure 8.2.). This result can be explained by the fact that even though *Listeria innocua* is defined as facultative anaerobe, preferred growth conditions of *Listeria innocua* is aerobic atmosphere which is limited in solid media growth conditions.



Figure 8.2. Petri dishes with *Listeria innocua* at different bacteria concentration : a) 100 µl, b) 200 µl, c) 300 µl.

8.4.2. *Bacillus subtilis*

In the case of *Bacillus subtilis*, growth of bacteria was observed easily after 24 hours. Several experiments were performed in order to evaluate antibacterial activity of Gramicidin.

8.4.2.1. Gramicidin activity in micelles without presence of methanol

To check the activity of Gramicidin entrapped in TRX micelles, experiments with the following solutions were designed:

1. PBS/CH₃OH solution
2. PBS/ TRX/ gA (50 µg/ml)
3. PBS/ CH₃OH / gA (50µg/ml)
4. PBS/ TRX/ gA (100µg/ml)
5. PBS/ CH₃OH / gA (100 µg/ml)

Concentration of methanol in samples 1,3 and 5 was 10%. Solution of PBS/ CH₃OH was used as control in order to check if methanol in this concentration had any effect on bacteria growth. Experiment was repeated 3 times and the results of this trial are visible on Figure 8.3.

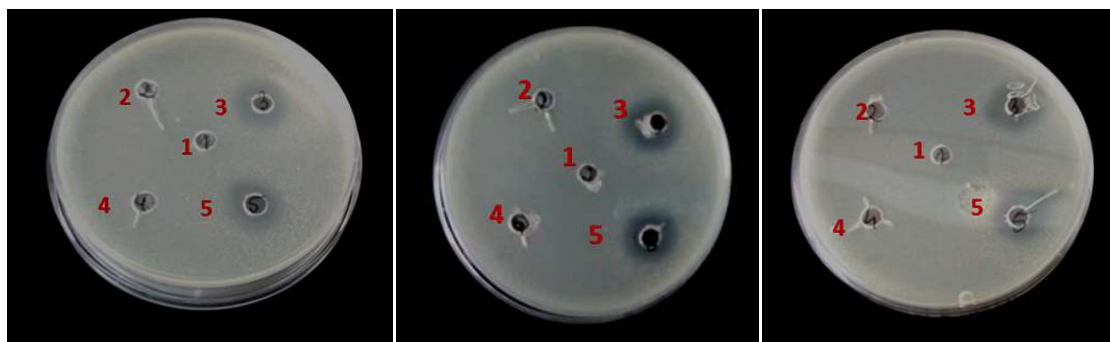


Figure 8.3. Results of the study of gA activity in micelles without presence of methanol.

As can be seen, in agreement with our expectations, methanol in concentration of 10% in PBS does not inhibit bacteria growth (nr 1). TRX/gA micelles in both concentrations, 50 and 100 $\mu\text{g/ml}$, when prepared in PBS solution do not exhibit neither any effect on bacteria growth. However, when gA is not entrapped in the micelle, in the presence of methanol, at both concentrations (50 and 100 $\mu\text{g/ml}$) it shows inhibiting effect on *Bacillus subtilis* growth, what proves its activity against this bacteria. This observation can be explained by low micelle permeability and very slow diffusion of gA from the surfactant capsule. Since it is likely that gA in the presence of methanol adapt its structure to form an active dimer, it is also possible that even though within the presence of surfactant it got dissolved, it was not oriented in its active form, and therefore, could not inhibit bacterial growth. To evaluate this hypothesis, two other experiments were performed.

8.4.2.2. Gramicidin activity in micelles without presence of methanol at different concentration of bacteria

To check if the lack of biological activity of Gramicidin entrapped in micelles is a result of low permeability of micelles in comparison to high concentration of bacteria, the previous experiment was repeated with different bacteria concentration. Perti dishes with nutrient agar with the content of 100, 200 and 300 μl of bacteria culture were prepared and the following solutions were tested:

1. PBS/ CH_3OH solution
2. PBS/ TRX/ gA (50 $\mu\text{g/ml}$)
3. PBS/ CH_3OH / gA (50 $\mu\text{g/ml}$)
4. PBS/ TRX/ gA (100 $\mu\text{g/ml}$)
5. PBS/ CH_3OH / gA (100 $\mu\text{g/ml}$)

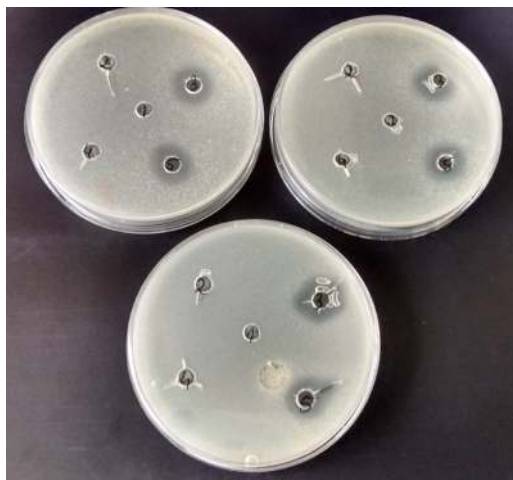


Figure 8.4. Results of experiment studying gA activity in micelles without presence of methanol at different concentration of bacteria.

As it may be seen in Figure 8.4., independently of the bacteria concentration applied, bacteria growth inhibition zone remains similar. This would suggest that gA entrapped in the micelle does not adapt its active form. Next experiment was designed in order to check if the presence of methanol influences the activity of micelles.

8.4.2.3. Gramicidin activity in micelles with presence of methanol

In order to check if the addition of methanol to the micelle solution would change the activity of gA the following solutions were tested:

1. PBS/ CH₃OH
2. PBS/ CH₃OH/ TRX
3. PBS
4. PBS/ CH₃OH / gA (25 µg/ml)
5. PBS/ CH₃OH/ TRX/ gA (100 µg/ml)

This time, PBS, PBS/CH₃OH, and PBS/CH₃OH/TRX were used as a control solutions. Also, to check if there is any limitation concerning gA concentration concerning activity against bacteria in solutions without surfactant; a concentration of gA of 25 µg/ml was considered. The results are visible in Figure 8.5.



Figure 8.5. Results of experiment studying gA activity in micelles with presence of methanol.

As expected and encountered before, methanol in concentration of 10% does not have harmful effect on bacteria, and so does not PBS alone. Also, Gramicidin in the PBS/CH₃OH solution when is at lower concentration (25 µg/ml) does not inhibit bacteria growth. Contrary, addition of methanol, TRX/gA micelles with protein concentration of 100µg/ml do inhibit growth of *Bacillus*. In the case of the solution containing only PBS/CH₃OH with TRX, bacteria growth inhibition was detected, although antibiotic was not present. To better understand this findings further experiments were performed.

8.4.2.4. Gramicidin activity in micelles with presence of methanol and at different concentration of protein

To check if lowering the gA concentration in micelles, together with addition of methanol would influence bioactivity, and to confirm inhibiting effect of PBS/CH₃OH/TRX mixture, the following solutions were tested.

1. PBS/CH₃OH/TRX/ 50µg gA
2. PBS/CH₃OH/TRX
3. PBS
4. PBS/CH₃OH /5 µg gA
5. PBS/CH₃OH

As control solutions again PBS/CH₃OH and PBS solutions were used. In order to study the minimum concentration of gA in methanol, which might cause bacteria growth inhibition, 5µg/ml of gA in PBS/CH₃OH mixture was used. Results are presented in Figure 8.6.



Figure 8.6. Results of the experiment carried out to study gA activity in micelles with presence of methanol and at different protein concentration.

No effect of PBS/CH₃OH and PBS was detected, neither PBS/CH₃OH with low content of gA (5 µg/ml) caused any effect on bacteria growth. On the other hand, growth inhibition was observed again for PBS/CH₃OH/TRX solution and for TRX/gA micelles with presence of methanol. Thus, in order to evaluate the low limit of gA concentration in micelles that is active and to understand the effect of the activity shown by the mixture of PBS/ CH₃OH/ TRX against *Bacillus*, further work was performed.

8.4.2.5. Gramicidin activity in micelles and in the solution with presence of methanol

The last experiment carried out employed a solution PBS/CH₃OH and PBS/CH₃OH/TRX as controls. Micelle solution with addition of methanol was tested with the content of 50µg/ml and 5 µg/ml of antibiotic. For comparison 25µg/ml of gA in PBS/CH₃OH solution was also used. The tested solutions were the following:

1. PBS/CH₃OH
2. PBS/CH₃OH/TRX/5 µg gA
3. PBS/CH₃OH/TRX
4. PBS/CH₃OH/TRX/50 µg gA
5. PBS/CH₃OH/25 µg gA

Results are shown in Figure 8.7.



Figure 8.7. Results of the experiment carried out to study gA activity in micelles and in the solution with the presence of methanol.

As previously confirmed, PBS/CH₃OH does not affect bacteria growth. Neither does the solution containing gA 25 µg/ml of gA in PBS/CH₃OH. In contrast, lower concentration of antibiotic (5 µg/ml) inhibit *Bacillus subtilis* growth when mixed together with TRX with addition of alcohol. The same effect was observed for PBS/CH₃OH/TRX without gA. It may be concluded that the combination of methanol and TRX exhibit antimicrobial

properties even without presence of antibiotic, while each one separately neither Triton nor methanol is harmful for bacteria. The results are summarized in Table 8.2.

Table 8.2. Growth inhibition diameter measured for all tested solutions.

Sample	Growth inhibition	Inhibition diameter (cm)
1. PBS	-	-
2. PBS/CH ₃ OH	-	-
3. PBS/CH ₃ OH/gA (100µg/ml)	+	2.12
4. PBS/CH ₃ OH/gA (50µg/ml)	+	1.82
5. PBS/CH ₃ OH/gA (25µg/ml)	-	-
6. PBS/CH ₃ OH/gA (5µg/ml)	-	-
7. PBS/ CH ₃ OH/Triton	+	1.86
8. PBS/TRX/gA (100µg/ml)	-	-
9. PBS/TRX/gA (50µg/ml)	-	-
10. PBS/CH ₃ OH/TRX/gA (100µg/ml)	+	2.58
11. PBS/CH ₃ OH/TRX/gA (50µg/ml)	+	2.33
12. PBS/CH ₃ OH/TRX/gA (5µg/ml)	+	2.05

None of the control solutions, neither PBS nor PBS/CH₃OH (samples 1 and 2) do not exhibit harmful effect on bacteria growth. The activity of free gA in comparison to TRX/gA micelles revealed, that at both concentrations, 50 and 100 µg/ml , micelles do not exhibit any effect on bacteria growth (samples 3 and 4). However, when gA is not entrapped within the surfactant molecules, in the presence of methanol (necessary to dissolve it), at the same concentrations (50 and 100 µg/ml), gA shows inhibiting effect on *Bacillus subtilis* growth (samples 5 and 6). Lower concentrations of free antibiotic (25 and 5 g/ml) were too low to prevent the growth (samples 7 and 8). This differences in activity

of free protein comparing to the micelles can be an effect of low TRX micelles permeability and very slow, or no diffusion of gA from the surfactant capsule.

Nevertheless, experiment performed with the same group of solutions using bacteria concentrations from 100-300 μ l showed, that even at lower bacteria concentration, the growth inhibition zone remains similar in size. Thus, it is likely that gA gets only dispersed by the surfactant, due to its low solubility in water, while the presence of methanol allow the actual dissolution. After addition of methanol, TRX/gA micelles with protein concentrations of 100 and 50 μ g/ml do inhibit growth of *Bacillus* (samples 9 and 10), and even stronger comparing to the free, non-micellized gA (inhibition growth diameter is: 2.12 cm and 1.82 cm for free gA, and 2.58 cm and 2.33 cm for TRX/gA micelle with methanol). At gA concentration of 5 μ g/ml, inhibition was observed (sample 11) while free gA, even at slightly higher concentration was already inactive (sample 7 and 8).

The PBS/CH₃OH/TRX solution, exhibited bacteria growth inhibition even without presence of antibiotic (sample 12). This result can be due to the presence of methanol, which was reported to exhibit toxic effect on bacteria when it is in concentration of around 5% [16]. In these experiments, all the tested solutions contained much more than 10% of alcohol. In the case of control solution (sample 2) growth inhibition was not observed, because probably the real concentration is lower, due to the fact that some amount of alcohol evaporates during preparation procedure (2 hours before incubation, when the plates are left with the solutions to let them diffuse into agar, as explained in this Chapter in Section 8.3.3.1). In contrast, when the surfactant is present, apart of the gA, also the methanol is entrapped within the micelles, what prevents it from evaporation. Thus, high methanol concentration is maintained what results in harmful effect on bacteria. This fact also explains the differences between the solutions with free gA (samples 5, 6) and the micelles (samples 9 and 10), where the visible effect of both, antibiotic and methanol, results in stronger bacteria growth inhibition. Statistical analysis of growth inhibition diameters was performed to evaluate if bacteria killing effect is caused rather by gA, or is it only a toxic behavior of methanol. The results are collected in Table 8.3.

Table 8.3. Statistical analysis of growth inhibition diameters of the samples containing TRX/gA micelles and methanol in comparison to the solution without gA.

Sample	p-value
PBS+ 10%CH ₃ OH+ 320 μl/ml TRX+ 100μg/ml gA	<0.0001
PBS+ 10%CH ₃ OH+ 320 μl/ml TRX+ 50μg/ml gA	0
PBS+ 10%CH ₃ OH+ 320 μl/ml TRX+ 5μg/ml gA	0.01

For the statistical evaluation, the following *hypothesis* was made: the growth inhibition diameter of the samples containing gA are bigger than the growth inhibition diameter of the sample without gA. The p-values **below** 0.05 correspond to the samples which are in agreement with those assumptions.

All of the p-values obtained for the samples 9-11 (containing both, gA and methanol) when compared with the sample 12 (without gA) indicate, that bacteria growth was inhibited significantly enhanced when both components were present. This proves that there is a direct effect of gA on bacteria growth inhibition, which however is enhanced by methanol. Besides, increase of p-value as the antibiotic concentration in the samples decreases, additionally supports this statement. This clearly indicates that the TRX/gA micelles in the presence of methanol exhibited the expected antibacterial activity.

8.4.3. Inhibitory activity of polysulfone membranes containing immobilized TRX/gA micelles

8.4.3.1. Experiment in solid medium

Similar like in the previous assay, the growth of *Bacillus subtilis* was already observed after 24 hours. The clear zones of growth inhibition were visible as shown in Figure 8.8. It

is clearly that when the micelles are immobilized on a membrane surface, the bacteria growth is inhibited and the inhibition zone average was 0.45 ± 0.3 cm.



Figure 8.8. Results of the experiment evaluating antibacterial activity study of TRX/gA micelles immobilized on MNP-OH membrane, against *Bacillus subtilis*. The clear zones refer to the range of bacteria growth inhibition. The membranes on the left side of the Petri plate are the polysulfone membranes without TRX/gA micelles, on the right- the membranes containing immobilized TRX/gA micelles.

8.4.3.2. Experiment in liquid medium

The latest result was also confirmed by an assay performed in liquid medium. The results of optical density measurement are presented on Figure 8.9. When the membrane with immobilized TRX/gA micelles is immersed in liquid medium, the bacteria growth is lower: after 24 hours the OD is of 0.32 while when the membrane does not contain micelles, OD value after the same time is of 0.41. After 48 hours of experiment the OD values are 0.39 and 0.5 for the sample with membrane containing micelles and without them, respectively. The statistical analysis confirms that the difference in OD

measurements between the samples investigated is significant (p-value of <0.001). This results undoubtedly proves that immobilized micelles maintains their antibacterial properties.

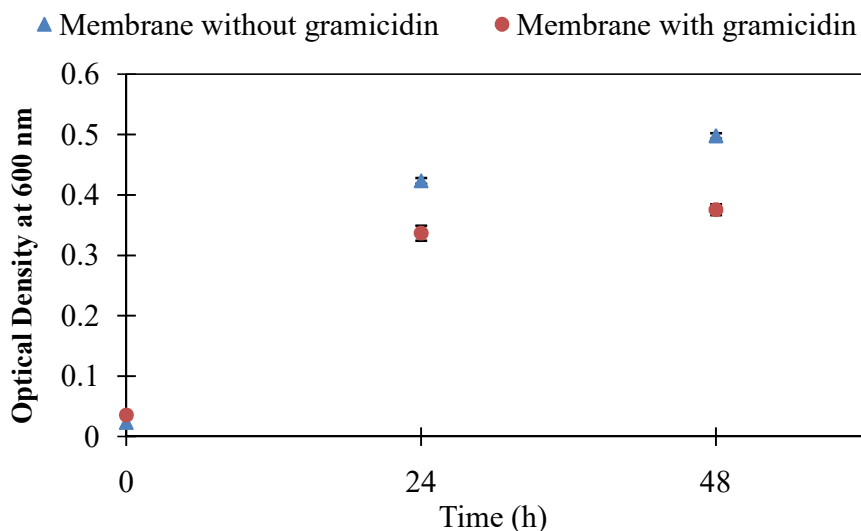


Figure 8.9. Optical density at 600 nm of the liquid media with immersed membranes: without and with immobilized TRX/gA micelles. Experiment was performed per triplicate. The error bars refer to the standard deviation from the 3 measurements taken from 3 different samples.

In Figure 8.10. a, which refers to the membrane which does not contain immobilized micelles, bacteria forming big colonies can be seen and it starts to form a biofilm. In contrast, in Figure 8.10. b, presenting the membrane with immobilized TRX/gA micelles such a extensive growth is not observed and only single bacteria are visible.

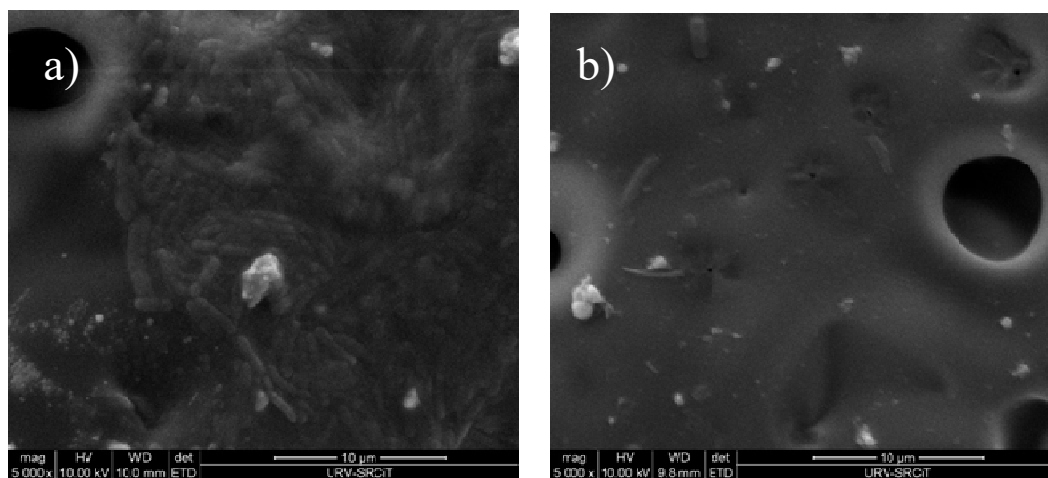


Figure 8.10. ESEM micrographs of the membranes after immersion in liquid media containing *Bacillus subtilis*: a) membrane without and b) with immobilized micelles.

8.4.4. Membrane biofouling determination

In regards to the soaking experiment, it is clearly visible that after 24 hours of incubation in the seawater the solution containing glucose and *Bacillus* (left hand side of the picture) is turbid in comparison to the other two solutions (Figure 8.11.).



Figure 8.11. Solutions under study after 24 hours of incubation, from the left to the right: seawater with glucose and *Bacillus subtilis*, seawater, MiliQ water.

This proves that *Bacillus subtilis* certainly grows in seawater conditions and that during 24 hours it is able to grow significantly. However, in the seawater sample, without addition of nutrients, turbidity was not observed. It has the same clearness as MiliQ water. Nevertheless, the ESEM analysis did not show any difference in bacteria growth and on both types of membranes (containing TRX/gA micelles and without them) very small colonies were present, only after soaking in seawater with *Bacillus* and glucose.

8.4.5. Characterization of membrane with micelles containing methanol

Characterization of MNP-NH₂ membrane containing micelles with addition of methanol is hereby presented and discussed. The preparation method of the membrane is the one described in a Chapter V, section 5.3.1. but instead of using only PBS as a bulk solution, the mixture contained 90% of PBS and 10% of methanol (v/v). The results have been compared with the results of MNP/TRX/gA membranes prepared without methanol and with MNP/glutar/gA membranes.

8.4.5.1. Permeability test

Permeability test results are presented in Figure 8.12. Ions permeability for the membrane prepared in PBS with addition of alcohol is higher in comparison to the same type of membrane prepared in PBS only, except for the biggest ion, that shows the lowest permeability value. This could suggest selective behavior of active Gramicidin, which results in high permeability for smaller species. The novel obtained membranes shows better performance in terms of permeability than the membranes obtained by glutaraldehyde coupling when prepared in water, but still worse than the one prepared in PBS. Statistical analysis confirmed that the membrane permeability value is higher than the MNP-NH₂ membrane without any modification.

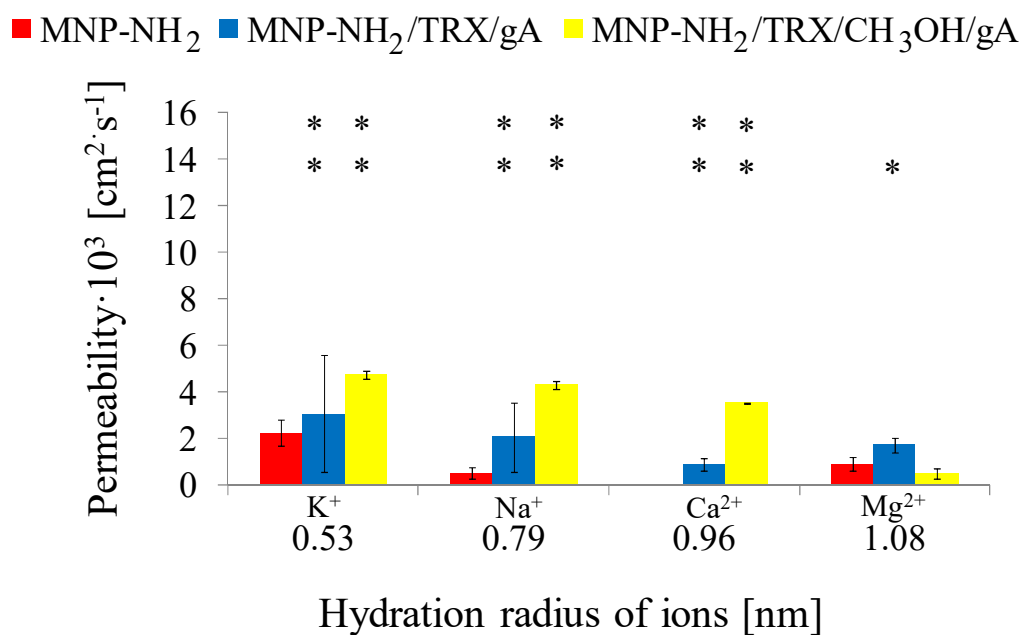


Figure 8.12. Permeability versus hydration radius of ions K⁺, Na⁺, Ca²⁺ and Mg²⁺ [17, 18] for membranes: MNP-NH₂/TRX/gA prepared in PBS, presented previously (see Chapter V, Figure 5.5. e), MNP-NH₂/glutar/gA prepared in H₂O and MNP-NH₂/glutar/gA prepared in PBS presented previously (see Chapter VI, Figure 6.3. a-b) and MNP-NH₂/TRX/gA membrane prepared in PBS/methanol mixture. Values of permeability are average of 3 measurements taken from 3 different membranes prepared under the same experimental conditions. The error bars refers to the standard deviation of the measurements. Columns highlighted with ** refers to the samples for which p-value was <0.01, columns highlighted with * refers to the samples for which p-value was <0.05. For the statistical evaluation, the following hypothesis was made: (i) the permeability value of membranes after TRX/gA micelles immobilization in the presence of methanol is different than permeability value of non-modified membrane. The p-values **below** 0.05 correspond to the samples which are in agreement with this assumption.

8.4.5.2. Current-Voltage measurement (CV)

The graphical representation of resistance data is collected in Figure 8.13.

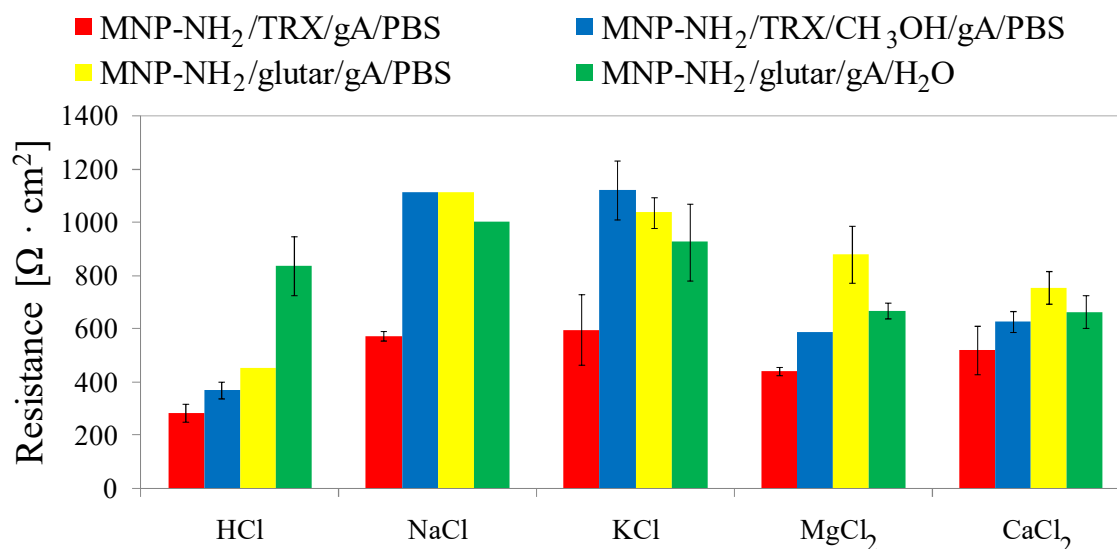


Figure 8.13. Ohmic resistance values of the membranes: MNP-NH₂/TRX/gA prepared in PBS presented previously (see Chapter V, Figure 5.10.), MNP-NH₂/glutar/gA prepared in H₂O presented previously (see Chapter VI, Figure 6.5.) and MNP-NH₂/glutar/gA prepared in PBS presented previously (see Chapter VI, Figure 6.6.) and MNP-NH₂/TRX/gA prepared in PBS/methanol mixture.

Comparing the results obtained for MNP-NH₂/TRX/gA membrane prepared in PBS or in PBS/methanol, it can be observed that the membrane prepared in the presence of alcohol, exhibits higher resistance values. This phenomenon will be discussed in Chapter IX, section 9.4.3. This results would imply, that the use of methanol during micelles immobilization process is not favourable in terms of ion conductivity. Nevertheless, to draw out the full conclusion it is necessary to analyze the selectivity calculation, collected in Table 8.4.

Taking into consideration the selectivity values of MNP-NH₂/TRX/gA/PBS/CH₃OH membrane, an enhancement of selectivity in comparison to the membrane MNP-NH₂/TRX/gA/PBS may be observed. Selectivity was improved and monovalent ions

passage decreased 33% in the case of sodium and 31% in the case of potassium. In the case of divalent ions, this improvement is not observed. When comparing selectivity of the MNP-NH₂/TRX/gA/PBS/CH₃OH membrane with the membranes prepared via glutaraldehyde coupling it can be seen that more selective behavior in terms of sodium and potassium passage, but according to divalent ions, still the best selectivity is shown by membrane with chemically attached gA, prepared in PBS (MNP-NH₂/glutar/gA/PBS).

Table 8.4. Selectivity values for the membranes: MNP-NH₂/TRX/gA/PBS, MNP-NH₂/TRX/gA/PBS/CH₃OH, MNP-NH₂/glutar/gA/H₂O and MNP-NH₂/glutar/gA/PBS.

Selectivity [Y_{ion}/Y_{H^+}]					
Ion	MNP-NH ₂ /TRX/gA/PBS	MNP-NH ₂ /TRX/gA/PBS/CH ₃ OH	MNP-NH ₂ /glutar/gA/H ₂ O	MNP-NH ₂ /glutar/gA/PBS	
H ⁺	1	1	1	1	
Na ⁺	0,50 ± 0.04	0.33 ± 0.03	0.54 ± 0.0	0.41 ± 0.0	
K ⁺	0.48 ± 0.05	0.33 ± 0.0	0.45 ± 0.0	0.44 ± 0.0	
Mg ²⁺	0.64 ± 0.05	0.63 ± 0.05	0.49 ± 0.0	0.52 ± 0.0	
Ca ²⁺	0.55 ± 0.03	0.59 ± 0.01	0.68 ± 0.0	0.60 ± 0.0	

8.5. Conclusions

Various experiments have been performed in order to evaluate the biological activity of antibiotic Gramicidin A against two gram-positive bacteria, which were selected based on the potential applications of the micelles immobilized on the membrane surface. The first bacteria, *Listeria innocua*, was chosen to study the effect of gA on harmful pathogen *Listeria monocytogenes* which is characterized by very similar genus with the non-pathogenic *innocua*. Bioactivity of gA against this microbe was not proved. The second bacteria selected, *Bacillus subtilis*, found to be a component of nanofiltration membranes biofouling and thus was chosen to study potential antifouling properties of membranes with immobilized micelles. It is also a model for gram-positive bacteria which could give an idea about general gA micelles activity. In the case of *Bacillus* several experiments were performed, which provided information about activity of both antibiotic and micelles with entrapped gA. It has been proved that gA is biologically active against gram positive *Bacillus subtilis*, when is dissolved in the presence of methanol. When it is immobilized within the micelle, without presence of alcohol, bioactivity is not observed, which may come from the inactivity of the protein or from the low micelle permeability. When the micelles are prepared in the presence of methanol, the active antibiotic effect is observed and it is enhanced by the effect of methanol, which in high concentration is harmful to bacteria. When the micelles prepared in presence of methanol are immobilized on the membrane surface, they also exhibit antimicrobial properties against *Bacillus*.

Besides, transport properties of the membrane with immobilized TRX/gA micelles prepared with methanol have been evaluated. Resistance of the membrane with TRX/gA micelles prepared with the presence of methanol is higher in comparison to the resistance shown by the membrane prepared in PBS only. Higher ion permeability velocity, improved selectivity is encountered as well for the former membrane. This is in an agreement with the results of bioactivity assay and suggests, that when methanol is added to the micelle solution, gA adapts its active form. In summary, prepared micelles contain

biologically active antibiotic when prepared with the presence of methanol and exhibit antimicrobial properties against gram-positive bacteria. This characteristics give them potential application as antifouling coatings for ultra and nanofiltration membranes and can serve also as a valuable guidance for other proteins immobilization strategies.

8.6. Acknowledgments

Dr. Magdalena Constantí is kindly acknowledged for her help during biological activity assay, which was performed in the microbiological laboratory of Interfibio research group of the Chemical Engineering Department of Universitat Rovira i Virgili.

8.7. References

- [1] J.-W. Liou, Y.-J. Hung, C.-H. Yang, Y.-C. Chen, The Antimicrobial Activity of Gramicidin A Is Associated with Hydroxyl Radical Formation, *PLoS ONE*, 10 (2015) e0117065.
- [2] K.B. Jadhav, C. Stein, O. Makarewicz, G. Pradel, R.J. Lichtenecker, H. Sack, S.H. Heinemann, H.-D. Arndt, Bioactivity of topologically confined Gramicidin A dimers, *Bioorganic & Medicinal Chemistry*, 25 (2017) 261-268.
- [3] J. Yang, Viscoelastic wormlike micelles and their applications, *Current Opinion in Colloid & Interface Science*, 7 (2002) 276-281.
- [4] I.M. Banat, Biosurfactants production and possible uses in microbial enhanced oil recovery and oil pollution remediation: A review, *Bioresource Technology*, 51 (1995) 1-12.
- [5] M.J. Rosen, H. Wang, P. Shen, Y. Zhu, Ultralow Interfacial Tension for Enhanced Oil Recovery at Very Low Surfactant Concentrations, *Langmuir*, 21 (2005) 3749-3756.
- [6] L.D. Rhein, M. Schlossman, A. O'Lenick, P. Somasundaran, *Surfactants in personal care products and decorative cosmetics*, crc press, 2006.
- [7] B. Wiegand, L. McCulloch, E. Lukenbach, Personal care formulations, in, *Google Patents*, 2000.
- [8] N. Pitakteeratham, A. Hafuka, H. Satoh, Y. Watanabe, High efficiency removal of phosphate from water by zirconium sulfate-surfactant micelle mesostructure immobilized on polymer matrix, *Water Research*, 47 (2013) 3583-3590.
- [9] K. Nakada, T.H.A. Hasanin, T. Tanaka, M. Ueda, S. Tsukahara, Y. Okamoto, T. Fujiwara, Synthesis of nylon-6.6 using cetyltrimethylammonium chloride reverse micelles immobilized on silica surfaces, *Journal of Molecular Liquids*, 219 (2016) 789-794.
- [10] X. Zhong, Y. Qian, J. Huang, D. Yang, Y. Deng, X. Qiu, Fabrication of Lignosulfonate Vesicular Reverse Micelles to Immobilize Horseradish Peroxidase, *Industrial & Engineering Chemistry Research*, 55 (2016) 2731-2737.
- [11] S. Kobayashi, T. Wakabayashi, S. Nagayama, H. Oyamada, Lewis acid catalysis in micellar systems. Sc(OTf)₃-Catalyzed aqueous aldol reactions of silyl enol ethers with aldehydes in the presence of a surfactant, *Tetrahedron Letters*, 38 (1997) 4559-4562.

- [12] M.R. Farrow, P.J. Camp, P.J. Dowding, K. Lewtas, The effects of surface curvature on the adsorption of surfactants at the solid–liquid interface, *Physical Chemistry Chemical Physics*, 15 (2013) 11653-11660.
- [13] X.S. Zhao, X.Y. Bao, W. Guo, F.Y. Lee, Immobilizing catalysts on porous materials, *Materials Today*, 9 (2006) 32-39.
- [14] P. McMorn, G.J. Hutchings, Heterogeneous enantioselective catalysts: strategies for the immobilisation of homogeneous catalysts, *Chemical Society Reviews*, 33 (2004) 108-122.
- [15] P.S. Mead, L. Slutsker, V. Dietz, L.F. McCaig, J.S. Bresee, C. Shapiro, P.M. Griffin, R.V. Tauxe, Food-related illness and death in the United States, *Emerging Infectious Diseases*, 5 (1999) 607-625.
- [16] T. Wadhvani, K. Desai, D. Patel, D. Lawani, P. Bahaley, P. Joshi, V. Kothari, Effect of various solvents on bacterial growth in context of determining MIC of various antimicrobials, *Internet J Microbiol*, 7 (2009).
- [17] F. Kara, G. Gurakan, F. Sanin, Monovalent cations and their influence on activated sludge floc chemistry, structure, and physical characteristics, *Biotechnology and bioengineering*, 100 (2008) 231-239.
- [18] R.P.a.S.M. E., *Processes Involved in Sodic Behaviour*, Oxford University Press, New York, 1998.

Chapter IX

Characterization of the thermophysical properties of Surfactant/Gramicidin micelles

9.1. Introduction

Since certain decades ago surfactants have been important technological tools in consumer products. With time people learned also how to use this valuable amphiphilic compounds to create structures called micelles, which possess a variety of applications, e.g. in cosmetology, ultrafiltration, food industry, controlled release etc. Until now, thermophysical properties of ionic or non-ionic surfactants have been widely studied, and their application in creation of micelles, reverse micelles and mixed micelles have been well characterized in different solvents. Triton X-100, a component widely used in biological science for cell permeabilization, have been also often employed in many research work. Due to its capability to mimic biological membranes, Triton X-100 micelles were also used to study the structure of various proteins, including Gramicidin, using spectroscopic methods. In order to better understand the results of TRX/gA micelles bioactivity assay and to extract more information about the micelles properties and performance, a complex characterization of micelle solution of Triton X-100 with Gramicidin have been carried out. This investigation involved measurement of interfacial tension, particle size distribution analysis via dynamic light scattering and viscosity determination.

Surface tension is a phenomenon related with cohesive forces (attraction) between solution molecules. The tension occurring at the interface of two non-miscible phases (in the present case liquid and air) is called interfacial tension (IFT). The molecules present on the interface of the solution do not have in their surrounding the same type of molecules as if they were in the bulk solution, and thus, they cohere stronger than the molecules in the solution. That causes the formation of surface “films”. High value of interfacial tension means, that the cohesive forces inside the phase A (liquid) are stronger than adhesive forces on the interface with phase B (air) and in consequence, the surface film is more difficult to break.

Dynamic light scattering have been widely used in the analysis of particle size of colloidal structures. It delivers information about particle size distribution, polydispersity or

diffusion coefficient. In its working principles it makes use of two colloid's properties which are Brownian motions and Tyndall effect. Those movements of particles in suspension causes scattering of the light at different intensities, which then is registered and analyzed using the Stokes-Einstein relationship.

Viscosity is a property of liquids and plastic solids and it correspond to the measure of the resistance of a sample to flow. At molecular level, viscosity is a result of internal interaction between the molecules of the substance, their friction. Viscosity values can deliver valuable information about the substance behavior in different environments, at different temperature or humidity conditions.

9.2. Materials

Gramicidin (gA) from *Bacillus aneurinolyticus* (*Bacillus brevis*) were purchased from Sigma Aldrich. Salts used for PBS (phosphate buffer saline) preparation: sodium chloride and potassium chloride were purchased from Sigma Aldrich, potassium phosphate dibasic trihydrate, disodium hydrogen phosphate dihydrate were purchased from Panreac. Surfactant Triton X-100 (TRX) was purchased from Sigma Aldrich. Methanol was purchased from Sigma Aldrich. All the solutions were prepared in MiliQ water from Millipore.

9.3. Methods

9.3.1. Micelles solution preparation

PBS used to prepare all the micelle solutions was made by dissolving the salts at the following concentrations: 137 mM of NaCl, 2.7 mM of KCl, 10 mM of Na₂HPO₄ and 1.8 mM of K₂HPO₄. Final pH value was 7.4± 0.05. For some of the samples preparation, 10wt% of CH₃OH was added. Next, the gA and TRX were added and the mixture was stirred overnight with use of magnetic stirrer.

9.3.2. Interfacial tension measurement (IFT)

The interfacial tension assessments were performed using a OCA-15EC instrument (DataPhysics, Germany), where the surface tension was determined using the pendant drop technique, with assist of the specific SCA software. Interfacial tension was determined through digitization and analysis of the droplet profile using the Young-Laplace equation. All measurements were repeated at least 3 times. The resulting data of interfacial tensions were subjected to statistical analysis using student-T test, performed with XLStat software, using means comparison method with a significance level of 0.05.

9.3.3. Dynamic Light Scattering analysis (DLS)

The average size of particles was determined through Dynamic Light Scattering (DLS) analysis using a Zetasizer Nano ZS (Malvern Instruments). In order to study the effect of temperature on this parameter, the analysis was performed at 25, 37 and 50 °C. Measurements were repeated 3 times.

9.3.4. Viscosity measurement

The kinematic viscosity of the micelle solutions was measured using the Micro Ostwald capillary viscometer (SI Analytics GmbH, Mainz, Apparatus number 1071677) with capillary 517 10 / I at 25°C. Dynamic viscosity was calculated by dividing the obtained value of kinematic viscosity over the density of each sample. Density was measured with the use of vibrating-tube densimeter (Anton Paar, mod. DMA 35N). This equipment was validated with water and the maximum deviation from literature values was 0.03%. The procedure to determine dynamic viscosity was validated using water, obtaining a maximum deviation of 3% when the experimental values were compared with the literature values [1, 2]. The measurements were repeated 6 times.

9.3.5. Conductivity measurement

Conductivity of the micelles solutions was measured using the Orion Dual Star (ThermoFisher Scientific) at the temperature of 25°C. The equipment was validated using water and PBS solution. The measurements were repeated five times. The list of samples prepared, together with their contents of protein and surfactant is presented below (Table 9.1.).

Table 9.1. List of the samples prepared for thermophysical properties analysis.

Samples
1. PBS+160 μ g/ml TRX
2. PBS+320 μ g/ml TRX
3. PBS+480 μ g/ml TRX
4. PBS+160 μ g/ml TRX+50 μ g/ml gA
5. PBS+320 μ g/ml TRX+50 μ g/ml gA
6. PBS+480 μ g/ml TRX+50 μ g/ml gA
7. PBS+10%CH ₃ OH +160 μ g/ml TRX
8. PBS+10%CH ₃ OH +320 μ g/ml TRX
9. PBS+10%CH ₃ OH +480 μ g/ml TRX
10. PBS+10%CH ₃ OH +160 μ g/ml TRX+ 50 μ g/ml gA
11. PBS+10%CH ₃ OH +320 μ g/ml TRX+ 50 μ g/ml gA
12. PBS+10%CH ₃ OH +480 μ g/ml TRX+ 50 μ g/ml gA

9.4. Results

9.4.1. Interfacial tension measurement (IFT)

Interfacial tension measurements were performed firstly for control solutions. The results are presented on the Figure 9.1. As it can be seen, addition of TRX to PBS solution decreases the IFT of the latest from over 70 to around 30 mN/m. This number is in good agreement with the reference value reported for aqueous solutions of this surfactant (ref supplier data sheet). Contrary, addition of CH₃OH to the PBS buffer, decreases the IFT value, but only from over 70 to 60 mN/m, what was also reported in the literature [3, 4]). When both components, surfactant and alcohol, are added to PBS buffer, IFT of PBS/CH₃OH/TRX sample is reduced to approx. 30 mN/m, similarly to the case where only

surfactant was added. This result implies, that in the presence of salts, a major effect on this surface property comes from the presence of surfactant, while methanol effect is negligible.

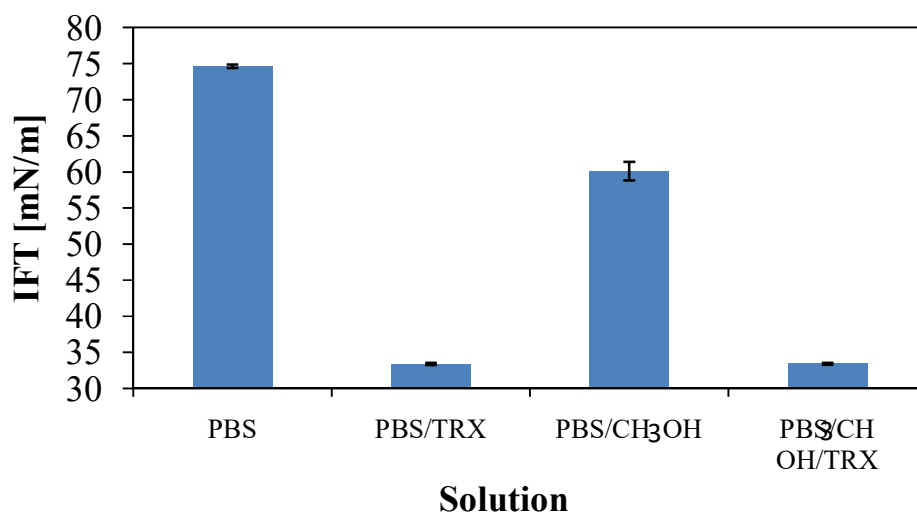


Figure 9.1. Interfacial tension measurements results for a control solutions.

This relation observed could explain the harmful effect on bacteria growth presented by the PBS/TRX/CH₃OH mixture, without Gramicidin. Presence of surfactant is indispensable for methanol to affect bacteria growth, because it decrease interfacial tension of solution what allows better cell penetration and permeabilization. Alcohol itself, when not mixed with TRX, do not affect bacteria growth, unless antibiotic was added.

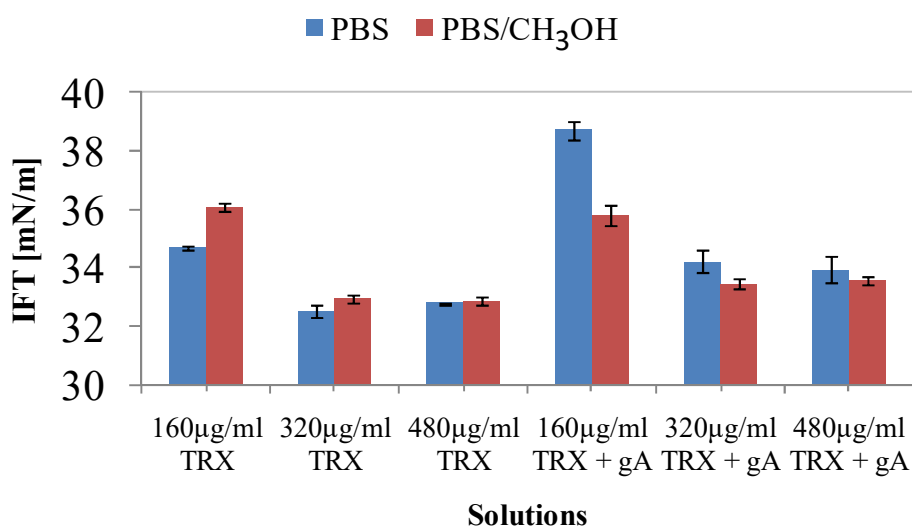


Figure 9.2. Interfacial tension of samples with different concentration of surfactant, without and with gA addition, in the presence or absence of methanol.

In the solutions that do not contain alcohol (blue bars) a huge decrease in IFT is observed, when the surfactant concentration exceeds critical micelle concentration (CMC, for Triton X100 is around 29 mM, which refers to 160µl of this surfactant). It can also be seen, that addition of Gramicidin increases the IFT values, especially at the lowest TRX concentration. Probably, at this concentration (around CMC) not all the surfactant molecules are in the form of micelles, thus there is not enough surfactant to solubilize all the protein. Regarding the solutions with methanol, after addition of more than 160ul of TRX, a significant decrease of IFT occurs. However, there is no increase of the IFT after addition of Gramicidin, as in the case of the samples without alcohol. This is most likely due to higher protein solubility in water, in the presence of methanol. This hypothesis is supported by the fact, that all the solutions containing gA have lower IFT values when the methanol is added. This is another explanation why methanol when combined with surfactant provide higher pathogens killing properties, as was observed in biological activity assay (see Chapter VIII, section 8.4.2.).

It is worth to mention, that further increase in the surfactant concentration does not influence IFT significantly. In Table 9.2. the results of statistical are presented. None of the

p-values demonstrates that the further increase of surfactant concentration enhances the interfacial tension properties.

Table 9.2. Statistical analysis of interfacial tension values for the samples containing 320 μ l of TRX in comparison to the ones containing 480 μ l of TRX .

Samples	p-value
PBS + 320 μ g/ml TRX	0.089
PBS + 480 μ g/ml TRX	
PBS + 320 μ g/ml TRX + 50 μ g/ml gA	0.45
PBS + 480 μ g/ml TRX + 50 μ g/ml gA	
PBS + 10% CH ₃ OH + 320 μ g/ml TRX	0.629
PBS + 10% CH ₃ OH + 480 μ g/ml TRX	
PBS + 10% CH ₃ OH + 320 μ g/ml TRX + 50 μ g/ml gA	0.541
PBS + 10% CH ₃ OH + 480 μ g/ml TRX + 50 μ g/ml gA	

For the statistical evaluation, the following *hypothesis* was made: the interfacial tension values of the samples containing 320 μ l of TRX is different than the ones for the samples with 480 μ l of TRX. The p-values **below** 0.05 correspond to the samples which are in agreement with those assumptions.

9.4.2. Dynamic Light Scattering analysis (DLS)

Dynamic Light Scattering experiments were performed in order to find out if there is a relation between surface tension and the size of the particles in the solution. Figures 9.3.a and 9.3.b present average particle size values obtained for the samples (without methanol), at temperatures :25, 37 (bacteria incubation temperature), and 50° C.

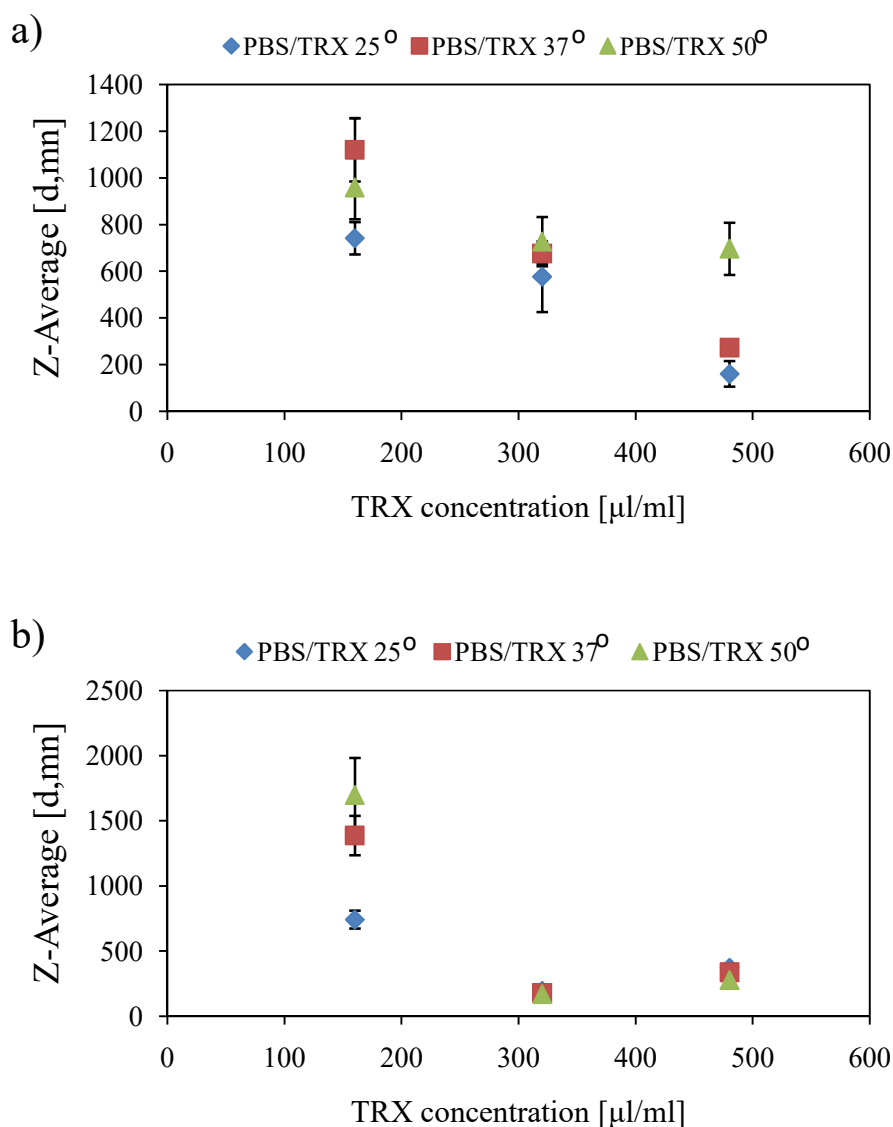
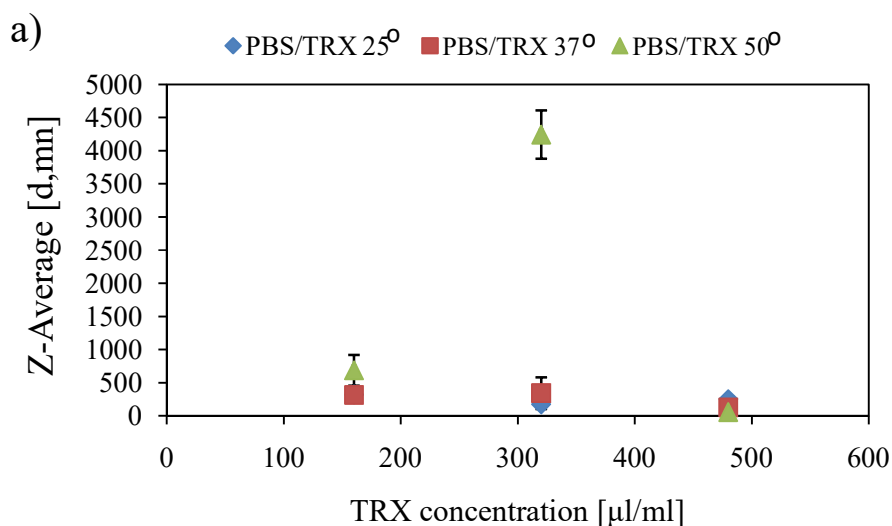


Figure 9.3. Dynamic light scattering measurement results for the samples with different concentration of surfactant, without (a) and with gA addition (b), in the absence of methanol.

Regarding the samples without gA, the particle size decreases with increasing surfactant concentration in all the cases. This is only partially in agreement with the IFT data which show, that after overcoming the CMC value, further decrease of IFT was not observed, thus a decrease of the particle size was not expected in that case. The particle diameter also seems to increase while increasing the temperature, what have been reported previously as

an increase of aggregation number [5, 6]. When the protein is present, at surfactant concentrations above 160 μl , the particle size decreases, however at the highest concentration of surfactant it seems to slightly increase again. This effect could be explained either by the interferences of the salts in the medium, or by the fact that the surfactant amount selected (320 $\mu\text{l}/\text{ml}$) is an optimal concentration at which the micelles are formed but do not form too much aggregates. Besides, no temperature effect was encountered when the surfactant concentration is higher than 160 μl . The relation with the IFT data is not evident, nevertheless it confirms, as well as IFT value, that particle size significantly decreases when the TRX concentration reaches 320 μl or upper. In Figures 9.4.a and 9.4.b data obtained for the samples with methanol are shown.

Addition of methanol seems to decrease the particle size of the samples, when no gA is added to the solution. Contrary, when the protein is present, the particle size in the samples with methanol is bigger compare to the samples without alcohol. This is unexpected, since IFT measurements showed, that addition of methanol to the samples containing gA decrease IFT value. This may be a consequence of complex composition of analytes. It is also possible, that although the protein is dissolved in alcohol, formed micelles are organized in big aggregates, which result in a big particle size.



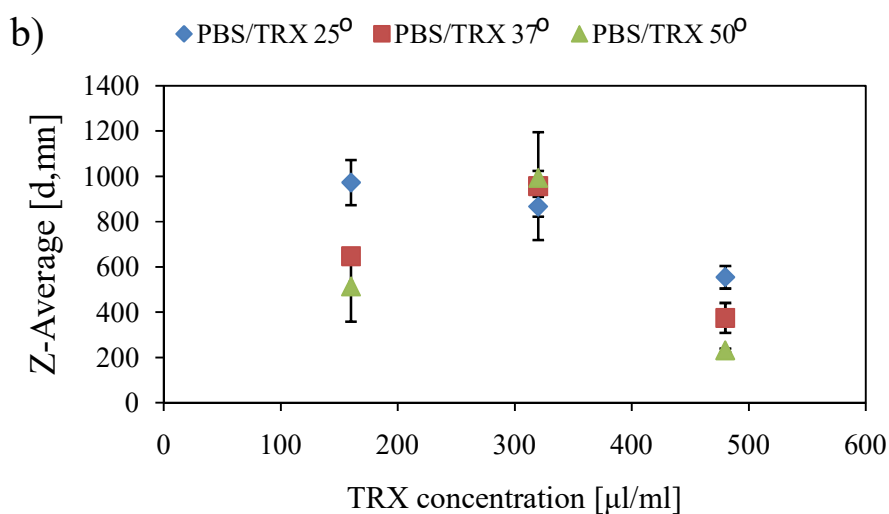


Figure 9.4. Dynamic light scattering measurement results for the samples with different concentration of surfactant, without (9.4. a) and with gA addition (9.4. b), in the presence of methanol.

9.4.3. Viscosity and Conductivity measurement

Measurements of viscosity and conductivity were carried out in order to further characterize system under study concerning the effect of the presence of micelles on the solution conditions. In Figure 9.5.9. the relation between the viscosity and conductivity of the studied samples is shown. As reported previously [1, 7] addition of surfactant decrease the viscosity of the solution, what is related with the formation of micelles. In more viscous fluids, molecules are moving slower and in consequence, conductivity is high [8-10]. Thus, it is expected that conductivity increases as the viscosity decreases. Viscosity of the samples containing methanol is higher than viscosity values of pure methanol (0.54 cP) or water (0.89 cP).

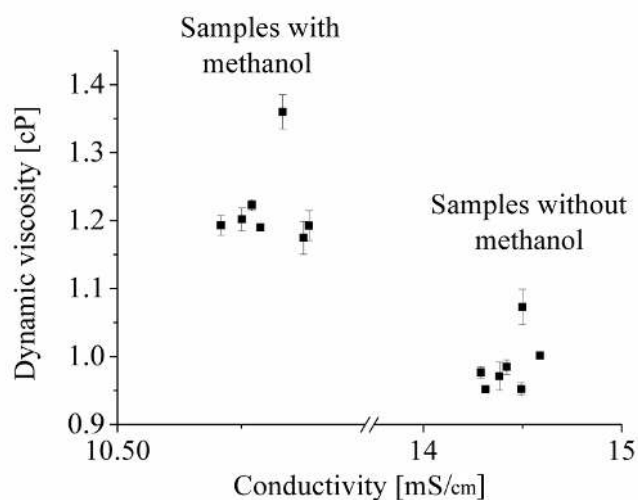


Figure 9.5. Relation of dynamic viscosity and conductivity of the tested micelle solutions.

This unusual behavior was reported for the water-methanol binary mixture [11] and is explained by very strong intermolecular forces between water and methanol, resulting in a fluid with higher viscosity compare to pure substances from which it is composed. Conductivity values of the micelle solutions are in the same range that the ones of the pure base solutions.

9.5. Conclusions

Thermophysical properties (interfacial tension, viscosity and electrical conductivity) of TRX/gA micelle solutions have been determined, together with particle size analysis with use of Diffraction Light Scattering technique. It can be concluded that, presence of surfactant decreases interfacial tension of the solution and decreases viscosity. Methanol addition, decreases interfacial tension of the PBS, but when the surfactant is present, the effect of alcohol is diminished. Regarding the viscosity, addition of methanol increases the viscosity, what was reported previously for water/methanol binary mixture. No effect of micelles on conductivity was observed. Dynamic light scattering data suggest that particle

size decrease with the increase of surfactant concentration. However, it does not provide a clear answer about the relation between the presence of methanol and the micelle size, probably due to the very complex solution composition and the interference effect of ionic strength.

In regard to the results of bioactivity assay discussed in the previous chapter, it has been proved herein that the solution containing both, methanol and Triton X100 has lower interfacial tension in comparison to the one without surfactant, what increases its toxicity versus bacteria. Interfacial tension study revealed also the probable effect of methanol on protein solubility, which is enhanced when the alcohol is present, what results in lower values of IFT.

9.6. Acknowledgments

Dr. Pierfrancesco Cerruti from the Institute of Polymers, Composites and Biomaterials – CNR, Via Campi Flegrei, 3480128 Pozzuoli (Naples), Italy is kindly acknowledged for performing Dynamic Light Scattering analysis and his collaboration.

9.7. References

- [1] B. González, Noelia Calvar, Elena Gómez, Ángeles Domínguez, Density, dynamic viscosity, and derived properties of binary mixtures of methanol or ethanol with water, ethyl acetate, and methyl acetate at $T=(293.15, 298.15, \text{ and } 303.15)$ K, *The Journal of Chemical Thermodynamics*, 39 (2007) 1578-1588.
- [2] W. Wagner, A. Pruss, The IAPWS formulation for the thermodynamic properties of ordinary water substance for general and scientific use., *Journal of Physical Chemistry Reference Data*, 31 (2002) 387-535.
- [3] W.J. Cheong, P.W. Carr, The Surface Tension of Mixtures of Methanol, Acetonitrile, Tetrahydrofuran, Isopropanol, Tertiary Butanol and Dimethyl-Sulfoxide with Water at 25°C, *Journal of Liquid Chromatography*, 10 (1987) 561-581.
- [4] G. Buckton, *Interfacial phenomena in drug delivery and targeting*, CRC press, 2000.
- [5] W.C. Zana R., Effect of temperature on the aggregation behaviour of nonionic surfactants in aqueous solutions. , *Journal de Physique Lettres*, 46 (1985) 953-960.
- [6] K. Streltzyk, G.D.J. Phillis, Temperature Dependence of Triton X-100 Micelle Size and Hydration, *Langmuir*, 11 (1995) 42-47.
- [7] K. Szymczyk, A. Taraba, Aggregation behavior of Triton X-114 and Tween 80 at various temperatures and concentrations studied by density and viscosity measurements, *Journal of Thermal Analysis and Calorimetry*, 126 315-326.
- [8] W.-J. Li, B.-X. Han, R.-T. Tao, Z.-F. Zhang, J.-L. Zhang, Measurement and Correlation of the Ionic Conductivity of Ionic Liquid-Molecular Solvent Solutions, *Chinese Journal of Chemistry*, 25 (2007) 1349-1356.
- [9] J.P. Southall, H.V.S.A. Hubbard, S.F. Johnston, V. Rogers, G.R. Davies, J.E. McIntyre, I.M. Ward, Ionic conductivity and viscosity correlations in liquid electrolytes for incorporation into PVDF gel electrolytes, *Solid State Ionics*, 85 (1996) 51-60.
- [10] J.N. Canongia Lopes, M.F. Costa Gomes, P. Husson, A.A.H. Pádua, L.P.N. Rebelo, S. Sarraute, M. Tariq, Polarity, Viscosity, and Ionic Conductivity of Liquid Mixtures Containing [C4C1im][Ntf₂] and a Molecular Component, *The Journal of Physical Chemistry B*, 115 (2011) 6088-6099.

- [11] S.Z. Mikhail, W.R. Kimel, Densities and Viscosities of Methanol-Water Mixtures, *Journal of Chemical and Engineering Data*, 6 (1961) 533-537.

Chapter X

Conclusions

10.1. Conclusions

From the performed work the following conclusions can be drawn:

- Polysulfone membrane containing Gramicidin protein, have been prepared by three different approaches: physical method which consist in protein entrapment within polymer matrix; physical method with use of magnetic nanoparticles suspended in the membrane with immobilized surfactant/protein micelles, which was performed with use of two types of nanoparticles: $-OH$ and $-NH_2$ functionalized, and with use of two preparation solutions: water and PBS buffer; and chemical method which consist in glutaraldehyde coupling.
- The novel membranes presented herein have been extensively characterized with the following techniques: Scanning Electron Microscope, Fourier-Transform Infrared, Contact Angle, Water Uptake, Permeability experiment, Current-Voltage measurement, Biological activity. Moreover, prepared surfactant/protein micelles were characterized in terms of Biological activity, Electrical conductivity, Dynamic Light Scattering, Interfacial Tension and Viscosity.
- Low protein concentration ($<10^{-7}$ M) disabled Gramicidin detection by conventional methods such as FTIR, XRD or Raman.
- Immobilization of protein in the membrane matrix within entrapment method have been proved by SEM analysis, which show an influence of Gramicidin addition on membrane morphology: sponge-like structure and pore size increase from 45 nm to 3 μm and reduction from 22 μm to 12 μm . Also, micrographs present precipitates of immobilized protein. Contact Angle measurements revealed that protein immobilization decreases hydrophobic character of polysulfone (decrease of CA from 96.6° to 89.5 °), what was confirmed by WU experiment (increase of water uptake from 0.51 to 0.57 mg of water per mg of membrane). Transport properties evaluation in terms of Permeability experiment and Current-Voltage measurement did not show any improvement compare to the unmodified polysulfone membrane.

- Immobilization of Gramicidin with use of magnetic nanoparticles did not affect membrane morphology (pore size and membrane thickness remained unchanged). CA measurements showed that use of magnetic nanoparticles increases hydrophilicity of polysulfone membrane, compare to Plain polysulfone membrane (CA decrease from 96.6° to 82.4° in the case of use -NH₂ functionalized nanoparticles; and from 96.6° to 73.3° in the case of use -OH functionalized nanoparticles). Protein immobilization, when performed in PBS solution, lead to membrane with higher hydrophilicity in the case of use MNP-NH₂ nanoparticles (decrease of CA from 83.8° to 69.9°), or higher hydrophobicity in the case of use MNP-OH nanoparticles (increase of CA from 61.9 ° to 68.4°). Membranes after Gramicidin immobilization swell more water, compare to the membranes without protein: water uptake increase from 1.35 to 2.63 mg of water per mg of membrane in the case of MNP-OH membrane prepared in PBS; from 1.74 to 2.24 mg of water per mg of membrane in the case of MNP-NH₂ membrane prepared in water; and from 1.22 to 2.25 mg of water per mg of membrane in the case of MNP-NH₂ membrane prepared in PBS. Immobilization of TRX/gA micelles is more effective in MNP-OH membranes, which maintains relatively high ion passage velocity when prepared either in water (7.89E-03 cm²·s⁻¹ for K⁺ and 6.33E-03 cm²·s⁻¹ for Na⁺) or in PBS (7.88E-03 cm²·s⁻¹ for K⁺ and 5.83E-03 cm²·s⁻¹ for Na⁺). Gramicidin immobilization drastically reduce Ohmic resistance of the membranes. In three of the four cases, immobilization of TRX/gA micelles enhances membrane selectivity. The best results in terms of ion transport efficiency and selectivity is disclosed by the membrane MNP-OH prepared in water, which has both, the lowest resistance values after gA immobilization (decrease from 83.3 Ω·cm²·10⁻¹ in unmodified membrane to 12.2 Ω·cm²·10⁻¹ for membrane after TRX/gA micelles immobilization, in the case of transport of H⁺ ion) and the highest selectivity (reduction of magnesium passage 51.56% and calcium 56.93%).
- Immobilization of Gramicidin by glutaraldehyde coupling did not affect membrane morphology (pore size and membrane thickness remained unchanged). CA measurements showed that use of magnetic nanoparticles increases hydrophilicity of the membrane (decrease of CA from 82.3° to 57.7° in the case of immobilization performed in water and to 57.1° in the case of

immobilization performed in PBS). The change in water uptake compare to unmodified membrane was not proved statistically (increase of water uptake from 1.23 to 1.53 mg of water per mg of membrane in the case of membrane prepared in water and decrease from 1.97 to 1.67 mg of water per mg of membrane in the case of membrane prepared in PBS). Nevertheless, immobilization of gA in PBS buffer leads to membrane with significantly enhanced ion diffusion properties (increase from $2.233 \cdot 10^{-3}$ to $7.53 \cdot 10^{-3} \text{ cm}^2 \cdot \text{s}^{-1}$ for K^+ and from $5.24 \cdot 10^{-4}$ to $1.06 \cdot 10^{-2} \text{ cm}^2 \cdot \text{s}^{-1}$ for Na^+). Gramicidin immobilization drastically reduces Ohmic resistance of the membranes (Ohmic resistance decrease from $1226 \text{ } \Omega \cdot \text{cm}^2$ to $454 \text{ } \Omega \cdot \text{cm}^2$ for membrane after gA immobilization, in the case of transport of H^+ ion) and improves selectivity (improvement of 6, 11, 16 and 4% for sodium, potassium, magnesium and calcium, respectively).

- The best performance in terms of ion conductivity was presented by the MNP-OH membranes with Gramicidin immobilized physically, which exhibit the highest conductivity (0.71 S/m) and selectivity (0.21; 0.29; 0.32 and 0.34 for potassium, sodium, calcium and magnesium respectively).
- The highest diffusion permeability values was obtained for the membrane with chemically immobilized Gramicidin, prepared in PBS buffer solution ($7.53 \cdot 10^{-3}$ for K^+ and $1.06 \cdot 10^{-2} \text{ cm}^2 \cdot \text{s}^{-1}$ for Na^+), which has also relatively high conductivity (0.45 S/m) and good selectivity values (0.41; 0.44; 0.52 and 0.6 34 for potassium, sodium, calcium and magnesium respectively).
- Biological activity assay revealed that Gramicidin maintains its antibacterial properties when the methanol is present in preparation solution (*Bacillus subtilis* growth inhibition diameter 2.12 cm).
- Micelles composed of surfactant Triton X100 and protein Gramicidin are biologically active in both, solution (*Bacillus subtilis* growth inhibition diameter 2.58 cm) and immobilized on a membrane surface (*Bacillus subtilis* growth inhibition diameter 0.45 cm).
- Membranes with immobilized micelles have higher resistance to bacteria growth, visible on SEM micrograph.

Appendices

Appendix A. List of Figures

Figure 1.1 Scheme of physical adsorption of biomolecules on a polymeric support.	7
Figure 1.2 Schematic representation of a covalent biomolecule attachment to the polymeric support.	8
Figure 1.3 Schematic representation of biomolecule immobilization by encapsulation method.	9
Figure 1.4. Scheme of biomolecule immobilization via entrapment.	9
Figure 1.5. Scheme of affinity membrane separation mechanism.	11
Figure 1.6. Schematic presentation of double mechanism of OP hydrolase-immobilized nanofibrous polymeric clothing.	13
Figure 1.7. Scheme of the sequential enzyme immobilization and co-immobilization.	14
Figure 1.8. Polysulfone structure.	18
Figure 1.9. Structure of Gramicidin.	20
Figure 2.1. Schematic representation of hopping mechanism through the sulfonic groups of sulfonated polymer.	31
Figure 2.2. Schematic design of diffusion mechanism as proton conduction.	32
Figure 3.1. Scheme of phase inversion/precipitation process for membrane fabrication.	44
Figure 3.2. Scheme of the gA interaction in lipid bilayer.	44
Figure 3.3. Scheme of the surfactant (Triton X100)/protein (gA) micelles immobilization on Psf membrane containing MNP's.	47
Figure 3.4. Schematic representation of glutaraldehyde coupling with biomolecule.	48
Figure 3.5. Scheme of Atomic Layer Deposition process.	50
Figure 3.6. Nystatin structure.	51
Figure 3.7. Water drop behaviour and contact angle on hydrophobic surface.	52
Figure 3.8. Scheme of the permeability experiments test cell consisting in Teflon cell with two compartments of 200 ml volume, separated by tested membrane placed between two rubber o-rings.	57
Figure 3.9. Typical Current-Voltage curve for proton exchange membranes, containing three characteristic regions: Ohmic (I), limiting current (II) and convective region (III).	58
Figure 3.10. Experimental set-up for Current-Voltage measurements.	59
Figure 3.11. Experimental procedure of antibacterial activity assay with use of solid media.	62
Figure 3.12. Schematic setup for pendant drop technique.	64
Figure 3.13. Ostwald viscometer scheme.	65

Figure 3.14. Theoretical dynamic light scattering of two samples: containing big particles on the top, and small particles on the bottom.	67
Figure 4.1. Cross-section micrographs of the membranes prepared by phase inversion/precipitation method in a water-coagulation bath, Plain Psf (left), 0.5 wt% of gA (middle) and 5 wt% of gA (right).	77
Figure 4.2. Cross-sectional view of the membrane containing 10^{-7} M of gA.	78
Figure 4.3. Plain polysulfone membrane (a) and Psf/ 10^{-7} M of gA membrane (b) prepared by phase inversion/precipitation method in water-coagulation bath (top surface).	79
Figure 4.5. SEM cross section micrographs of membranes: a) Plain Psf, b) 0,75 wt% of gA, c) 1 wt% of gA, d) 1,5 wt% of gA in magnification 500x times.	79
Figure 4.6. SEM micrographs of cross section of membranes: a) Psf/1wt% of gA and b) Psf/0.75 wt% of gA, with visible protein aggregates.	80-81
Figure 4.7. Water uptake results for membranes prepared by entrapment. The error bars refers to the standard deviation of the measurements.	83
Figure 5.1. Scheme of the reaction of the synthesis of magnetite nanoparticles (Fe_3O_4) from iron salts FeCl_2 and FeCl_3 .	93
Figure 5.2. Scheme of the MNP-OH functionalization through the silanization reaction with APTS. The products of the reaction are MNPs functionalized with - NH_2 groups.	93
Figure 5.3. ESEM micrographs of cross sections in magnification x500: a) MNP- NH_2 , b) MNP- NH_2 /TRX/gA, c) MNP-OH, d) MNP-OH/TRX/gA membranes, with visible particles.	100-101
Figure 5.4. Water uptake experiment results for MNP membranes: MNP-OH membranes prepared in H_2O (a) and in PBS (b). MNP- NH_2 membranes prepared in H_2O (c) and in PBS (d).	104-105
Figure 5.5. Permeability test results in respect to the hydration radius of ions K^+ , Na^+ , Ca^{2+} and Mg^{2+} respectively for Psf membranes: Plain Psf prepared in H_2O (a) and in PBS (b), MNP-OH prepared in H_2O (c) and in PBS (d), MNP- NH_2 prepared in H_2O (e) and in PBS (f).	109-111
Figure 5.6. Current- Voltage curve of MNP- NH_2 /TRX membrane prepared in PBS, with visible 3 characteristic regions: limiting current (0-1 V), pseudo-plateau (1-3 V) and convective region (3-5 V).	115
Figure 5.7. Ohmic resistance of MNP	116
Figure 5.8. Ohmic resistance of the MNP	117
Figure 5.9. Ohmic resistance of the MNP	118
Figure 5.10. Ohmic resistance of the MNP	119
Figure 6.1. ESEM micrographs of membrane cross sections in magnification x500: a) MNP- NH_2 /glutar/gA prepared in PBS, b) MNP- NH_2 /glutar/gA prepared in water.	135
Figure 6.2. Water uptake experiment results for MNP- NH_2 membranes: described	

previously Plain MNP-NH ₂ and MNP-NH ₂ /TRX/gA (see Chapter V, Figure 4 c-d) and MNP-NH ₂ /glutar/gA prepared in water (a) and PBS (b).	137
Figure 6.3. Permeability test results versus the hydration radius of ions K ⁺ , Na ⁺ , Ca ²⁺ and Mg ²⁺ respectively [7, 8] for membranes: MNP-NH ₂ , MNP-NH ₂ /TRX/gA presented previously (see Chapter V, Figure 5.5. e-f) and MNP-NH ₂ /glutar/gA prepared in H ₂ O (a) and in PBS (b).	138
Figure 6.4. Current-Voltage curves obtained for all electrolyte solutions for the membrane MNP-NH ₂ /glutar prepared in PBS solution.	140
Figure 6.5. Ohmic resistance values the membranes: MNP-NH ₂ , MNP-NH ₂ /TRX/gA presented previously (see Chapter V, Figure 5.9.) and MNP-NH ₂ /glutar/gA prepared in water.	141
Figure 6.6. Ohmic resistance values for the membranes: MNP-NH ₂ , MNP-NH ₂ /TRX/gA presented previously (see Chapter V, Figure 5.10.) and MNP-NH ₂ /glutar/gA prepared in PBS.	142
Figure 7.1. Nystatin structure.	151
Figure 7.2. Permeability of track etched membranes with conical pores, before and after TRX/gA micelles immobilization versus the hydration radius of ions K ⁺ , Na ⁺ , Ca ²⁺ and Mg ²⁺ respectively.	153
Figure 7.3. Permeability of HMDS functionalized track etched membranes with conical pores, before and after gA immobilization versus the hydration radius of ions K ⁺ , Na ⁺ , Ca ²⁺ and Mg ²⁺ respectively.	154
Figure 7.4. Permeability of HMDS functionalized track etched membranes with cylindrical pores of initial size of 40 (a) and 80 nm (b), before and after gA immobilization versus the hydration radius of ions K ⁺ , Na ⁺ , Ca ²⁺ and Mg ²⁺ respectively.	155
Figure 7.5. Permeability of all the track etched membranes modified with various techniques.	156
Figure 7.6. Permeability of track etched membranes with conical pores, before and after TRX/gA micelles immobilization versus the hydration radius of ions Cl ⁻ , NO ₃ ⁻ , CO ₃ ⁻ and SO ₄ ²⁻ respectively.	157
Figure 7.7. Permeability trends of all the track etched membranes modified with various techniques.	158
Figure 7.8. Permeability of polysulfone membranes modified with various techniques: previously presented Plain Psf, Psf/TRX and Psf/TRX/gA membrane (see Chapter V, Figure 5.6.b) and Psf/Nystatine membrane versus the hydration radius of ions K ⁺ , Na ⁺ , Ca ²⁺ and Mg ²⁺ respectively.	159
Figure 7.9. FTIR spectra of track etched membranes: plain PET film, functionalized with isopropylamine and gA, and with TRX/gA micelles.	160
Figure 8.1. Petri dishes with <i>Listeria innocua</i> , without visible growth of bacteria culture.	171
Figure 8.2. Petri dishes with <i>Listeria innocua</i> at different bacteria concentration : a) 100 µl, b) 200 µl, c) 300 µl.	171

Figure 8.3. Results of the study of gA activity in micelles without presence of methanol.	172
Figure 8.4. Results of experiment studying gA activity in micelles without presence of methanol at different concentration of bacteria.	174
Figure 8.5. Results of experiment studying gA activity in micelles with presence of methanol.	175
Figure 8.6. Results of the experiment carried out to study gA activity in micelles with presence of methanol and at different concentration of protein.	176
Figure 8.7. Results of the experiment carried out to study gA activity in micelles and in the solution with the presence of methanol.	177
Figure 8.8. Results of the experiment evaluating antibacterial activity study of TRX/gA micelles immobilized on MNP-OH membrane, against <i>Bacillus subtilis</i> .	181
Figure 8.9. Optical density at 600 nm of the liquid media with immersed membranes: without and with immobilized TRX/gA micelles.	182
Figure 8.10. ESEM micrographs of the membranes after immersion in liquid media containing <i>Bacillus subtilis</i> : a) membrane without and b) with immobilized micelles.	183
Figure 8.11. Solutions under study after 24 hours of incubation, from the left to the right: seawater with glucose and <i>Bacillus subtilis</i> , seawater, MiliQ water.	183
Figure 8.12. Permeability versus hydration radius of ions K^+ , Na^+ , Ca^{2+} and Mg^{2+} for membranes: MNP-NH ₂ /TRX/gA prepared in PBS, presented previously (see Chapter V, Figure 5.5. e), MNP-NH ₂ /glutar/gA prepared in H ₂ O and MNP-NH ₂ /glutar/gA prepared in PBS presented previously (see Chapter VI, Figure 6.3. a-b) and MNP-NH ₂ /TRX/gA membrane prepared in PBS/methanol mixture.	185
Figure 8.13. Ohmic resistance values of the membranes: MNP-NH ₂ /TRX/gA prepared in PBS presented previously (see Chapter V, Figure 5.10.), MNP-NH ₂ /glutar/gA prepared in H ₂ O presented previously (see Chapter VI, Figure 6.5.) and MNP-NH ₂ /glutar/gA prepared in PBS presented previously (see Chapter VI, Figure 6.6.) and MNP-NH ₂ /TRX/gA prepared in PBS/methanol mixture.	186
Figure 9.1. Interfacial tension measurements results for a control solutions.	200
Figure 9.2. Interfacial tension of samples with different concentration of surfactant, without and with gA addition, in the presence or absence of methanol.	201
Figure 9.3. Dynamic light scattering measurement results for the samples with different concentration of surfactant, without (a) and with gA addition (b), in the absence of methanol.	203
Figure 9.4. Dynamic light scattering measurement results for the samples with different concentration of surfactant, without (9.4. a) and with gA addition (9.4. b), in the presence of methanol.	204-205
Figure 9.5. Relation of dynamic viscosity and conductivity of the tested micelle solutions.	206

Appendix B. List of Tables

Table 1.1 Reactions on the electrodes in different fuel cells.	3
Table 4.1. Pore sizes of the membranes prepared by phase inversion/precipitation method in water-coagulation bath.	79
Table 4.2. Pore sizes and thicknesses of the membranes prepared by gA entrapment.	82
Table 4.3. Contact angle (CA) measurement for membranes prepared by gA entrapment.	82
Table 5.1. List of all the membranes used in this investigation and characterization performed.	96
Table 5.2. Pore sizes and thicknesses of membranes prepared before and after TRX/gA immobilization.	101
Table 5.3. Results of contact angle (CA) measurement for MNP membranes.	103
Table 5.4. Statistical analysis performed for WU experiments corresponding to MNP membranes.	106
Table 5.5. Statistical analysis performed for permeability tests for Plain Psf and MNP membranes.	112
Table 5.6. Results of Mg^{2+} ion concentration in the stripping solution according to the pH meter measurements and Atomic Absorption Spectrometry	113
Table 5.7. Ohmic resistance values for all the tested membranes.	114
Table 5.8. Statistical analysis of the Ohmic resistance values.	115
Table 5.9. Selectivity values for MNP-OH membranes prepared in water.	117
Table 5.10. Selectivity values for MNP-OH membranes prepared in PBS.	118
Table 5.11. Selectivity values for the MNP-NH ₂ membranes prepared in water.	119
Table 5.12. Selectivity values for the MNP-NH ₂ membranes prepared in PBS.	120
Table 5.13. Results of conductivity and self-diffusion coefficient calculated from the resistance data, and the diffusion coefficient values calculated from permeability data, for the membranes prepared in water and in PBS.	122
Table 6.1. Pore sizes and thicknesses of membranes prepared before and after glutaraldehyde coupling reaction, compared also with the values obtained previously for the MNP-NH ₂ membrane with physically immobilized TRX/gA micelles and MNP-NH ₂ membrane before modification (Chapter V, Table 5.2.).	135
Table 6.2. Results of contact angle (CA) measurement for MNP membranes with gA immobilized via glutaraldehyde coupling (5-6) compared with the values obtained previously for the MNP-NH ₂ membrane with physically immobilized TRX/gA micelles and MNP-NH ₂ membrane before modification (1-4, see Chapter V, Table 5.3.).	136
Table 6.3. Ohmic resistance values for the membranes: MNP-NH ₂ , MNP-NH ₂ /TRX/gA presented previously (see Chapter V, Table 6.7.) and MNP-	140

NH₂/glutar/gA prepared in water and in PBS.

Table 6.4. Selectivity values the membranes: MNP-NH₂, MNP-NH₂/TRX/gA presented previously (see Chapter V, Table 5.11.) and MNP-NH₂/glutar/gA prepared in water. 141

Table 6.5. Selectivity values for the membranes: MNP-NH₂, MNP-NH₂/TRX/gA presented previously (see Chapter V, Table 5.12.) and MNP-NH₂/glutar/gA prepared in PBS. 142

Table 6.6. Results of conductivity and self-diffusion coefficient calculated from the resistance data, and the diffusion coefficient values calculated from permeability data, for the membranes: MNP-NH₂, MNP-NH₂/TRX/gA presented previously (see Chapter V, Table 5.14.) and MNP-NH₂/glutar/gA. 144

Table 8.1. List of the samples prepared for bioactivity assay. 168

Table 8.2. Growth inhibition diameter measured for all tested solutions. 178

Table 8.3. Statistical analysis of growth inhibition diameters of the samples containing TRX/gA micelles and methanol in comparison to the solution without gA. 180

Table 8.4. Selectivity values for the membranes: MNP-NH₂/TRX/gA/PBS, MNP-NH₂/TRX/gA/PBS/CH₃OH, MNP-NH₂/glutar/gA/H₂O and MNP-NH₂/glutar/gA/PBS. 188

Table 9.1. List of the samples prepared for thermophysical properties analysis. 199

Table 9.2. Statistical analysis of interfacial tension values for the samples containing 320 µl of TRX in comparison to the ones containing 480 µl of TRX . 202

Appendix C. Publications

- Kamila Szalata, Gaurav Pande, Tania Gumi. Novel bioinspired polysulfone membranes with physically immobilized gramicidin for ion exchange applications. Submitted to Industrial & Engineering Chemistry Research.
- Kamila Szalata, Magda Constanti, Tania Gumi. Antibacterial properties of polysulfone membranes with immobilized Triton X100/Gramicidin micelles. Submitted to Industrial & Engineering Chemistry Research.
- Kamila Szalata, Tania Gumi, Bartosz Tylkowski. "BioArtificial polymers" in Tylkowski, B. (Ed.), Wieszczycka, K. (Ed.), Jastrzab, R. (Ed.), et al. (2017). Polymer Engineering. Berlin, Boston: De Gruyter.
- Kamila Szalata, Tania Gumi. BioArtificial polymers, Physical Sciences Reviews. 2,2 (2017).

Appendix D. Contribution to Congresses

- Kamila Szałata, Tània Gumí. Proton conductive polysulfone biomimetic membranes. 4th of May 2016, 13th Doctoral Day, Tarragona (Poster).
- Kamila Szałata, Gaurav Pande, Tània Gumí. Proton conductive polysulfone biomimetic membranes. May 15-19, 2016, PERMEA & MELPRO, Prague (Oral presentation).
- Kamila Szałata, Tània Gumí. Biomimetyczne membrany polisulfonowe przewodzące protony. III Poznańskie Sympozjum Młodych Naukowców, November 2016, Poznań (Poster).
- Kamila Szałata, Magda Constantí, Tània Gumí. Właściwości antybakteryjne membran polisulfonowych z zimobilizowaną gramicydyną. IV Poznańskie Sympozjum Młodych Naukowców, November 2017, Poznań (Poster).
- Tània Gumí, Kamila Szałata, Magda Constanti. Characterization of transport properties and the bioactivity of polysulfone membranes containing gramicidin. April 5-7, 2017, 4th World Congress and Expo on Nanotechnology and Materials Science, Barcelona (Oral presentation).
- Kamila Szałata, Jie Ma, Tània Gumí. Novel bioinspired proton exchange polysulfone membrane containing Gramicidin. December 12-15, 2017, European Membrane Fuel Cells, Naples (Poster).

Appendix E. Other contributions

- El-Feky, Hany Hassan; Briceno, Kelly; Szałata, Kamila; Hevia, Miguel A.G.; Gumí, Tània. Characterization of Metal-Doped Methylated Microporous Silica for Molecular Separations. International Journal of Membrane Science and Technology. 2,2 (2015).

Research stay

- The European Membrane Institute
Period: February 2016- May 2016
Advisor: Dr. Sébastien Balme
Topic: Preparation and characterization of different polymeric membranes containing Gramicidin ion channel.

Appendix F. Curriculum Vitae

Kamila Szalata

HIGHLIGHT

October 2014- current	PhD student at Univeristy Rovira i Virgili, Tarragona, Spain
October 2013- July 2014	Master Internship in DOW Chemical Iberica, DW&PS Department in Tarragona, Spain
July- September 2013	LLP Erasmus Training Placement in DOW Chemical Iberica company, DW&PS Department in Tarragona, Spain
September 2012-June 2013	Memeber of “METEOR” research group, Membrane Technology and Process Engineering Centre, Tarragona, Spain

ACADEMIC INFORMATION

February 2016- May 2016	Doctoral Research Stage European Membrane Institute in Montpellier, France
September 2012- June 2014	Master in Materials Chemistry Faculty of Chemistry, Adam Mickiewicz University in Poznań, Poland Master’s Thesis: Nanofiltration for high salinity water treatment October 2012-July 2013 Erasmus student at Chemical Engineering Faculty, University Rovira i Virgili in Tarragona, Spain
October 2009-June 2012	Bachelor in Chemistry Faculty of Chemistry, Adam Mickiewicz University in Poznań, Poland Specialization: Cosmetics chemistry

SCHOLARSHIPS

Doctoral Scholarship Marti-Franques	2014-2018
EU funds scholarship for the best students, POKL <i>Poczuj chemię do chemii</i>	2009-2013
Polish National Education Minister’s Scholarship	2008

CERTIFICATIONS AND TRAINING

Certificate of training on the internal auditor of quality management system in laboratory research by norm PN-EN ISO/IEC 17025:2005.